AN ABSTRACT OF THE THESIS OF

Daniel S. Wilks for the degree of Doctor of Philosophy in Atmospheric Sciences presented on November 26, 1986.

Title: Specification of Local Surface Weather Elements from Large-Scale General Circulation Model Information, with Application to Agricultural Impact Assessment

Abstract Approved: —Redacted for Privacy—

A procedure for model-assisted climate impact assessment is developed. The approach combines data from observations and atmospheric general circulation models (GCMs), and provides the basis for a potentially valuable means of using information derived from GCMs for climate impact assessments on local scales.

The first component of this procedure is an extension of the "climate inverse" method of Kim et al. (1984). Daily mesoscale temperature and precipitation values are stochastically specifed on the basis of observational data representing the average over an area corresponding to a GCM grid element. Synthetic local data sets generated in this manner resemble the corresponding observations with respect to various spatial and temporal statistical measures.

A method for extrapolation to grid-scale "scenarios" of a changed climate on the basis of control and experimental integrations of a

GCM, in conjunction with observational data, is also presented. The statistical characteristics of daily time series from each of these data sources are portrayed in terms of the parameters of a multivariate time-domain stochastic model. Significant differences between the model data sets are applied to the corresponding parameters derived from the observations, and synthetic data sets representing the inferred changed climate are generated using Monte-Carlo simulations.

The use of the procedure is illustrated in a case study. The potential climatic impacts of a doubling of atmospheric carbon dioxide concentrations on three important North American grain cropping regions is investigated using two "physiological" crop models. Although the specific results must be interpreted with caution, they are moderately optimistic and demonstrate possible means by which agricultural production may adapt to climatic changes.

# Specification of Local Surface Weather Elements from Large-Scale General Circulation Model Information, with Application to Agricultural Impact Assessment

by

Daniel S. Wilks

A THESIS

submitted to

Oregon State University

in partial fulfillment of
the requirements for the
degree of

Doctor of Philosophy

Completed November 26, 1986

Commencement June 7, 1987

APPROVED:

Redacted for Privacy

Professor of Atmospheric Sciences, in charge of major

Redacted for Privacy

Chairman of Department of Atmopheric Sciences

Redacted for Privacy

Dean of Graduate School

Date thesis is presented: November 26, 1986

## Acknowledgements

The contributions of Drs. W. Lawrence Gates and Allan H. Murphy in suggesting, encouraging, and supporting this work are gratefully acknowledged. Drs. Steven K. Esbensen and Daniel W. Schafer also provided valuable comments on this manuscript. The necessary GCM data was generously provided through Dr. Gates. Thanks are also due to Dr. William Dugas of the Texas Agricultural Experiment Station for supplying the crop models.

This research was supported by the National Science Foundation under grant ATM-8411003.

Table of Contents

## List of Figures

List of Tables

# Specification of Local Surface Weather Elements from Large-Scale General Circulation Model Information, with Application to Agricultural Impact Assessment

## Section 1

## Introduction

Skillful climate forecasts have the potential to be of immense economic value for the purposes of agricultural impact assessment, planning, and decision making. Among the potential methods of producing such forecasts, large-scale coupled atmosphere-ocean general circulation models (GCMs) appear to be the most promising. This promise is principally a consequence of the ability of these models to provide data sets that contain a wide variety of meteorological variables, that are complete (within the limits of model resolution) in space and time, and that are physically consistent both internally and with experimentally specified boundary conditions (Gates, 1985).

One especially attractive aspect of information generated by GCMs for the purpose of climate impact assessment is the regularity and fineness of their time resolution. Impact assessment tools such as physiological crop simulation models typically require data at daily or even hourly intervals (e.g., Baier, 1977; World Climate Applications Programme, 1984), which are not provided by other potential means of climate forecasting. This degree of time resolution is necessary to detect some extreme weather events (e.g., temperature extremes on a single day or several consecutive days) which may dominate the response, particularly of crops, to variations or changes in climate (e.g., Mearns _et al_., 1984; Nield _et al_., 1980; Parry and Carter, 1985).

Gates (1985) has recently outlined the elements of a strategy for obtaining (climate) model-assisted estimates of climatic impacts, and has identified several critical steps related to the use of GCMs for local impact assessment. These steps, presented schematically in Figure 1, are (1) determining which aspects of the modeled climate change are significant, (2) translating the large-scale information generated by the climate model to the smaller spatial scales relevant to potential impacts, and (3) using the inferred local climate information for estimation of biological and economic impacts. The first of the above steps may be viewed as the problem of constructing climate "scenarios" (e.g., Bach _et al_., 1984). The second and third steps have become known as the "climate inverse" problem (Kim _et al_., 1984), and the problem of "climate impacts" assessment, repspectively.

The relevance of the climate inverse problem to the issue of impact assessment using GCMs results from the intrinsic coarseness of the spatial resolution of these models relative to the scales on which the impacts of weather or climate are accumulated. Typical spatial resolutions for GCMs are approximately 200,000 km$^2$. Relatively little work has been done to date in investigating the size of areas that are fairly homogeneous from the standpoint of agronomic prediction. However, the results of Dugas _et al_. (1983a), derived from physiological crop models, and of Galliani and Filippini (1985),

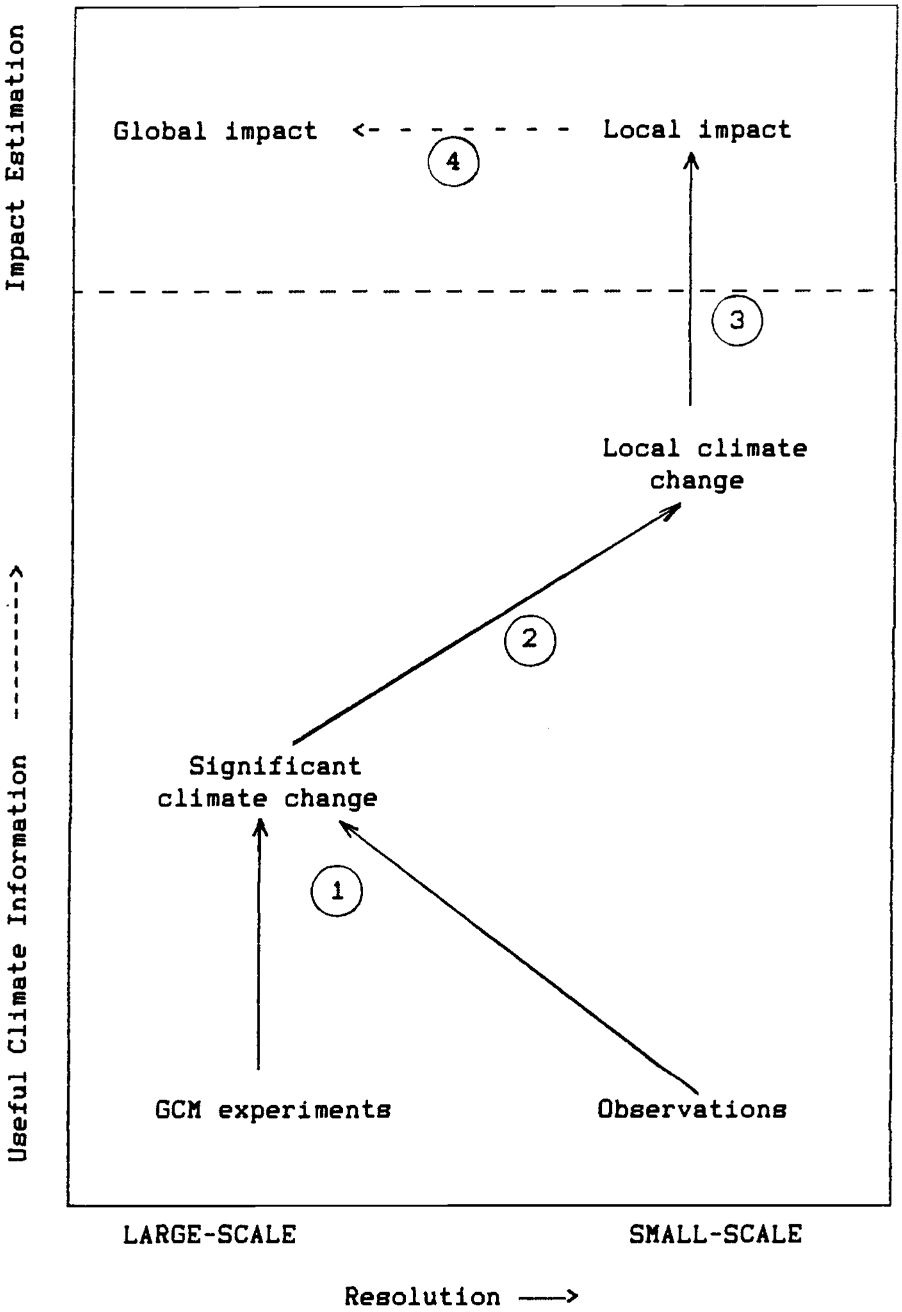


Figure 1. Schematic illustration of the elements of a model-assisted methodology for estimation of ecosystem impacts of climate change. After Gates (1985).

obtained from a cluster analysis of daily temperature and rainfall data, both indicate that this area may be approximately 1500 $km^2$. That scale appears to be controlled by the fineness of spatial variations in precipitation.

Several approaches to the climate inverse problem have appeared in the literature. One possible procedure is to add temperature changes linearly and apply proportional precipitation changes to observed data (Terjung et al., 1984; Waggoner, 1983; Williams, 1985). However, this approach only considers changes in first-moment characteristics, and does not allow treatment of possible changes in variance (at least for temperature) or autocorrelation. Also, the above studies have employed highly generalized scenarios for the changed climates, none of which have included variations in time or space. Another possible treatment of the climate inverse problem is interpolation between grid points (Santer, 1985), although this procedure almost certainly results in unrealistic spatial homogeneity, particularly for precipitation.

Kim et al. (1984) addressed the climate inverse problem by performing a principal component analysis of monthly temperature and precipitation data for stations within an area comparable in size to the gridbox of a GCM. The time-dependent structure of the data, with respect to the principal component basis set, was then predicted from the respective large-scale data by linear regression. Predictions were made separately for each of the two variables. Although this work is the most complete treatment of the problem to date, its applicability to problems such as agricultural impact assessment is limited by the consideration of only monthly-averaged quantities.

To date, no specific protocol for implementing the schematic outline of Gates (1985) on the daily timescale has been proposed. The present work seeks to develop specific methods to implement this framework for estimation of climate impacts using results from general circulation models. Section 2 extends the climate inverse approach of Kim *et al*. (1984) to the analysis of daily data necessary for impact assessment using physiological crop models. This work relates to step 2 in Figure 1. Section 3 describes and implements a methodology for the construction of climate change scenarios (step 1 in Figure 1) that utilizes the fine time-resolution of the available GCM information, and that may be used in a Monte Carlo setting with the climate inverse procedure developed in Section 2. The application of the coupling of the above two procedures to climate impact assessment (step 3 in Figure 1) is illustrated in Section 4, with a case study of possible effects of carbon dioxide-induced climate change on North American grain agriculture. Section 5 contains a summary, conclusions, and outlook for future work.

# Section 2

## Statistical Specification of Daily Local Surface Weather Elements from Large-Scale Information

### 2.1 Introduction

One of the critical elements of a procedure involving use of GCM data for local climate impact assessments is a means to translate the large-scale information to a more local scale (Gates, 1985). This topic has been called the climate inverse problem (Kim *et al.*, 1984). One possible approach to this problem would involve deterministic dynamical modeling of local flow regimes as forced by small-scale topography (Deardorff *et al.*, 1984; Han *et al.*, 1982), using the large-scale data as boundary conditions. However, the computer resources required for extended integrations using this approach appear at the present time to be prohibitive for climate impacts work.

This section presents a statistical formulation of the climate inverse problem. The starting point for the present treatment is the approach of Kim *et al.* (1984). In that work, monthly-averaged values of temperature and precipitation were subjected to separate principal component (empirical orthogonal function) analyses. The time-dependent structure of each data set, with respect to the principal component basis set, was then separately predicted from the corresponding large-scale data by linear regression. The same basis functions were used for all months, and the intercorrelation between temperature and precipitation was ignored. Also, only a generalized evaluation of the performance of the scheme was attempted.

The present work seeks to extend the approach of Kim _et al._ (1984), with a view toward use of the results as input to crop simulation models. Toward that end, daily values of three relevant surface weather variables are analyzed, and treatment of their mutual intercorrelations is included. The performance of the procedure is explicitly assessed through compilation of verification statistics derived from independent data. Section 2.2 describes the spatial domain and the data set used in the analysis. Section 2.3 develops a rotated principal component representation of the data, which is used in Section 2.4 as the basis of a climate inverse procedure. Section 2.5 contains a summary and a brief set of conclusions.

## 2.2 Domain and Data

The study area for the present work is comprised of three 4° by 5° (latitude by longitude) regions within North America. The size and boundaries of these areas were selected to conform to the 4° by 5° grid spacing of the Oregon State University Atmospheric GCM (Ghan et al., 1982), and the locations were chosen to encompass important grain cropping regions. These gridboxes are hereafter designated as Box 1 (centered at 38°N, 100°W, and comprised primarily by central and western Kansas), Box 2 (centered at 42°N, 95°W, and comprised primarily by central and western Iowa), and Box 3 (centered at 46°N, 100°W, and located in the eastern and central portions of North and

South Dakota).

Daily maximum and minimum temperature and daily accumulated precipitation data were obtained from the Oklahoma Climate Survey for 24, 27, and 26 stations within Boxes 1, 2, and 3, respectively, for the years 1948-1983. To the extent possible, stations were chosen from the list of candidate stations for the National Climatic Data Center Historical Climatology Network (Brower, 1984) to minimize problems associated with changes in station location or instrument height. Also when feasible, only stations with PM observation times throughout the 36-year data record were selected. The stations, locations, and elevations are given in Table 1. A few stations with morning observation times or missing data for portions of the record, noted in Table 2, are used in order to improve the homogeneity of station distribution or to include stations with solar radiation measurements. Flagged estimates of missing data, derived from weighted averages of near neighbors in space and time (Oklahoma Climate Survey, private communication), were included in the data set.

Temperature data for each station are converted to series of deviations from an annual cycle by removing the 12-monthly Fourier harmonic, and as many of the 6-monthly, 4-monthly, 3-monthly, 12/5-monthly, and 2-monthly harmonics as were deemed "significant." Significance was determined using an F-test at the 0.83% level (6 tests simultaneously at the 5% level), although lack of independence of the residuals renders the true level of the test to be much less stringent. Typically harmonics with amplitudes less than 0.2°C are not retained. Fourier harmonics are fit to the full data records in order to avoid filtering the very low frequency variations (Trenberth,

Table 1. Station index, name, latitude, longitude, elevation (m), and relative weight.

a. Box 1

| Station | Name | N Lat | W Lon | Elev(m) | Weight |
|---|---|---|---|---|---|
| 1 | Cheyenne Wells, CO | 38°49' | 102°21' | 1295 | .02088 |
| 2 | Belleville, KS | 39°50' | 97°38' | 469 | .01084 |
| 3 | Beloit, KS | 39°29' | 98°06' | 445 | .01850 |
| 4 | Coldwater, KS | 37°16' | 99°20' | 634 | .01909 |
| 5 | Dodge city WSO AP, KS | 37°46' | 99°58' | 786 | .03788 |
| 6 | Goodland WSO AP, KS | 39°22' | 101°42' | 1113 | .06963 |
| 7 | Greensburg, KS | 37°37' | 99°18' | 680 | .01897 |
| 8 | Healy, KS | 38°36' | 100°37' | 869 | .03305 |
| 9 | Hoxie, KS | 39°21' | 100°27' | 820 | .05768 |
| 10 | Larned, KS | 38°11' | 99°06' | 610 | .05203 |
| 11 | Liberal, KS | 37°02' | 100°55' | 866 | .04740 |
| 12 | Lincoln 1 ESE, KS | 39°02' | 98°08' | 427 | .02963 |
| 13 | McPherson, KS | 38°22' | 97°40' | 454 | .04211 |
| 14 | Medicine Lodge, KS | 37°16' | 98°35' | 442 | .05384 |
| 15 | Minneapolis, KS | 39°08' | 97°42' | 402 | .01313 |
| 16 | Plainville, KS | 39°14' | 99°18' | 655 | .05247 |
| 17 | Scott City, KS | 38°29' | 100°54' | 905 | .02983 |
| 18 | Smith Center, KS | 39°47' | 98°47' | 546 | .03035 |
| 19 | Sublette, KS | 37°29' | 100°51' | 890 | .04917 |
| 20 | Tribune 1 W, KS | 38°28' | 101°46' | 1100 | .06207 |
| 21 | Buffalo, OK | 36°50' | 99°37' | 549 | .07363 |
| 22 | Goodwell Res. Sta., OK | 36°36' | 101°37' | 1009 | .09849 |
| 23 | Jefferson, OK | 36°43' | 97°48' | 326 | .03839 |
| 24 | Okeene, OK | 36°07' | 98°19' | 366 | .04094 |

Table 1, continued.

b. Box 2

| Station | Name | N Lat | W Lon | Elev(m) | Weight |
|---|---|---|---|---|---|
| 1 | Algonia 3 W, IA | 43°04' | 94°18' | 375 | .02731 |
| 2 | Ames 8 WSW & 3SW, IA | 42°01' | 93°44' | 320 | .02917 |
| 3 | Atlantic 1 N, IA | 41°25' | 95°00' | 366 | .02444 |
| 4 | Carroll 2 SSW, IA | 42°02' | 94°53' | 381 | .02333 |
| 5 | Chariton, IA | 41°00' | 93°19' | 293 | .02260 |
| 6 | Charles City, IA | 43°03' | 92°40' | 308 | .01205 |
| 7 | Clarinda, IA | 40°44' | 95°01' | 322 | .02835 |
| 8 | Glenwood, IA | 41°02' | 95°45' | 302 | .02348 |
| 9 | Harlan, IA | 41°39' | 95°19' | 354 | .03141 |
| 10 | Indianola 2, IA | 41°21' | 93°34' | 256 | .01983 |
| 11 | Iowa Falls, IA | 42°32' | 93°16' | 357 | .03384 |
| 12 | Le Mars, IA | 42°48' | 96°10' | 363 | .01228 |
| 13 | Logan, IA | 41°38' | 95°48' | 320 | .01686 |
| 14 | Mason City, IA | 43°09' | 93°12' | 344 | .02868 |
| 15 | Onawa, IA | 42°02' | 96°06' | 320 | .03294 |
| 16 | Osage, IA | 43°17' | 92°48' | 357 | .02461 |
| 17 | Oskaloosa, IA | 41°19' | 92°39' | 253 | .02075 |
| 18 | Rockwell City, IA | 42°24' | 94°37' | 369 | .03285 |
| 19 | Spencer 1 N, IA | 43°10' | 95°09' | 405 | .03110 |
| 20 | Albert Lea, MN | 43°39' | 93°21' | 372 | .00979 |
| 21 | Trenton, MO | 40°05' | 93°38' | 256 | .01910 |
| 22 | Crete, NE | 40°37' | 96°57' | 439 | .04012 |
| 23 | Madison, NE | 41°50' | 97°27' | 482 | .01435 |
| 24 | Omaha (North) WSFO, NE | 41°22' | 96°01' | 399 | .01962 |
| 25 | Seward, NE | 40°54' | 97°05' | 451 | .02751 |
| 26 | Wakefield, NE | 42°16' | 96°52' | 430 | .02334 |
| 27 | Sioux Falls SD | 43°34' | 96°44' | 433 | .02271 |

Table 1, continued.

c. Box 3

| Station | Name | N Lat | W Lon | Elev(m) | Weight |
|---|---|---|---|---|---|
| 1 | Bismarck WSO AP, ND | 46°46' | 100°46' | 503 | .03199 |
| 2 | Cooperstown, ND | 47°26' | 98°07' | 436 | .04962 |
| 3 | Fessenden, ND | 47°39' | 99°37' | 494 | .03876 |
| 4 | Fullerton, ND | 46°09' | 98°24' | 439 | .03662 |
| 5 | Gackle, ND | 46°38' | 99°08' | 594 | .02770 |
| 6 | Jamestown St Hosp., ND | 46°53' | 98°41' | 445 | .02201 |
| 7 | McLusky, ND | 47°29' | 100°28' | 591 | .02184 |
| 8 | Mott, ND | 46°23' | 102°20' | 738 | .01654 |
| 9 | Pettibone, ND | 47°07' | 99°31' | 597 | .03067 |
| 10 | Richardton Abbey, ND | 46°53' | 102°19' | 753 | .03979 |
| 11 | Washburn, ND | 47°17' | 101°02' | 546 | .02916 |
| 12 | Aberdeen WSO AP, SD | 45°27' | 98°26' | 396 | .01324 |
| 13 | Britton, SD | 45°47' | 97°45' | 408 | .02974 |
| 14 | Clark, SD | 44°53' | 97°44' | 543 | .02830 |
| 15 | Dupree, SD | 45°03' | 101°36' | 722 | .03159 |
| 16 | Eureka, SD | 45°47' | 99°38' | 570 | .02185 |
| 17 | Faulkton 1 NW, SD | 45°02' | 99°08' | 479 | .02606 |
| 18 | Forestburg 3 NE, SD | 44°02' | 98°04' | 375 | .03479 |
| 19 | Gann Valley, SD | 44°02' | 98°58' | 533 | .02344 |
| 20 | Highmore 1 W, SD | 44°31' | 99°28' | 576 | .02832 |
| 21 | Hopewell 1 SE, SD | 44°30' | 100°52' | 585 | .06116 |
| 22 | Huron WSO AP, SD | 44°23' | 98°13' | 390 | .04354 |
| 23 | Lemmon, SD | 45°56' | 102°10' | 792 | .02939 |
| 24 | Midland, SD | 44°04' | 101°09' | 576 | .01148 |
| 25 | Pierre FAA AP, SD | 44°23' | 100°17' | 527 | .01607 |
| 26 | Timber Lake, SD | 45°26' | 101°04' | 655 | .03389 |

Table 2. Stations and dates of missing data and morning observation times.

| | | | |
|---|---|---|---|
| Box 1 | Station 10 | Sep 1983 - Dec 1983 | AM Observations |
| | Station 11 | Sep 1979 - Dec 1983 | AM Observations |
| | Station 19 | Jan 1948 - Dec 1949 | AM Observations |
| | Station 22 | Dec 1972 - Dec 1983 | AM Observations |
| | Station 24 | Jan 1948 - Jan 1950 | AM Observations |
| Box 2 | Station 8 | May 1958 - Nov 1960 | AM Observations |
| | Station 20 | Aug 1979 - Dec 1983 | AM Observations |
| | Station 23 | Jan 1981 - Dec 1983 | AM Observations |
| | Station 24 | Jan 1948 - Dec 1953 | Missing |
| Box 3 | Station 3 | Jan 1982 - Dec 1983 | Missing |
| | Station 7 | Jan 1948 - Sep 1950 | AM Observations |
| | Station 8 | Dec 1980 - Dec 1983 | AM Observations |
| | Station 11 | Feb 1966 - Nov 1970 | AM Observations |
| | Station 21 | Jan 1948 - Dec 1949 | Missing |

1984).

Trace precipitation values are assigned the value 0.1 mm. Precipitation data is square-root transformed to mitigate the very strong positive skewness exhibited. This transformation was chosen as being most satisfactory, after some experimentation involving comparisons with logarithmic and cube-root transformations, and no transformation.

Box-scale time series of daily maximum and minimum temperatures and daily precipitation were calculated by area-averaging station values using the weights listed in Table 1. These weights specify the proportion of the study areas closest to each station. Maximum and minimum temperatures for each station were adjusted, before averaging, to the nominal box elevations as specified in the GCM (Box 1 = 913 m, Box 2 = 381 m, Box 3 = 629 m) using an assumed lapse rate of 6.5°C/km. Morning-observed maximum temperatures were assigned to the previous day. Morning-observed precipitation data were considered to be missing, and the weights recalculated for these cases.

## 2.3 Rotated Principal Component Representation

### 2.3.1. Spatial patterns

Eigenvectors and eigenvalues are calculated, separately for each month and gridbox, from the correlation matrix $\underset{\sim}{R}$ of the data for all stations and variables. This matrix is defined as

$$\underset{\sim}{R} = \langle \underset{\sim}{z}\, \underset{\sim}{z}' \rangle . \tag{2.1}$$

Here the angle brackets denote an ensemble average over all non-missing data, calculated separately (and with sample sizes possibly varying) for each element of $\underset{\sim}{R}$, and the prime denotes a transpose. Morning-observed maximum temperatures are assigned to the previous day and considered valid. All estimated data and morning-observed precipitation are considered missing. The ensemble average is taken over a randomly selected 27-year training sample only, the omitted years being 1950, 1955, 1957, 1962, 1966, 1969, 1973, 1974, and 1980.

The data vectors $\underset{\sim}{z}$ are of dimension equal to the number of stations in the gridbox J multiplied by 3, and are comprised of three sub-vectors, each of dimension J. That is,

$$\underset{\sim}{z} = \begin{vmatrix} \underset{\sim}{\tilde{h}} \\ -\!-\!- \\ \underset{\sim}{\tilde{\ell}} \\ -\!-\!- \\ \underset{\sim}{\widetilde{\sqrt{p}}} \end{vmatrix}, \qquad (2.2)$$

where the vector elements $h_j$ denotes maximum temperature, $\ell_j$ denotes minimum temperature, and $\sqrt{p}_j$ denotes the square-root of the precipitation, for station $j$. The tildes above each vector variable indicate data standardization by subtraction of the annual cycle (significant Fourier harmonics, varying daily, for temperatures, and monthly means for transformed precipitation) and division by standard deviations from the annual cycle for that variable, month, and station. That is,

$$\tilde{x}_j = (x_j - \bar{x}_j) / \sigma_{x_j} , \qquad (2.3)$$

where

$$\bar{x}_j = A_{oj} + \sum_{m=1}^{6} A_{mj} \sin[(2\pi m t)/365.25 + B_{mj}] , \quad j = 1, 2J; \qquad (2.4a)$$

$$\bar{x}_j = \frac{1}{N_j} \sum_{n=1}^{N_j} x_{jn} , \qquad j = 2J+1, 3J; \qquad (2.4b)$$

and

$$\sigma_{x_j} = [ \frac{1}{N_j} \sum_{n=1}^{N_j} (x_{jn} - \bar{x}_j)^2 ]^{1/2} . \qquad (2.5)$$

Here $x_j$ represents either maximum temperature, minimum temperature, or square-root transformed precipitation (depending on the index $j$), the A's are the Fourier amplitudes, the B's are the phases, and t is the julian date.

Thus, for Box 1, where J = 24, $z_{24}$ is the scaled maximum temperature deviation for station 24, and $z_{25}$ is the scaled minimum temperature deviation for station 1. This simultaneous treatment of all variables is analogous to the approach of Kutzbach (1967). Note also that this formulation is different from that of Kim <u>et al.</u> (1984), who considered scaled deviations of station data from the box-scale values, rather than from the individual average values for each station.

The largest eigenvectors for each month (scaled to have lengths equal to the square-roots of the corresponding eigenvalues) are then subjected to a varimax rotation (Horel, 1981; Kaiser, 1958). Recommendations in the literature as to precisely how many vectors to rotate vary widely (e.g., Richman, 1981; Richman and Lamb, 1985). The criterion used in the present formulation is to include in the rotation the number of eigenvectors sufficient to describe 98% of the variance for each month. This number is smallest for the cool months and largest for the warm months, and ranges from 35, 34, and 36 (respectively for Boxes 1, 2, and 3) for February to 52, 55, and 56 for July. The cutoff value was arrived at by examining the result of rotating successively more vectors, and observing the point at which the result ceased to change appreciably. The rotated vectors are scaled to unit length and, for convenience, multiplied by -1 if necessary to insure that the loading (i.e., vector element) with the largest absolute value is positive.

Rotation of principal components is a means of avoiding the somewhat artificial (for purposes other than data compression only) constraint on the unrotated solution that each vector in decreasing importance be orthogonal to the previous vectors while simultaneously being oriented along the line with maximum variance in the remaining subspace. Not rotating the initial solution can lead to vectors which do not represent any feature (pattern or cluster of data points) of the data. A particular unrotated mode may include only a residual fraction of a particular feature of the data, or may compromise between several features by being oriented between them (e.g., Richman, 1981, Richman 1986; Walsh and Richman, 1981).

The varimax procedure seeks to find rotations of the eigenvectors that will maximize the variance of the squared (scaled) rotated vector loadings. The usual result is that only a few loadings of a given rotated vector are substantially different from zero. This result is sometimes referred to as "simple structure," (e.g., Harman, 1967; Horel, 1981; Richman, 1986), and often aids in interpreting these vectors in terms of features in the data.

In the present data sets, simple structure is manifested by vectors having distinctly more length in one of the three J-dimensional subspaces that correspond to each of the three surface weather variables. The first J loadings of each vector are the elements of the "maximum temperature subspace", the second J loadings are the elements of the "minimum temperature subspace", and the last J loadings are the elements of the "precipitation subspace." The fact that these portions of the vectors correspond in this way to the three variables can be seen from the definition of the correlation matrix $\underset{\sim}{R}$ in (2.1) and (2.2), from which the rotated vectors are derived. The relative division of emphasis of each vector between these three subspaces may be examined quantitatively (since the rotated vectors have been scaled to unit length) by summing the squared loadings in each of the three subspaces. For example, Table 3 presents this decomposition for the 39 rotated January vectors for Box 1, and Table 4 does the same for the corresponding 52 rotated July vectors. These tables show that, except for some of the least important modes (which will subsequently be truncated), each mode may be rather unambiguously characterized as a "maximum temperature," a "minimum temperature," or a "precipitation" vector. Results for the other months and gridboxes are quite similar.

Table 3. Index number, percent of total variance described, and relative partition between maximum temperature, minimum temperature, and precipititation for rotated Box 1 January vectors. Asterisk indicates dominant emphasis of mode. Truncation for stochastic data generation indicated by K.

| Mode # | Variance ($\lambda_k$ x 100) | Sum of squared loadings for elements of: Max. Temp. | Min. Temp. | Precipitation |
|---|---|---|---|---|
| 1 | 30.69 % | .227 | .771 * | .002 |
| 2 | 26.75 % | .783 * | .181 | .036 |
| 3 | 14.60 % | .053 | .007 | .940 * |
| 4 | 2.10 % | .063 | .021 | .915 * |
| 5 | 1.80 % | .053 | .021 | .926 * |
| 6 | 1.60 % | .024 | .011 | .964 * |
| 7 | 1.58 % | .017 | .007 | .976 * |
| 8 | 1.53 % | .024 | .010 | .966 * |
| 9 | 1.03 % | .021 | .009 | .970 * |
| 10 | 1.00 % | .016 | .010 | .974 * |
| 11 | 0.98 % | .015 | .005 | .981 * |
| 12 | 0.93 % | .156 | .829 * | .015 |
| 13 | 0.83 % | .015 | .005 | .980 * |
| 14 | 0.82 % | .028 | .016 | .955 * |
| 15 | 0.79 % | .021 | .005 | .974 * |
| 16 | 0.78 % | .020 | .016 | .964 * |
| 17 | 0.76 % | .015 | .031 | .955 * |
| 18 | 0.67 % | .018 | .017 | .965 * |
| 19 | 0.65 % | .954 * | .041 | .006 |
| 20 | 0.63 % | .952 * | .040 | .008 |
| 21 | 0.55 % | .921 * | .069 | .010 |
| 22 | 0.55 % | .032 | .966 * | .002 |
| 23 | 0.54 % | .039 | .954 * | .008 |
| 24 | 0.51 % | .936 * | .056 | .008 |
| 25 | 0.50 % | .085 | .908 * | .007 |
| 26 | 0.50 % | .019 | .018 | .964 * |
| 27 | 0.49 % | .108 | .885 * | .007 |
| 28 | 0.48 % | .027 | .016 | .957 * |
| 29(=K) | 0.46 % | .041 | .038 | .922 * |
| 30 | 0.38 % | .024 | .025 | .951 * |
| 31 | 0.38 % | .022 | .023 | .955 * |
| 32 | 0.37 % | .027 | .019 | .954 * |
| 33 | 0.30 % | .059 | .939 * | .002 |
| 34 | 0.29 % | .893 * | .079 | .028 |
| 35 | 0.28 % | .823 * | .165 | .012 |
| 36 | 0.27 % | .901 * | .091 | .008 |
| 37 | 0.24 % | .136 | .844 * | .020 |
| 38 | 0.22 % | .162 | .394 | .443 |
| 39 | 0.22 % | .053 | .062 | .886 * |

Table 4. Index number, percent of total variance described, and relative partition between maximum temperature, minimum temperature, and precipititation for rotated Box 1 July vectors. Asterisk indicates dominant emphasis of mode. Truncation for stochastic data generation indicated by K.

| Mode # | Variance ($\lambda_k$ x 100) | Sum of squared loadings for elements of: Max. Temp. | Min. Temp. | Precipitation |
|---|---|---|---|---|
| 1 | 23.53 % | .773 * | .150 | .077 |
| 2 | 22.69 % | .192 | .804 * | .004 |
| 3 | 3.70 % | .825 * | .160 | .015 |
| 4 | 1.68 % | .053 | .023 | .924 * |
| 5 | 1.56 % | .055 | .038 | .906 * |
| 6 | 1.54 % | .061 | .033 | .906 * |
| 7 | 1.50 % | .043 | .012 | .946 * |
| 8 | 1.50 % | .032 | .021 | .946 * |
| 9 | 1.48 % | .055 | .010 | .935 * |
| 10 | 1.47 % | .049 | .017 | .934 * |
| 11 | 1.47 % | .051 | .023 | .926 * |
| 12 | 1.46 % | .059 | .011 | .931 * |
| 13 | 1.46 % | .041 | .027 | .932 * |
| 14 | 1.45 % | .035 | .013 | .952 * |
| 15 | 1.44 % | .047 | .017 | .936 * |
| 16 | 1.43 % | .057 | .016 | .927 * |
| 17 | 1.43 % | .039 | .023 | .938 * |
| 18 | 1.42 % | .908 * | .082 | .010 |
| 19 | 1.42 % | .074 | .024 | .902 * |
| 20 | 1.40 % | .048 | .016 | .935 * |
| 21 | 1.37 % | .061 | .035 | .903 * |
| 22 | 1.34 % | .034 | .013 | .953 * |
| 23 | 1.33 % | .077 | .903 * | .020 |
| 24 | 1.30 % | .118 | .085 | .798 * |
| 25 | 1.29 % | .047 | .014 | .938 * |
| 26 | 1.27 % | .035 | .019 | .946 * |
| 27 | 1.26 % | .045 | .017 | .938 * |
| 28 | 1.13 % | .050 | .014 | .937 * |
| 29 | 1.05 % | .044 | .014 | .942 * |
| 30 | .96 % | .065 | .921 * | .014 |
| 31 | .90 % | .036 | .958 * | .006 |
| 32 | .81 % | .070 | .919 * | .011 |
| 33 | .80 % | .958 * | .038 | .005 |
| 34 | .75 % | .080 | .911 * | .009 |
| 35 | .71 % | .938 * | .049 | .013 |
| 36 | .66 % | .039 | .954 * | .006 |
| 37 | .58 % | .078 | .921 * | .002 |
| 38 | .55 % | .051 | .944 * | .005 |
| 39 | .46 % | .979 * | .020 | .001 |
| 40(=K) | .46 % | .063 | .931 * | .006 |
| 41 | .44 % | .052 | .945 * | .002 |
| 42 | .41 % | .956 * | .042 | .001 |

Table 4, continued.

| | Variance | Sum of squared loadings for elements of: | | |
|---|---|---|---|---|
| Mode # | $(\lambda_k \times 100)$ | Max. Temp. | Min. Temp. | Precipitation |
| 43 | .41 % | .132 | .867 * | .002 |
| 44 | .39 % | .055 | .944 * | .001 |
| 45 | .39 % | .061 | .937 * | .002 |
| 46 | .34 % | .082 | .916 * | .002 |
| 47 | .30 % | .107 | .892 * | .001 |
| 48 | .30 % | .255 | .745 | .001 |
| 49 | .28 % | .320 | .680 | .000 |
| 50 | .27 % | .907 * | .092 | .001 |
| 51 | .27 % | .436 | .564 | .000 |
| 52 | .23 % | .460 | .539 | .000 |

Figures 2, 3, and 4 illustrate the above for the case of the leading three vectors, respectively, for the January Box 1 data. Panel (a) in each figure depicts the structure in (2-dimensional geographical) space of the first 24 (maximum temperature) elements for that mode, the (b) panels show the second 24 elements (minimum temperature), and the (c) panels show the final 24 (precipitation) elements. Looking at the three panels of Figure 2 illustrates the result, indicated in Table 3, that the first vector primarily represents variations in minimum temperature. The loadings in Figure 2b are of the same sign and of approximately the same magnitude, indicating that minimum temperatures are broadly coherent across the domain. The loadings in Figure 2a (for maximum temperature) are also all positive and comparable in magnitude, but are smaller than those for minimum temperature in Figure 2b. This result indicates a positive correlation between maximum and minimum temperatures, but also that the spatial correlation among minimum temperatures is stronger than their correlation with maximum temperatures. The loadings for precipitation in the first January mode, shown in Figure 2c, are all essentially zero. This result indicates that, to a first approximation, the relationship between precipitation and broad-scale minimum temperature is weak.

The second vector, depicted in the three panels of Figure 3 has a similar interpretation. In this case, however, it is primarily variations in maximum temperature which are represented, since the largest loadings are those in Figure 3a. Minimum temperatures exhibit substantial and coherent positive correlation with maximum temperatures, as seen in Figure 3b. The loadings for precipitation in

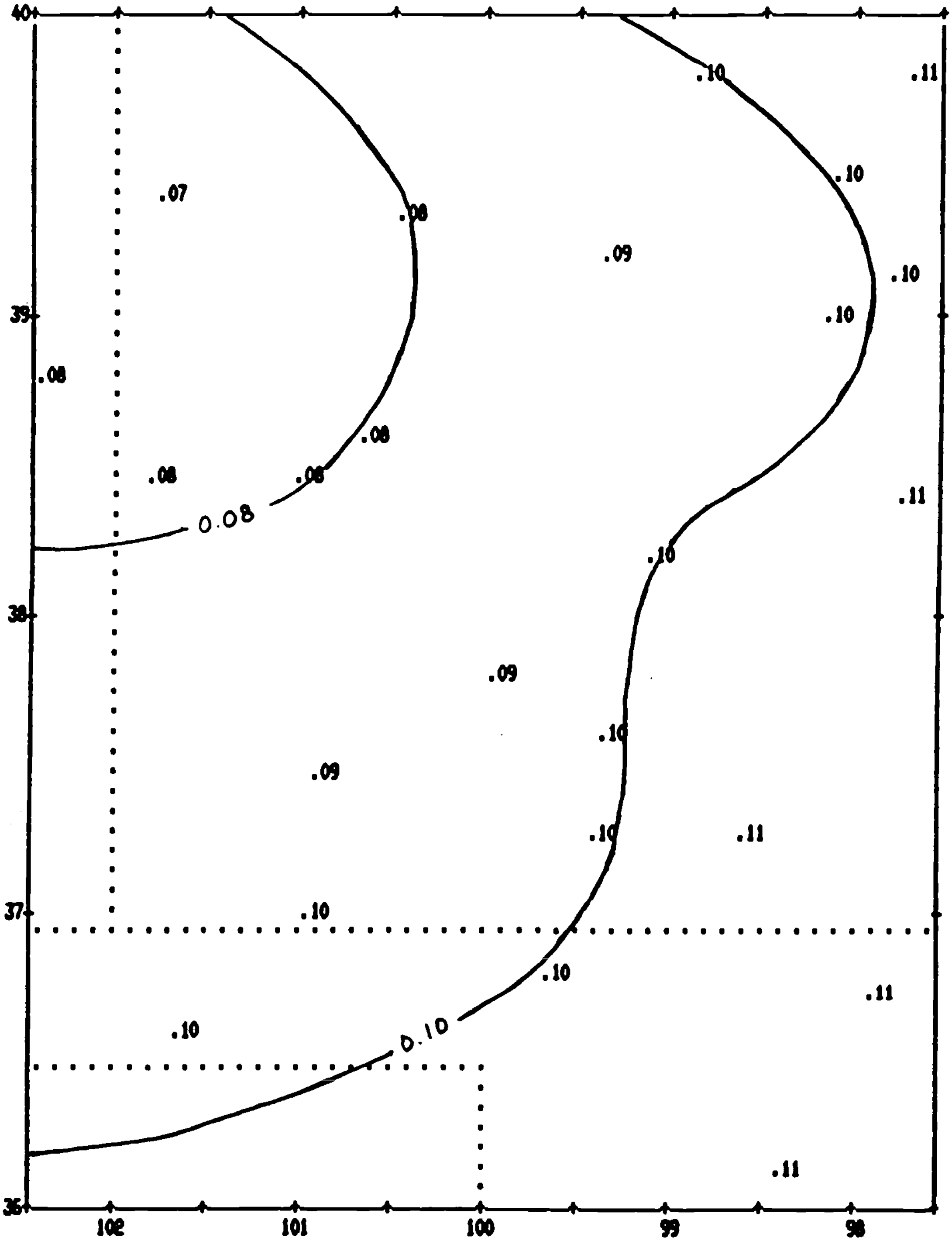


Figure 2a. Spatial distribution of elements of the leading (varimax rotated) vector for January Box 1. First 24 (maximum temperature) elements.

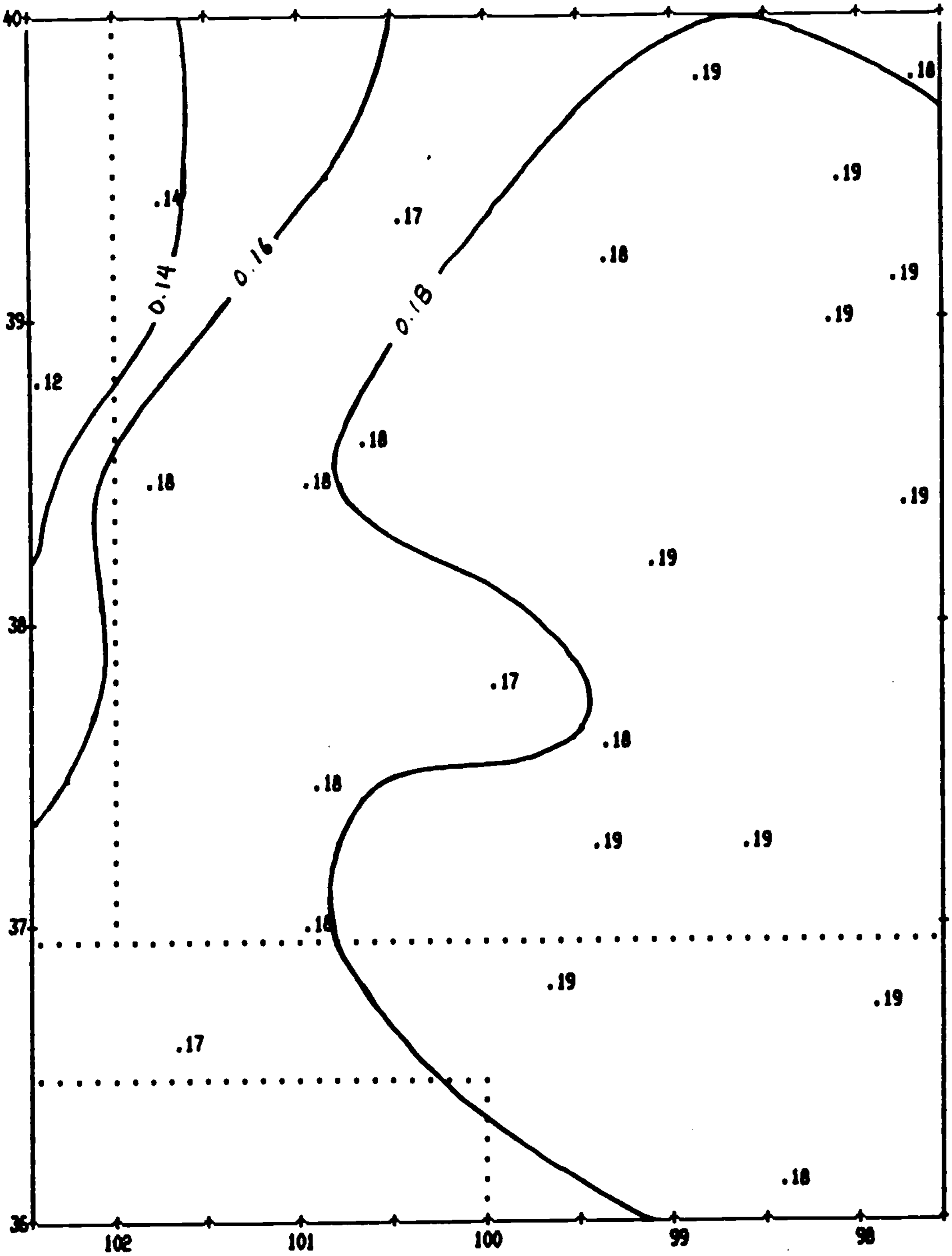


Figure 2b. Spatial distribution of elements of the leading (varimax rotated) vector for January Box 1. Second 24 (minimum temperature) elements.

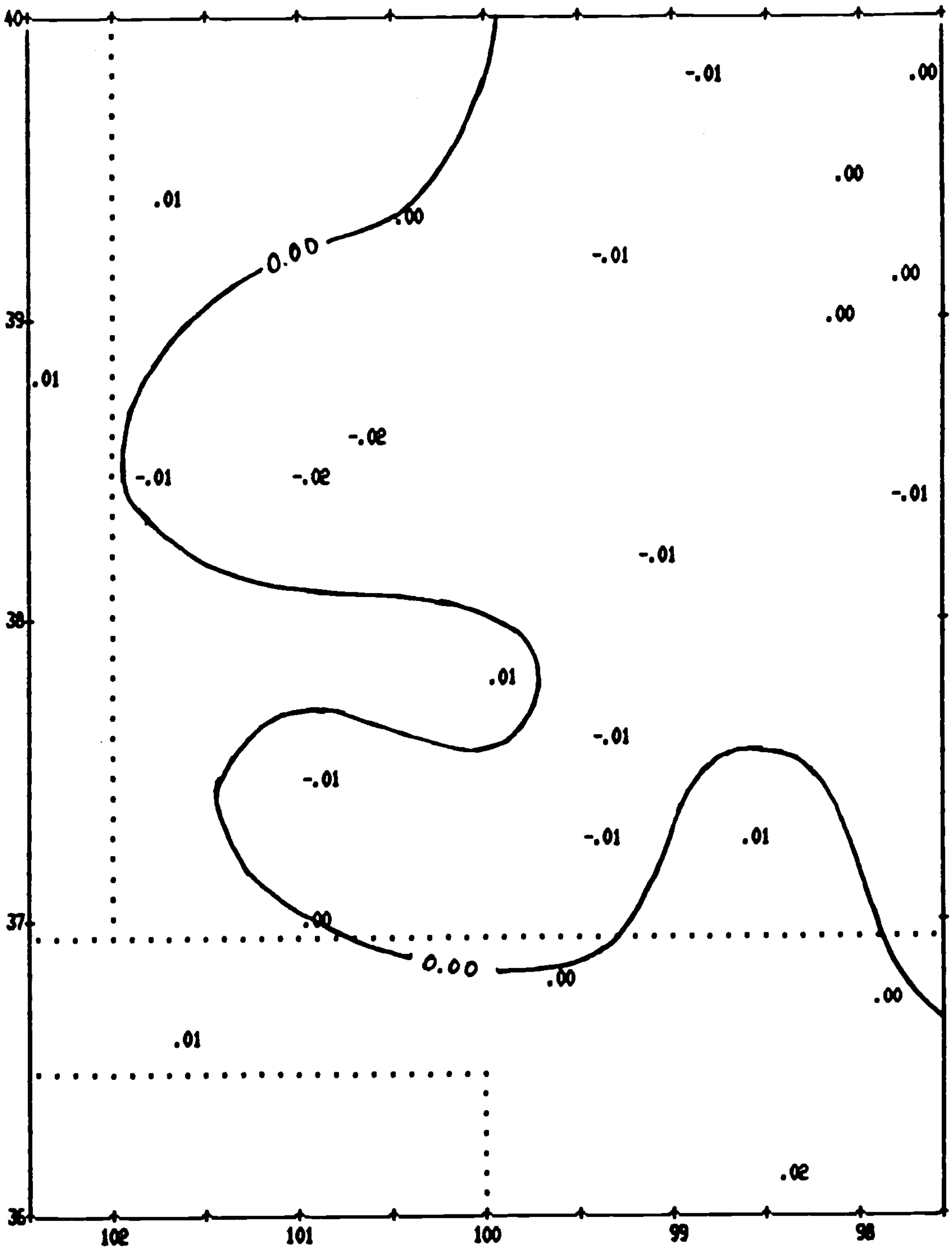


Figure 2c. Spatial distribution of elements of the leading (varimax rotated) vector for January Box 1. Last 24 (precipitation) elements.

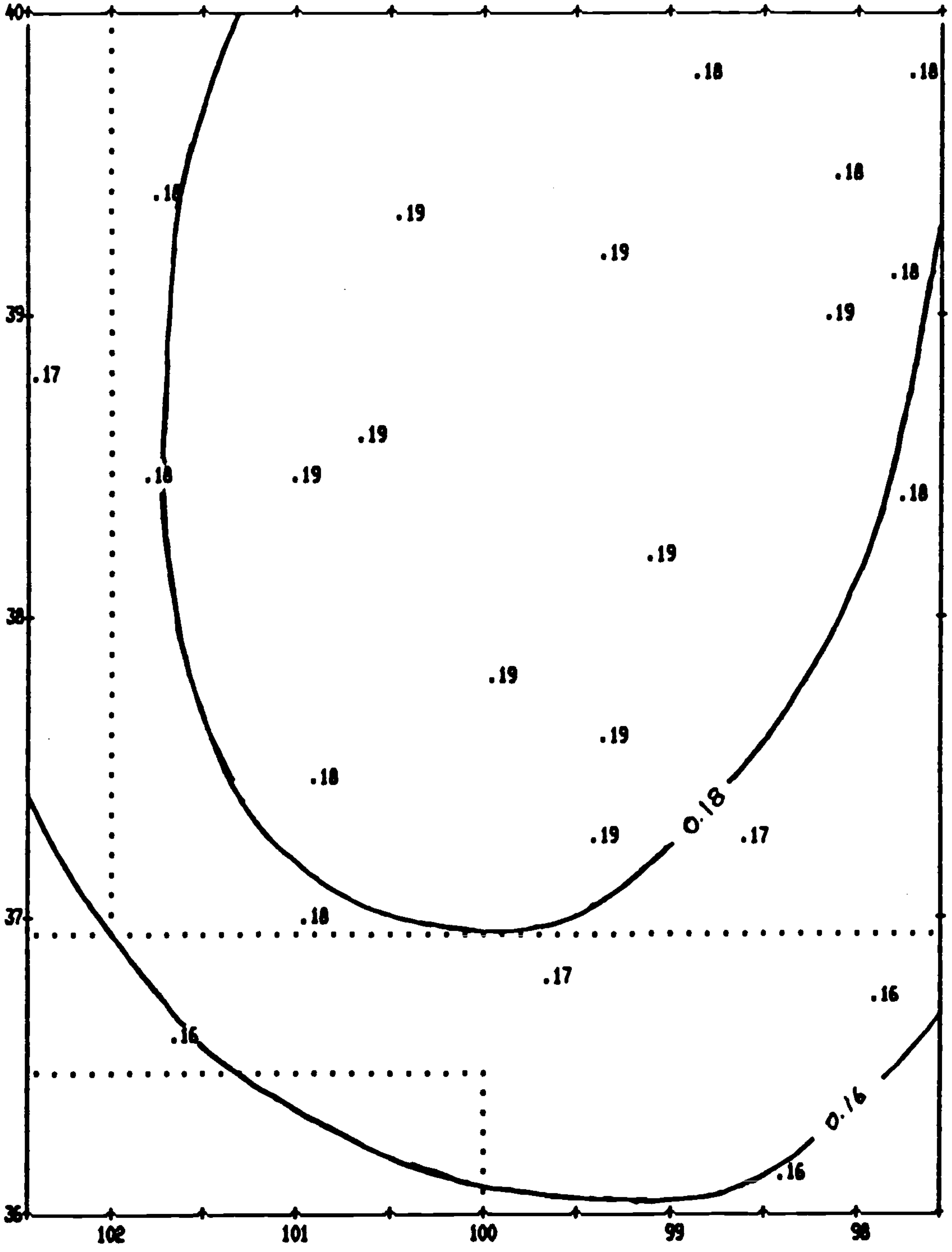


Figure 3a. Spatial distribution of elements of the second (varimax rotated) vector for January Box 1. First 24 (maximum temperature) elements.

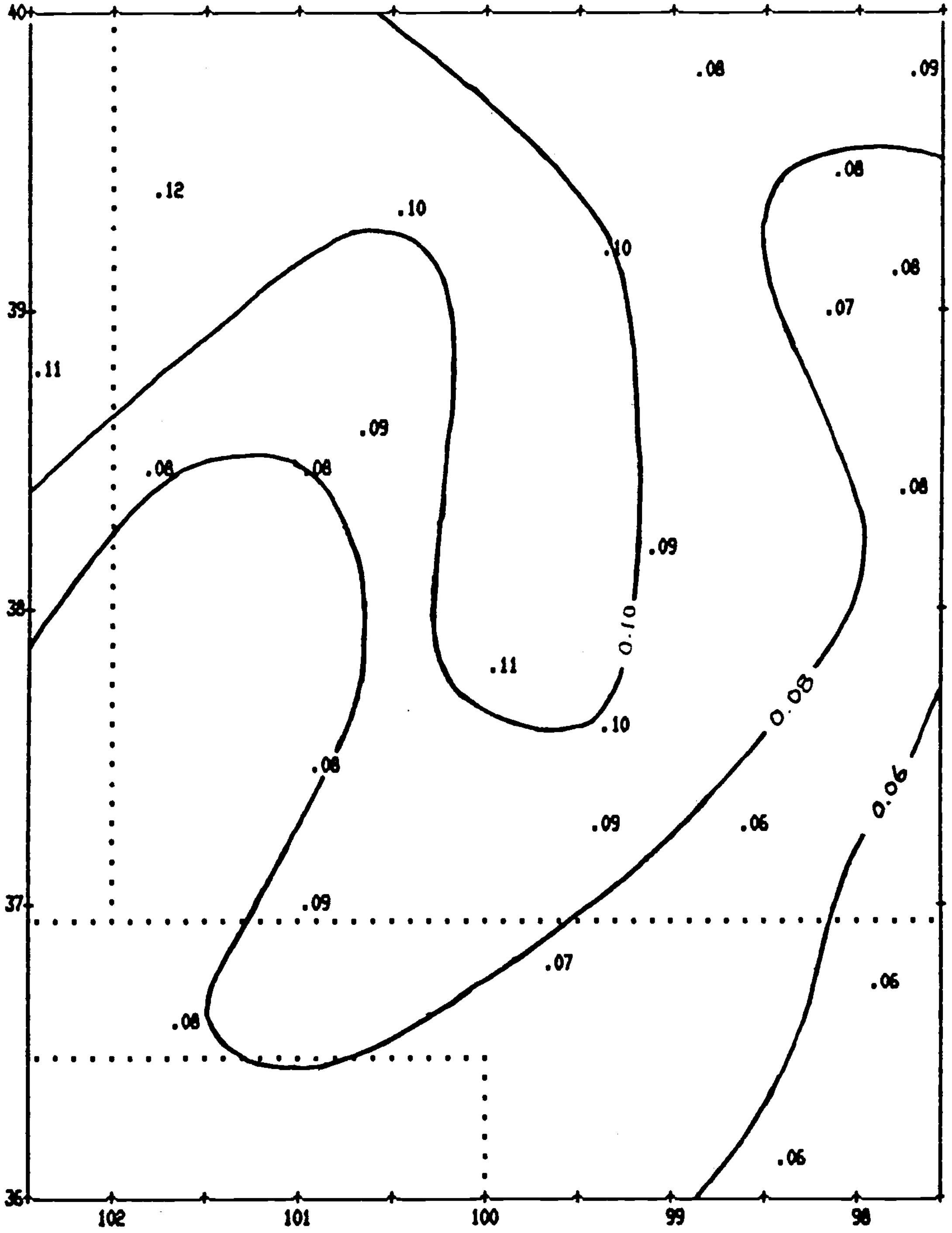


Figure 3b. Spatial distribution of elements of the second (varimax rotated) vector for January Box 1. Second 24 (minimum temperature) elements.

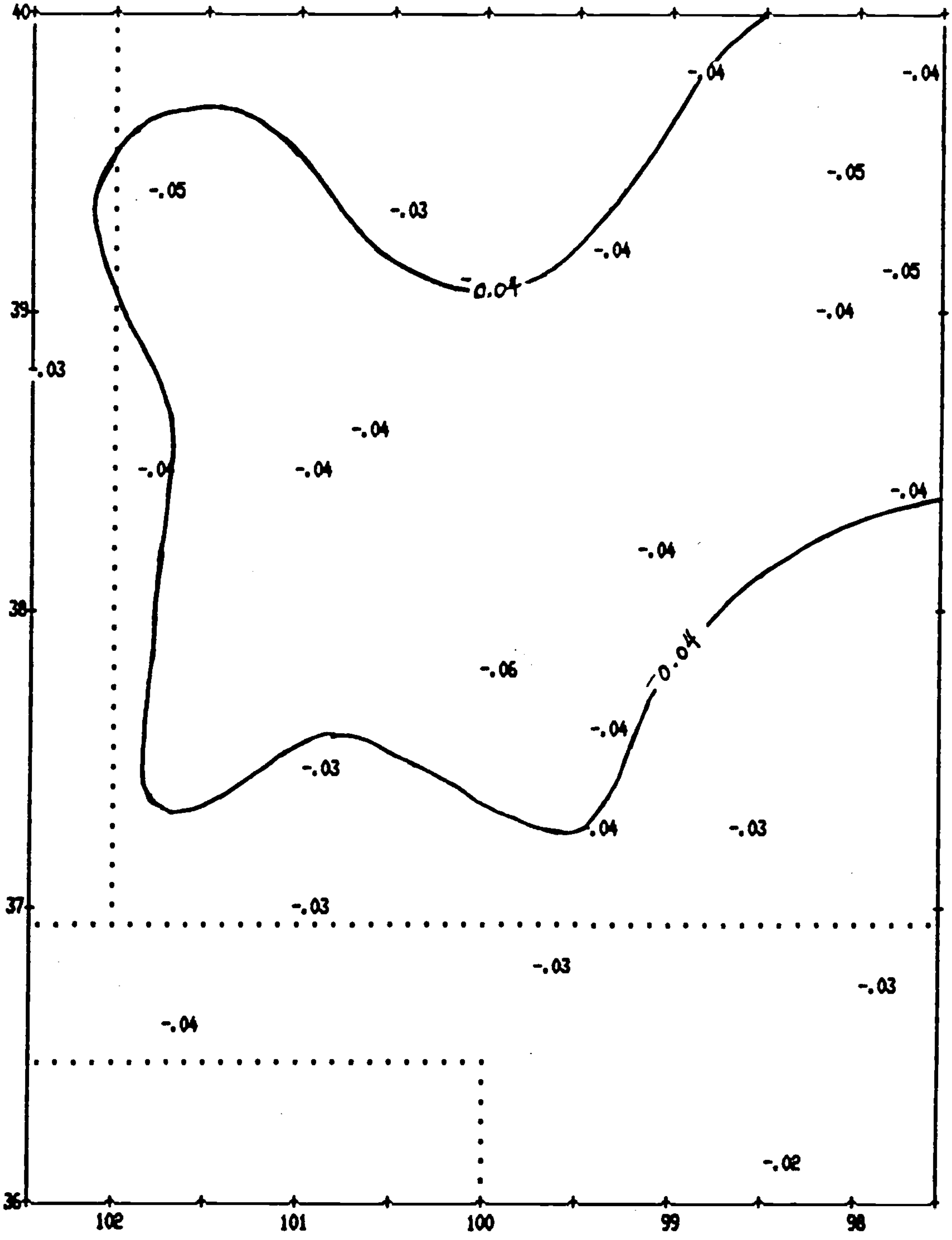


Figure 3c. Spatial distribution of elements of the second (varimax rotated) vector for January Box 1. Last 24 (precipitation) elements.

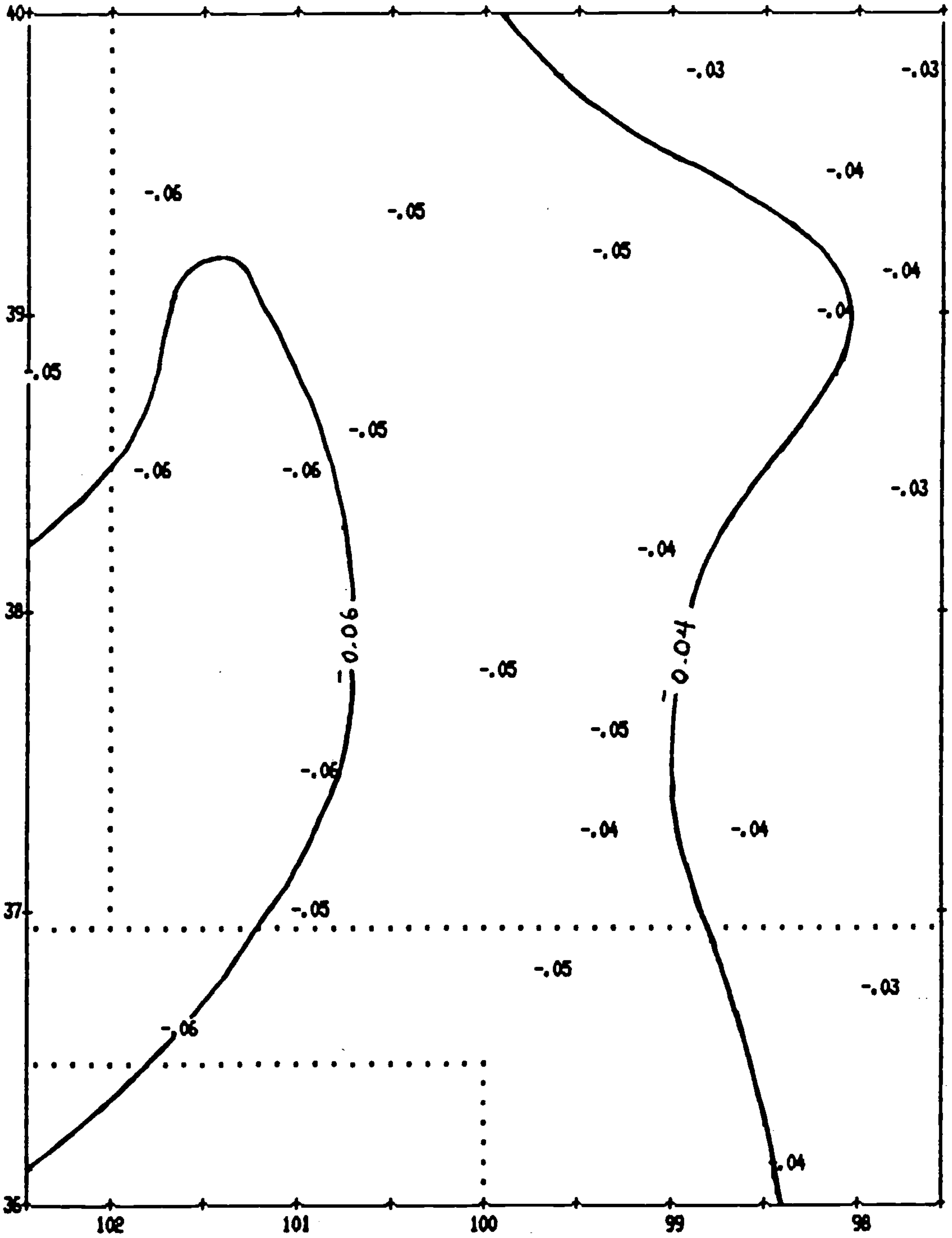


Figure 4a. Spatial distribution of elements of the third (varimax rotated) vector for January Box 1. First 24 (maximum temperature) elements.

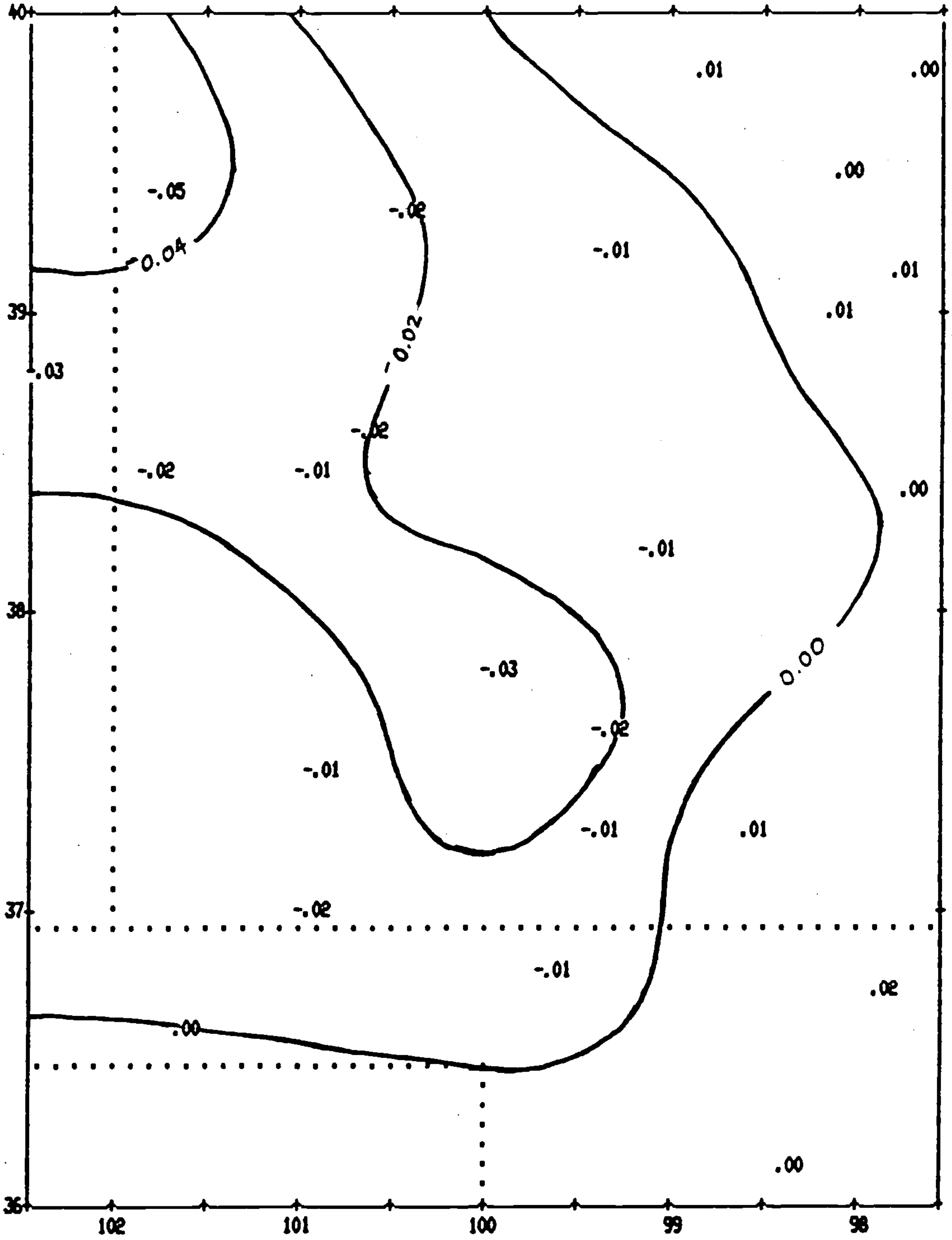


Figure 4b. Spatial distribution of elements of the third (varimax rotated) vector for January Box 1. Second 24 (minimum temperature) elements.

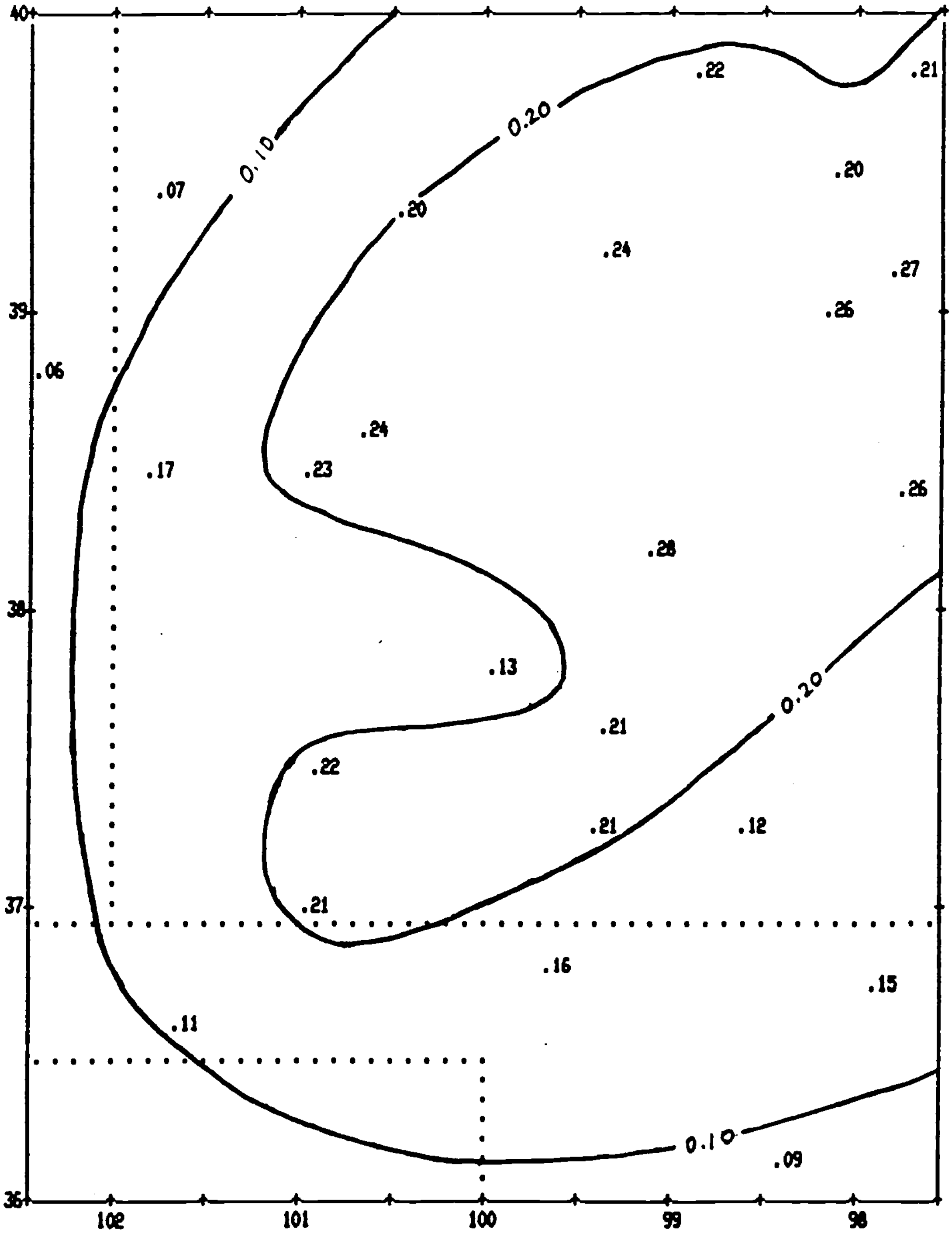


Figure 4c. Spatial distribution of elements of the third (varimax rotated) vector for January Box 1. Last 24 (precipitation) elements.

Figure 3c are consistently negative although small, and reflect a tendency for relatively dry conditions to be associated with higher than average maximum temperatures (and vice versa).

The third January vector, represented in Figure 4, apparently corresponds to relatively coherent synoptic-scale precipitation over much of the domain. Many of the loadings in Figure 4c are roughly equal and of positive sign, and the larger loadings tend to occur in the wetter (eastern) part of the domain. Figures 4a and 4b indicate negative relationships between large-scale January precipitation and temperatures, particularly for the case of maximum temperature.

These results are broadly representative of the cool season for all three gridboxes. For these months (October through March or April) the first two vectors are of approximately equal importance and each describe approximately 25-30% of the variance; one is a maximum temperature vector resembling Figure 3, and the other is a minimum temperature vector resembling Figure 2. In each of these months, the third vector is a precipitation vector resembling Figure 4, which describes approximately 10% to 15% of the variance. Subsequent precipitation modes (for example, 4 through 11, 12 through 17, 26, and 28 through 32 for Box 1 January -- see Table 3) each describe a relatively small portion of the total variation, and can generally be identified with a single station.

An exception to the above pattern occurs for the months of December, January, and February in Box 3. In this case, the primary variations in maximum and minimum temperature are both contained in a single (the first) mode, which accounts for approximately 55% of the total variation. This result may reflect a tendency for temperatures to be decoupled from the diurnal cycle of solar radiation as a result of the influence of snowcover on albedo.

For the warm-season months the temperature analysis is essentially the same as presented above, but no vector representing large-scale precipitation exists (compare Table 3 and Table 4). This result is physically reasonable considering the small-scale nature of warm-season, convective precipitation in this region. Instead, variations in precipitation are described by a series of precipitation modes, a typical example of which (the July vector 6 for Box 1) is shown in Figure 5. Figure 5c shows clearly that this vector primarily describes precipitation variations at and near Buffalo, Oklahoma. This and other single-station precipitation modes represent the positive spatial correlation in rainfall amounts that drops off more or less regularly with distance, and is a familiar feature of observed precipitation data (e.g., Hendrick and Comer, 1970; Zawadzki, 1973). Also represented (in Figures 5a and 5b) are the negative correlations between precipitation at Buffalo and temperatures at moderately large distances from that station. The larger regions of negative temperature loadings centered geographically on areas of high positive precipitation loadings seem to reflect the influence of non- or lightly-precipitating clouds on scales larger than that of the intense convective precipitation. Again, the relationship is strongest with maximum temperature, and inspection of Tables 3 and 4 indicates that this result is common in this data set.

Taken together, the warm-season precipitation vectors for a given month, each describing a small portion of total variance identified with a single station, present a picture such as that shown in Figure

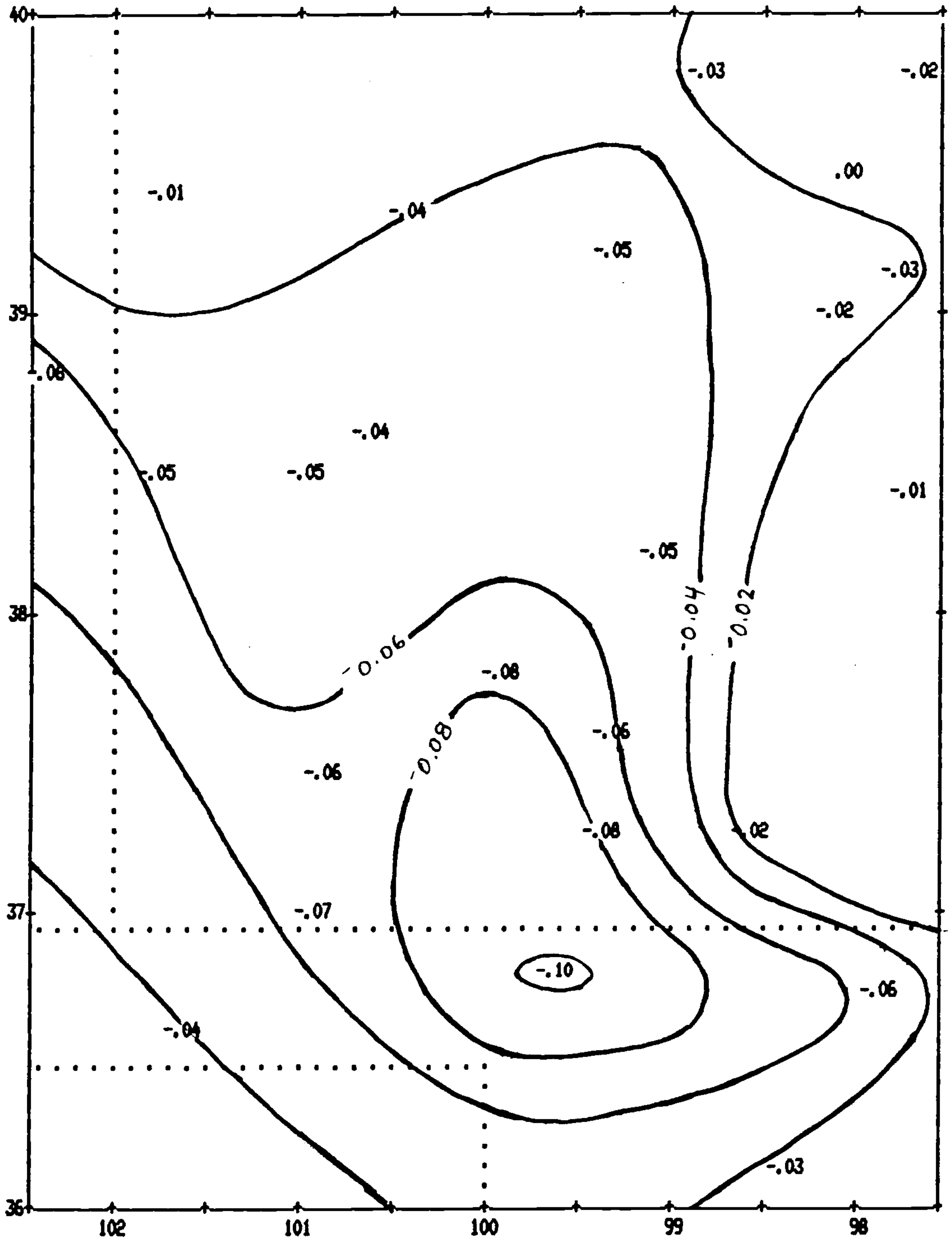


Figure 5a. Spatial distribution of elements of rotated July vector number 6 for January Box 1, representing precipitation variations at Buffalo, Oklahoma. First 24 (maximum temperature) elements).

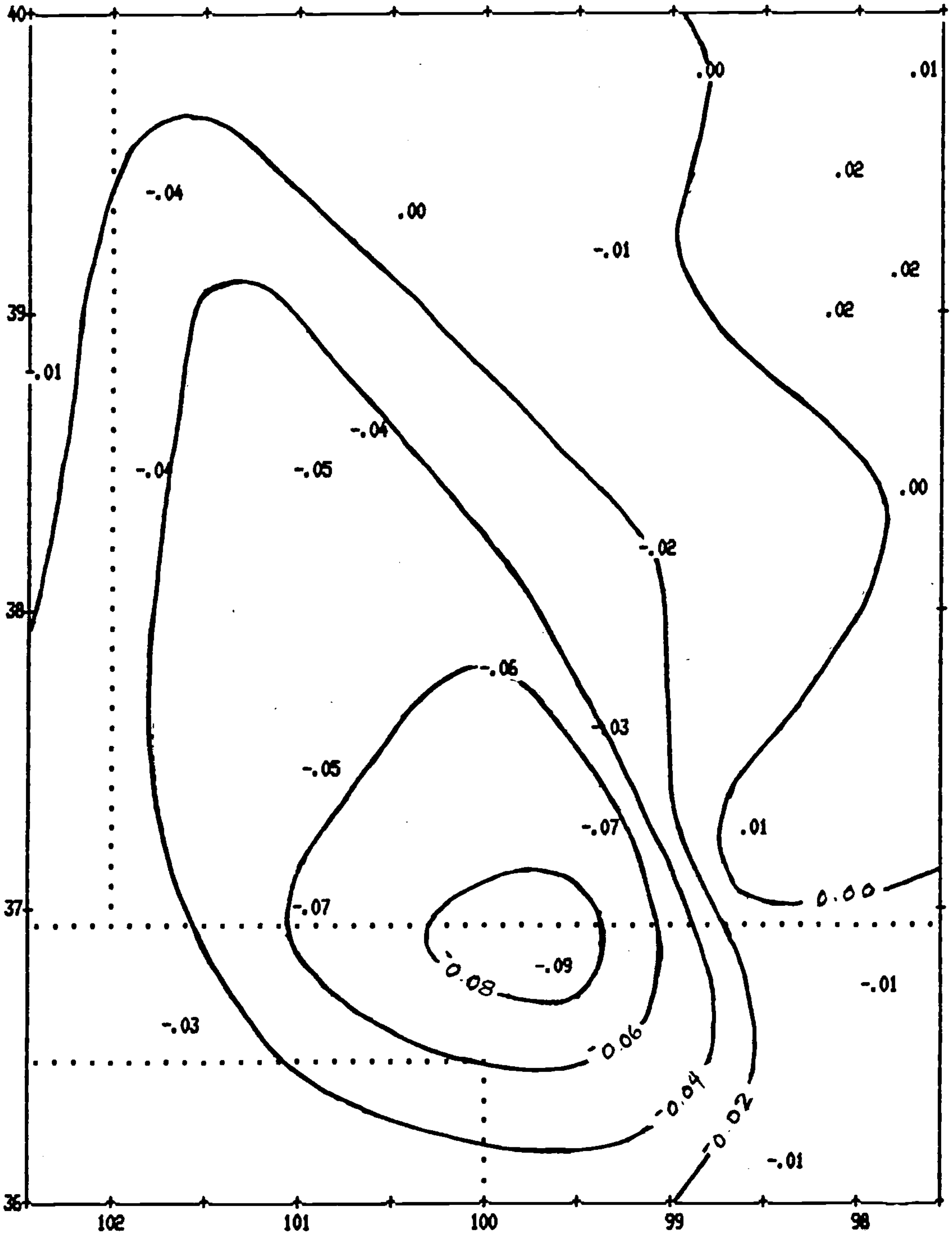


Figure 5b. Spatial distribution of elements of rotated July vector number 6 for January Box 1, representing precipitation variations at Buffalo, Oklahoma. Second 24 (minimum temperature) elements).

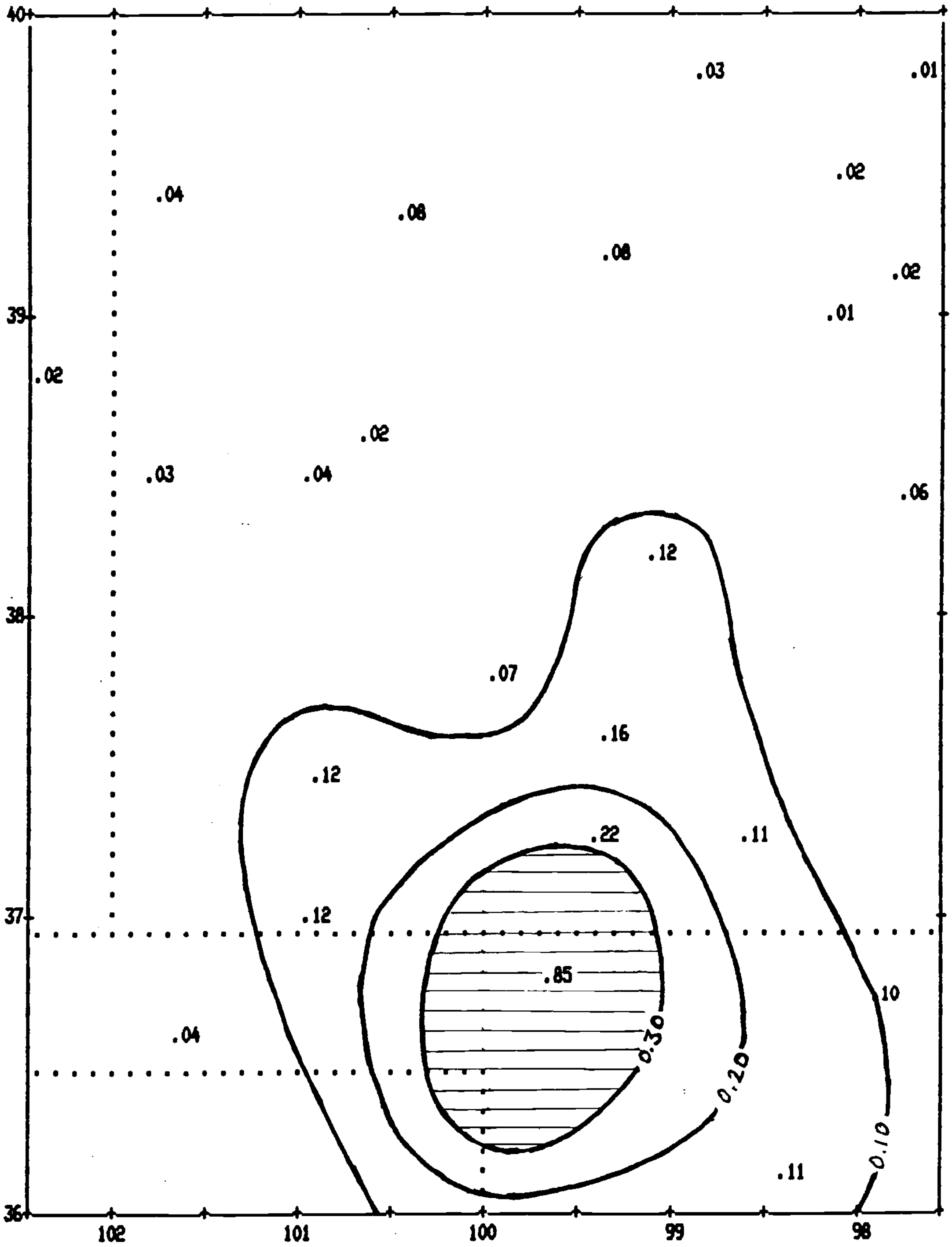


Figure 5c. Spatial distribution of elements of rotated July vector number 6 for January Box 1, representing precipitation variations at Buffalo, Oklahoma. Last 24 (precipitation) elements. Areas over 0.30 are hatched.

6. This figure superimposes the 0.30 contours for all July precipitation modes, again for Box 1. The selection of the 0.30 contour for Figure 6 is a convenience that serves to illustrate the completeness of the representation over the sample of stations available, and the interconnectedness of the precipitation patterns for nearby stations. It portrays a "collective regionalization" of daily precipitation similar to that presented by Richman and Lamb (1985) for 3- to 7-day precipitation totals over a larger domain. This type of partition of the precipitation variance is completely general for the warm season over the gridboxes considered. For all three cases the analyses for June, July, and August exhibit exactly J of these small precipitation modes.

The small cool-season precipitation vectors resemble that shown in Figure 5 as well, and thus may be representing similar physical phenomena. In that context they seem to correspond to precipitation produced by convective elements imbedded in a larger-scale precipitation event (represented by the third, broad-scale precipitation vector), which appear to be general features of extratropical synoptic-scale cyclones (e.g., Houze and Hobbs, 1982).

A demonstration of the utility of the rotation of the initial principal component solution in meteorological pattern representation is provided in Figure 7. This figure shows a typical unrotated July precipitation vector comparable in importance (1.6% of variance) to that shown in Figure 5. The precipitation subspace of this unrotated vector, shown in Figure 7c, includes both large positive and negative loadings, with a pattern not apparently related to any physical mode of precipitation. Moreover, the corresponding temperature portions of

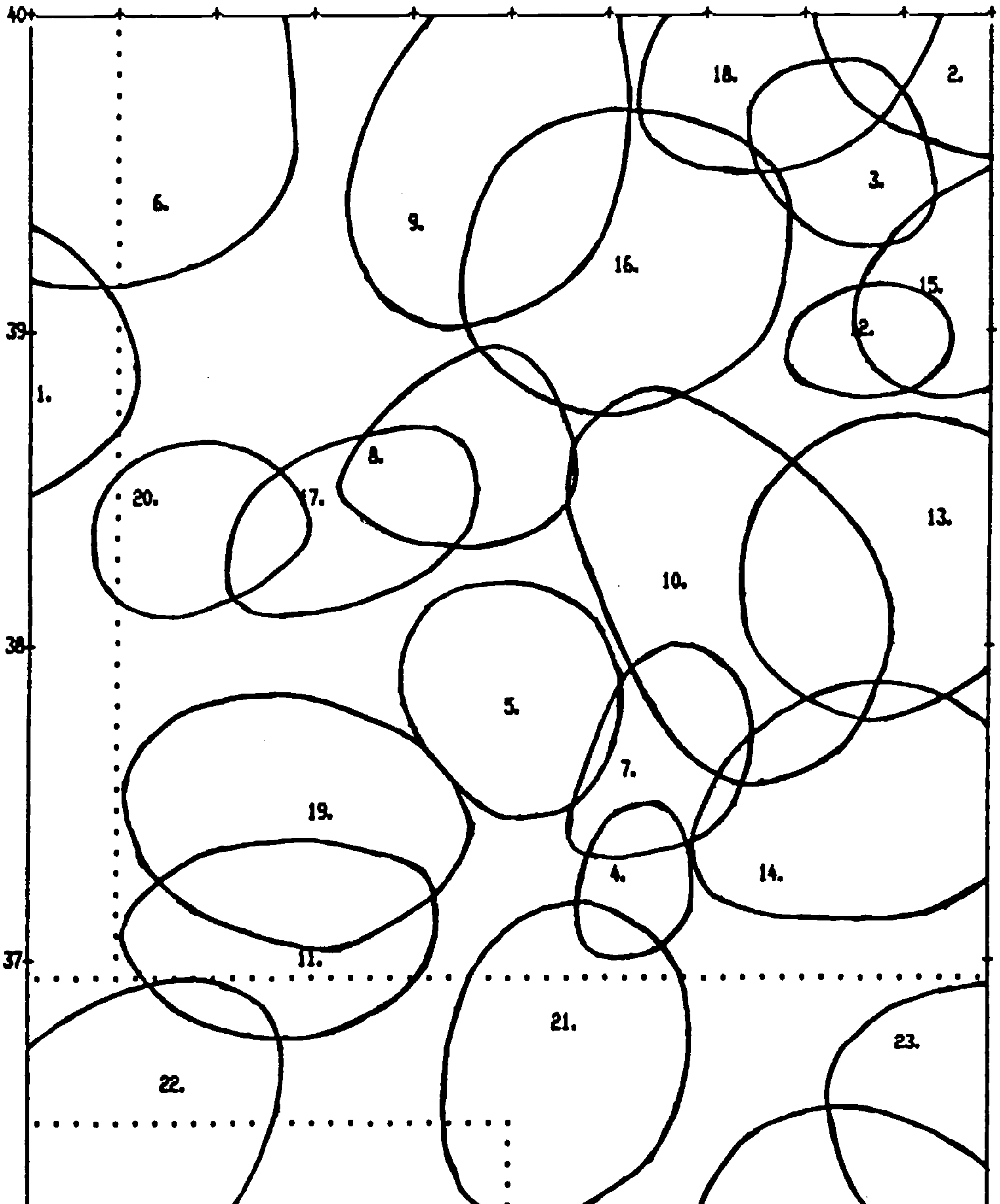


Figure 6. Superposition of the 0.30 loading contours for Box 1 July precipitation vectors.

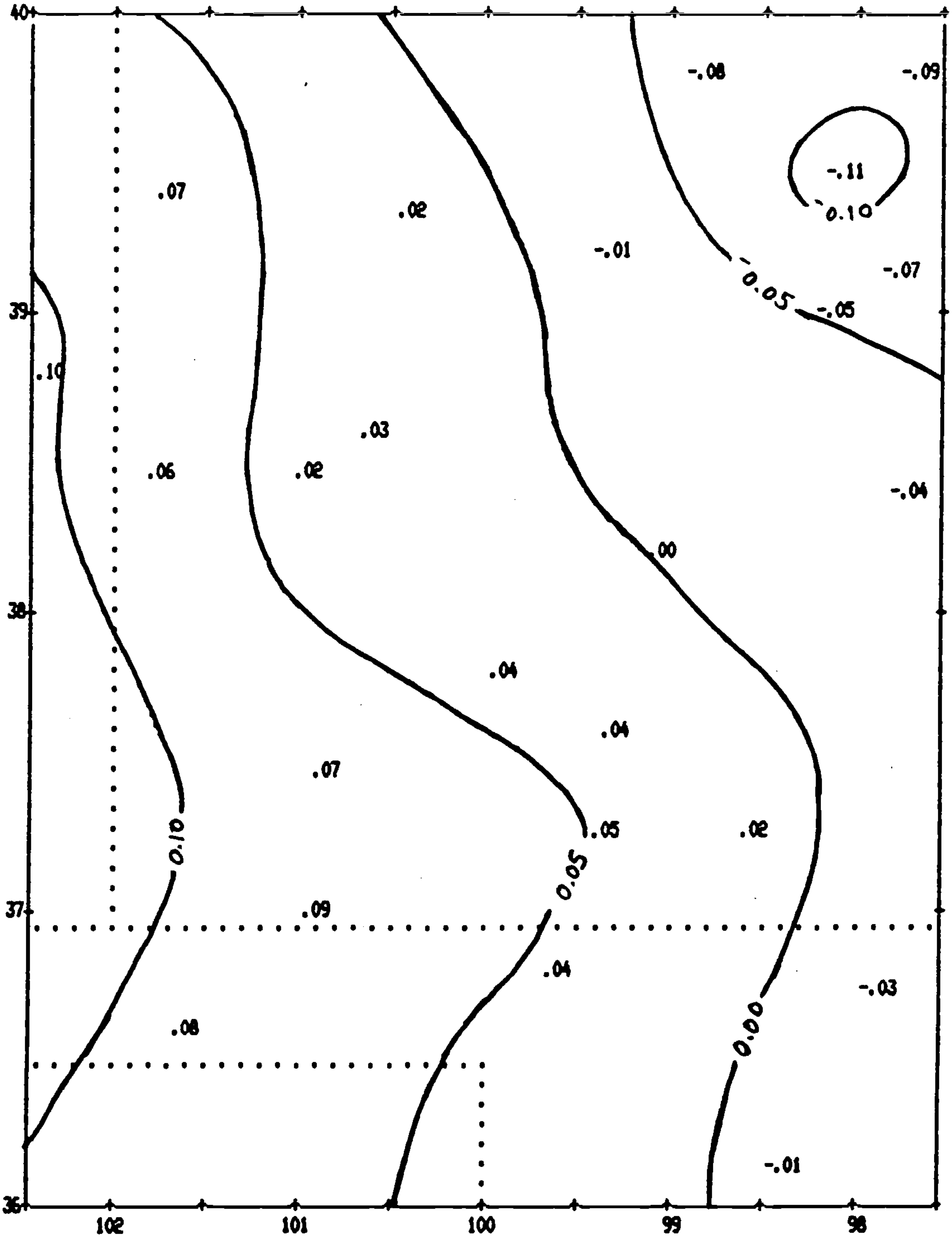


Figure 7a. Spatial distribution of elements of an unrotated July precipitation vector, illustrating difficulties in pattern interpretation. First 24 (maximum temperature) elements.

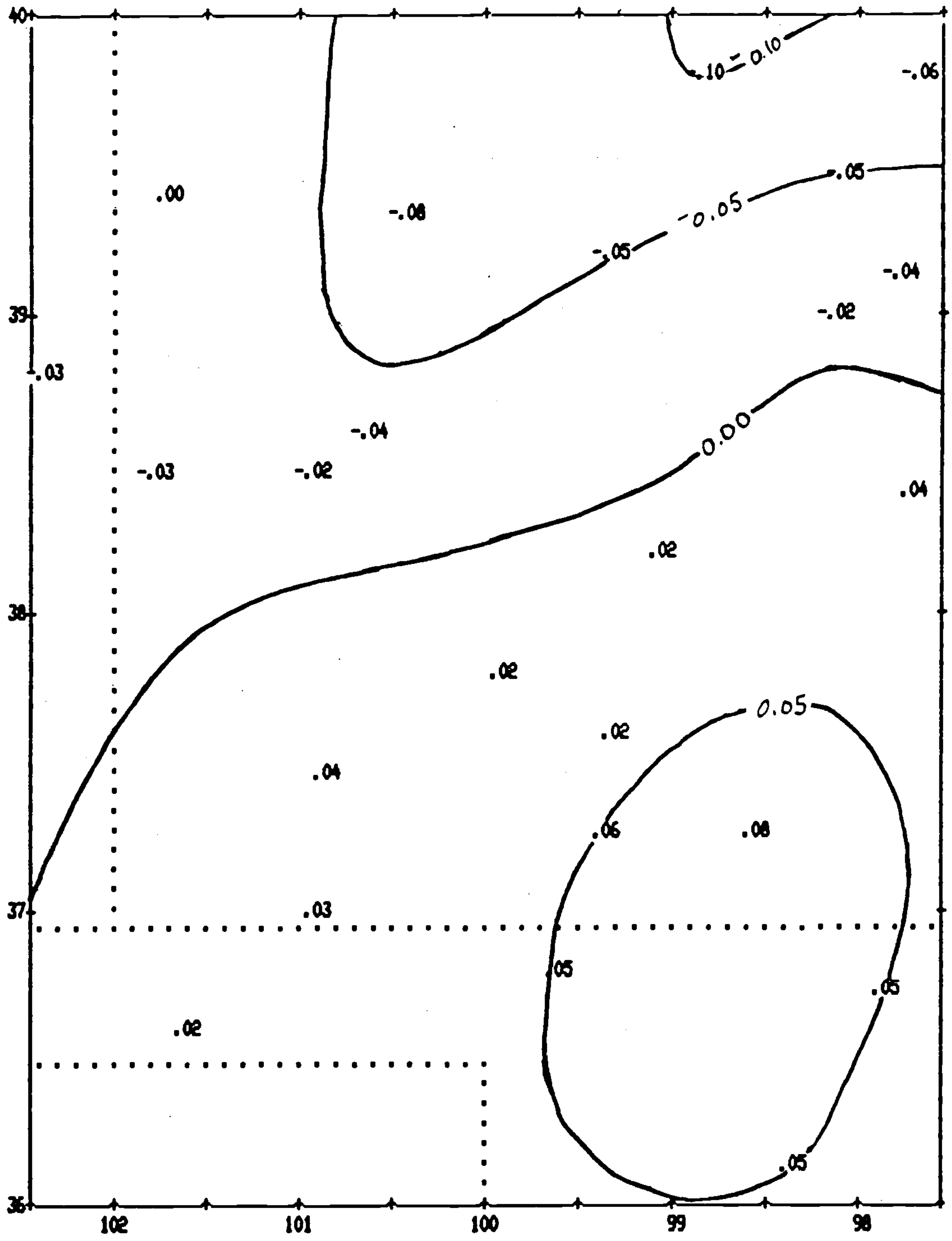


Figure 7b. Spatial distribution of elements of an unrotated July precipitation vector, illustrating difficulties in pattern interpretation. Second 24 (minimum temperature) elements.

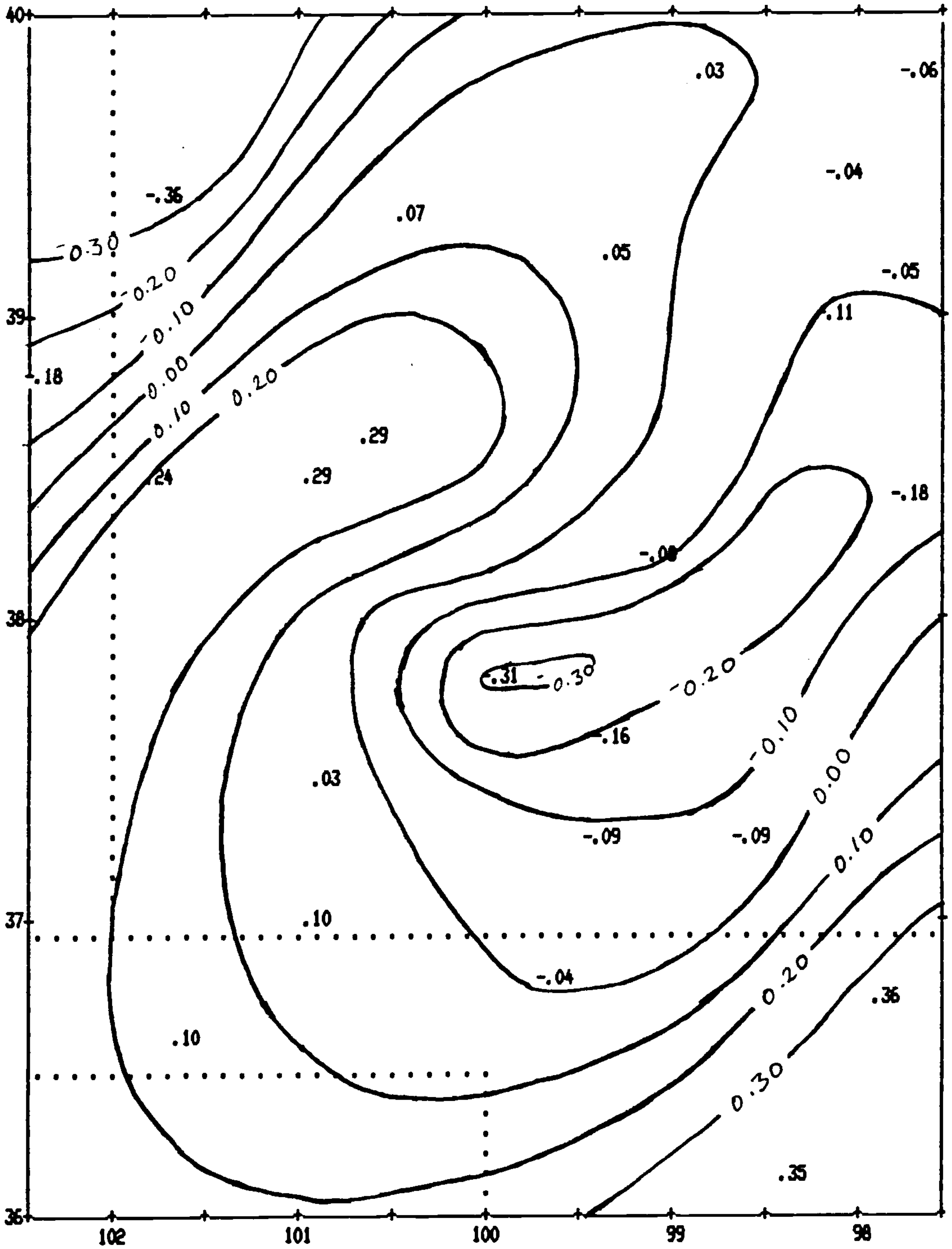


Figure 7c. Spatial distribution of elements of an unrotated July precipitation vector, illustrating difficulties in pattern interpretation. Third 24 (precipitation) elements.

this vector shown in Figures 7a,b appear to be equally arbitrary, and not discernably related to the precipitation pattern portrayed in Figure 7c or to each other.

By contrast, consider the effect of the spatial- and cross-correlations (preserved by the varimax rotation), shown in the panels of Figure 5, on the representation of the corresponding meteorological data. A daily precipitation total of 18.0 mm in July at Buffalo, Oklahoma implies, in the absence of contributions from other precipitation modes, 2.0 mm at the nearest station, Coldwater, Kansas (Station 4, cf. Figure 5c). This precipitation amount at Buffalo also implies an adjustment of −1.0°C to the maximum temperature at Buffalo, and adjustments of between −0.4°C and −0.8°C at the other stations in southwestern Kansas and northwestern Oklahoma (cf. Figure 5a). A similarly large precipitation amount at Medicine Lodge, Kansas (Station 14) would produce (through the corresponding correlation structure portrayed in the precipitation mode for that station) comparable and additive effects on the temperatures at these stations. A contribution to the precipitation at Coldwater would be made as well, but its effect in combination with that from the Buffalo precipitation mode would be more than additive, as a result of the square-root transformation to which the precipitation data have been subjected. The implied precipitation at Buffalo would of course increase as well.

Finally, it is interesting to compare the spatial representation obtained from a rotated principal component analysis derived using the correlation matrix formed in the manner of Kim et al. (1984); that is, using scaled deviations of station data from the box-scale values, rather than from the individual average values for each station. As might have been anticipated, there are no counterparts to the two leading large temperature modes indicated in Tables 3 and 4, and there are correspondingly more small "noise" modes. Since the large leading temperature modes represent broadly coherent temperature variations, these variations are closely paralleled by the grid-scale time series. This source of variance is removed from the data before the correlation matrix is formed, and is automatically reflected in reconstructed data as a consequence of the correct back-transformation.

Other aspects of this alternative formulation resemble those discussed above, although some appreciable differences exist. Convective precipitation is again represented by local modes, but there are fewer than J of these modes for the warm season. Some closely spaced stations share a single mode. Others are not most important in any one mode, but rather are represented as clearly secondary components of several vectors. The manifestation of "simple structure" is less clear in this case, with moderately large negative preciptitation loadings (on the order of -0.10 to -0.15) appearing for some stations in precipitation modes (compare Figure 5c). Also, the intercorrelation between precipitation and the temperature variables in the precipitation modes seems less physically plausible. Although moderately large negative temperature loadings occur at stations for which the precipiation loading is highest, those for the nearest stations are sometimes small or even positive. These differences may result from the inability of the Kim et al. (1984) formulation to distinguish, for example, cases for which all stations within a box are dry from cases for which precipitation at a particular station is near the box-averaged value.

### 2.3.2. Time-dependent structure

In the present setting the mathematical model for the data in terms of the rotated eigenvectors may be written in matrix form as

$$\underset{\sim}{z}(t) = \underset{\sim}{E}\ \underset{\sim}{a}(t), \tag{2.6}$$

where $\underset{\sim}{E}$ is a matrix whose columns are the rotated eigenvectors, and $\underset{\sim}{a}(t)$ is the time-dependent vector of "scores" or "amplitudes." In the present work this latter term is adopted for the $\underset{\sim}{a}$ vector (cf. Kim _et al_., 1984; Richman, 1986), which arises from the analogy between the matrix $\underset{\sim}{E}$ and a basis set such as the Fourier harmonics. The vector $\underset{\sim}{z}(t)$ is defined as in (2.2) for each day t. The 2% of total variance contained in the unrotated vectors has therefore been assumed to be of negligible importance.

Various approaches to calculating the amplitudes have been advanced (e.g., Harris, 1967; McDonald and Burr, 1967), and most of these methods were found to yield essentially identical results for the present data set. The amplitudes here are calculated directly, according to

$$\underset{\sim}{a}(t) = [\ \underset{\sim}{E}'\ \underset{\sim}{E}\ ]^{-1}\ \underset{\sim}{E}'\ \underset{\sim}{z}(t) \quad , \tag{2.7}$$

which is obtained by elementary manipulation of (2.6) (Kaiser, 1962).

## 2.4 Climate Inverse Procedures

### 2.4.1. Regression specification of local data from box-scale information

Following Kim et al. (1984), regression equations were developed that related the box-scale values of temperature and precipitation to the amplitudes (as predictands) calculated according to (2.7). Note that this procedure is the reverse of the usual principal component regression, where the aim is to produce a set of orthogonal predictor variables (Draper and Smith, 1981). The relationships were fit only to amplitudes calculated from the 27-year training sample. Morning-observed precipitation, and all estimated values were accepted in this calculation, as a complete data set is required. Potential predictors were deviations of box-scale maximum and minimum temperatures from an annual cycle (calculated in the same way as for station data in Section 2), the box-scale precipitation, and its square root. Other predictors, such as a dummy variable for precipitation occurrence, and the values for box-scale variables on previous days were found not to be useful in exploratory analyses, and are therefore not included.

The regression coefficients for the first four Box 1 January and July amplitudes, and the respective $r^2$ values are listed in Table 5. In both cases, amplitudes of the leading two temperature modes are very well predicted by box-scale information, particularly for January. This result should not be surprising in view of the high degree of coherence exhibited by maximum and minimum temperatures in

Table 5. Regression coefficients, $r^2$, and partition of variance described, for prediction of first four amplitudes from box-scale values for Box 1, January and July.

| | Coefficient for: | | | | | $r^2$ | $3r^2_k \lambda_{j*} \Sigma e^2_{jk}$ | | |
|---|---|---|---|---|---|---|---|---|---|
| | Const. | Max T. | Min T. | $\sqrt{Ppt}$ | Ppt | | max | min | ppt |
| January: | | | | | | | | | |
| $a_1$ | .091 | -.435 | 1.228 | -- | -.324 | .977 | .204 | .693 | .002 |
| $a_2$ | -.561 | .971 | -.679 | 1.471 | .426 | .974 | .612 | .141 | .028 |
| $a_3$ | -1.200 | .117 | -.087 | 2.782 | 1.235 | .698 | .016 | .002 | .287 |
| $a_4$ | -.281 | -- | -- | .311 | -- | .020 | .000 | .000 | .001 |
| | | | | | | Totals | .832 | .836 | .318 |
| July: | | | | | | | | | |
| $a_1$ | -.730 | 1.715 | -1.191 | -- | .224 | .880 | .480 | .093 | .048 |
| $a_2$ | .040 | -.656 | 2.287 | -- | -- | .900 | .118 | .493 | .002 |
| $a_3$ | -.053 | .112 | -- | -- | -- | .056 | .005 | .001 | .000 |
| $a_4$ | -.224 | -- | -- | .179 | -- | .032 | .000 | .000 | .002 |
| | | | | | | Totals | .603 | .587 | .052 |

the study area (cf. Figures 2b and 3a). Variations in broad-scale winter precipitation are moderately well predicted (e.g., $r^2$ = .698 for Box 1 January mode 3). However, the smaller-scale precipitation modes, typified in Table 5 by $a_4$ for both January and July, appear to be essentially unpredictable from only box-scale information. For the summer months, in which all precipitation variations are represented by these small-scale precipitation modes (cf. Table 4), knowledge of the weighted-average box-scale values gives essentially no information as to where within the domain or with what intensity the contributing precipitation may have fallen. This result is of course not unexpected considering the nature of warm-season precipitation.

A partition of variance described by the combination of the rotated principal component representation of the data and the specification of the amplitudes by the regression equations may be calculated. The proportion of variance described by a particular principal component which is contributed by each loading is given (for vectors of unit length) by the square of that loading (e.g., Harman, 1967). The proportion of variance (over all stations), for maximum temperature, minimum temperature, and precipitation separately, described by the combined analysis for the kth mode, is thus given by

$$s_{j^*k} = 3r^2 \lambda_k \sum_{j^*} e^2_{jk} . \qquad (2.8)$$

Here $r^2$ is the proportion of variance described by the regression equation, $\lambda_k$ is the proportion of total variance described by the kth rotated principal component, the $e_{jk}$ are elements of the matrix $\underset{\sim}{E}$ defined above, and the summation over $j^*$ denotes either the maximum temperature, minimum temperature, or precipitation subspace. The factor 3 enters since basing the principal component analysis on the correlation matrix $\underset{\sim}{R}$ weights all combinations of stations and variables equally, and the summations in (2.8) are over one-third of the vector elements.

Table 5 also gives values of $s_{j \cdot k}$ for the first 4 Box 1 modes for January and July. Approximately 80% of the variations in the training sample of January temperatures and 60% of the variations in July temperatures are captured by the combined specification procedure. Almost all of this specification is attributable to the first two modes in each case. The procedure also describes approximately 30% of the variations in January precipitation, which is derived almost entirely from the single broad-scale precipitation component $a_3$, and essentially none of the variations in July precipitation. These results are typical for cool- and warm-season months in all three gridboxes considered.

Regression specification of the local-scale variables from the box-scale data proceeds in the following manner. First, amplitudes that exhibit predictability using regression coefficients such as those presented in Table 5 are specified. Expected (i.e., average) values, which are zero in all cases, are assumed for the remaining amplitudes. Scaled deviations for the meteorological variables are then calculated according to (2.6), which are back-transformed by the inverses of (2.2) and (2.3). The precipitation is then squared to recover the dimensional values (taking care that imaginary precipitation values are first set to zero). Precipitation amounts less than 0.1 mm are truncated to zero, and nonzero values are proportionally scaled such that their weighted average (with weights defined from Table 1) equals the box-scale value. Note that this procedure specifies all station precipitation amounts must be zero if the box-scale value is zero. Examination of the original data indicates that this relationship is not strictly true, but that exceptions are nearly always trace amounts, and can of course never be substantial.

Results of this process for the 27-year training sample and the 9-year independent sample are presented in Tables 6 and 7, again for the case of Box 1 data which is representative. Table 6 shows the average over the 24 stations of mean squared errors for maximum temperature, minimum temperature, and precipitation amount specifications made according to climatology [i.e., (2.4a) and (2.4b)], the procedure described above, and a "simple inverse" procedure. The regression procedure was carried out using the four equations specified by the parameters presented in Table 5, and verifications were made only with nonmissing data and PM-observed precipitation. The simple inverse procedure specifies temperatures by adding the unscaled box-scale maximum and minimum temperature deviations from their respective means for that date to each of the respective station mean values. It specifies precipitation by assuming that it is uniform over the entire study area; that is, it assumes that all station values are equal to the box-scale value. Note that the performance of the "simple inverse" procedure is very similar to that of the rotated principal component representation derived from the Kim et al. (1984) formulation for the correlation matrix. This result occurs because the amplitudes for the vectors of

Table 6. Empirical verification statistics (MSE and skill score with respect to climatology) for specification of temperature and precipitation amount by means of climatolological values, a simple inverse procedure, and the regression procedure for Box 1 January and July. Tabulated separately for the 27-year training samples and the 9-year independent samples.

| | Training Sample | | | Independent Sample | | |
|---|---|---|---|---|---|---|
| | max | min | ppt | max | min | ppt |
| January: | | | | | | |
| MSE | | | | | | |
| Climatology | 61.7 | 36.1 | 3.8 | 70.2 | 45.0 | 3.4 |
| Simple inverse | 8.5 | 5.5 | .1 | 9.4 | 6.1 | 2.0 |
| Regression procedure | 8.2 | 5.1 | 2.5 | 9.1 | 5.8 | 2.3 |
| Skill score (%) | | | | | | |
| Simple inverse | 86.3 | 84.8 | 43.2 | 86.6 | 86.4 | 43.0 |
| Regression procedure | 86.6 | 85.8 | 34.0 | 87.1 | 87.0 | 33.0 |
| July: | | | | | | |
| MSE | | | | | | |
| Climatology | 16.5 | 8.1 | 67.7 | 17.4 | 8.6 | 74.9 |
| Simple inverse | 4.3 | 2.6 | 52.7 | 3.4 | 2.5 | 57.0 |
| Regression procedure | 4.6 | 2.6 | 54.0 | 3.6 | 2.4 | 60.6 |
| Skill score (%) | | | | | | |
| Simple inverse | 74.0 | 67.2 | 22.2 | 80.5 | 71.3 | 23.9 |
| Regression procedure | 72.4 | 68.4 | 20.2 | 79.1 | 72.2 | 19.1 |

Table 7. Average over the 24 stations for Box 1 January and July, of verification tables and threat scores for precipitation specified by the regression procedure. Tabulated separately for the 27-year training sample and the 9-year independent sample.

**January:**

| | Training Sample: Forecast Y | Training Sample: Forecast N | Independent Sample: Forecast Y | Independent Sample: Forecast N |
|---|---|---|---|---|
| Obs Y | 88 | 58 | 40 | 26 |
| Obs N | 55 | 602 | 23 | 182 |

| | Training Sample | Independent Sample |
|---|---|---|
| Threat Score: | .434 | .436 |
| Fale Alarm Rate: | .385 | .365 |

**July:**

| | Training Sample: Forecast Y | Training Sample: Forecast N | Independent Sample: Forecast Y | Independent Sample: Forecast N |
|---|---|---|---|---|
| Obs Y | 222 | 8 | 73 | 29 |
| Obs N | 496 | 79 | 157 | 40 |

| | Training Sample | Independent Sample |
|---|---|---|
| Threat Score: | .304 | .309 |
| False Alarm Rate: | .691 | .683 |

the latter representation exhibit essentially no predictability on the basis of the large-scale data, so that grid-scale variations are transferred directly to the stations.

It is evident that there is no appreciable degradation of the specifications from the training sample to the independent sample. Temperature specifications appear to be reasonably good, with skill scores ranging from 67% to 87%. Average root-mean-squared errors for temperature specifications range from approximately 1.5°C for July minima to 3.0°C for January maxima. The simple inverse scheme performs essentially as well as the regression procedure for temperature, which is probably a consequence of the relatively homogeneous physiography of the study area. Either approach appears to be a suitable basis for temperature specifications in the present study area. The simple scheme would be expected to perform less well in more complex terrain, a supposition that could be tested by extending the analysis to other areas.

In contrast, the precipitation specifications of both schemes appear to be entirely unsatisfactory for the deterministic generation of acceptably realistic (from the standpoint of crop simulation) synthetic station weather data using large-scale information. This conclusion is reinforced by the data in Table 7, which presents verification tables and threat scores for precipitation occurrence specified by the regression procedure, averaged over the 24 stations. Again, no appreciable degradation is evident in the independent sample. However, particularly for July, the false alarm rate (specification of precipitation when none is observed) is extremely high. Evidently, widespread light precipitation is being specified.

Increasing the threshold of "trace" from 0.1 mm does not appreciably improve this situation.

### 2.4.2. Stochastic generation of station weather data consistent with box-scale values

The spatial distribution of convective precipitation (presuming now that such preciptation is represented by the small, single-station precipitation modes in both the cool and warm seasons) within the domain is evidently not predictable from the box-scale data with satisfactory accuracy. It is natural, then, to model the particular locations and intensities of the convective precipitation conditional on the box-scale average as random phenomena. In formulating a climate inverse procedure in this setting, the objective is to stochastically generate time series of 3J-dimensional weather vectors which represent the 3 surface weather elements and J stations under consideration. Of course, such a procedure must produce data that are both consistent with the (specified) box-scale weather data, and that exhibit acceptable resemblance to the observed data in terms of statistical characteristics such as mean, variance, distributional form, and autocorrelation structure in time and space. Successful development of such a procedure would represent a practical solution to this portion of the climate inverse problem from the standpoint of impact assessment using, for example, crop simulation models. The utility of this solution relates to the fact that a longer record than could be economically generated directly by GCM runs or would be available from observational data is likely to be desired for this purpose.

It is in this context that the utility of employing the varimax rotation, rather than an oblique rotation which might better represent the spatial variations in the data (Richman, 1986), becomes apparent. The advantage of the former arises because the amplitudes are temporally orthogonal, which greatly simplifies the task of simulating them in a stochastic sense. In addition, the amplitudes of these small-scale precipitation modes exhibit a very small degree of serial correlation.

The data generation then proceeds in the following manner. Only amplitudes for the most important modes are simulated. This truncation is determined by including enough modes so that at least 75% of the variance for each of the combinations of stations and variables is included. That is, truncation K is chosen such that

$$3J \sum_{k=1}^{K} \lambda_k e_{jk}^2 \geq 0.75 \,, \qquad \text{for all } j = 1, 3J \,, \tag{2.9}$$

where all symbols are as defined above. Again, the factor 3J enters as a result of the equal weighting of all 3J combinations of variables and stations. The truncations K for Box 1 January and July are indicated in Tables 3 and 4, respectively.

Given the box-scale values for the variables of interest, values for the first two (or three in the cool-season months) amplitudes are calculated using regression coefficients such as those presented in Table 5. A Gaussian noise term is then added to simulate variation about the mean level predicted by the least-squares regression. That is,

$$a_k = \beta_0 + \beta_1 T_{max} + \beta_2 T_{min} + \beta_3 \sqrt{P_L} + \beta_4 P_L + \epsilon_k , \qquad (2.10)$$

where the $\beta$'s are the regression coefficients, $T_{max}$ and $T_{min}$ are the deviations of the box-scale temperatures from their respective means for that date, and $P_L$ is the large-scale precipitation value for the date. The independent Gaussian noise $\epsilon_k$ has zero mean and variance equal to the mean-squared error of the regression.

Unlike the amplitudes for the small precipitation modes, those for the small temperature modes exhibit moderate positive serial correlation. For a majority of these modes, this serial correlation is adequately modeled by first-order autoregressive models, as judged by examination of the Bayesian Information Criterion (BIC) statistic (Katz, 1982; Schwartz, 1978). For simplicity, all of the small (i.e. not explicitly predictable) temperature-mode amplitude series are modeled as first-order autoregressions with parameter (i.e., lag-one autocorrelation) of 0.3, and (Gaussian) white-noise variance consistent with this choice of parameter and with the proportion of total variance accounted for by each mode.

Preliminary amplitudes for the small-scale precipitation modes are drawn randomly from their respective empirical distributions; that is, from the collection of amplitudes for that mode calculated from the data. Since all stations are assumed dry on days for which $P_L$, the box-scale precipitation, is zero, these empirical distributions include only box-scale wet days. Also, amplitudes are included in the empirical distributions only if observed precipitation for stations that are "dominant" in a given mode are nonmissing and not morning-observed. Dominant stations are defined to have precipitation loadings of at least 0.15 in magnitude. The empirical precipitation-mode amplitude distributions are calculated from data taken from the full 36-year record.

A histogram for a typical empirical amplitude distribution, that corresponding to the vector shown in Figure 5, is included in Figure 8. It is evident that the distribution is highly skewed, and that its representation by a member of one of the usual families of parametric probability distributions would lead to serious distortions of its character. In particular, extreme positive values, corresponding to the largest precipitation amounts, would be difficult to portray accurately in a parametric setting.

The most serious difficulty with stochastic generation of station precipitation data according to the above procedure is that the results derived from the initial sampling just described will in general not lead to a weighted-average box-scale precipitation value equal to $P_L$. This difficulty is circumvented using the following procedure. First, the approximation

$$\tilde{\sqrt{\underset{\sim}{p}}} \approx \underset{\sim}{E}^{*} \underset{\sim}{a}^{*} , \tag{2.11}$$

corresponding to (2.6), is employed, where $\underset{\sim}{E}^{*}$ is the matrix whose columns (of dimension J) are comprised of the precipitation elements of the precipitation vectors only, and $a^{*}$ is the vector of precipitation mode amplitudes. Initial dimensional values of precipitation values at station j, $p_j$, are calculated in a manner similar to that in Section 2.4a, using (2.11) and the inverses of (2.2) and (2.3). Values less than 0.33 mm are set equal to zero.

A scaling factor F is defined as

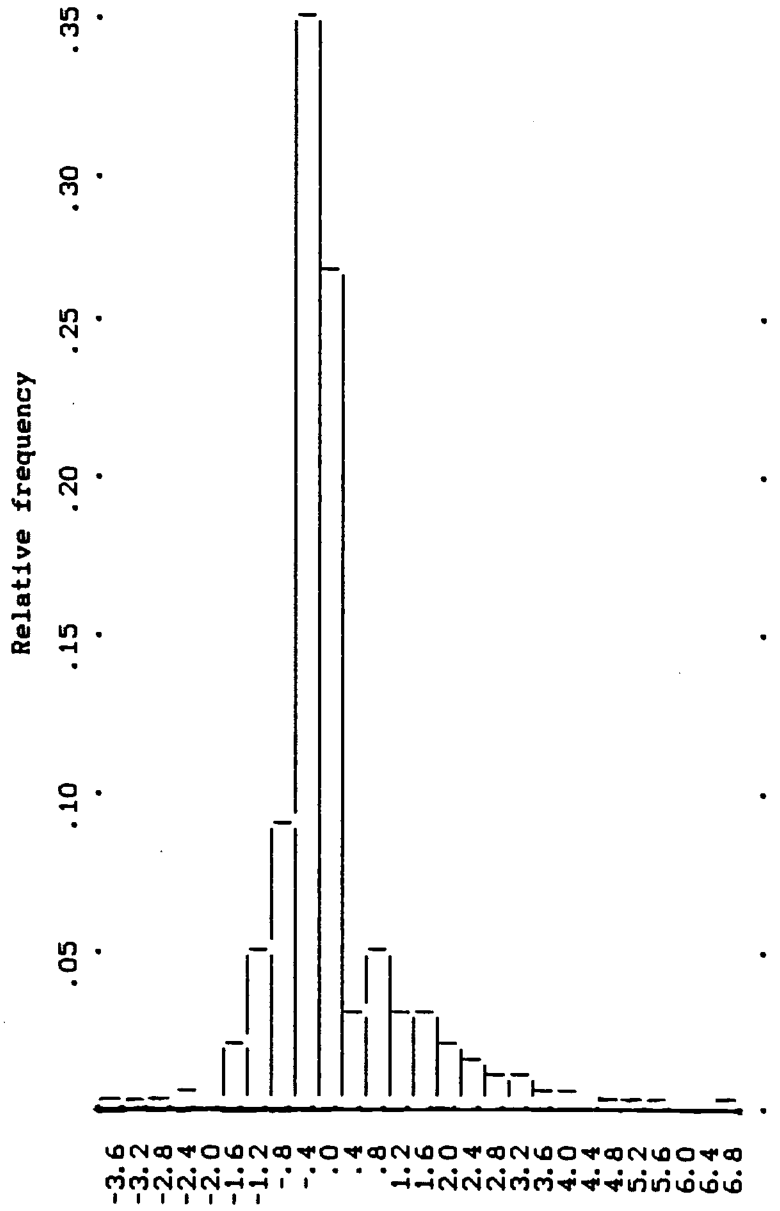


Figure 8. Histogram of a typical empirical amplitude distribution, pertaining to Box 1 July vector 6 (cf. Figure 5).

$$F = P_L \Big/ \sum_{j=1}^{J} w_j p_j \,, \tag{2.12}$$

where the weights $w_j$ are given in Table 1. A modified scaling factor S is then calculated according to

$$S = 1/3 + 2/3 \exp\{-F^2/100\} \,. \tag{2.13}$$

The scaled precipitation estimates $\hat{p}$ are calculated as

$$\hat{p}_j = (p_j)^S (P_L / P_L^*) \,, \tag{2.14}$$

where

$$P_L^* = \sum_{j=1}^{J} w_j (p_j)^S \,. \tag{2.15}$$

This moderately complex procedure is adopted because simple proportional scaling (i.e., S = 1 for all F) produces extremely high individual station precipitation amounts on the relatively rare occasions where all but a few of the randomly drawn amplitudes are negative or close to zero. In that case, F is necessarily very large (on the order of 10 to 100), and all the box-scale precipitation must be concentrated at the few stations whose amplitudes are not small or negative. For F less than 2 or 3, which occurs in the great majority of cases, (2.13) implies that S will be very nearly equal to 1, and precipitation amounts will be scaled nearly in proportion to their dimensional values. For large F, the scaling is performed in proportion to their cube roots. The adjustable constants in this procedure have been "tuned" empirically to provide a reasonable compromise between rare generation of extremely unrealistic large station precipitiation amounts, and excessive frequency of relatively small precipitation amounts. Note finally that this approach insures congruence between the synthetic and box-scale precipitation; that is,

$$\sum_{j=1}^{J} w_j \hat{p}_j = P_L . \tag{2.16}$$

The rescaled precipitation amounts no longer correspond, in general, to those produced by the amplitudes originally drawn at random. Therefore direct use of the original random amplitudes would not produce contributions to temperature anomalies, implied by the patterns such as those shown in Figure 6, that would correspond correctly to the rescaled precipitation. Therefore, once the final station precipitation values have been specified, estimates of precipitation mode amplitudes consistent with those amounts are calculated according to

$$\underset{\sim}{\hat{a}}^{*} = [\underset{\sim}{E}^{*\prime} \underset{\sim}{E}^{*}]^{-1} \underset{\sim}{E}^{*\prime} \sqrt{\tilde{\hat{\underset{\sim}{p}}}} , \tag{2.17}$$

which is analogous to (2.7). Finally, these estimates and the temperature mode amplitudes generated as described above are used to derive temperature specifications using the relevant sub-matrices in (2.6) and the inverses of (2.2) and (2.3).

### 2.4.3. Comparison of the statistical characteristics of the synthetic and observed data

This section presents a comparison of the statistical characteristics (spatial and temporal) of the observed 36-year set of station data with a particular realization of the process described in the previous section. For convenience, only results for Box 1 are presented although, as before, these results are representative of those for the other boxes. The synthetic data were generated using grid-scale values derived from the observed 36-year time series and are therefore of the same length.

The averages, over the 24 stations, of observed and synthetic correlation matrices for maximum and minimum temperature and square-root transformed precipitation are shown in Table 8 for January and July. These data indicate that the procedure described in Section 2.4b has successfully reproduced this aspect of the observed correlation structure of the data. Maximum and minimum temperatures are moderately positively correlated; and precipitation is negatively correlated with both temperature variables, the relationship being stronger with maximum temperature. Variances of observed and synthetic data are comparable in magnitude except for July maximum temperature, for which the variance of the synthetic data is 10-20% higher.

Intercorrelations between stations for particular variables are also well portrayed. Table 9 presents the correlation matrices for observed and synthetic maximum temperatures between the 24 stations for July. Table 10 does the same for square-root transformed precipitation. There is a consistent tendency evident in Table 9 for the synthetic maximum temperature data to exhibit somewhat stronger correlation between stations than the corresponding observed data, but the relative relationships are well preserved. The data in Table 10

Table 8. Observed and synthetic correlation matrices for maximum temperature, minimum temperature, and square-root transformed precipitation, averaged over the 24 stations, for Box 1 January and July.

| January | | | | | | July | | | | | |
|---|---|---|---|---|---|---|---|---|---|---|---|
| Observed | | | Synthetic | | | Observed | | | Synthetic | | |
| 1.00 | | | 1.00 | | | 1.00 | | | 1.00 | | |
| .72 | 1.00 | | .76 | 1.00 | | .61 | 1.00 | | .69 | 1.00 | |
| -.27 | -.10 | 1.00 | -.26 | -.07 | 1.00 | -.33 | -.18 | 1.00 | -.32 | -.19 | 1.00 |

Table 9. Matrix of correlations of maximum temperature between Box 1 stations for July, observed and synthetic data.

a. Observed data

| | | | | | | | | | | | | | | | | | | | | | | | |
|---|---|---|---|---|---|---|---|---|---|---|---|---|---|---|---|---|---|---|---|---|---|---|---|
| 1. | | | | | | | | | | | | | | | | | | | | | | | |
| .66 | 1. | | | | | | | | | | | | | | | | | | | | | | |
| .63 | .87 | 1. | | | | | | | | | | | | | | | | | | | | | |
| .63 | .62 | .65 | 1. | | | | | | | | | | | | | | | | | | | | |
| .74 | .70 | .74 | .83 | 1. | | | | | | | | | | | | | | | | | | | |
| .84 | .72 | .68 | .58 | .74 | 1. | | | | | | | | | | | | | | | | | | |
| .68 | .70 | .73 | .91 | .89 | .67 | 1. | | | | | | | | | | | | | | | | | |
| .77 | .73 | .76 | .73 | .86 | .86 | .77 | 1. | | | | | | | | | | | | | | | | |
| .79 | .75 | .76 | .71 | .82 | .84 | .73 | .88 | 1. | | | | | | | | | | | | | | | |
| .66 | .72 | .78 | .88 | .88 | .67 | .88 | .82 | .81 | 1. | | | | | | | | | | | | | | |
| .66 | .52 | .62 | .85 | .82 | .59 | .78 | .70 | .69 | .79 | 1. | | | | | | | | | | | | | |
| .64 | .84 | .88 | .78 | .79 | .67 | .80 | .76 | .80 | .87 | .66 | 1. | | | | | | | | | | | | |
| .59 | .74 | .73 | .84 | .78 | .58 | .82 | .72 | .75 | .89 | .71 | .88 | 1. | | | | | | | | | | | |
| .58 | .61 | .64 | .91 | .81 | .54 | .88 | .67 | .66 | .85 | .77 | .76 | .83 | 1. | | | | | | | | | | |
| .63 | .87 | .85 | .76 | .76 | .66 | .78 | .75 | .79 | .84 | .63 | .94 | .88 | .74 | 1. | | | | | | | | | |
| .74 | .86 | .85 | .74 | .82 | .80 | .80 | .85 | .86 | .84 | .65 | .87 | .80 | .71 | .86 | 1. | | | | | | | | |
| .81 | .71 | .73 | .81 | .86 | .77 | .83 | .89 | .88 | .87 | .82 | .81 | .78 | .78 | .78 | .85 | 1. | | | | | | | |
| .68 | .86 | .88 | .71 | .78 | .71 | .76 | .79 | .86 | .84 | .66 | .89 | .79 | .71 | .89 | .89 | .79 | 1. | | | | | | |
| .69 | .58 | .63 | .86 | .84 | .61 | .84 | .76 | .74 | .84 | .92 | .71 | .75 | .80 | .68 | .73 | .85 | .69 | 1. | | | | | |
| .87 | .69 | .72 | .74 | .85 | .85 | .78 | .88 | .86 | .80 | .77 | .74 | .70 | .68 | .71 | .82 | .91 | .76 | .81 | 1. | | | | |
| .54 | .49 | .53 | .88 | .78 | .48 | .80 | .64 | .62 | .79 | .82 | .67 | .75 | .83 | .64 | .63 | .72 | .62 | .83 | .66 | 1. | | | |
| .66 | .51 | .59 | .80 | .76 | .58 | .73 | .66 | .64 | .72 | .88 | .61 | .64 | .72 | .60 | .62 | .78 | .64 | .86 | .75 | .76 | 1. | | |
| .48 | .52 | .58 | .86 | .71 | .43 | .78 | .59 | .56 | .79 | .73 | .69 | .79 | .89 | .69 | .63 | .68 | .65 | .73 | .59 | .83 | .68 | 1. | |
| .42 | .44 | .50 | .81 | .63 | .35 | .72 | .49 | .46 | .70 | .72 | .60 | .71 | .82 | .59 | .54 | .61 | .56 | .70 | .52 | .81 | .68 | .89 | 1. |
| 1 | 2 | 3 | 4 | 5 | 6 | 7 | 8 | 9 | 10 | 11 | 12 | 13 | 14 | 15 | 16 | 17 | 18 | 19 | 20 | 21 | 22 | 23 | 24 |

Table 9, continued.

b. Synthetic data

| | | | | | | | | | | | | | | | | | | | | | | | |
|---|---|---|---|---|---|---|---|---|---|---|---|---|---|---|---|---|---|---|---|---|---|---|---|
| 1. | | | | | | | | | | | | | | | | | | | | | | | |
| .74 | 1. | | | | | | | | | | | | | | | | | | | | | | |
| .71 | .97 | 1. | | | | | | | | | | | | | | | | | | | | | |
| .74 | .75 | .79 | 1. | | | | | | | | | | | | | | | | | | | | |
| .84 | .83 | .87 | .92 | 1. | | | | | | | | | | | | | | | | | | | |
| .93 | .81 | .77 | .72 | .86 | 1. | | | | | | | | | | | | | | | | | | |
| .80 | .84 | .87 | .98 | .96 | .81 | 1. | | | | | | | | | | | | | | | | | |
| .84 | .83 | .84 | .84 | .95 | .93 | .91 | 1. | | | | | | | | | | | | | | | | |
| .88 | .86 | .84 | .83 | .95 | .93 | .90 | .97 | 1. | | | | | | | | | | | | | | | |
| .77 | .84 | .87 | .95 | .96 | .78 | .97 | .91 | .92 | 1. | | | | | | | | | | | | | | |
| .77 | .66 | .73 | .92 | .91 | .72 | .90 | .81 | .81 | .88 | 1. | | | | | | | | | | | | | |
| .72 | .93 | .93 | .87 | .88 | .75 | .91 | .84 | .87 | .94 | .76 | 1. | | | | | | | | | | | | |
| .69 | .82 | .82 | .92 | .87 | .67 | .92 | .80 | .83 | .95 | .80 | .95 | 1. | | | | | | | | | | | |
| .73 | .75 | .79 | .98 | .91 | .70 | .97 | .82 | .81 | .94 | .89 | .88 | .92 | 1. | | | | | | | | | | |
| .72 | .94 | .93 | .86 | .88 | .74 | .90 | .84 | .87 | .93 | .75 | .99 | .95 | .86 | 1. | | | | | | | | | |
| .81 | .94 | .94 | .87 | .94 | .88 | .94 | .95 | .95 | .94 | .78 | .95 | .88 | .86 | .95 | 1. | | | | | | | | |
| .88 | .80 | .82 | .92 | .97 | .88 | .95 | .95 | .96 | .95 | .91 | .88 | .88 | .90 | .87 | .93 | 1. | | | | | | | |
| .77 | .95 | .97 | .85 | .93 | .82 | .92 | .89 | .91 | .93 | .78 | .95 | .87 | .86 | .95 | .97 | .89 | 1. | | | | | | |
| .79 | .70 | .77 | .94 | .94 | .75 | .93 | .86 | .86 | .92 | .98 | .82 | .84 | .91 | .80 | .84 | .95 | .83 | 1. | | | | | |
| .93 | .80 | .80 | .86 | .95 | .94 | .91 | .95 | .96 | .89 | .87 | .82 | .79 | .83 | .81 | .92 | .97 | .87 | .91 | 1. | | | | |
| .69 | .66 | .71 | .97 | .89 | .64 | .93 | .78 | .76 | .90 | .92 | .79 | .86 | .96 | .78 | .79 | .87 | .79 | .93 | .81 | 1. | | | |
| .74 | .61 | .69 | .88 | .84 | .67 | .85 | .74 | .73 | .80 | .96 | .70 | .73 | .83 | .69 | .73 | .85 | .73 | .94 | .83 | .88 | 1. | | |
| .62 | .67 | .71 | .95 | .83 | .59 | .91 | .72 | .70 | .88 | .83 | .80 | .87 | .97 | .79 | .77 | .80 | .78 | .84 | .73 | .96 | .78 | 1. | |
| .56 | .58 | .64 | .91 | .75 | .50 | .86 | .63 | .59 | .79 | .81 | .71 | .79 | .93 | .70 | .68 | .73 | .69 | .80 | .65 | .94 | .79 | .97 | 1. |
| 1 | 2 | 3 | 4 | 5 | 6 | 7 | 8 | 9 | 10 | 11 | 12 | 13 | 14 | 15 | 16 | 17 | 18 | 19 | 20 | 21 | 22 | 23 | 24 |

Table 10. Matrix of correlations of square-root transformed precipitation for Box 1 July, observed and synthetic data.

a. Observed data

| | | | | | | | | | | | | | | | | | | | | | | | |
|---|---|---|---|---|---|---|---|---|---|---|---|---|---|---|---|---|---|---|---|---|---|---|---|
| 1. | | | | | | | | | | | | | | | | | | | | | | | |
| .07 | 1. | | | | | | | | | | | | | | | | | | | | | | |
| .12 | .57 | 1. | | | | | | | | | | | | | | | | | | | | | |
| .16 | .18 | .19 | 1. | | | | | | | | | | | | | | | | | | | | |
| .23 | .21 | .22 | .43 | 1. | | | | | | | | | | | | | | | | | | | |
| .29 | .10 | .11 | .15 | .25 | 1. | | | | | | | | | | | | | | | | | | |
| .18 | .19 | .22 | .68 | .41 | .14 | 1. | | | | | | | | | | | | | | | | | |
| .23 | .28 | .34 | .38 | .32 | .19 | .37 | 1. | | | | | | | | | | | | | | | | |
| .26 | .31 | .39 | .23 | .28 | .19 | .26 | .49 | 1. | | | | | | | | | | | | | | | |
| .17 | .33 | .36 | .52 | .36 | .15 | .60 | .45 | .38 | 1. | | | | | | | | | | | | | | |
| .11 | .16 | .18 | .45 | .29 | .11 | .40 | .33 | .21 | .35 | 1. | | | | | | | | | | | | | |
| .10 | .54 | .55 | .26 | .20 | .13 | .30 | .32 | .38 | .44 | .15 | 1. | | | | | | | | | | | | |
| .12 | .40 | .42 | .36 | .23 | .12 | .45 | .26 | .29 | .57 | .23 | .58 | 1. | | | | | | | | | | | |
| .15 | .21 | .20 | .57 | .36 | .15 | .57 | .30 | .20 | .48 | .39 | .26 | .38 | 1. | | | | | | | | | | |
| .08 | .52 | .55 | .23 | .18 | .08 | .25 | .31 | .33 | .38 | .15 | .72 | .52 | .20 | 1. | | | | | | | | | |
| .16 | .44 | .51 | .29 | .27 | .18 | .25 | .47 | .57 | .46 | .27 | .50 | .37 | .34 | .44 | 1. | | | | | | | | |
| .25 | .23 | .30 | .33 | .34 | .16 | .36 | .71 | .44 | .41 | .36 | .25 | .24 | .33 | .24 | .36 | 1. | | | | | | | |
| .11 | .60 | .62 | .17 | .21 | .11 | .18 | .36 | .50 | .33 | .19 | .51 | .31 | .18 | .49 | .55 | .30 | 1. | | | | | | |
| .16 | .15 | .16 | .39 | .34 | .16 | .41 | .37 | .26 | .35 | .59 | .15 | .18 | .28 | .15 | .27 | .35 | .20 | 1. | | | | | |
| .30 | .21 | .26 | .34 | .31 | .13 | .31 | .50 | .37 | .33 | .35 | .22 | .19 | .24 | .18 | .34 | .57 | .26 | .34 | 1. | | | | |
| .13 | .11 | .14 | .55 | .26 | .15 | .46 | .21 | .26 | .39 | .39 | .16 | .26 | .39 | .15 | .27 | .22 | .16 | .38 | .21 | 1. | | | |
| .12 | .00 | .08 | .31 | .19 | .11 | .29 | .28 | .16 | .20 | .48 | .03 | .20 | .26 | .05 | .11 | .25 | .08 | .41 | .26 | .24 | 1. | | |
| .07 | .04 | .05 | .40 | .08 | .05 | .29 | .21 | .09 | .29 | .25 | .15 | .28 | .36 | .15 | .14 | .16 | .05 | .15 | .14 | .35 | .23 | 1. | |
| .04 | .05 | .03 | .27 | .00 | .01 | .23 | .10 | .04 | .18 | .16 | .09 | .16 | .27 | .09 | .09 | .06 | .04 | .09 | .06 | .33 | .09 | .51 | 1. |
| 1 | 2 | 3 | 4 | 5 | 6 | 7 | 8 | 9 | 10 | 11 | 12 | 13 | 14 | 15 | 16 | 17 | 18 | 19 | 20 | 21 | 22 | 23 | 24 |

Table 10, continued.

b. Synthetic data

| | | | | | | | | | | | | | | | | | | | | | | | |
|---|---|---|---|---|---|---|---|---|---|---|---|---|---|---|---|---|---|---|---|---|---|---|---|
| 1. | | | | | | | | | | | | | | | | | | | | | | | |
| .11 | 1. | | | | | | | | | | | | | | | | | | | | | | |
| .17 | .47 | 1. | | | | | | | | | | | | | | | | | | | | | |
| .13 | .10 | .10 | 1. | | | | | | | | | | | | | | | | | | | | |
| .17 | .14 | .14 | .32 | 1. | | | | | | | | | | | | | | | | | | | |
| .20 | .10 | .10 | .11 | .24 | 1. | | | | | | | | | | | | | | | | | | |
| .13 | .12 | .14 | .52 | .37 | .13 | 1. | | | | | | | | | | | | | | | | | |
| .21 | .14 | .20 | .24 | .20 | .16 | .29 | 1. | | | | | | | | | | | | | | | | |
| .30 | .20 | .32 | .16 | .24 | .19 | .17 | .35 | 1. | | | | | | | | | | | | | | | |
| .18 | .20 | .32 | .35 | .27 | .15 | .46 | .40 | .32 | 1. | | | | | | | | | | | | | | |
| .16 | .18 | .22 | .29 | .20 | .16 | .24 | .26 | .16 | .31 | 1. | | | | | | | | | | | | | |
| .14 | .36 | .37 | .13 | .12 | .05 | .17 | .27 | .31 | .30 | .13 | 1. | | | | | | | | | | | | |
| .11 | .32 | .35 | .20 | .16 | .16 | .32 | .19 | .21 | .45 | .16 | .42 | 1. | | | | | | | | | | | |
| .08 | .16 | .20 | .42 | .31 | .10 | .44 | .22 | .16 | .38 | .28 | .20 | .30 | 1. | | | | | | | | | | |
| .19 | .42 | .47 | .18 | .17 | .07 | .15 | .23 | .25 | .29 | .15 | .56 | .44 | .20 | 1. | | | | | | | | | |
| .16 | .27 | .39 | .17 | .17 | .15 | .16 | .33 | .45 | .31 | .21 | .39 | .32 | .24 | .35 | 1. | | | | | | | | |
| .21 | .19 | .26 | .20 | .23 | .13 | .32 | .60 | .29 | .38 | .26 | .18 | .20 | .25 | .20 | .21 | 1. | | | | | | | |
| .10 | .48 | .52 | .10 | .15 | .07 | .12 | .28 | .43 | .31 | .18 | .37 | .22 | .14 | .39 | .44 | .20 | 1. | | | | | | |
| .11 | .11 | .17 | .23 | .22 | .17 | .25 | .21 | .18 | .26 | .51 | .06 | .10 | .20 | .09 | .24 | .22 | .17 | 1. | | | | | |
| .20 | .15 | .21 | .30 | .24 | .13 | .28 | .35 | .25 | .35 | .33 | .22 | .20 | .25 | .16 | .20 | .38 | .20 | .28 | 1. | | | | |
| .16 | .11 | .11 | .36 | .19 | .14 | .32 | .19 | .26 | .35 | .27 | .13 | .25 | .29 | .24 | .21 | .12 | .14 | .27 | .20 | 1. | | | |
| .16 | .12 | .19 | .20 | .22 | .15 | .25 | .22 | .23 | .26 | .40 | .14 | .20 | .26 | .12 | .12 | .21 | .20 | .27 | .25 | .23 | 1. | | |
| .14 | .12 | .11 | .30 | .06 | .02 | .17 | .24 | .10 | .27 | .21 | .15 | .21 | .20 | .23 | .11 | .13 | .08 | .14 | .18 | .42 | .26 | 1. | |
| .23 | .08 | .15 | .28 | .08 | .11 | .26 | .28 | .18 | .25 | .21 | .13 | .20 | .21 | .19 | .13 | .16 | .11 | .14 | .23 | .39 | .23 | .49 | 1. |
| 1 | 2 | 3 | 4 | 5 | 6 | 7 | 8 | 9 | 10 | 11 | 12 | 13 | 14 | 15 | 16 | 17 | 18 | 19 | 20 | 21 | 22 | 23 | 24 |

for precipitation are noisier, as would be expected, but the observed spatial correlation structure again seems to be well reproduced.

Much of the time dependence of the data at the individual station level also appears to be captured by this method of data generation. One aspect of the degree of serial correlation of temperature data is the "effective time between independent samples" $T_0$ (e.g., Leith, 1973; Trenberth, 1984). Using the result that estimates of $T_0$ are approximately normally distributed for present sample sizes, with variance depending nonlinearly on $T_0$ (Wilks, 1987; Appendix A), the equality of $T_0$ estimates from observed and synthetic January and July data was tested for each station. Agreement for January data is excellent, with none of the maximum temperature differences declared significant, and the difference for a single station declared significant (at the 5% level) for minimum temperature. Results for July indicate less agreement, with 11 tests of 24 significant for maximum temperature, and 3 tests significant for minimum temperature. Locations of stations with significant differences appear to be highly clustered (e.g., all four Oklahoma stations produce significant results for tests of July maximum temperature), so that a conclusion of a significant overall difference is not clearcut (cf. Livezey and Chen, 1983). There is a consistent tendency, however, for synthetic data for stations for which the test gives a significant result to exhibit lower $T_0$ than the corresponding observed data. This tendency is also evident in a comparison of the synthetic autocorrelation functions, which decay too rapidly with time for these stations.

Serial correlation of precipitation occurrence may be characterized by the parameters of a two-state Markov process, and by the order of the model necessary to adequately fit the data (e.g., Katz, 1985). Determiniation of the appropriate model order is accomplished by the application of the BIC statistic applied to Markov chains (Katz, 1981; Schwartz, 1978). Observed serial correlation of precipitation occurrence is adequately represented by Markov chains of order 1 for all combinations of stations and months in January and July. The synthetic January data for one station required a second-order model, whereas July data for seven stations were adequately described by zero-order models (i.e., precipitation occurrence independent from day to day). However, in most of these cases, a first-order model fit the data nearly as well. The results regarding optimal model order for the synthetic data appear to vary substantially between realizations, another trial yielding only three stations (all different from the above seven), with July data requiring only zero-order models. Averages over the 24 stations for January and July (Table 11) indicate that the portrayal of serial correlation of precipitation occurrence in the synthetic data is reasonably close to that in the observed data. In general, parameter values for different stations are similar, and deviations from these means for particular stations are generally no more than 10%.

Another important aspect of the observed data that should be reproduced by a successful specification procedure is the distributional form of the daily precipitation amounts. This feature is particularly important from the standpoint of agricultural impacts assessment. Daily precipitation amounts are generally very strongly skewed, and often a two-parameter gamma distribution is fit to this type of data, which is first censored to include only nonzero amounts

Table 11. Average first-order Markov chain parameters for observed and synthetic data; Box 1 January and July. Averages over the 24 stations.

| | January | | July | |
|---|---|---|---|---|
| | Observed | Synthetic | Observed | Synthetic |
| Pr {dry following dry} | .849 | .895 | .763 | .694 |
| Pr {wet following dry} | .621 | 675 | .599 | .586 |

Table 12. Average scale and shape parameters of gamma distributions for precipitation amount: observed and synthetic data for Box 1 January and July. Averages over 24 stations.

| | January | | July | |
|---|---|---|---|---|
| | Observed | Synthetic | Observed | Synthetic |
| Scale parameter | 4.3 | 3.9 | 16.2 | 14.5 |
| Shape parameter | 0.55 | 0.84 | 0.59 | 0.54 |

(e.g., Katz, 1977; Stern and Coe, 1984; Waymire and Gupta, 1981). The density function of the gamma distribution may be written in a number of alternative ways. Here it is described in a form such that the mean is given by the product of the shape and scale parameters. A comparison of the averages of the shape and scale paramters over the 24 stations is contained in Table 12. It should be noted that individual station values for the scale parameter deviate substantially from these mean values (up to 50% or so), particularly as a result of one or more very large summer precipitation amounts, but overall there is reasonable agreement between the observed and synthetic data.

The scaling procedure (2.12)-(2.15) succeeds to a large degree in supressing wildly extreme daily precipitation amounts, although the synthetic data still exhibit larger extreme values than the corresponding observations. Table 13 presents a comparison of frequencies with which selected daily precipitation amounts are exceeded for January and July. These figures are pooled over all 24 Box 1 stations for the 36-year record in each case. The correspondence for January is reasonably good. For July, twenty-two days with more than 150 mm occurred in this realization of the synthetic data, compared to one day for the observations. The maximum precipitation amount for the present realization of the synthetic data is 331 mm, compared to 164 mm in the observations. Use of proportional scaling rather than (2.12)-(2.15), by comparison, produces maximum daily precipitation amounts greater than 600 mm. Note that this tendency to produce occasional unrealistically large precipitation amounts would probably be exacerbated in a

Table 13. Frequencies with which selected daily precipitation amounts are exceeded in the synthetic and observational data, January and July. Figures are pooled over 24 stations of Box 1 for 36-year records.

January:

| Amount | Times exceeded in: Observations | Times exceeded in: Synthetic data |
|---|---|---|
| 50 mm | 0 | 1 |
| 40 mm | 1 | 5 |
| 30 mm | 12 | 14 |
| 20 mm | 49 | 54 |

July:

| Amount | Times exceeded in: Observations | Times exceeded in: Synthetic data |
|---|---|---|
| 300 mm | 0 | 1 |
| 250 mm | 0 | 2 |
| 200 mm | 0 | 9 |
| 150 mm | 1 | 22 |
| 100 mm | 8 | 62 |

representation based on the Kim et al. (1984) formulation for the correlation matrix, as a result of the presence of moderately large negative precipitation loadings in the precipitation modes that would accentuate the relative differences between stations.

Table 14 presents a comparison of average monthly total (untransformed) precipitation for each station for January and July, and the corresponding standard deviations (with respect to the 36-year means for each station). There is moderately good agreement for most of the stations, with the synthetic data correctly producing largest average totals on the eastern margin of the domain (north-central Kansas and Jefferson, Oklahoma), and the lowest average totals in southwestern Kansas. Note also that for both data sources the standard deviations are of the same magnitude as the mean values. This result indicates (for this necessarily nonnegative quantity) that the strong positive skewness of the observed distribution is reproduced in the monthly totals of the synthetic data. Such a result would be expected to follow from the near-equality for the two data sources of the daily occurrence and intensity parameters presented above (Katz, 1977).

Finally, Table 15 presents analogous data for mean monthly maximum and minimum temperatures. The 36-year averages of mean monthly tempeatures and the standard deviations of these averages from the overall means are very well reproduced in the synthetic data for all stations, for both months, and for both temperature variables.

Table 14. Average monthly total precipitation (mm) and standard deviations of individual monthly totals from the overall mean monthly total, Box 1 January and July.

a. January

| | Observed | | Synthetic | |
|---|---|---|---|---|
| Station | Mean | Std. Dev | Mean | Std. Dev |
| 1 | 6.7 | 6.0 | 6.2 | 5.9 |
| 2 | 17.2 | 14.6 | 23.0 | 20.9 |
| 3 | 16.4 | 14.3 | 24.5 | 21.7 |
| 4 | 15.5 | 16.2 | 15.0 | 14.3 |
| 5 | 12.2 | 11.0 | 15.0 | 14.2 |
| 6 | 10.5 | 7.5 | 9.1 | 7.2 |
| 7 | 13.6 | 13.1 | 11.4 | 11.2 |
| 8 | 10.8 | 9.8 | 12.9 | 15.0 |
| 9 | 10.0 | 8.4 | 8.8 | 9.3 |
| 10 | 12.5 | 12.0 | 15.8 | 16.2 |
| 11 | 12.3 | 12.3 | 9.6 | 9.8 |
| 12 | 15.7 | 14.9 | 19.1 | 18.9 |
| 13 | 17.4 | 19.8 | 20.7 | 20.0 |
| 14 | 14.1 | 16.2 | 11.0 | 10.4 |
| 15 | 16.7 | 17.1 | 23.4 | 21.1 |
| 16 | 10.2 | 8.9 | 12.5 | 12.0 |
| 17 | 13.2 | 12.1 | 16.4 | 19.1 |
| 18 | 10.6 | 9.4 | 13.9 | 12.5 |
| 19 | 8.1 | 8.0 | 7.5 | 9.5 |
| 20 | 7.9 | 7.6 | 8.9 | 9.6 |
| 21 | 13.8 | 14.5 | 11.2 | 10.6 |
| 22 | 7.2 | 7.3 | 4.1 | 3.9 |
| 23 | 20.5 | 22.9 | 16.9 | 15.2 |
| 24 | 17.2 | 19.6 | 9.2 | 10.9 |

Table 14, continued.

b. July

| Station | Observed Mean | Observed Std. Dev | Synthetic Mean | Synthetic Std. Dev |
|---|---|---|---|---|
| 1 | 68.6 | 46.5 | 84.7 | 90.2 |
| 2 | 99.6 | 66.6 | 107.5 | 70.9 |
| 3 | 88.0 | 72.4 | 92.4 | 70.2 |
| 4 | 77.4 | 59.1 | 86.3 | 80.8 |
| 5 | 81.3 | 52.3 | 79.1 | 53.9 |
| 6 | 63.0 | 31.0 | 86.8 | 80.0 |
| 7 | 72.5 | 52.6 | 60.8 | 58.8 |
| 8 | 77.0 | 54.5 | 61.3 | 49.4 |
| 9 | 81.5 | 48.9 | 69.3 | 49.8 |
| 10 | 87.4 | 54.1 | 78.9 | 56.6 |
| 11 | 77.7 | 60.9 | 70.3 | 52.6 |
| 12 | 93.6 | 58.6 | 105.7 | 99.6 |
| 13 | 91.3 | 65.0 | 84.8 | 71.1 |
| 14 | 77.7 | 52.8 | 57.6 | 57.1 |
| 15 | 95.6 | 64.8 | 100.8 | 98.7 |
| 16 | 80.1 | 50.1 | 82.1 | 62.2 |
| 17 | 78.2 | 60.9 | 58.4 | 48.5 |
| 18 | 73.3 | 42.5 | 76.4 | 51.8 |
| 19 | 67.1 | 44.6 | 63.3 | 55.8 |
| 20 | 65.6 | 49.7 | 67.2 | 65.4 |
| 21 | 87.8 | 55.6 | 76.3 | 58.3 |
| 22 | 80.3 | 49.9 | 83.6 | 59.6 |
| 23 | 97.2 | 61.0 | 112.3 | 96.0 |
| 24 | 67.1 | 48.4 | 60.1 | 60.0 |

Table 15. Average monthly maximum and minimum temperatures, (C), and standard deviations of individual monthly means from overall mean values, Box 1 January and July.

a. January

| | Maximum temperature | | | | Minimum Temperature | | | |
|---|---|---|---|---|---|---|---|---|
| | Observed | | Synthetic | | Observed | | Synthetic | |
| Station | mean | s.d. | mean | s.d. | mean | s.d. | mean | s.d. |
| 1 | 6.23 | 3.31 | 6.22 | 3.35 | -10.07 | 3.06 | -10.09 | 2.91 |
| 2 | 1.81 | 3.02 | 1.87 | 3.01 | -10.13 | 3.05 | -10.23 | 3.02 |
| 3 | 3.02 | 3.18 | 2.78 | 3.11 | -9.93 | 3.01 | -10.17 | 3.02 |
| 4 | 6.74 | 3.46 | 6.68 | 3.58 | -6.92 | 2.58 | -7.16 | 2.56 |
| 5 | 5.10 | 3.52 | 5.10 | 3.75 | -7.85 | 2.74 | -7.80 | 2.75 |
| 6 | 4.68 | 3.50 | 4.77 | 3.66 | -10.11 | 3.09 | -10.05 | 2.98 |
| 7 | 5.59 | 3.50 | 5.55 | 3.63 | -7.85 | 2.72 | -7.92 | 2.70 |
| 8 | 5.78 | 3.52 | 5.83 | 3.66 | -9.55 | 2.83 | -9.53 | 2.89 |
| 9 | 5.25 | 3.52 | 5.32 | 3.59 | -9.44 | 2.81 | -9.32 | 2.84 |
| 10 | 5.50 | 3.37 | 5.56 | 3.53 | -7.61 | 2.70 | -7.60 | 2.68 |
| 11 | 8.58 | 3.55 | 8.77 | 3.70 | -6.67 | 2.54 | -6.80 | 2.59 |
| 12 | 4.42 | 3.26 | 4.44 | 3.36 | -9.45 | 3.12 | -9.53 | 2.86 |
| 13 | 4.07 | 3.13 | 4.00 | 3.19 | -7.61 | 2.64 | -7.72 | 2.69 |
| 14 | 6.96 | 3.63 | 6.87 | 3.45 | -7.12 | 2.70 | -7.18 | 2.43 |
| 15 | 3.63 | 2.97 | 3.67 | 3.10 | -8.43 | 2.86 | -8.40 | 2.70 |
| 16 | 3.91 | 3.40 | 3.92 | 3.53 | -9.00 | 2.93 | -8.91 | 2.76 |
| 17 | 6.55 | 3.46 | 6.52 | 3.70 | -8.97 | 2.74 | -9.10 | 2.77 |
| 18 | 3.08 | 3.14 | 2.83 | 3.10 | -10.23 | 2.98 | -10.30 | 2.95 |
| 19 | 7.61 | 3.65 | 7.63 | 3.68 | -8.12 | 2.59 | -8.25 | 2.68 |
| 20 | 6.42 | 3.57 | 6.54 | 3.63 | -9.87 | 2.79 | -9.86 | 2.85 |
| 21 | 9.04 | 3.70 | 9.16 | 3.61 | -6.48 | 2.56 | -6.58 | 2.47 |
| 22 | 9.27 | 4.25 | 9.49 | 3.82 | -7.62 | 2.68 | -7.70 | 2.62 |
| 23 | 7.85 | 3.43 | 7.82 | 3.35 | -5.44 | 2.54 | -5.65 | 2.36 |
| 24 | 9.46 | 3.76 | 9.51 | 3.51 | -4.98 | 2.48 | -5.09 | 2.29 |

Table 15, continued.

b. July

| | Maximum temperature | | | | Minimum Temperature | | | |
|---|---|---|---|---|---|---|---|---|
| | Observed | | Synthetic | | Observed | | Synthetic | |
| Station | mean | s.d. | mean | s.d. | mean | s.d. | mean | s.d. |
| 1 | 32.95 | 5.76 | 32.93 | 5.87 | 15.13 | 2.76 | 14.95 | 2.68 |
| 2 | 32.72 | 6.02 | 32.60 | 5.84 | 19.35 | 3.52 | 19.31 | 3.51 |
| 3 | 33.91 | 6.23 | 33.82 | 6.08 | 19.13 | 3.49 | 19.10 | 3.50 |
| 4 | 34.93 | 6.24 | 34.78 | 6.25 | 19.67 | 3.57 | 19.55 | 3.53 |
| 5 | 33.52 | 6.10 | 33.49 | 6.18 | 19.68 | 3.62 | 19.50 | 3.53 |
| 6 | 32.41 | 5.78 | 32.17 | 5.85 | 16.28 | 2.99 | 16.06 | 2.90 |
| 7 | 34.16 | 6.17 | 34.04 | 6.16 | 19.60 | 3.64 | 19.52 | 3.53 |
| 8 | 34.37 | 6.13 | 34.15 | 6.20 | 17.88 | 3.23 | 17.68 | 3.18 |
| 9 | 33.98 | 6.08 | 33.85 | 6.13 | 17.84 | 3.25 | 17.65 | 3.19 |
| 10 | 34.16 | 6.22 | 34.13 | 6.25 | 19.78 | 3.58 | 19.73 | 3.59 |
| 11 | 35.11 | 6.21 | 35.06 | 6.23 | 19.46 | 3.49 | 19.30 | 3.41 |
| 12 | 34.90 | 6.40 | 34.79 | 6.28 | 19.52 | 3.59 | 19.41 | 3.60 |
| 13 | 34.20 | 6.32 | 34.17 | 6.18 | 20.04 | 3.67 | 20.02 | 3.68 |
| 14 | 35.14 | 6.29 | 35.09 | 6.31 | 19.84 | 3.57 | 19.67 | 3.48 |
| 15 | 34.42 | 6.32 | 34.38 | 6.21 | 19.88 | 3.67 | 19.94 | 3.64 |
| 16 | 33.60 | 6.17 | 33.45 | 6.14 | 18.89 | 3.45 | 18.83 | 3.41 |
| 17 | 33.73 | 5.96 | 33.62 | 6.07 | 17.79 | 3.17 | 17.67 | 3.13 |
| 18 | 33.96 | 6.23 | 33.82 | 6.16 | 18.88 | 3.53 | 18.95 | 3.53 |
| 19 | 34.30 | 6.08 | 34.19 | 6.10 | 18.32 | 3.27 | 18.21 | 3.22 |
| 20 | 33.57 | 5.98 | 33.43 | 6.05 | 16.37 | 2.95 | 16.18 | 2.89 |
| 21 | 36.00 | 6.47 | 35.87 | 6.35 | 20.66 | 3.77 | 20.47 | 3.70 |
| 22 | 34.04 | 6.04 | 33.93 | 5.97 | 18.22 | 3.26 | 18.17 | 3.23 |
| 23 | 35.71 | 6.41 | 35.66 | 6.34 | 21.33 | 3.81 | 21.24 | 3.79 |
| 24 | 36.13 | 6.41 | 36.00 | 6.29 | 21.29 | 3.84 | 21.04 | 3.72 |

## 2.5 Summary and Conclusions

The present work has extended the initial study of Kim *et al.* (1984) by formulating a solution to the "climate inverse" problem for the case of daily values of maximum temperature, minimum temperature, and precipitation. The formulation presented differs from that of Kim *et al.* (1984) by simultaneously analyzing all three variables, and by forming the correlation matrix, separately for each month, using deviations of station values from their (local) mean values rather than deviations from the box-scale values.

It is found that varimax rotation of the initial principal component solution produces, consistent with the notion of "simple structure," pattern vectors that permit reasonable meteorological interpretations. These vectors are qualitatively different for the warm and cool seasons, but are similar from month to month within seasons. They reflect the strong spatial coherence of temperature, the moderately coherent nature of cool-season precipitation, the relatively small-scale character of convective precipitation, and the negative correlation of precipitation with (especially maximum) temperature.

Although it is possible to specify individual station temperature data from the larger scale average with moderate success, the particular location and intensity of convective rainfall within a 4° latitude by 5° longitude region is found to be essentially unpredictable from the larger-scale information. A stochastic approach to daily weather representation at the station level is therefore adopted, making use of the temporal orthogonality preserved by the varimax rotation procedure. Various spatial and temporal statistical characteristics of the resulting synthetic data at the station level correspond reasonably well to the observations. Much simpler procedures may be employed if realistic spatial representations of precipititation are not required.

Successful modeling of the spatial distribution of precipitation indicates that the present approach could be of use in climate impacts work where a means to produce spatially coherent synthetic meteorological data is needed. However, the result that exactly J small preciptitaion modes occur in the analyses for all warm-season months in each of the three gridboxes considered dictates that some caution should be exercised in the application of this procedure. In particular, this result indicates that the station density used here (even though some of the station spacings are as small as 20 km) is insufficient to capture the spatial scale of the convective precipitation. This result is consistent with results obtained using dense raingage networks (e.g., Changnon, 1981; Griffith et al., 1981). The application of the procedure should therefore be limited to data estimation at availabile stations only, as attempts at interpolation will likely result in underestimation of precipitation amounts between stations.

One possible application is in studies involving physiological crop models under present climatic conditions, where the observed record of meteorological data is shorter than desired. Perhaps the most serious defect of the present method for this purpose is the occasional production of unrealistically high daily precipitation amounts. This effect could be minimized, however, by including a parameterization within the crop model for limiting soil infiltration rate to physically realizable values.

Another potential application is as part of a procedure for using general circulation model results to estimate the consequences of a possible climate change on agricultural production. For this purpose, the method provides a means of producing meteorological data on scales small enough for use with crop models, which is consistent with the imposed box-scale data and which exhibits realistic statistical characteristics. This application is the focus of the remaining sections of the present work.

# Section 3

## Characterization of Grid-Scale Time Series and Construction of Climate Scenarios Using a Multivariate Stochastic Model

### 3.1 Introduction

The second major element in the design of a procedure for estimation of local impacts of a changed climate is a means to specify the characteristics of the changed climate on the larger scale. However, the problem of using data from general circulation model (GCM) integrations to extrapolate to a 2X-$CO_2$ world is not a straightforward one. Substantial errors in the control integrations indicate that direct acceptance of the output from 2X-$CO_2$ runs as literally representative of a future changed climate would be unwise. However, to the extent that significant features of the climate system are captured in these models, sensible estimates of future climate may be possible through careful use of the information.

This section describes an approach to this problem that involves a quantitative description of the statistical structure of daily GCM data. Surprisingly, only one previous paper in the meteorological literature (Reed, 1986) has reported investigation of this potentially rich source of information. In the present work, the statistical characteristics of the time series of daily surface weather elements at the scale of the GCM gridbox are portrayed in terms of the parameters of a multivariate time-domain stochastic model. This stochastic model and its parameters provide a statistical description of the climate represented by particular time series of surface weather elements, and thus may be regarded as a basis for the representation of the corresponding climatic states (National Academy of Sciences, 1975). The form of the statistical model is chosen with the intent of describing important features of the data in terms of readily interpretable parameters, while at the same time maintaining a structure that is directly applicable to Monte Carlo simulation.

The inferred climatic state of a 2X-$CO_2$ world is constructed by considering relative changes in the parameters of this stochastic model when fit to 1X- and 2X-$CO_2$ GCM data. This approach is the basic procedure often used in the evaluation of climate change studies using GCMs (e.g., Schlesinger, 1986). Several applications of this approach (using changes in monthly, seasonally, or annually averaged temperature levels and preciptitaion rates) for construction of "scenarios" of changed climate have been made on the basis of climatic variations within the period of instrumental records (e.g., Jager and Kellogg, 1983; Lough *et al.*, 1983; Namias, 1980; Pittock and Salinger, 1982; Wigley *et al.*, 1980; Williams, 1980). Some similar extrapolations, of the same averaged variables and at the same time scales, have been made with a view toward impact assessments using GCM data (Bach *et al.*, 1984; Gates and Bach, 1981; Rosenzweig, 1985; Santer, 1985).

The present approach is conceptually the same as that in the above works, but the procedure is used here with a much richer parameter set. In addition to time-dependent mean values, possible changes in variances, and in auto- and cross-correlations on the daily time scale are considered. The (statistically significant) differences in the values of parameters representing these aspects of the 1X- and 2X-$CO_2$ GCM data are applied to the corresponding values derived from observations. In this way time series consistent with observational data, and reflecting relative differences in the climate states generated by the GCM, may be produced in a Monte Carlo setting. It is implicitly assumed that no drastic changes in global circulation regimes will accompany the accomodation of the atmosphere to $CO_2$ increases, an assumption that is given some support by recent modeling efforts (Manabe and Bryan, 1985; Rind, 1986).

Finally, these results are combined with the climate inverse procedure of Section 2 to stochastically generate time series of daily weather data on the local (observing station) scale consistent with either the current climate or with the inferred 2X-$CO_2$ climate scenario. Since the ultimate objective is to use the results in conjunction with "physiological" crop simulation models, equations are also developed to specify total daily solar radiation on the station scale in terms of the generated surface weather variables.

The domain and data sources used are described in Section 3.2. The form of the stochastic model is described in Section 3.3, and the significance of differences in the values of its parameters for the 1X-$CO_2$ versus 2X-$CO_2$ GCM data sets is assessed in Section 3.4. Finally, the significant differences are applied to parameters characterizing the observational data, and the stochastic model is used in conjunction with the climate inverse procedure, in Section 3.5.

## 3.2 Domain and Data

The geographical domain for the work described in the present section is the same as that for Section 2. It is comprised of the three 4° by 5° (latitude by longitude) gridboxes centered at 38°N, 100°W (Box 1); 42°N, 95°W (Box 2); and 46°N, 100°W (Box 3).

Three time series, each comprised of daily values of maximum temperature, minimum temperature, and precipitation, are considered. The first is the area-weighted time series of (observed) cooperative station data described in Section 2.2. The remaining two are daily time series of the same variables derived from 1X-$CO_2$ and 2X-$CO_2$ integrations of a GCM for the same three gridboxes.

The GCM data is from the OSU Atmospheric GCM (Ghan et al., 1982) coupled to a two-layer, variable depth mixed-layer model of the upper ocean and sea ice (Pollard, 1982). Hourly model data for years 14 through 25 of the two integrations were obtained. Since the 2X-$CO_2$ realization of the model had not yet reached equilibrium (W.L. Gates, private communication), it was necessary to adjust the temperature data from this source to compensate for the nonstationarity. This adjustment was accomplished by removing a linear trend from the temperature data (separately for maximum and minimum temperature, and for each gridbox), and then adding back the values of the respective trend lines corresponding to the end of year 25.

Highest and lowest temperatures from 07 GMT through 06 GMT in the model are taken to represent the maximum and minimum temperatures. This period corresponds approximately to 00 hours through 23 hours local time. Daily precipitation from the GCM is summed over the same hours. Data from each of the three time series is stratified by calendar month, and parameters for the stochastic models are, with the exception of mean level for temperature, fit separately for each of the 12 months.

## 3.3 Description of the Stochastic Model

### 3.3.1. Precipitation

Stochastic models of daily precipitation are typically comprised of two parts: a formulation for the occurrence of sequences of wet and dry days, and another for the intensity (amount) of precipitation on wet days (Coe and Stern, 1982; Ison <u>et al</u>., 1971; Katz, 1977a,b; Stern and Coe, 1984; Waymire and Gupta, 1981; Woolhiser and Pegram, 1979). Typically the occurrence component is taken to be a 2-state Markov chain (usually of order 1), and the intensity is modeled using a gamma distribution.

To model precipitation occurrence, the present work adopts a modified form of the model proposed by Garcia Guzman and Torrez (1985). It is a Markov chain model, but the transition probabilites from wet days are allowed to change as a function of precipitation amount on the previous day. The matrix of transition probabilities is given by

$$P(y) = \begin{bmatrix} 1 - P_{01} & P_{01} \\ P_{10}\theta^{y} & 1 - P_{10}\theta^{y} \end{bmatrix} . \tag{3.1}$$

Here $\theta$ is the "feedback parameter," which scales the dependence of the probabilities on the previous day's precipitation, and is constrained such that $0 < \theta \leq 1$. The parameter $y$ is taken to be the natural logarithm of the previous day's precipitation divided by the minimum observable amount (in the present case the minimum is trace = 0.1 mm), $P_{01}$ is the probability of a wet day following a dry day, and $P_{10}$ is the probability of a dry day following a wet day for which $y = 0$. Garcia Guzman and Torrez (1985) propose that $y$ be equal simply to the previous day's precipitation, but exploration of the nature of the dependence in observed grid-averaged data indicated that a logarithmic relationship was more appropriate. That is, the probability of consecutive wet days increases much more strongly as precipitation increases from trace to small measurable amounts than it does over comparable ranges of large precipitation amounts. Precipitation amount is scaled by the minimum observable amount before the logarithm is taken in order to insure that $0 < \theta^y \leq 1$.

The model (3.1) is of course a first-order Markov chain, since the dependence of a given day's precipitation state on the previous history of the system is completely specified by the precipitation state and amount on the previous day (e.g., Katz, 1985). For $\theta = 1$, the probabilities in (3.1) reduce to those for the usual two-state, first-order Markov model. The assumption of first-order time dependence does appear to be adequate to model the dependence structure of precipitation occurrence in the present data. When (3.1) is fit, with $\theta$ assumed equal to unity, to the 36 combinations of grid-box and calendar month, the BIC procedure (Katz, 1981; Schwartz, 1978) specifies first-order models in 29 cases.

The parameters in (3.1) are fit by maximum likelihood. For the probability of precipitation following a dry day, the estimate is given simply by the relative frequency. That is,

$$\hat{P}_{01} = N_{01} / (N_{00} + N_{01}) , \qquad (3.2)$$

where $\hat{P}_{01}$ is the estimate of $P_{01}$, $N_{00}$ is the number of dry days in the data followed by dry days, and $N_{01}$ is the number of dry days in the sample followed by wet days. [Note: The corresponding equation in Garcia Guzman and Torrez (1985) is in error and should read as above.] For the probability of precipitation following a wet day, the parameters $P_{10}$ and $\theta$ must be fit simultaneously. The log-likelihood function is

$$\Lambda\,(\theta, P_{10}; y) = N_{10} \ln (P_{10}) + (\sum_{\Omega_{10}} y) \ln (\theta) + \sum_{\Omega_{11}} \ln (1 - P_{10}\,\theta^{y}) . \qquad (3.3)$$

Here $\Omega_{10}$ and $\Omega_{11}$ denote wet days followed by dry days, and wet days followed by wet days, respectively. The two parameters are fit iteratively using the Newton-Raphson algorithm (e.g., Beaumont, 1980).

The model (3.1) evidently captures an important feature of the observed gridscale precipitation data. A generalized likelihood test (e.g., Morrison, 1976) rejects the null hypothesis $\{\theta = 1\}$ at the 5% level for all combinations of the three gridboxes and twelve calendar months except December for Box 1. The data for individual stations within the gridboxes support this model for precipitation occurrence much less strongly. Individual stations may receive precipitation from the same storm and contribute to the area-averaged precipitation on different (consecutive) days. This could account for the observed correlation of grid-scale precipitation occurrence with grid-averaged intensity on the previous day.

Precipitation intensities on wet days are modeled as independent gamma variates. That is, the probability density for daily precipitation, given that a nonzero amount occurs, is

$$f(x;\alpha,\gamma) = \frac{(x/\alpha)^{\gamma-1} \exp(-x/\alpha)}{\alpha\,\Gamma(\gamma)}, \tag{3.4}$$

where $\alpha$ is the "scale" parameter, $\gamma$ is the "shape" parameter, and $\Gamma$ denotes the gamma function. This flexible distribution is able to fit daily precipitation data quite well, and is commonly chosen for this purpose (Coe and Stern, 1982; Neyman and Scott, 1967; Stern and Coe, 1984; Waymire and Gupta, 1981). The parameters are fit, again by maximum likelihood using the Newton-Raphson procedure, separately for the cases of wet days following wet days and wet days following dry days. The generalized likelihood ratio test strongly rejects the null hypothesis of equality of the parameters for these two cases for all three gridboxes and in all months.

The modest serial correlation present in precipitation amounts for consecutive wet days (typical correlation coefficients for logarithmically- or square-root transformed data are in the range 0.2 to 0.3) is ignored. Reports in the literature indicate that serial correlation of nonzero daily precipitation amounts is weak for individual station data as well (Chin and Miller, 1980; Katz, 1977b).

### 3.3.2. Temperature

Maximum and minimum temperatures are modeled using a bivariate autoregressive model. This model is a generalization of the usual univariate autoregressive model (e.g., Box and Jenkins, 1976), and may be written as

$$(\mathbf{T}_t - \bar{\mathbf{T}}_t) = \sum_{i=1}^{p} \boldsymbol{\Phi}_i \, (\mathbf{T}_{t-i} - \bar{\mathbf{T}}_{t-i}) + \boldsymbol{\epsilon}_t \, . \tag{3.5}$$

Here $\mathbf{T}$ is the vector of temperatures ($T_{max}$, $T_{min}$), the overbars denote the time-dependent mean values, p is the order of the autoregression, and the $\boldsymbol{\Phi}$'s are (2x2) matrices of the autoregressive constants to be determined. The $\boldsymbol{\epsilon}$'s are vectors of Gaussian random noise with zero mean, and variance-covariance matrix $\mathbf{V}$. Equivalent models are treated in the literature in, for example, Jones (1964), Tiao and Box (1981), and Whittle (1963). Note that (3.5) allows intercorrelation of the Gaussian stochastic forcing of the model, but requires that it be serially independent. Mean temperatures are allowed to vary continuously throughout the year by fitting Fourier series, separately for each gridbox:

$$\bar{T}_t = A_o + \sum_{m=1}^{6} A_m \sin[(2\pi m t)/365 + B_m] \, , \tag{3.6}$$

where the A's are the Fourier amplitudes, the B's are the phases, and t denotes the julian date. Only harmonics deemed significant in the manner described in Section 2.2 are retained.

As in the case of precipitation, the other parameters in (3.5) are fit separately for each combination of gridbox and calendar month.

Also, separate sets of all temperature parameters are fit for wet and dry days, as is usual in stochastic weather models (e.g., Bond, 1979; Larsen and Pense, 1982; Richardson, 1981). Thus, the parameters that characterize the temperature series -- mean, autocorrelation structure, variance, and cross-correlation -- are regarded as conditional on the precipitation state, and vary throughout the year.

Although use of the multivariate generalization of the Yule-Walker equations to fit the parameters in (3.5) has been advocated (Jones, 1964; Whittle 1963), this method was found to give unstable results for some subsets of the present data. In particular, the procedure can produce estimates of $\underset{\sim}{V}$ with determinants which increase with p. In the present work, parameters were fit to (3.5) directly by multivariate least-squares (e.g., Johnson and Wichern, 1982), modified to include no constant term (i.e., the design matrices have 2p rather than 2p+1 columns). Parameter estimation by least-squares is equivalent to multivariate maximum likelihood estimation for pure autoregressions (Hillmer and Tiao, 1979).

The appropriate order of the autoregressions (3.5) was estimated using an extension of the BIC procedure as formulated for univariate autoregressions (Katz, 1982). In general, the form of the BIC statistic is (Schwartz, 1978)

$$\mathrm{BIC}\,(p) = \Lambda\,(p) - \frac{q \ln (N)}{2}, \tag{3.7}$$

where p indicates the order of the model being tested, $\Lambda(p)$ is the log-likelihood for that model, q is the number of parameters estimated from the data, and N is the sample size. Written in this way, the order p that maximizes (3.7) is chosen as the most appropriate. For the model (3.5), where bivariate normal stochastic forcing (noise) is assumed, (3.7) becomes

$$\mathrm{BIC}\ (p) \;=\; \frac{-\,N\ \ln\ (\det\ [\hat{\underset{\sim}{V}}])}{2} \;-\; \frac{(4p + 4)\ \ln\ (N)}{2}, \qquad (3.8)$$

where $\hat{\underset{\sim}{V}}$ is the sample estimate of the variance-covariance matrix of the Gaussian noise, since 4p autoregressive coefficients, two variances, one covariance, and approximately one parameter representing the mean (per month) are estimated from the data.

Autoregressions of order 0 through 5 were fit to the observed data. Over the 72 combinations of gridbox, month, and precipitation state, p=1 was chosen in 19 cases, p=2 was chosen in 43 cases, and p=3 was chosen in 10 cases. Sequential F-tests (Anderson, 1958; Jones, 1964) produced substantially the same results. For those cases where BIC(3) was maximum, the values were close to those for BIC(2), so that, for uniformity, all temperature series were modeled as second-order bivariate autoregressions. Nearly all empirical residuals of (3.5) exhibit lag autocorrelations of magnitude less than 0.05, and appear to be have distributions that approximate the Gaussian. Typical examples of the latter are shown, converted to standard normal form (i.e., values minus sample means and divided by sample standard deviations) in Figures 9a,b and 10a,b. These results show Box 2 residuals for January minimum temperatures on dry and wet days, and residuals for July maximum temperatures on dry and wet days, respectively.

Once the parameter estimates for (3.5) have been obtained,

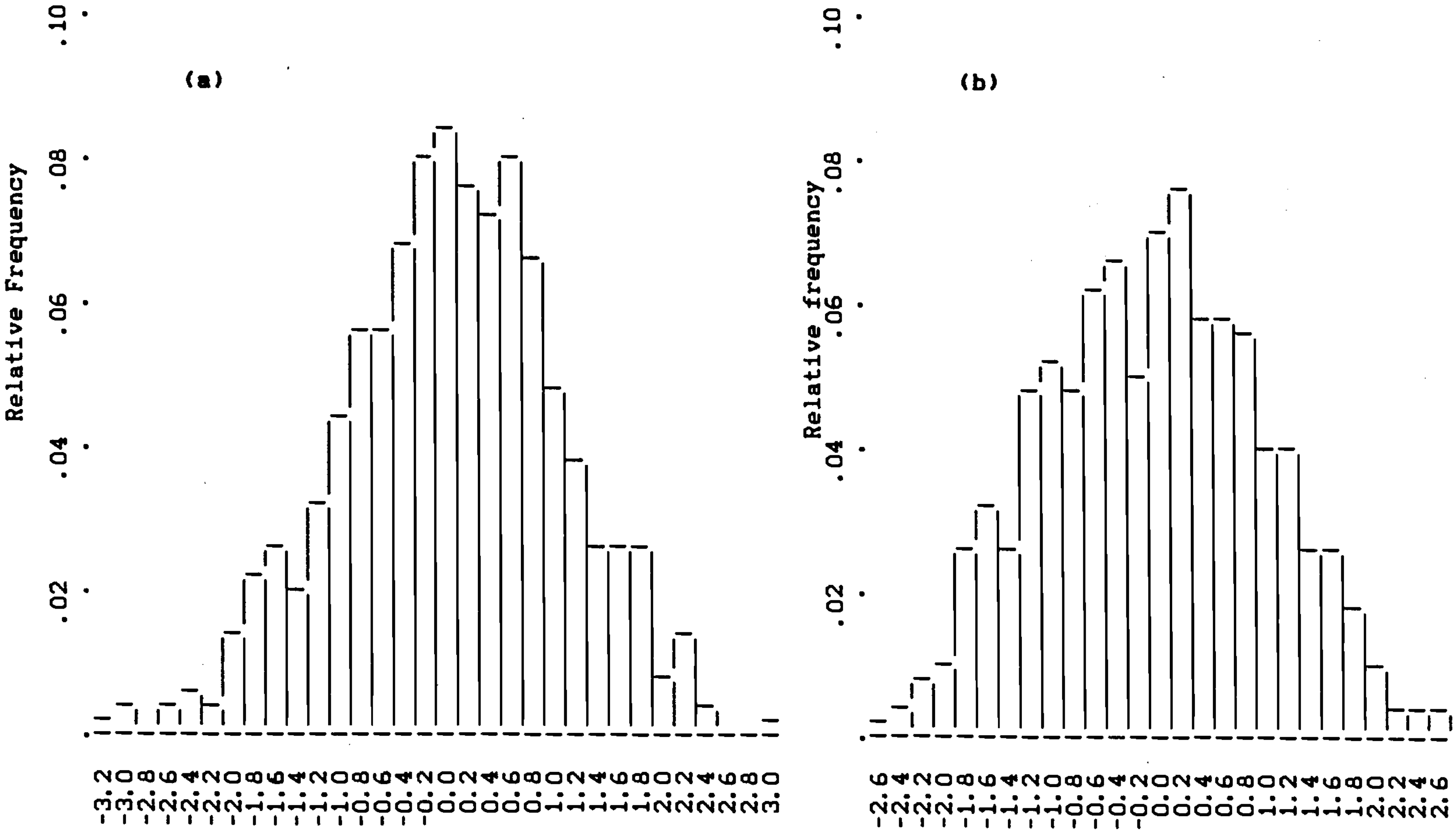


**Figure 9.** Empirical distributions of residuals for the autoregressive model (3.5) for January Box 2 minimum temperatures, converted to standard normal form. (a) dry days, (b) wet days.

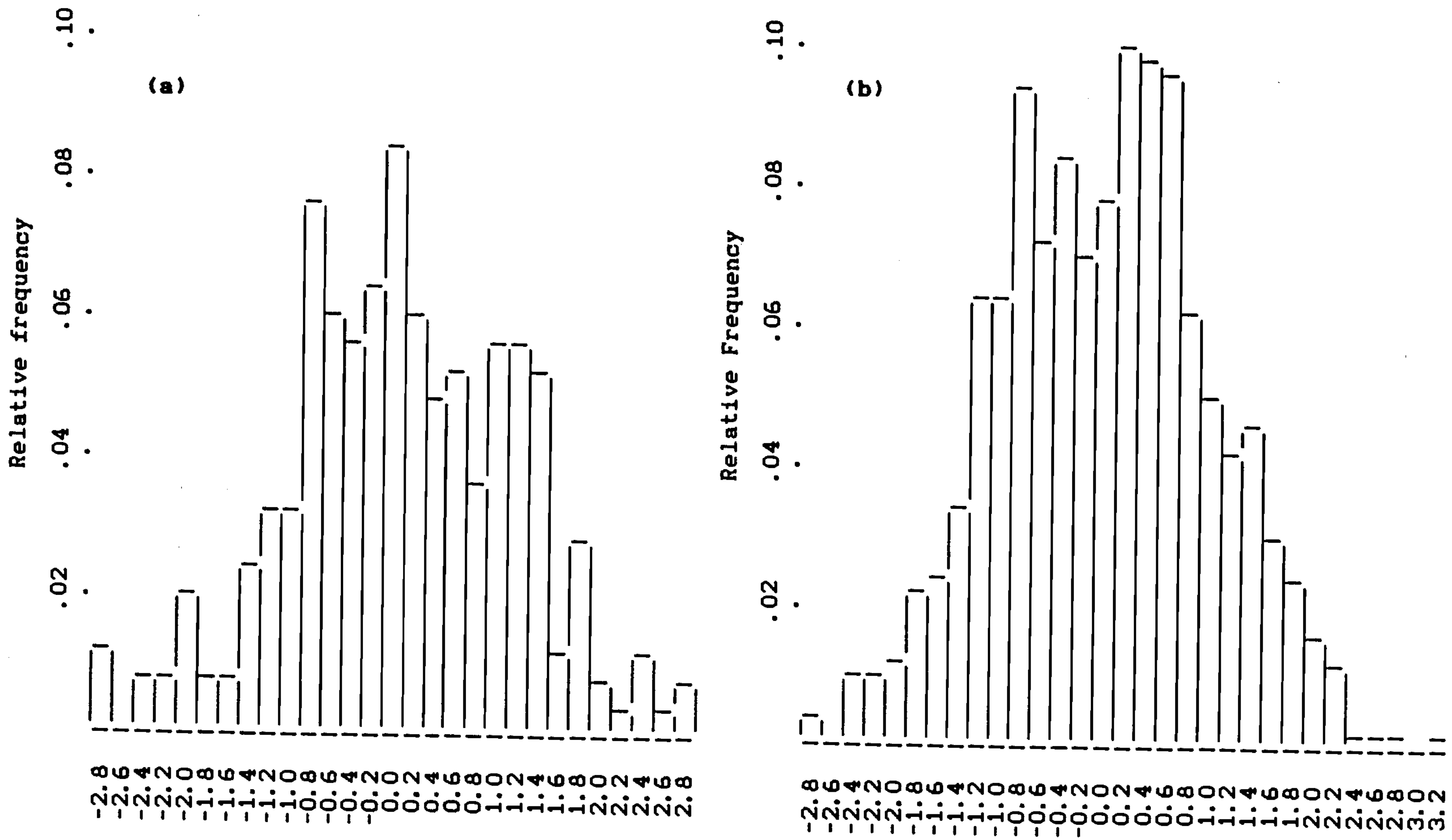


**Figure 10.** Empirical distributions of residuals for the autoregressive model (3.5) for July Box 2 maximum temperatures, converted to standard normal form. (a) dry days, (b) wet days.

implementation as a generating algorithm for Monte Carlo simulations is direct except for the specific nature of the random noise term $\underset{\sim}{\epsilon}$. Gaussian random number generators (e.g., Box and Muller, 1958) produce independent variates with zero mean and unit variance. A two-dimensional vector of these quantities, say $\underset{\sim}{g}$, has variance-covariance matrix

$$E \left[ \underset{\sim}{g}_t \; \underset{\sim}{g}'_t \right] = \underset{\sim}{I} \quad , \tag{3.9}$$

where E denotes statistical expectation, the prime denotes transpose, and $\underset{\sim}{I}$ is the (2 x 2) identity matrix. Some transformation, embodied in a (2 x 2) matrix $\underset{\sim}{C}$, is required, such that

$$\underset{\sim}{\epsilon}_t = \underset{\sim}{C} \; \underset{\sim}{g}_t \tag{3.10}$$

and

$$E \left[ \underset{\sim}{\epsilon}_t \; \underset{\sim}{\epsilon}'_t \right] = \underset{\sim}{V} \; . \tag{3.11}$$

Substitution of (3.9) and (3.10) into (3.11) yields

$$\underset{\sim}{C} \; \underset{\sim}{C}' = \underset{\sim}{V} \; . \tag{3.12}$$

Since any solution of (3.12) will produce the desired result and $\underset{\sim}{V}$ is symmetric, a simple procedure is to use the Cholesky (lower triangular) factorization of $\underset{\sim}{V}$ to calculate $\underset{\sim}{C}$ (Bratley et al., 1983), and substitute (3.10) into (3.5).

## 3.4 Intercomparison of GCM-Derived and Observed Data

### 3.4.1. Precipitation

Annual cycles for the parameter $P_{01}$ for gridboxes 1,2,and 3 are shown in Figures 11a, 12a, and 13a, respectively. The probability values in these figures are plotted on a log-odds scale, that is

$$\lambda ( P ) = \ln [ P / (1 - P)] \quad . \tag{3.13}$$

Cycles for observed data as well as for data from the 1X- and 2X-$CO_2$ GCM simulations are shown. The observed data for all three boxes exhibit strong and similar annual cycles, indicating that dry spells are most likely to persist in the cool season and least likely to persist in the warm season. The general shapes (and, for Box 2, the magnitudes) of the cycles for the model data are similar to those for the observed data for all except the summer months. For these months both model runs evidently exhibit longer dry spells than are present in the observations. Figures 11b, 12b, and 13b present estimates for the parameter $P_{10}$, derived using data from the three gridboxes, and again on a log-odds scale. For the case of estimates derived from the observations, the minima during the summer months indicate that the tendency for wet spells to terminate is lowest during this part of the year. Thus, both of these measures of precipitation occurrence favor wet days during the warm season. The general shape of the cycles derived from the GCM data is similar, although for most months the magnitudes are substantially larger. Again, differences between parameters derived from the two GCM data sets are small, and only that

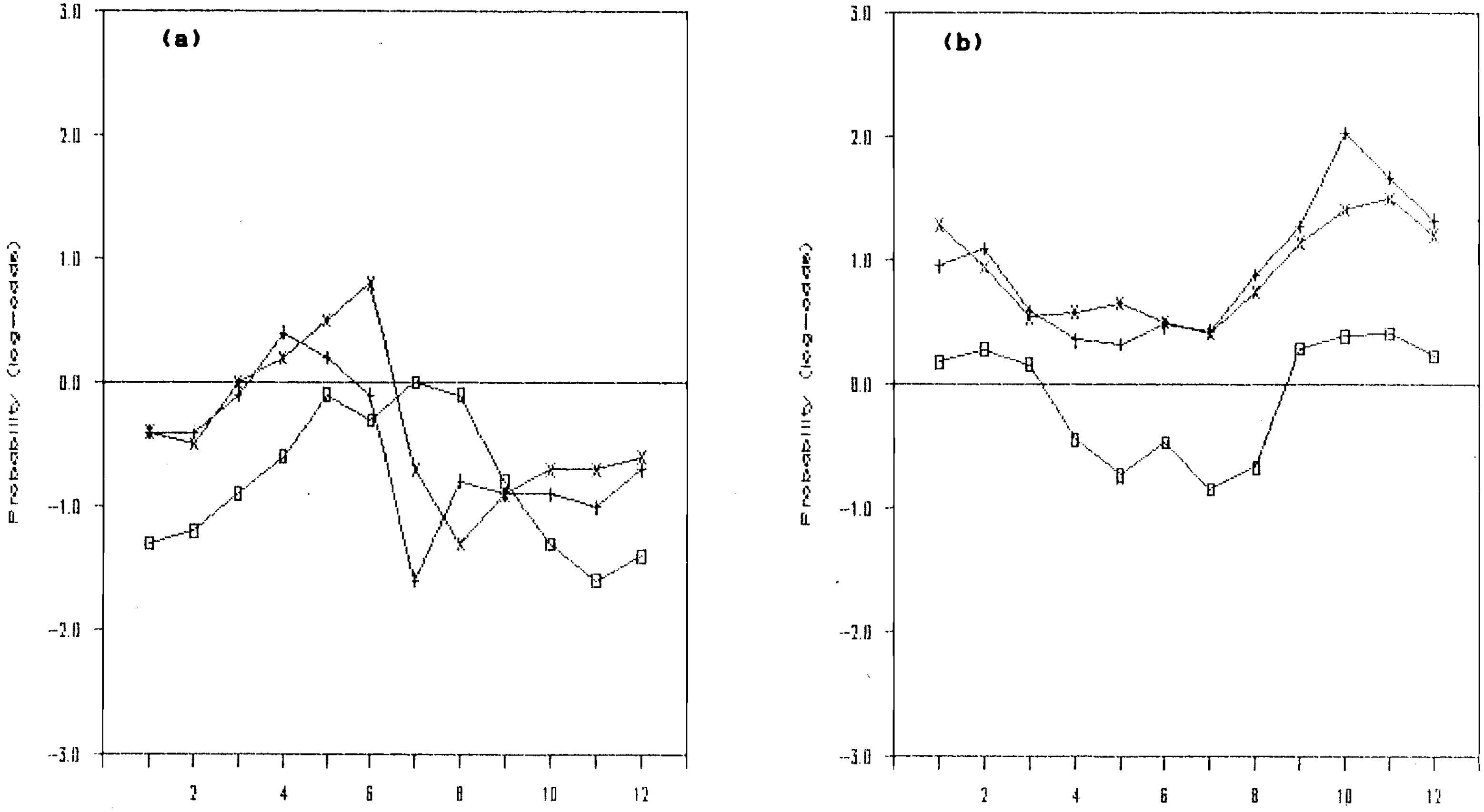


Figure 11. Annual cycles of the (log-odds) probabilities of (a) a wet day following a dry day, $P_{01}$, and (b) a dry day following a wet day with minimum observable precipitation, $P_{10}$ for Box 1; observations (■), 1X-$CO_2$ data (X), and 2X-$CO_2$ data (+).

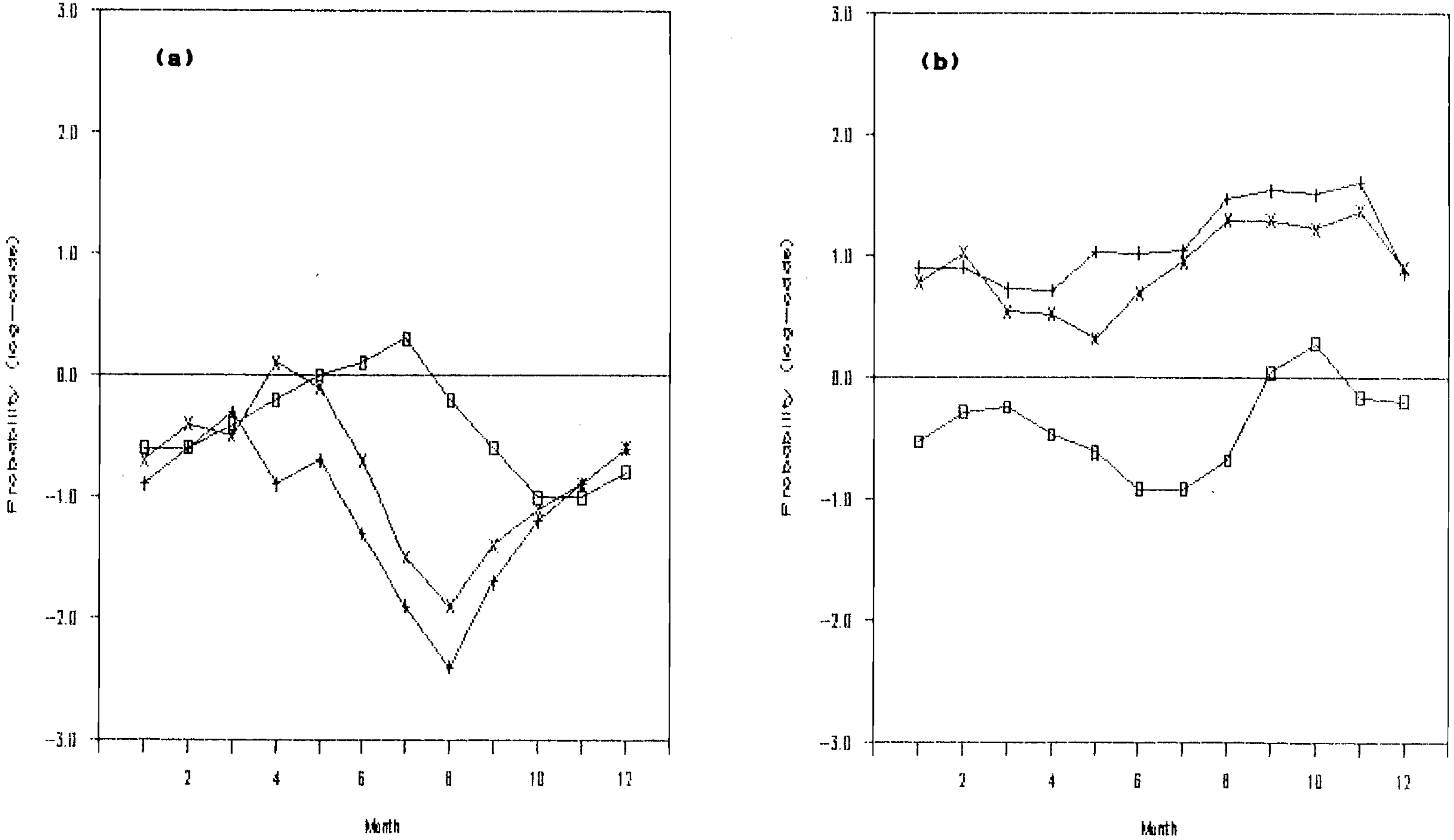


Figure 12. Annual cycles of the (log-odds) probabilities of (a) a wet day following a dry day, $P_{01}$, and (b) a dry day following a wet day with minimum observable precipitation, $P_{10}$ for Box 2; observations (▪), 1X-$CO_2$ data (X), and 2X-$CO_2$ data (+).

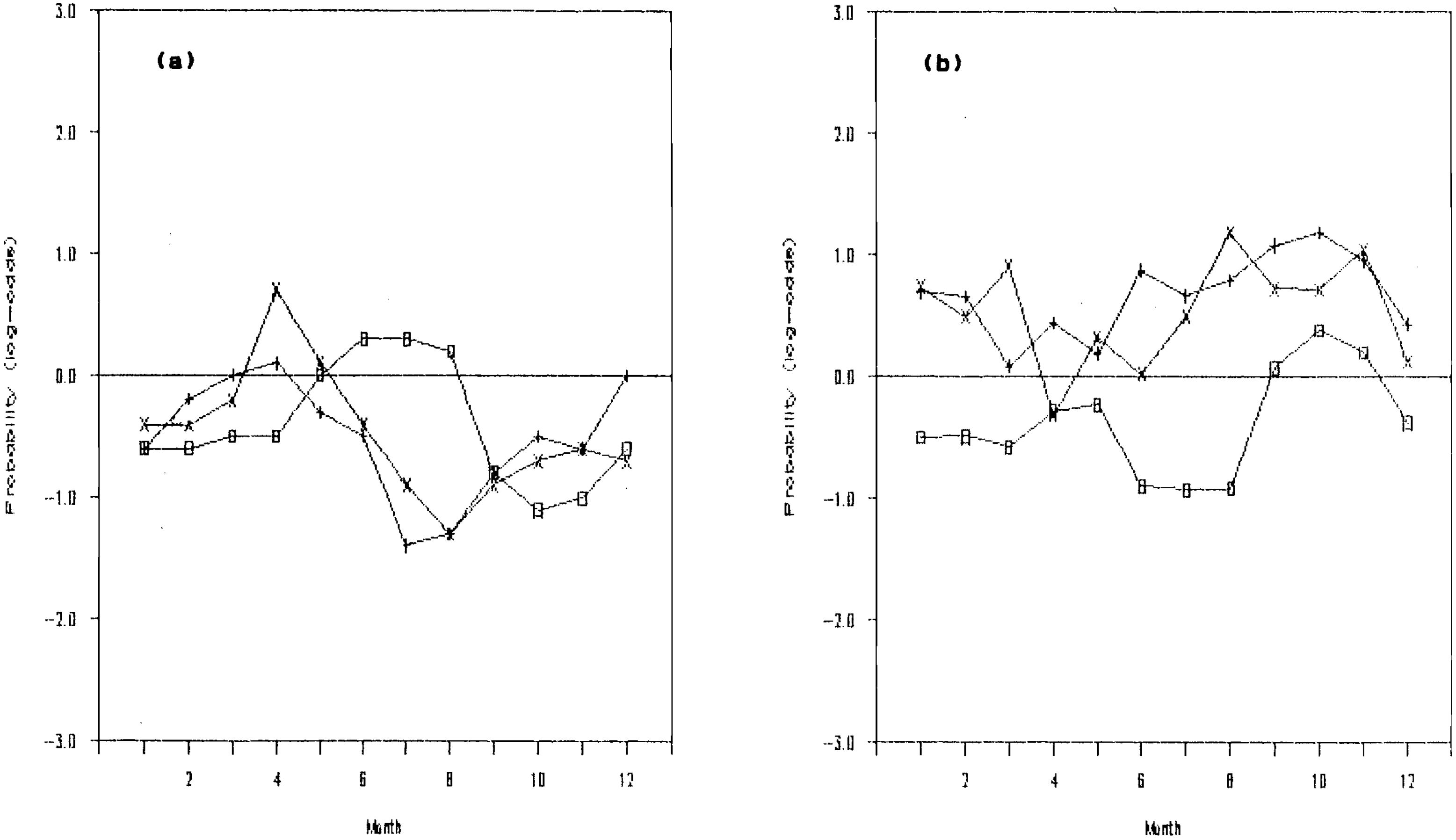


Figure 13. Annual cycles of the (log-odds) probabilities of (a) a wet day following a dry day, $P_{01}$, and (b) a dry day following a wet day with minimum observable precipitation, $P_{10}$ for Box 3; observations (▪), 1X-$CO_2$ data (X), and 2X-$CO_2$ data (+).

for Box 3 in March is significant at the 5% level.

Although the general shapes of the annual cycles of $P_{01}$ values derived from the two model data sets are quite similar, some statistically significant differences exist. These differences were assesed using the normal approximation to the binomial, which Gabriel (1959) has found to be adequate for this type of data using a sample size approximately 20% of those available in the present context. Table 16 indicates the months for which the differences are significant, and the level and direction of these differences. For example, "))" indicates that the $P_{01}$ value for the 2X-$CO_2$ data is significantly greater than that for the 1X-$CO_2$ data at the 1% level, and "(" indicates that $P_{01}$ for the 2X-$CO_2$ data is significantly less than that for the 1X-$CO_2$ data at the 5% level. It is evident that the primary difference is a relative decrease in $P_{01}$ (increase in the probability persistence of dry spells) during the warm season.

The corresponding data for the annual cycles of the "feedback parameter" $\theta$ are given in Figures 14a,b,c. Annual cycles in the parameter estimates derived from the observational data are less clear than for the case of $P_{01}$, although the larger interannual changes are statistically significant, as judged by the approximation of the sampling distribution of the maximum likelihood estimatiors to the normal distribution. As in the case of $P_{01}$, the annual cycles derived from the two GCM data sources correspond to each other closely, and none of the differences for particular months are significant at the 5% level.

Figures 15, 16, and 17 show the annual cycles for the scale parameter $\alpha$, of the gamma distribution model (3.4) for precipitation

Table 16. Distribution in time of significant differences in the parameter $P_{01}$ between 1X- and 2X-$CO_2$ model. Single symbols indicate differences significant at the 5% level and double symbols indicate differences significant at the 1% level. The symbol "<" indicates the value for 2X-$CO_2$ is less than that for 1X-$CO_2$.

| Box No. | Jan | Feb | Mar | Apr | May | Jun | Jul | Aug | Sep | Oct | Nov | Dec |
|---|---|---|---|---|---|---|---|---|---|---|---|---|
| 1 | | | | | | < | << | | | | | |
| 2 | | | | << | < | < | | < | | | | |
| 3 | | | | | | | < | | | | | >> |

Table 17. As Table 16, but for gamma distribution scale parameter, α, on consecutive wet days.

| Box No. | Jan | Feb | Mar | Apr | May | Jun | Jul | Aug | Sep | Oct | Nov | Dec |
|---|---|---|---|---|---|---|---|---|---|---|---|---|
| 1 | | | > | | | | | | | | | |
| 2 | | | | | | | >> | | | | | |
| 3 | | | | | | | >> | | | | >> | > |

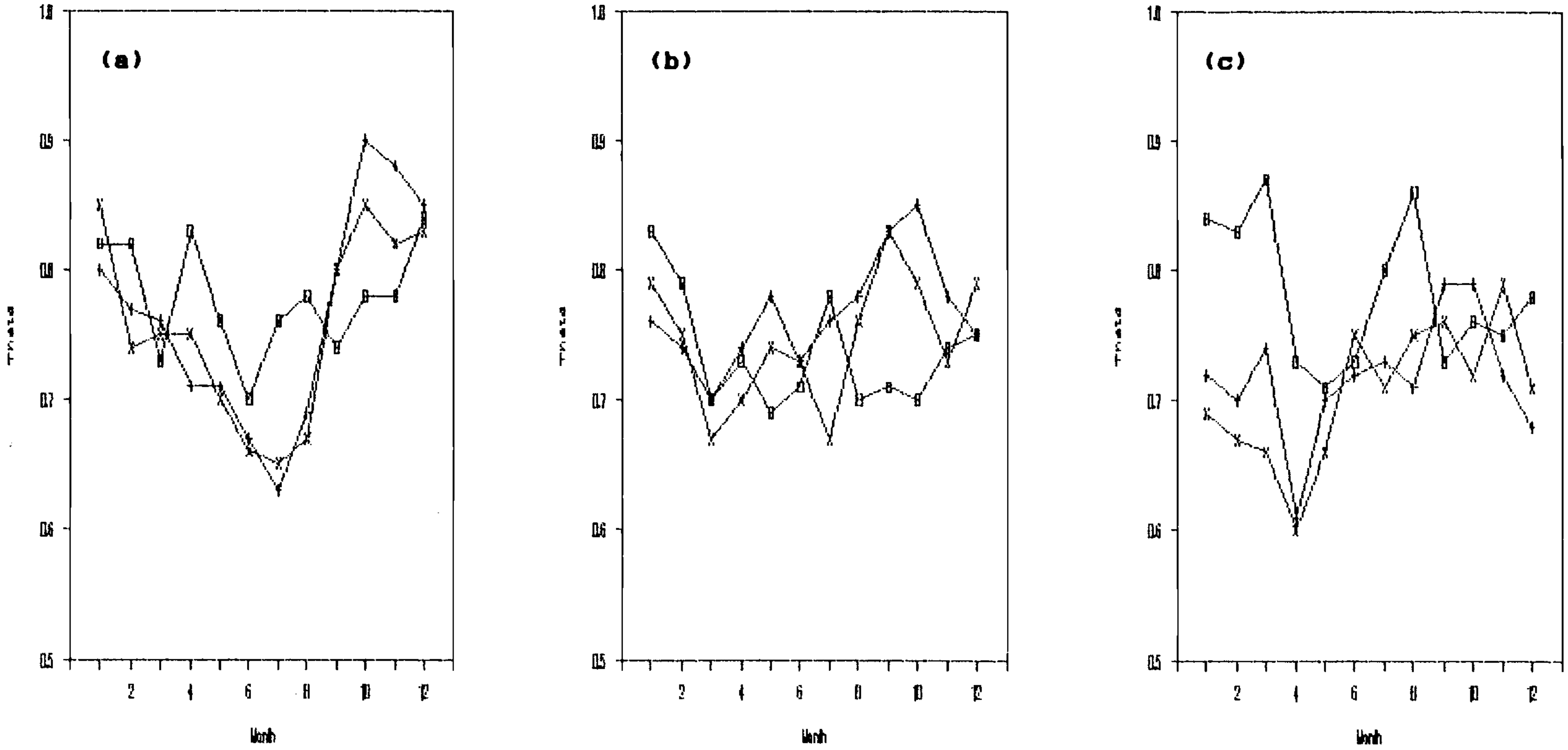


Figure 14. Annual cycles for the "feedback" parameter, θ in (a) Box 1, (b), Box (2), and (c) Box 3; for observations (▪), $1X\text{-}CO_2$ data (X), and $2X\text{-}CO_2$ data (+).

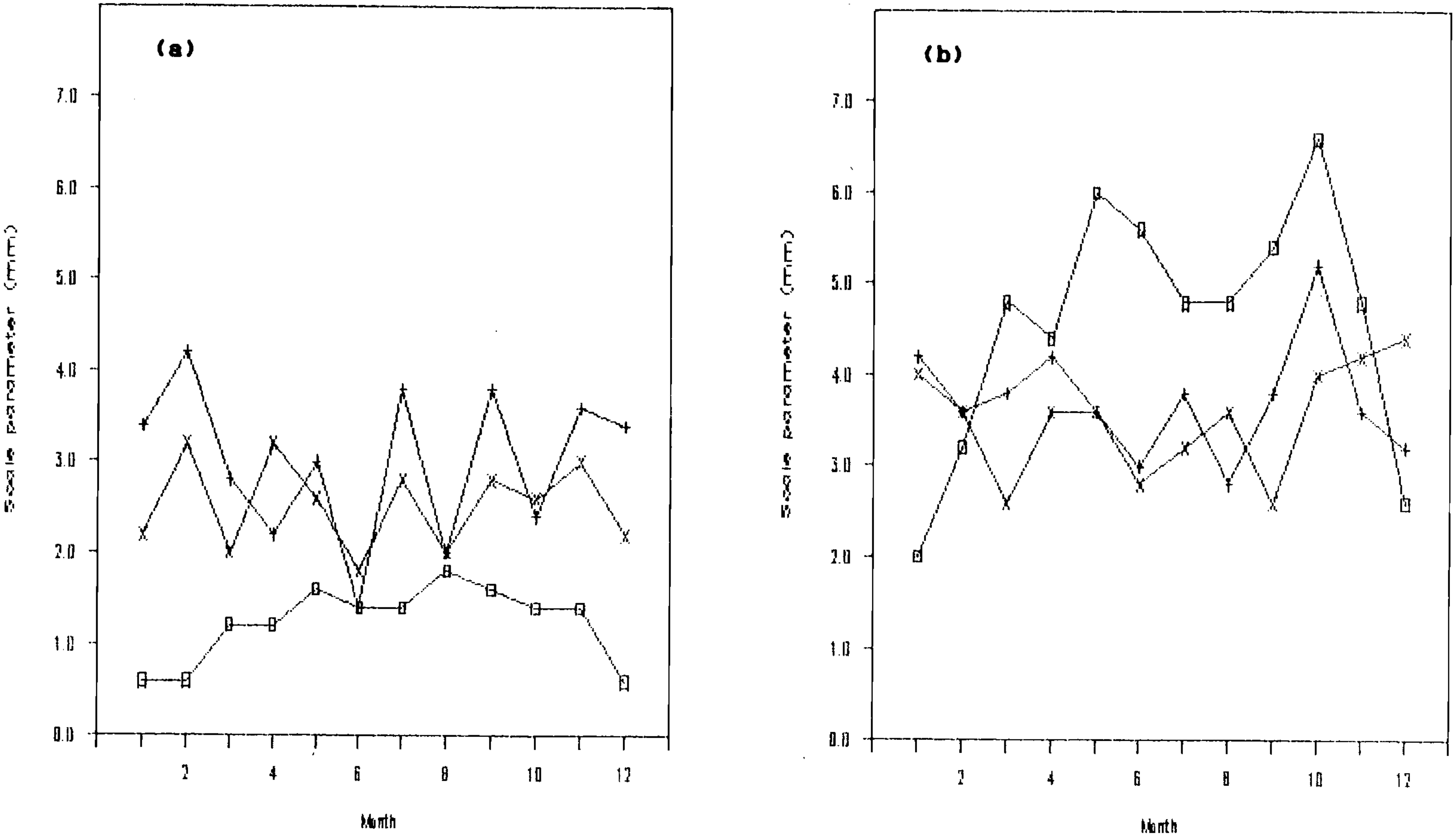


**Figure 15.** Annual cycles of the scale parameter, α, of the gamma distribution describing precipitation intensity for Box 1 (a) wet days following dry days, and (b) wet days following wet days; for observations (■), 1X-$CO_2$ data (X), and 2X-$CO_2$ data (+).

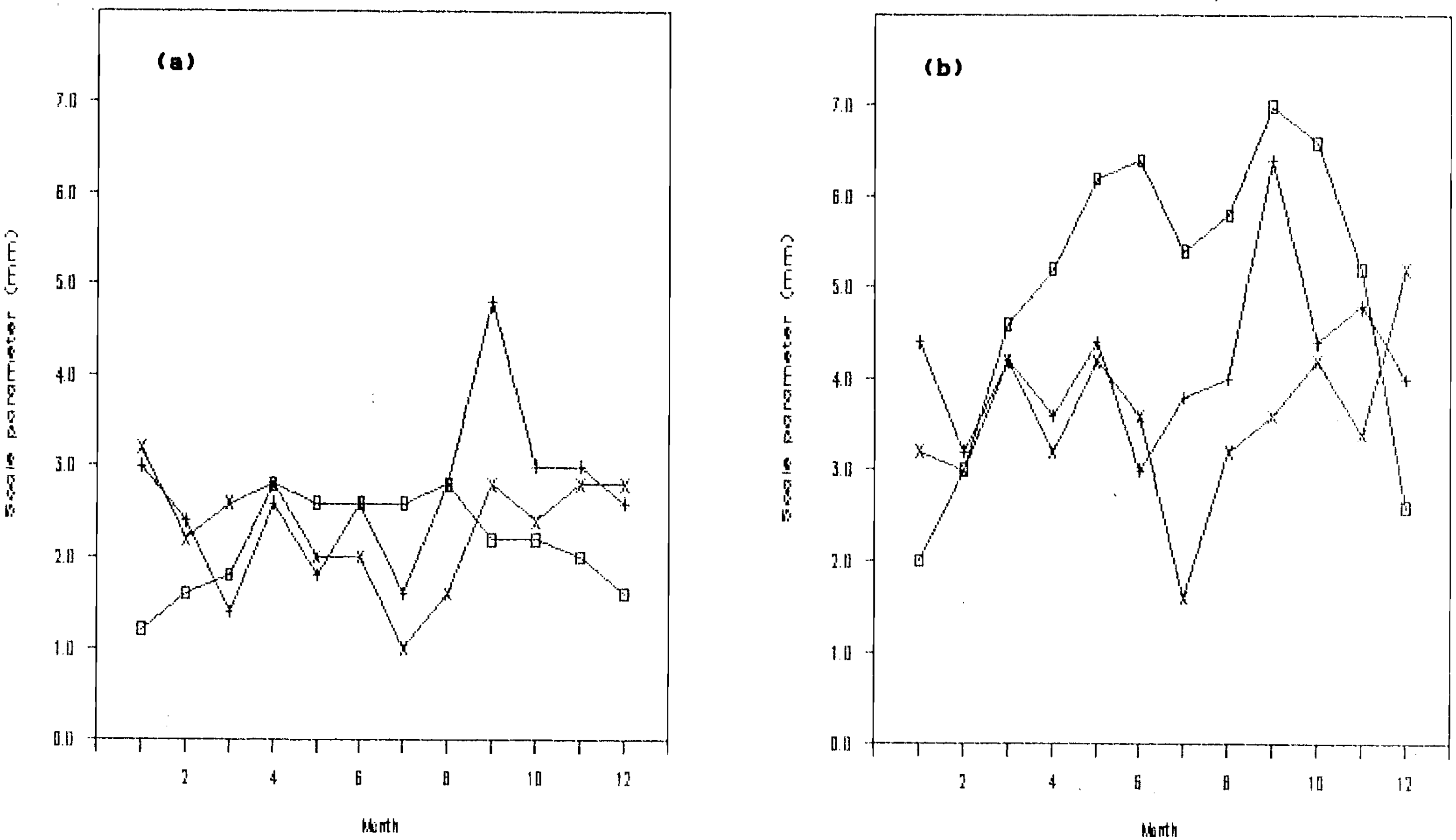


Figure 16. Annual cycles of the scale parameter, α, of the gamma distribution describing precipitation intensity for Box 2 (a) wet days following dry days, and (b) wet days following wet days; for observations (▪), $1X\text{-}CO_2$ data (X), and $2X\text{-}CO_2$ data (+).

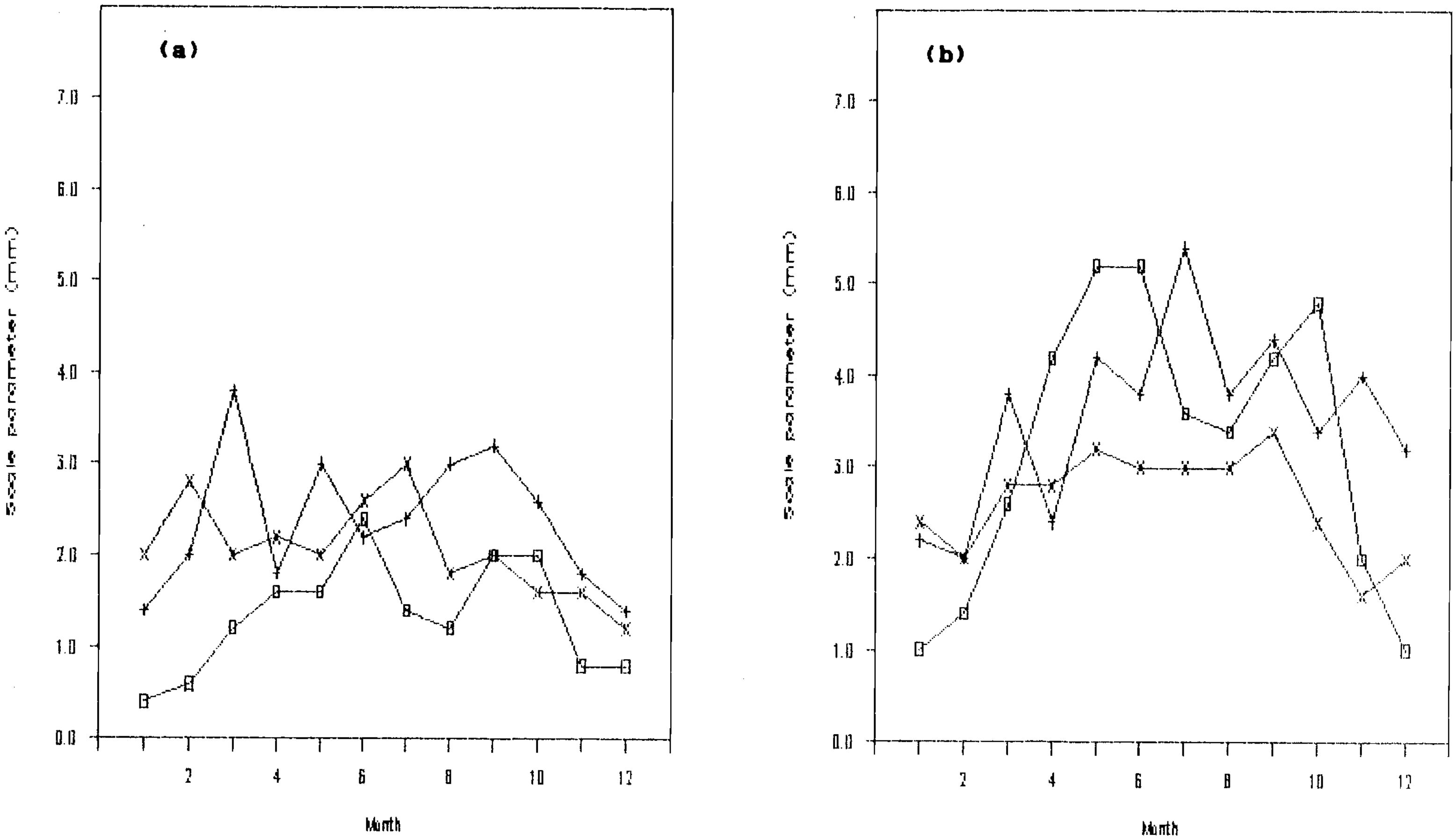


Figure 17. Annual cycles of the scale parameter, α, of the gamma distribution describing precipitation intensity for Box 3 (a) wet days following dry days, and (b) wet days following wet days; for observations (▪), 1X-$CO_2$ data (X), and 2X-$CO_2$ data (+).

intensity for Boxes 1, 2, and 3, respectively. The (a) panels in these figures are for precipitation intensities following dry days, and the (b) panels are precipitation intensities for consecutive wet days. Again, the largest values derived from the observational data occur in the warmer months, reflecting the fact that precipitation is more intense in this region during the summer. The seasonal difference is most striking when precipitation has occurred on the previous day. The corresponding curves for the GCM-derived parameters exhibit considerably less fluctuation throughout the year. For the case of the preceding day dry the differences are significant at the 5% level (as judged by the generalized likelihood test) only for Box 3 in March. More of the differences between the two GCM data sets are significant for the case of consecutive wet days, and at higher significance levels. These results are presented in Table 17. In particular, large increases in July precipitation intensity are indicated for Boxes 2 and 3.

Finally, Figures 18, 19, and 20 present the corresponding annual cycles for the shape parameter $\gamma$ of the precipitation intensity distributions. With the exception of the GCM-derived curves for Box 1 (Figure 18), all are fairly flat. The GCM-derived curves are rather noisy relative to those for the observations. Three of the monthly differences are judged to be significant, however; these are Box 1 August (1% level), Box 2 July (5% level), and Box 3 November (5% level).

### 3.4.2. Temperature

Figure 21 shows the annual cycles of maximum and minimum

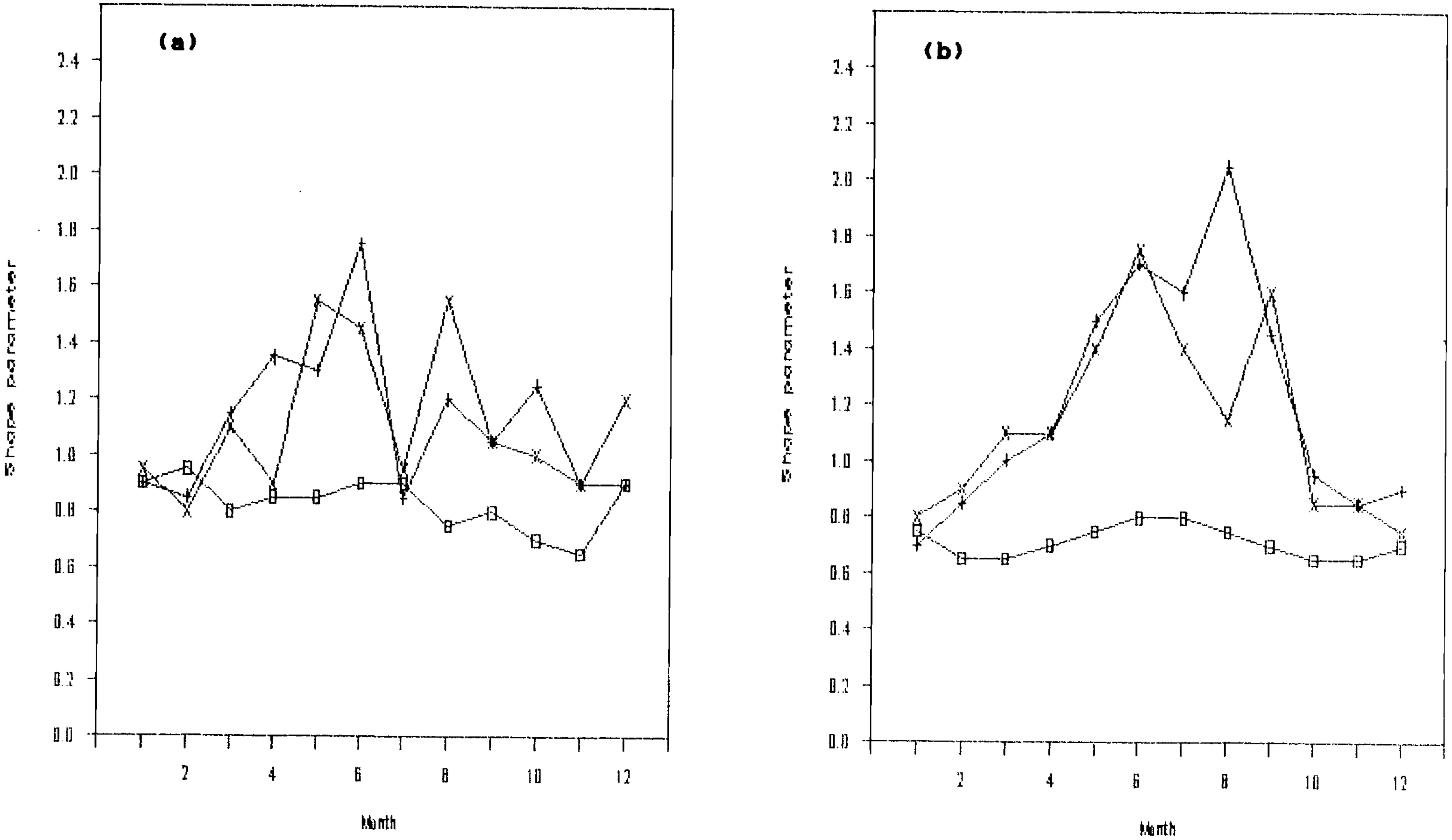


Figure 18. Annual cycles of the shape parameter, $\gamma$, of the gamma distribution describing precipitation intensity for Box 1 (a) wet days following dry days, and (b) wet days following wet days; for observations (▪), 1X-$CO_2$ data (X), and 2X-$CO_2$ data (+).

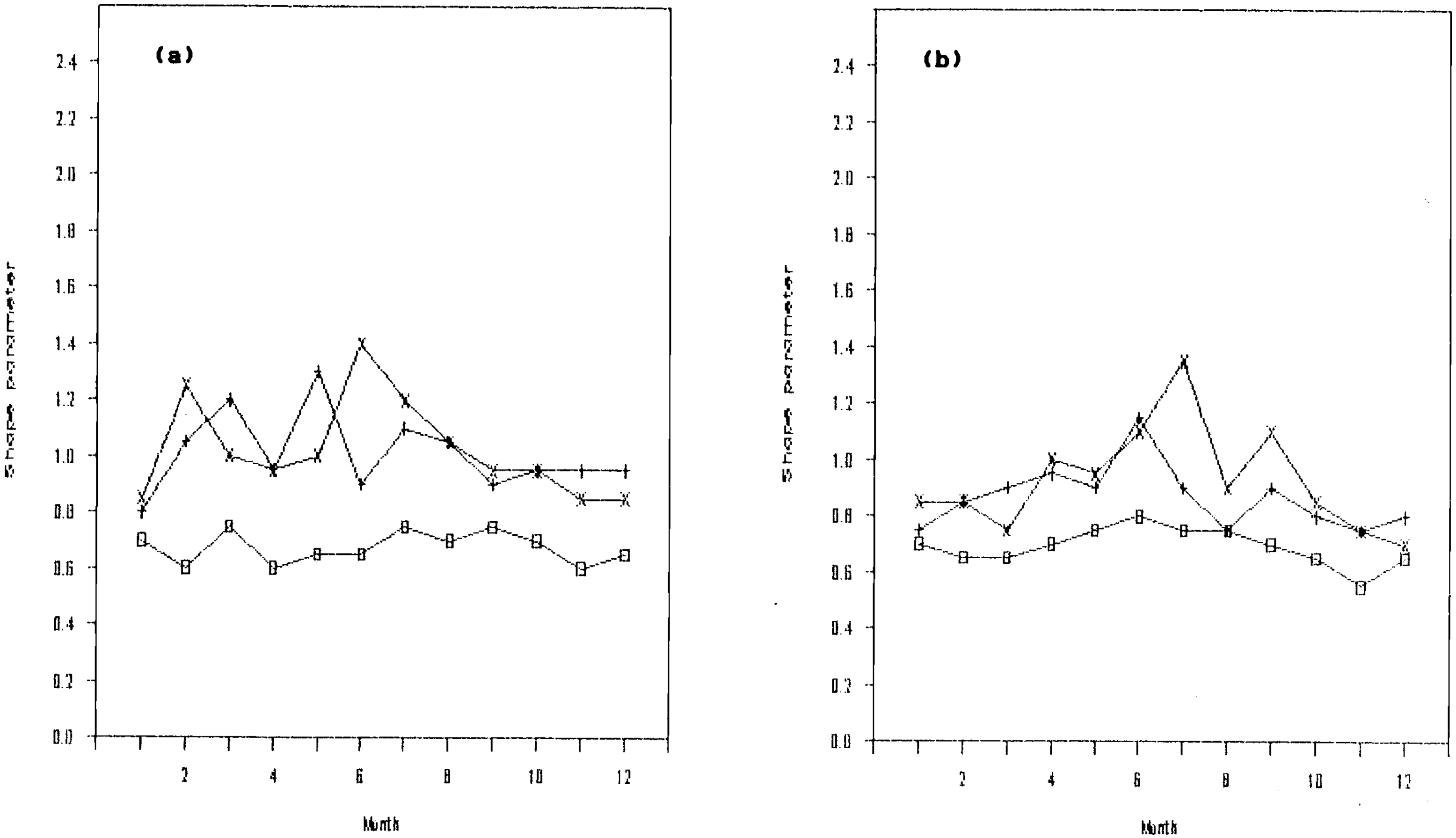


Figure 19. Annual cycles of the shape parameter, $\gamma$, of the gamma distribution describing precipitation intensity for Box 2 (a) wet days following dry days, and (b) wet days following wet days; for observations (▪), 1X-$CO_2$ data (X), and 2X-$CO_2$ data (+).

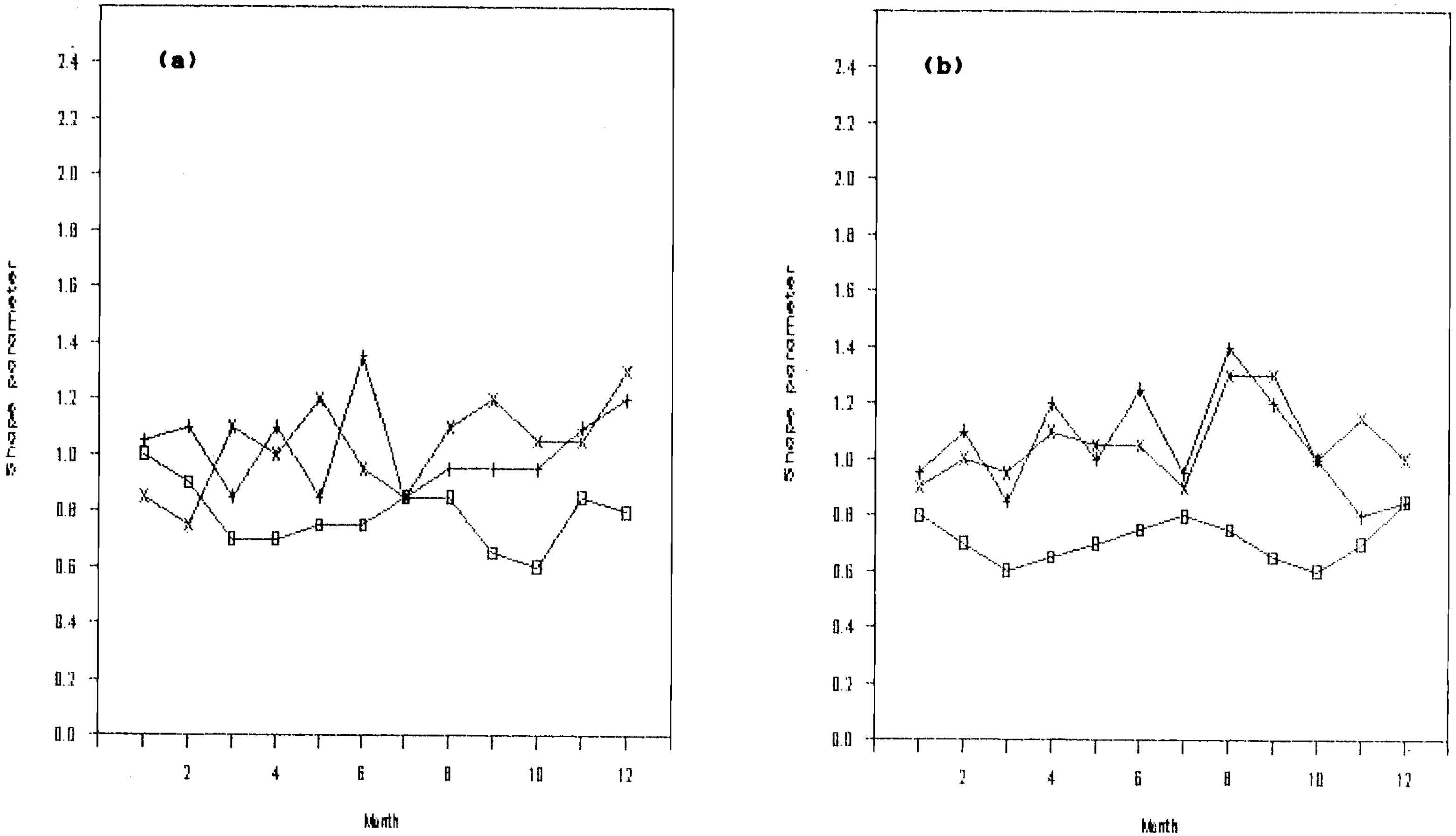


Figure 20. Annual cycles of the shape parameter, $\gamma$, of the gamma distribution describing precipitation intensity for Box 3 (a) wet days following dry days, and (b) wet days following wet days; for observations (▪), $1X\text{-}CO_2$ data (X), and $2X\text{-}CO_2$ data (+).

temperatures, for each of the three data sources, reconstructed from the "significant" Fourier modes for Box 1. Panel (a) shows dry day maxima, panel (b) shows dry day minima, panel (c) shows wet day maxima, and panel (d) shows wet day minima. Figures 22 and 23 present the corresponding information for Boxes 2 and 3. It is evident that the 1X-$CO_2$ climates in these gridboxes are in general substantially colder than the observations, which is a common feature of GCMs (Barnett, 1986). It is also clear that 2X-$CO_2$ climate is substantially warmer than the 1X-$CO_2$ climate. Interestingly, the largest differences between the GCM-derived temperatures occur during the warm season in the two southernmost gridboxes. Although it would be possible to conduct formal tests of statistical significance for differences in average temperature by, say, calendar month (Katz, 1982), the differences are so large in comparison to the white-noise variances (presented later in this section) scaled by the (effective) sample sizes, that such tests are scarcely necessary.

Although the magnitudes of the GCM temperatures exhibit large errors, the amplitudes and phases, particularly for the annual modes, are in closer agreement. Differences in the former are on the order of 2°C, and differences in the latter are approximately 10 days.

The autocorrelation structure of the temperature data is modeled in (3.5) by the parameter matrices $\underset{\sim}{\Phi}_i$. Comparison of variations through the year, or comparison of autocorrelation structure for different data sources, is difficult in that eight coefficients must be judged simultaneously for the second-order autoregressions considered here. One approach to intercomparison could be examination of spectra and cross-spectra, either derived directly from the data

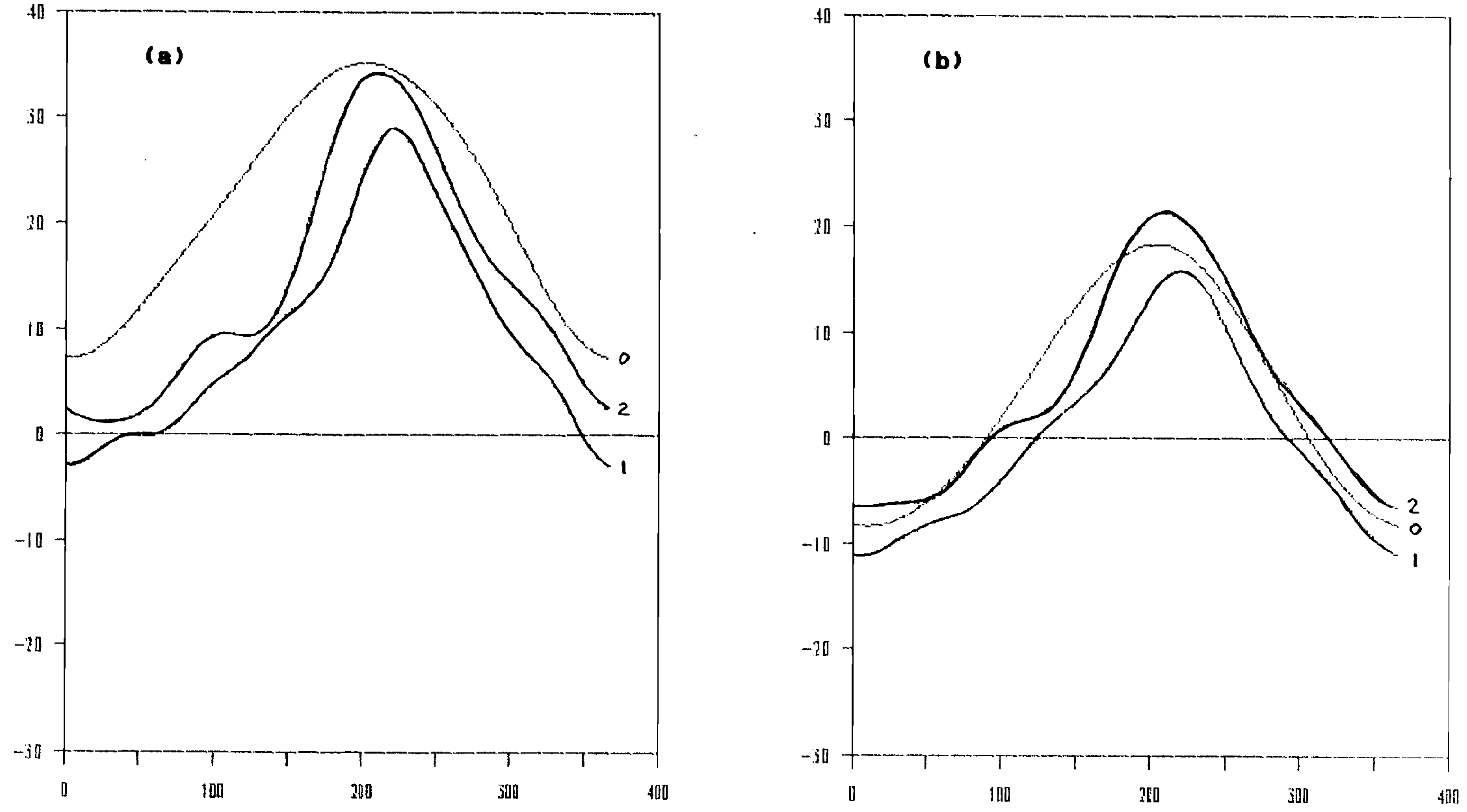


Figure 21. Annual temperature cycles for Box 1 observed (broken line), 1X-$CO_2$, and 2X-$CO_2$ data: (a) dry day maximum temperatures, and (b) dry day minimum temperatures.

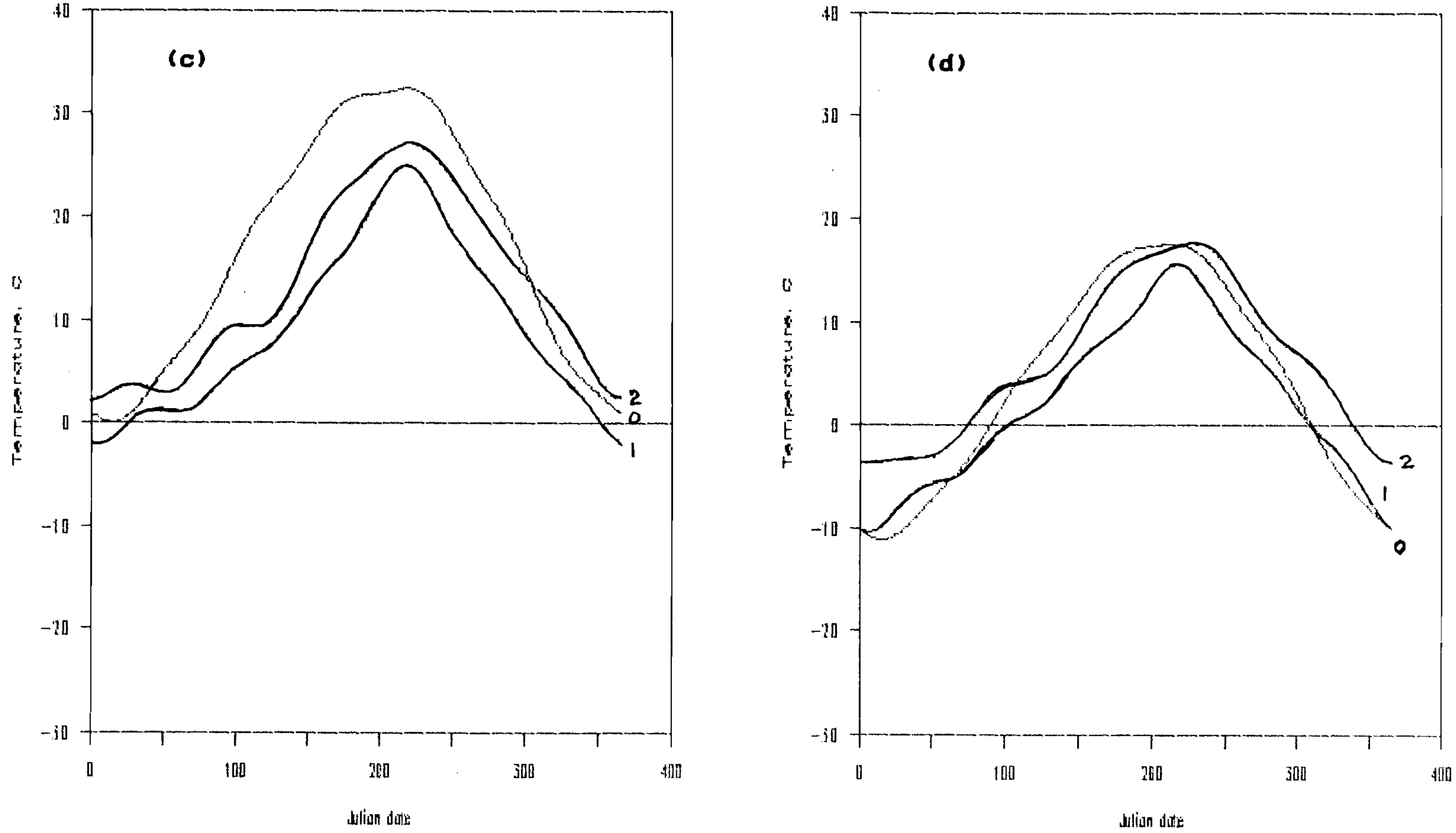


Figure 21, continued.
(c) wet day maximum temperatures, and (d) wet day minimum temperatures.

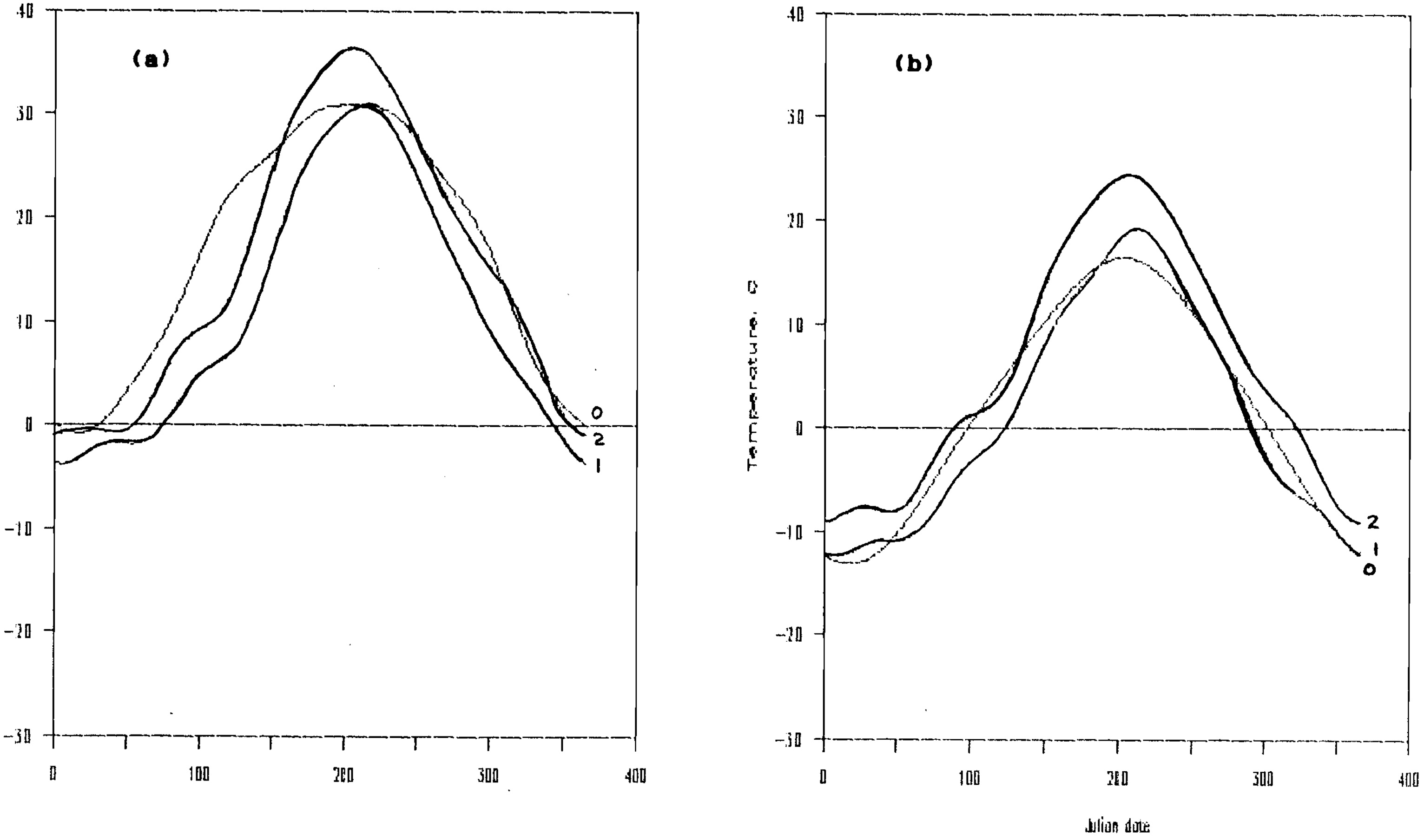


Figure 22. Annual temperature cycles for Box 2 observed (broken line), $1X\text{-}CO_2$, and $2X\text{-}CO_2$ data: (a) dry day maximum temperatures, and (b) dry day minimum temperatures.

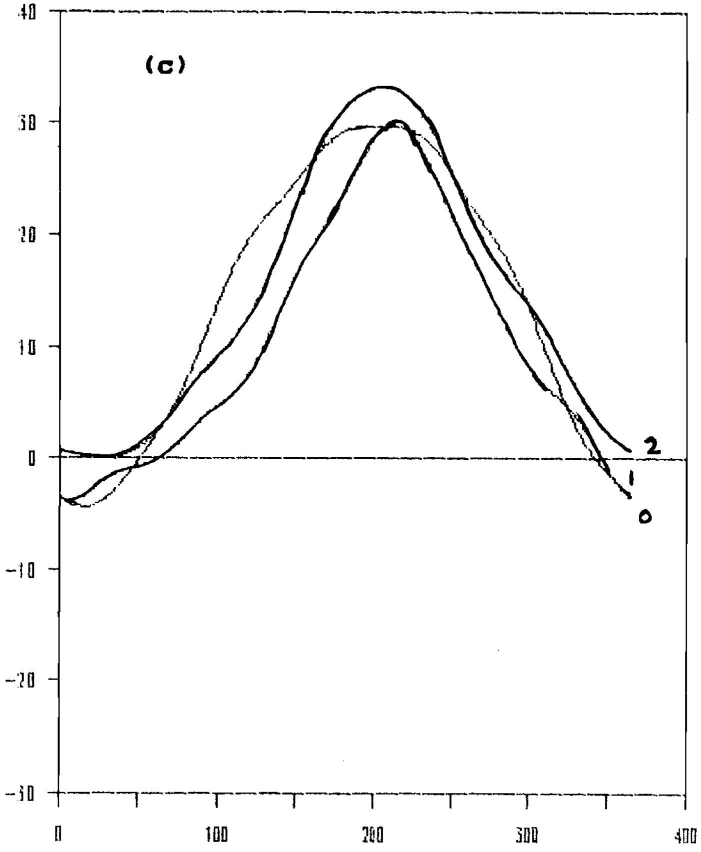


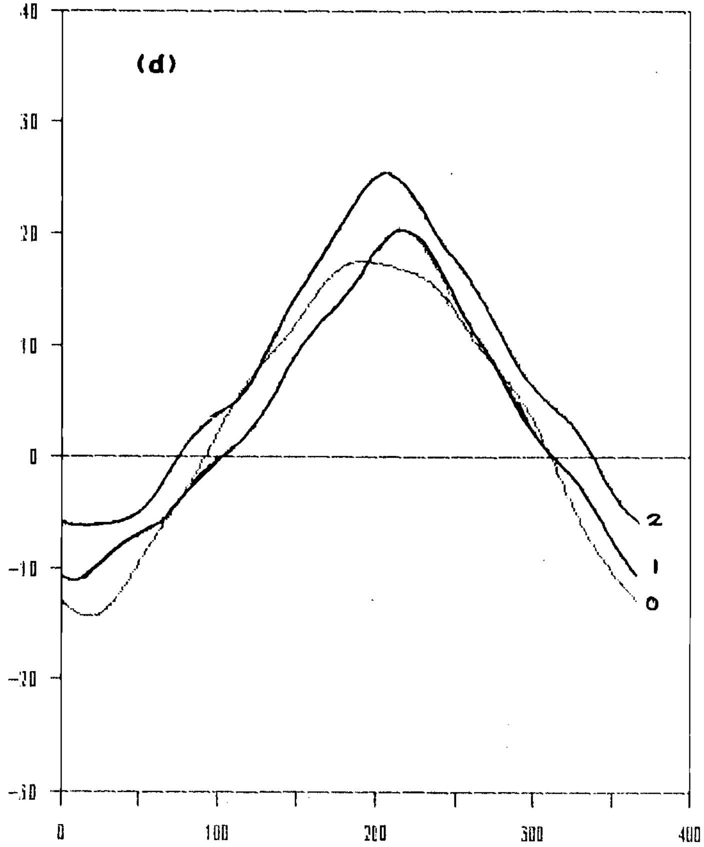


Figure 22, continued.
(c) wet day maximum temperatures, and (d) wet day minimum temperatures.

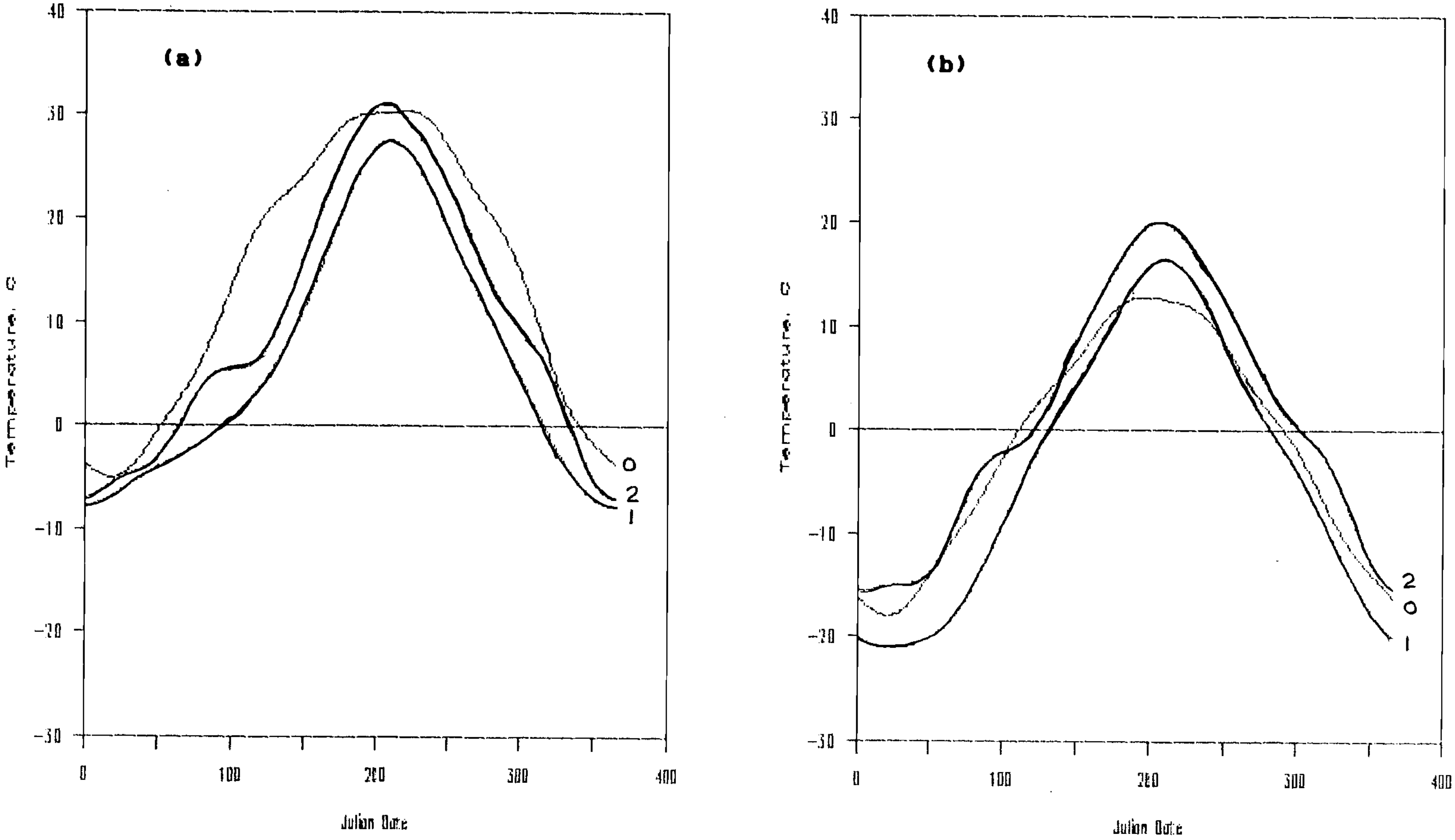


Figure 23. Annual temperature cycles for Box 3 observed (broken line), $1X\text{-}CO_2$, and $2X\text{-}CO_2$ data: (a) dry day maximum temperatures, and (b) dry day minimum temperatures.

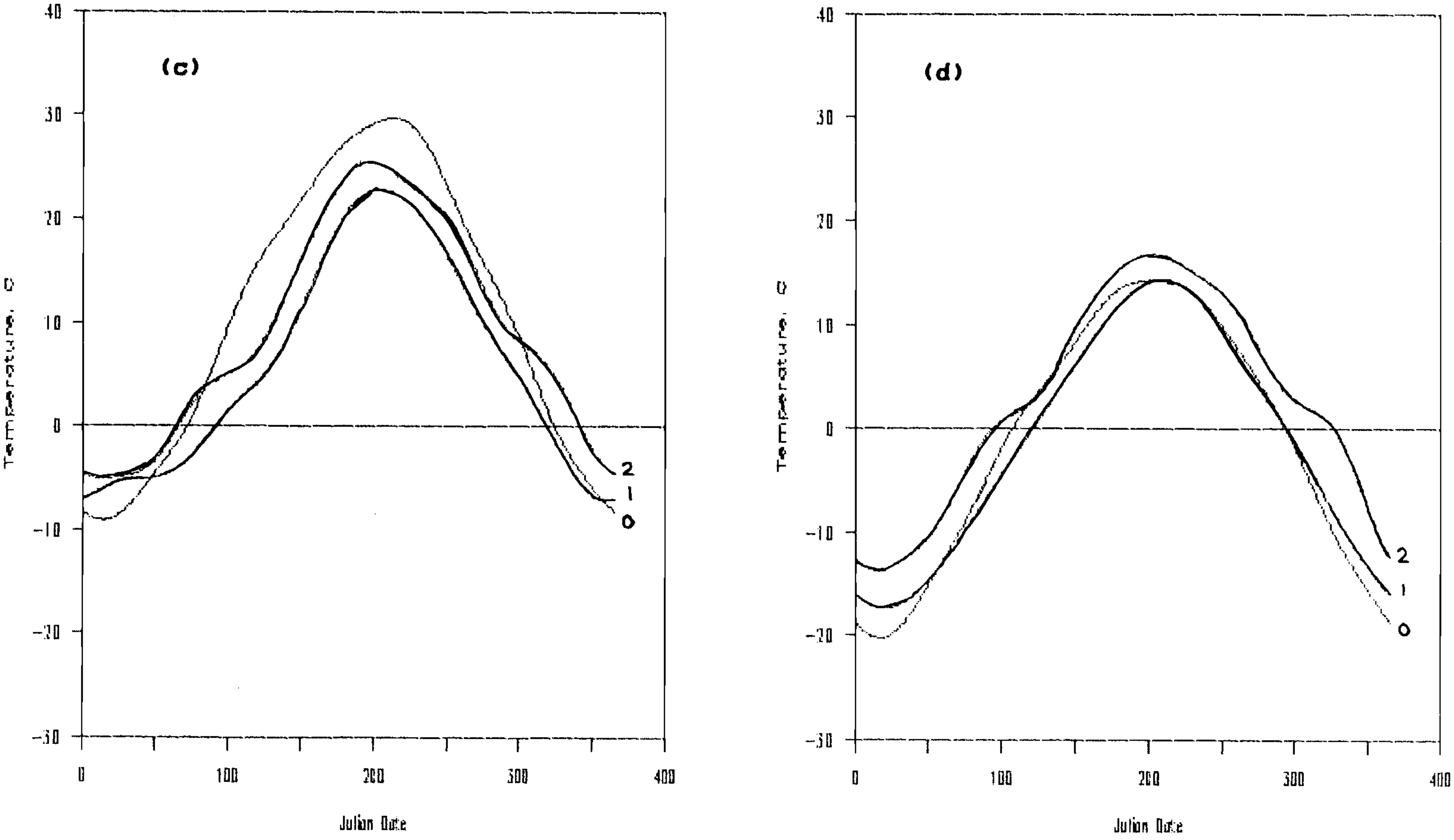


Figure 23, continued.
(c) wet day maximum temperatures, and (d) wet day minimum temperatures.

sets (e.g., Jenkins and Watts, 1968) or from the autoregressive coefficients themselves (Jones, 1974). It would be necessary in the present context to examine many plots using either approach, and difficult to present these results compactly.

The alternative employed here is use of the summary statistic $T_0$, or "time between effectively independent samples" (e.g., Leith, 1973; Madden, 1976; Trenberth, 1984). This statistic is constructed from a weighted average of sample autocorrelation estimates (see Appendix A for details), and is a compact characterization of the degree of autocorrelation present in a time series. Figures 24, 25, and 26 present annual cycles of $T_0$ for maximum temperature series from Boxes 1, 2, and 3, respectively. The (a) panels in these figures are for maximum temperatures, and the (b) panels are for minimum temperatures. For the most part, the cycles for maximum and minimum temperatures for each data source are similar with respect to both shape and magnitude for all three boxes. For the observed data, the cycle of $T_0$ exhibits apparent minima in the transition seasons for Box 1, and hints of a similar feature can be seen for Box 2. For Box 3 there is a broad warm-season minimum. These features may reflect the seasonal advance and retreat of the mean jet stream position over North America (e.g., Palmen and Newton, 1969), since the increased frequency of the associated cyclonic storms would tend to diminish the tendency of daily temperatures to persist. This pattern of two maxima in the annual cycles is also present in the GCM-derived data from Boxes 1 and 2, although the summer maxima are greatly exaggerated.

The GCM evidently does not reproduce this aspect of the observed climate with great fidelity, but the relative changes between the two

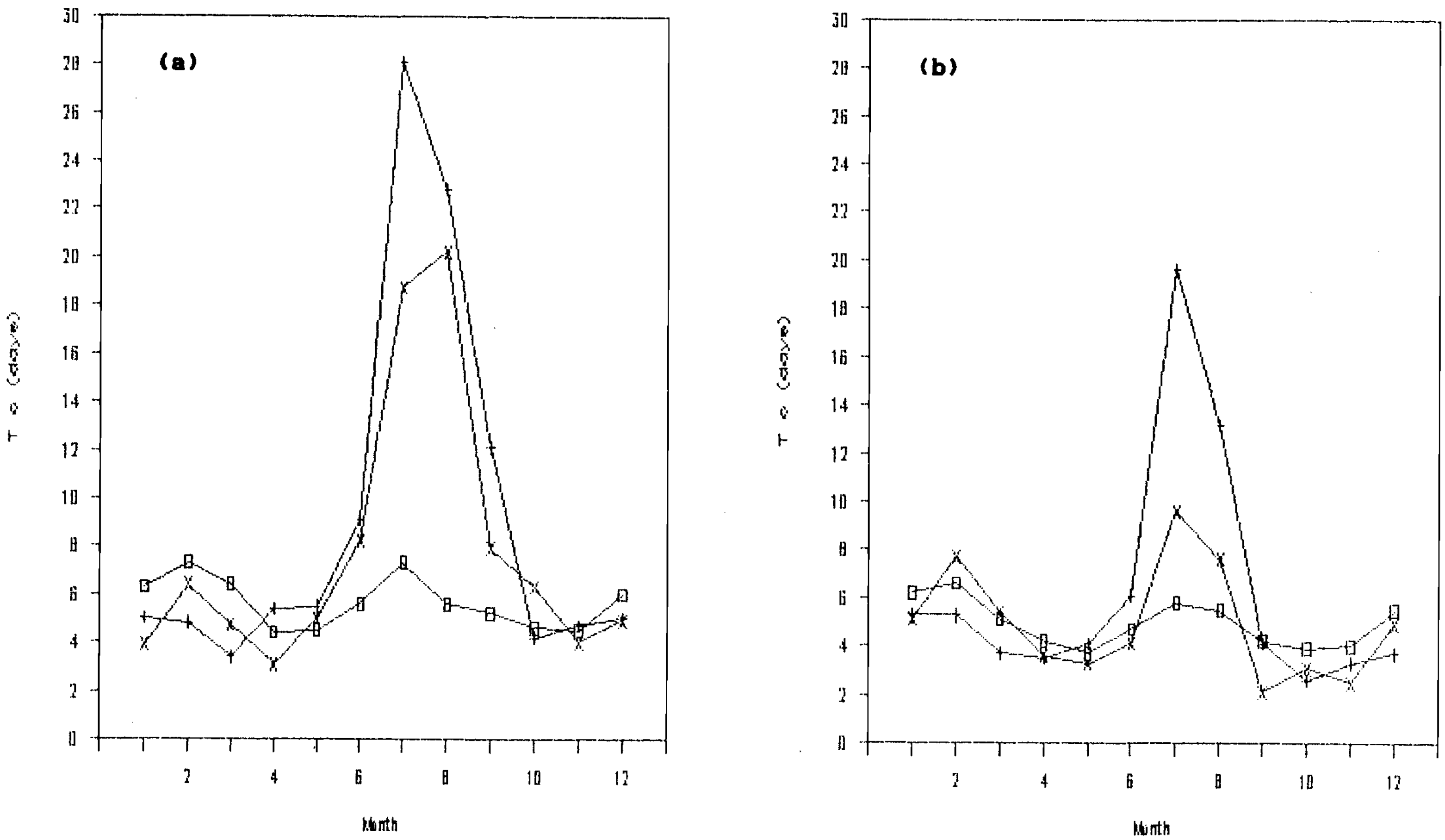


Figure 24. Annual cycles of the time between effectively independent samples, $T_e$, for Box 1: (a) maximum temperatures, and (b) minimum temperatures; for observations (▪), 1X-$CO_2$ data (X), and 2X-$CO_2$ data (+).

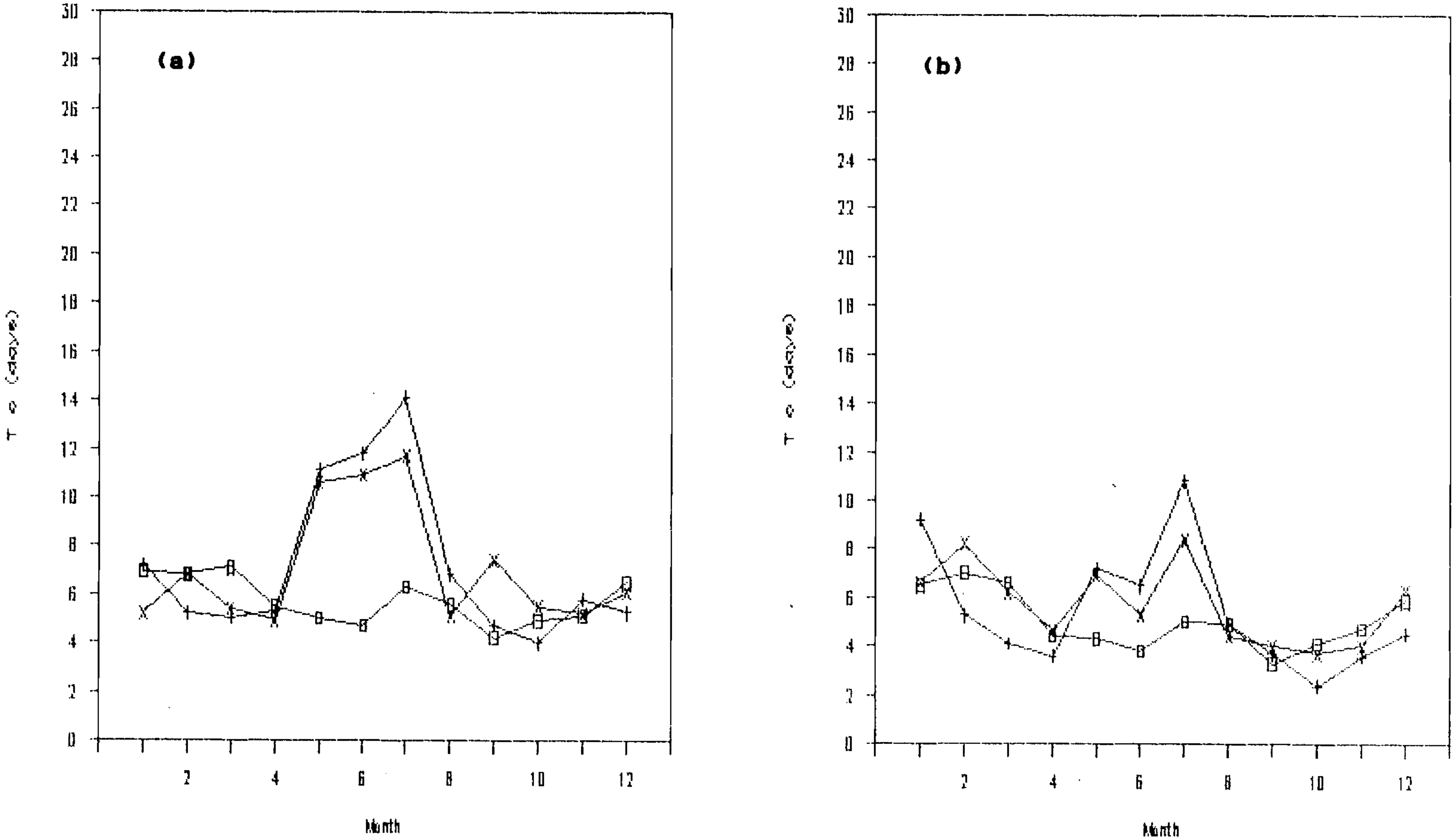


Figure 25. Annual cycles of the time between effectively independent samples, $T_0$, for Box 2: (a) maximum temperatures, and (b) minimum temperatures; for observations (▪), 1X-$CO_2$ data (X), and 2X-$CO_2$ data (+).

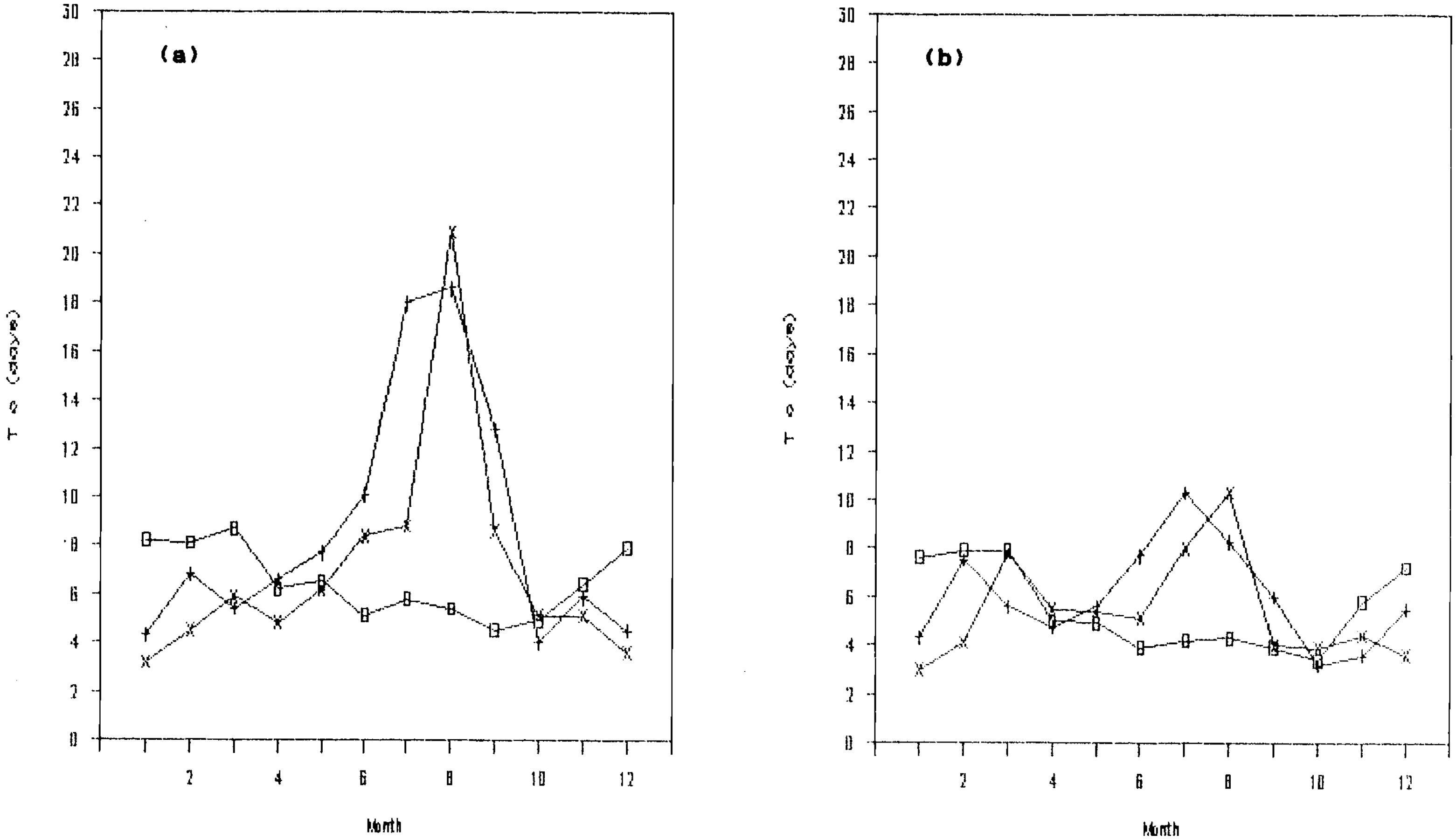


Figure 26. Annual cycles of the time between effectively independent samples, $T_e$, for Box 3: (a) maximum temperatures, and (b) minimum temperatures; for observations (▪), 1X-$CO_2$ data (X), and 2X-$CO_2$ data (+).

GCM data sets again are slight. Application of the normal approximation to the distribution of $T_0$ (Wilks, 1987; Appendix A) indicates a significant difference between the two GCM data sets at the 5% level only for Box 1 minimum temperatures for September.

Figures 27, 28, and 29 show the annual cycles of (for convenience, the square-roots of) white-noise variances for maximum temperatures on (a) dry days and (b) wet days, for Boxes 1, 2, and 3, respectively. Figures 30, 31, and 32 show the corresponding cycles for white-noise variances for minimum temperatures. These quantities are the square-roots of the diagonal elements of the matrices $\underset{\sim}{V}$ in (3.11). All of these figures indicate distinct warm-season minima and cool-season maxima for the observational data. The parameters derived from the GCM data exhibit the same primary feature, although often with much smaller amplitudes. Although the curves for the 1X- and 2X-$CO_2$ data tend to follow one another fairly closely, some substantial differences exist. Those differences which are significant, as determined using the method of Katz (1983), are tabulated in Table 18 for maximum temperature and in Table 19 for minimum temperature.

Similarly, differences in the white-noise correlation (the scaled off-diagonal elements of $\underset{\sim}{V}$), calculated using the normal approximation to the distribuiton of the Fisher z-transformation (e.g., Lindgren, 1976), are presented in Table 20. These tables indicate a tendency for relative increases in variability in temperature, as well as in correlations between maximum and minimum temperatures, during the warm season for the 2X-$CO_2$ simulations. This result is especially evident for wet days. Some tendency for

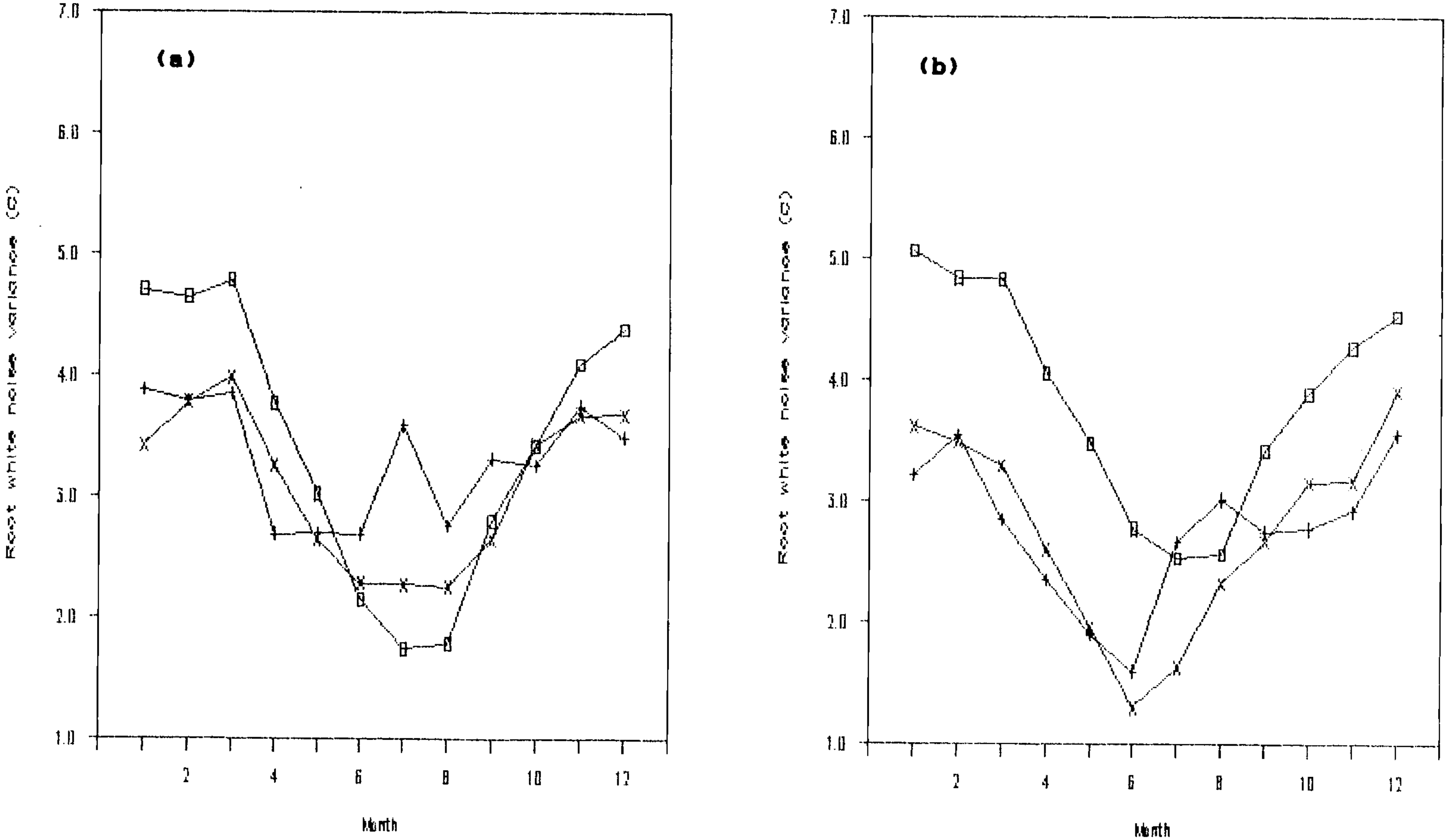


Figure 27. Annual cycles of (square-root of) white-noise variance for Box 1 maximum temperatures: (a) dry days, and (b) wet days; for observations (▪), 1X-$CO_2$ data (X), and 2X-$CO_2$ data (+).

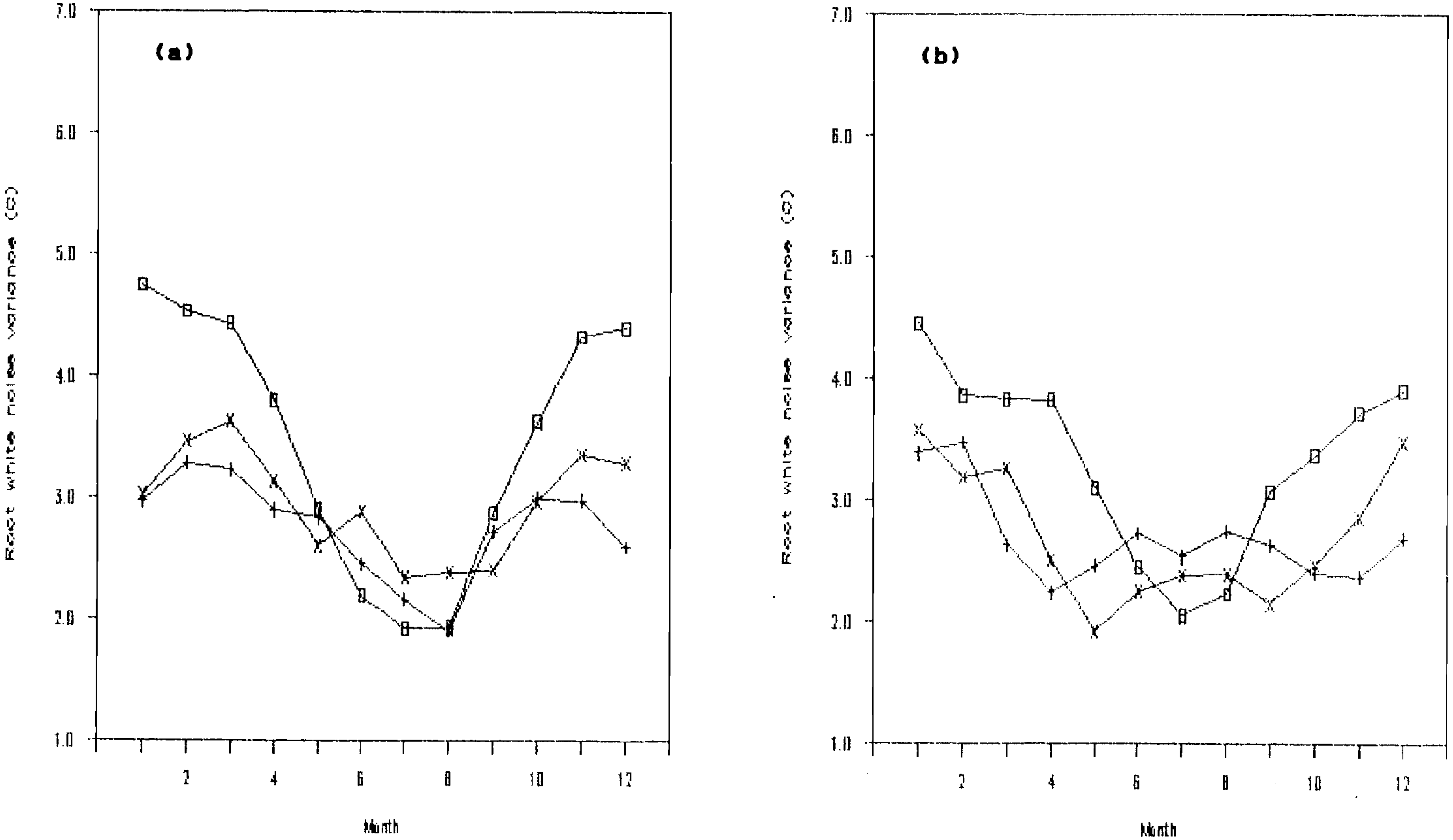


Figure 28. Annual cycles of (square-root of) white-noise variance for Box 2 maximum temperatures: (a) dry days, and (b) wet days; for observations (□), $1X-CO_2$ data (X), and $2X-CO_2$ data (+).

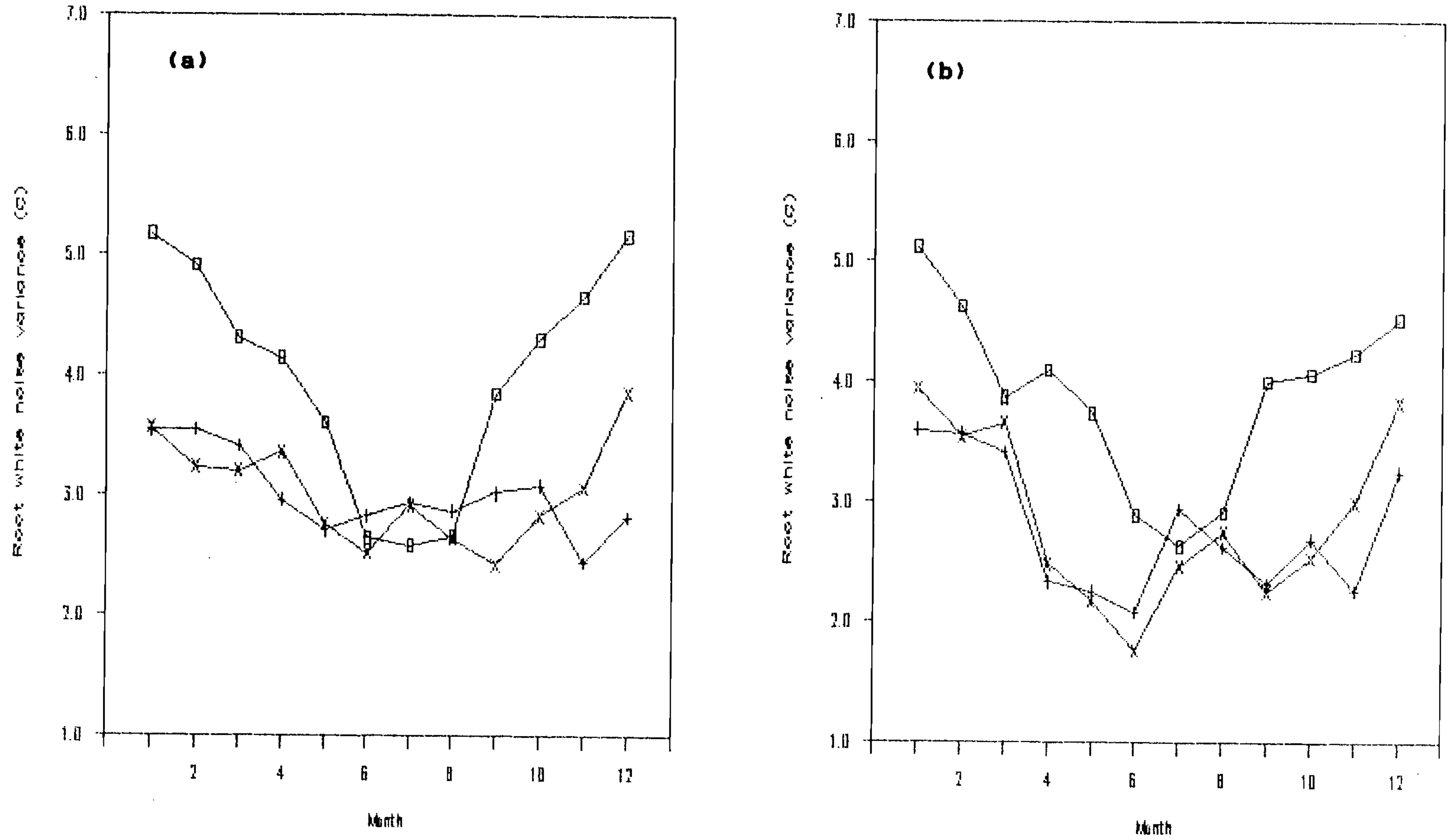


Figure 29. Annual cycles of (square-root of) white-noise variance for Box 3 maximum temperatures: (a) dry days, and (b) wet days; for observations (▪), 1X-$CO_2$ data (X), and 2X-$CO_2$ data (+).

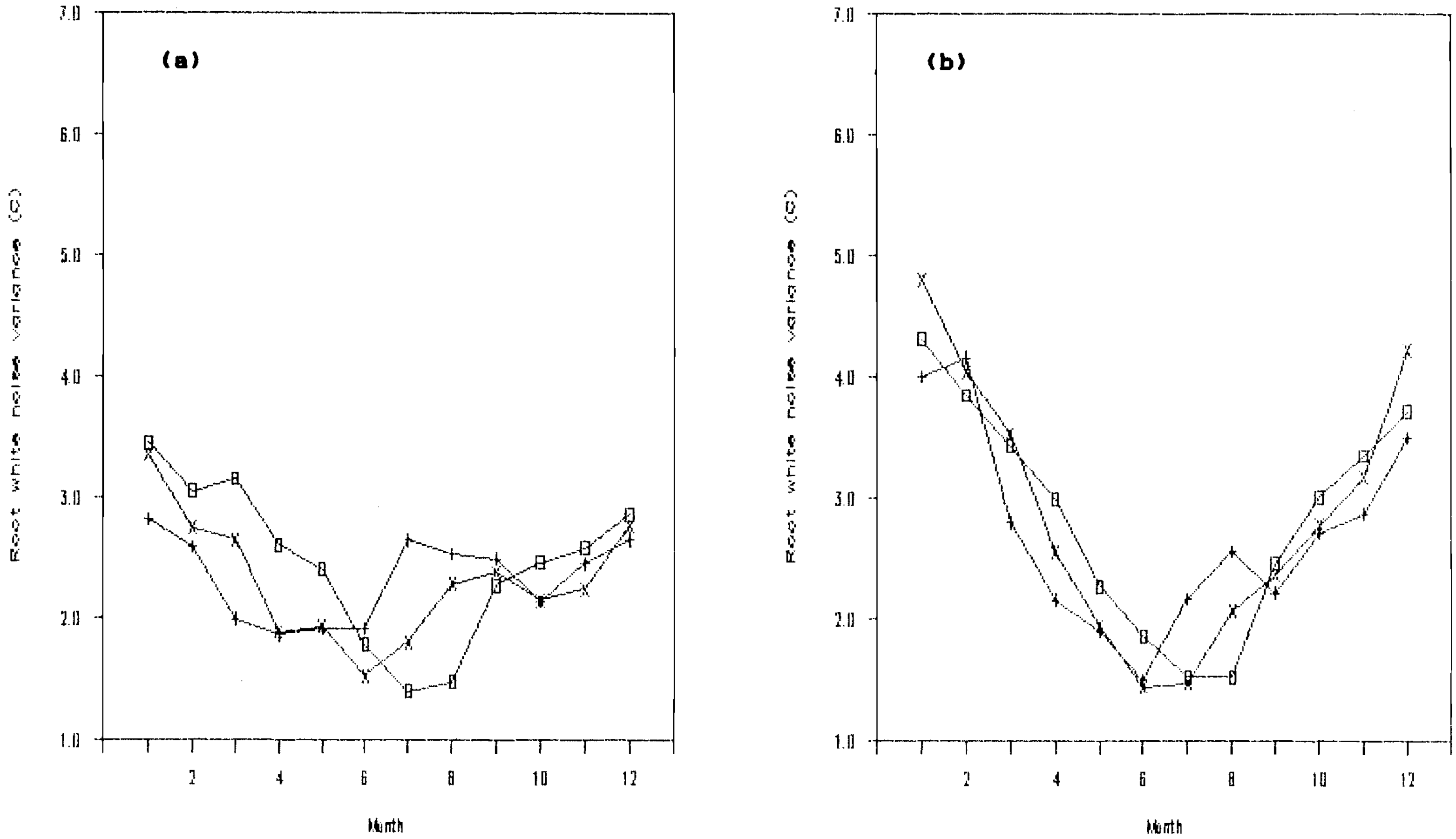


**Figure 30.** Annual cycles of (square-root of) white-noise variance for Box 1 minimum temperatures: (a) dry days, and (b) wet days; for observations (▪), 1X-$CO_2$ data (X), and 2X-$CO_2$ data (+).

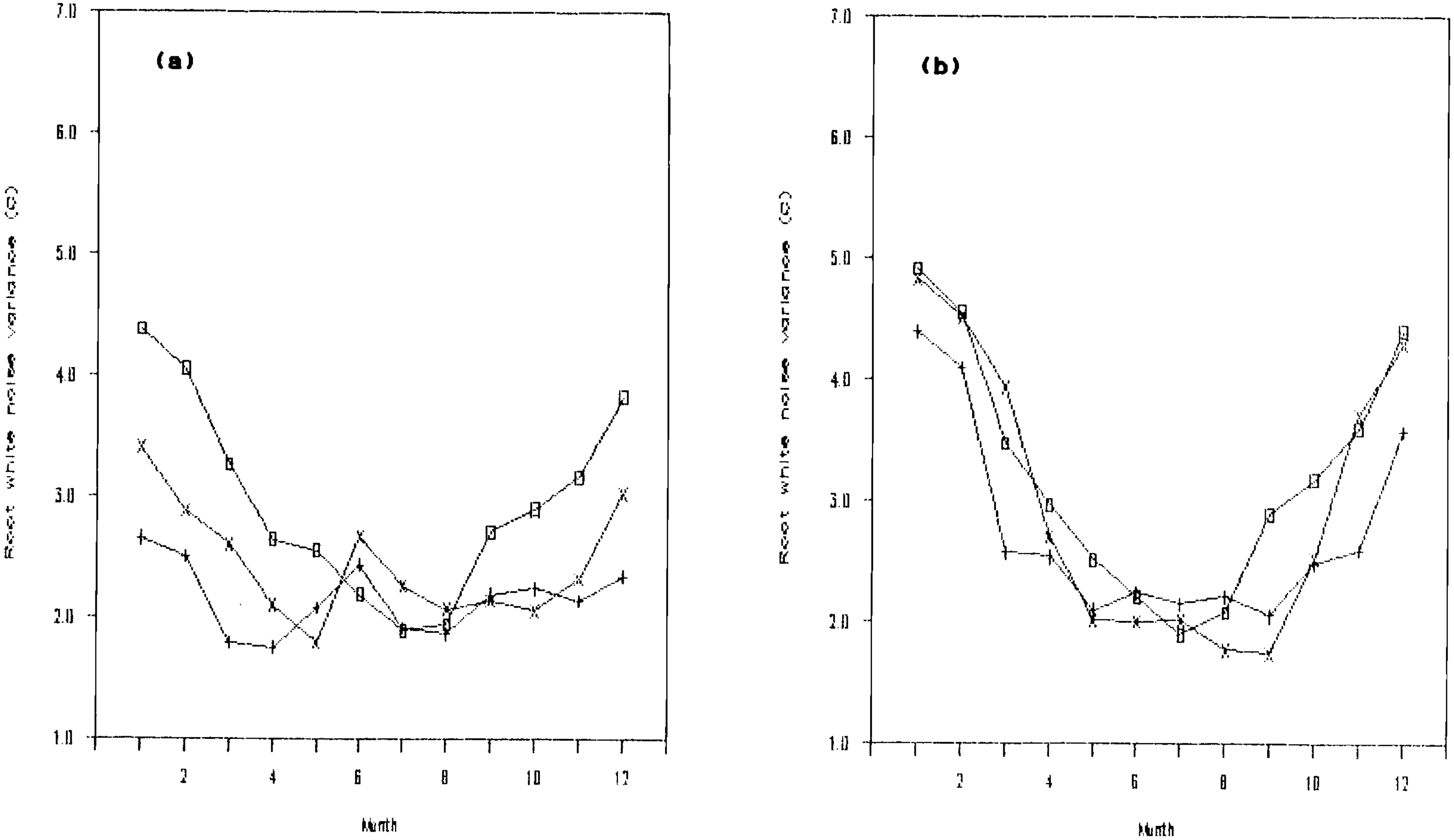


Figure 31. Annual cycles of (square-root of) white-noise variance for Box 2 minimum temperatures: (a) dry days, and (b) wet days; for observations (▪), 1X-$CO_2$ data (X), and 2X-$CO_2$ data (+).

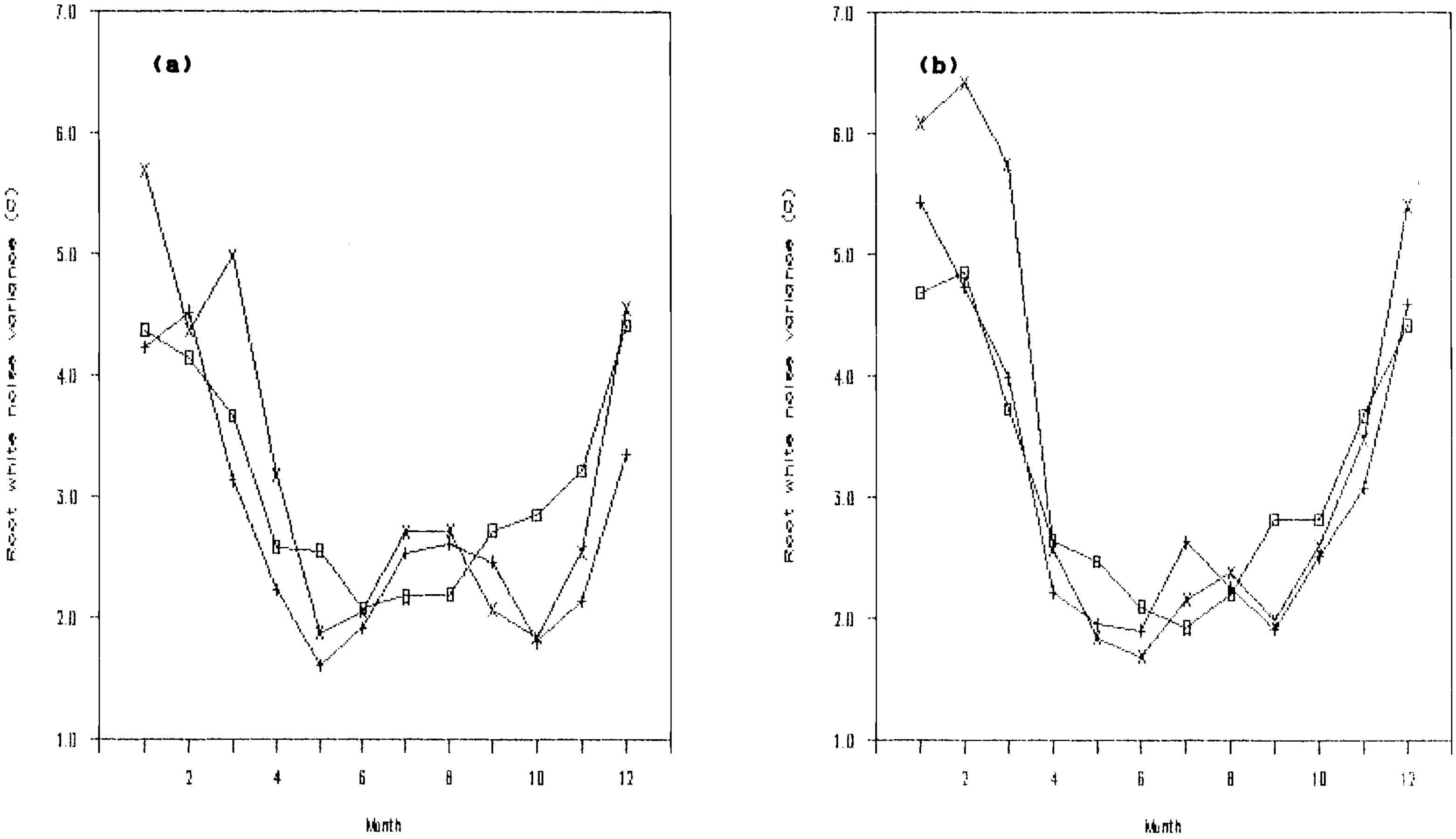


Figure 32. Annual cycles of (square-root of) white-noise variance for Box 3 minimum temperatures: (a) dry days, and (b) wet days; for observations (▪), 1X-$CO_2$ data (X), and 2X-$CO_2$ data (+).

Table 18. As Table 16, but for white-noise variance of maximum temperatures.

Dry days

| Box No. | Jan | Feb | Mar | Apr | May | Jun | Jul | Aug | Sep | Oct | Nov | Dec |
|---|---|---|---|---|---|---|---|---|---|---|---|---|
| 1 | > | | | < | | | >> | >> | >> | | | |
| 2 | | | | | | < | | << | > | | < | << |
| 3 | | | | | | | | | >> | | << | << |

Wet days

| Box No. | Jan | Feb | Mar | Apr | May | Jun | Jul | Aug | Sep | Oct | Nov | Dec |
|---|---|---|---|---|---|---|---|---|---|---|---|---|
| 1 | | | < | | | >> | >> | >> | | | | |
| 2 | | | << | | >> | >> | | | > | | < | << |
| 3 | | | | | | >> | >> | | | | << | << |

Table 19. As Table 16, but for white-noise variance of minimum temperatures.

Dry Days

| Box No. | Jan | Feb | Mar | Apr | May | Jun | Jul | Aug | Sep | Oct | Nov | Dec |
|---|---|---|---|---|---|---|---|---|---|---|---|---|
| 1 | << | | << | | | | >> | | | | | |
| 2 | << | > | << | < | > | | << | < | | | | << |
| 3 | << | | << | << | | | | | > | | < | << |

Wet days

| Box No. | Jan | Feb | Mar | Apr | May | Jun | Jul | Aug | Sep | Oct | Nov | Dec |
|---|---|---|---|---|---|---|---|---|---|---|---|---|
| 1 | << | | << | << | | | >> | >> | | | | << |
| 2 | | | << | | | | | > | > | | << | << |
| 3 | | << | << | << | | > | >> | | | | | << |

Table 20. As Table 16, but for white-noise correlation.

Dry Days

| Box No. | Jan | Feb | Mar | Apr | May | Jun | Jul | Aug | Sep | Oct | Nov | Dec |
|---|---|---|---|---|---|---|---|---|---|---|---|---|
| 1 | | | | | | | >> | >> | | | | < |
| 2 | | | | | | << | > | | >> | >> | | |
| 3 | | | | | | | | > | >> | | | |

Wet days

| Box No. | Jan | Feb | Mar | Apr | May | Jun | Jul | Aug | Sep | Oct | Nov | Dec |
|---|---|---|---|---|---|---|---|---|---|---|---|---|
| 1 | | | | | | >> | >> | >> | | | << | |
| 2 | > | > | << | | | | | > | >> | < | | |
| 3 | | | > | | | | > | | | | | > |

decreases in temperature variability during the cool season is also notable.

## 3.5 Stochastic Generation of Local 1X-$CO_2$ and Possible 2X-$CO_2$ Climate Data

### 3.5.1. Extrapolation to the 2X-$CO_2$ climate scenario on the grid-scale

The stochastic weather model described in Section 3.3 has been constructed so as to be directly applicable to Monte Carlo simulation of daily weather data on the grid scale. The stochastic forcing acts through the probabilities in (3.1), the precipitation intensity variates whose probability density function is given by (3.4), and the $\tilde{\epsilon}$ vectors in (3.5). Application of the model to generation of data representative of present climate is of course accomplished through use of parameters fit to the observational data.

The present approach to extrapolation to the possible climate of a 2X-$CO_2$ world is through use of relative changes in the parameters fit to the 1X-$CO_2$ and 2X-$CO_2$ GCM data. The inferred 2X-$CO_2$ climate scenario is constructed by applying changes in those parameters that are deemed to be statistically significant in Section 3.4 to the corresponding parameters derived from the observational data. There is no unique means of accomplishing this objective, and no theoretical guidance. The approach taken in the following is to apply the relative changes additively, but on transformed scales suggested by the forms of the usual statistical tests involving each parameter.

As discussed in Section 3.4, the statistical characteristics of the $1X\text{-}CO_2$ and $2X\text{-}CO_2$ data sets, with respect to many of the parameters described in Section 3.3, are rather similar. The only parameters to undergo adjustment are those for which significant differences are tabulated in Tables 16 through 20, and the annual cycles of mean daily temperature. For other parameters, the values fit to the observed data are assumed to describe the $2X\text{-}CO_2$ world as well.

The only precipitation occurrence parameter in (3.1) to be adjusted is $P_{01}$, the probability of precipitation given that the previous day was dry. Probabilities for those months and gridboxes indicated in Table 16 are adjusted additively on the log-odds scale (3.12). That is,

$$\lambda\,[P^*_{01}] = \lambda\,[P_{01}(\mathrm{obs})] + \lambda\,[P_{01}(2X)] - \lambda\,[P_{01}(1X)] \;, \qquad (3.14)$$

where $P^*_{01}$ is the value adopted to represent the $2X\text{-}CO_2$ world. In this case and in the following, starred parameters are equal to those fit to the observational data if the corresponding differences between the $1X\text{-}CO_2$ and $2X\text{-}CO_2$ data sets are not significant. Equation (3.14) leads to the formula

$$P^*_{01} = W^* / (1 + W^*) \;, \qquad (3.15)$$

where

$$W^* = \frac{[P_{01}(obs)]\,[P_{01}(2X)]\,[1 - P_{01}(1X)]}{[1 - P_{01}(obs)]\,[1 - P_{01}(2X)]\,[P_{01}(1X)]} . \qquad (3.16)$$

The only precipitation intensity parameter to be adjusted is the scale parameter $\alpha$ for days following wet days. This adjustment is performed multiplicatively for those combinations of gridbox and month indicated in Table 17:

$$\alpha^* = \frac{\alpha(obs)\ \alpha(2X)}{\alpha(1X)} . \qquad (3.17)$$

Note that the method adopted for examining and adjusting the parameters of the gamma distribution (3.4) is not the only one possible. An equally reasonable procedure would be to reparameterize (3.4) in terms of the mean of the distribution, $\mu = \alpha\gamma$, and a "nuisance" parameter (e.g., Beaumont, 1980), and then to consider relative changes in $\mu$ alone.

As discussed above, the nature of the autocorrelation of the temperatures is regarded as being unchanged for the 2X-$CO_2$ climate, and the matrices of autoregressive coefficients $\underset{\sim}{\Phi}_1$, derived from the observational data, are used to characterize the 2X-$CO_2$ climate as well. These quantities are presented separaately for wet and dry days in Table 21 for Box 1, Table 22 for Box 2, and Table 23 for Box 3.

Mean daily maximum and minimum temperatures are adjusted additively, and separately for wet and dry days:

$$\bar{T}^*_t = \bar{T}_t(obs) + \bar{T}_t(2X) - \bar{T}_t(1X) , \qquad (3.18)$$

Table 21. Autoregressive coefficient matrices, $\underset{\sim}{\Phi}$, and white-noise variance-covariance matrices, $\underset{\sim}{V}$, for Box 1. $\underset{\sim}{V}$* denotes assumed variance-covariance matrices for 2X-$CO_2$ climate.

a. Dry days

| | $\underset{\sim}{\Phi}_1$ | | $\underset{\sim}{\Phi}_2$ | | $\underset{\sim}{V}$ | | $\underset{\sim}{V}^*$ | |
|---|---|---|---|---|---|---|---|---|
| Jan | .641 | .122 | -.009 | -.079 | 22.08 | 10.89 | 28.42 | 10.40 |
| | .392 | .421 | -.150 | .027 | 10.89 | 11.89 | 10.40 | 8.43 |
| Feb | .712 | .020 | .001 | -.097 | 21.50 | 8.05 | 21.50 | 8.05 |
| | .356 | .382 | -.112 | .018 | 8.05 | 9.28 | 8.05 | 9.28 |
| Mar | .671 | .024 | .016 | -.099 | 22.83 | 8.82 | 22.83 | 6.63 |
| | .398 | .356 | -.041 | -.108 | 8.82 | 9.94 | 6.63 | 5.61 |
| Apr | .687 | -.039 | -.048 | -.177 | 14.21 | 5.33 | 9.73 | 4.41 |
| | .547 | .246 | -.088 | -.083 | 5.33 | 6.76 | 4.41 | 6.76 |
| May | .723 | -.001 | .011 | -.169 | 9.13 | 4.24 | 9.13 | 4.24 |
| | .458 | .471 | -.119 | -.134 | 4.24 | 5.77 | 4.24 | 5.77 |
| Jun | .702 | -.084 | .062 | -.094 | 4.61 | 2.19 | 4.61 | 2.19 |
| | .509 | .485 | -.185 | -.066 | 2.19 | 3.17 | 2.19 | 3.17 |
| Jul | .622 | .042 | .072 | -.060 | 3.03 | 1.40 | 7.57 | 4.89 |
| | .238 | .678 | -.050 | -.173 | 1.40 | 1.96 | 4.89 | 4.24 |
| Aug | .842 | -.102 | -.118 | .054 | 3.17 | 1.23 | 4.78 | 2.29 |
| | .548 | .485 | -.273 | .025 | 1.23 | 2.18 | 2.29 | 2.18 |
| Sep | .680 | -.022 | -.036 | -.055 | 7.86 | 3.45 | 12.26 | 4.30 |
| | .464 | .510 | -.268 | .004 | 3.45 | 5.17 | 4.30 | 5.17 |
| Oct | .686 | -.059 | -.079 | -.043 | 11.71 | 4.01 | 11.71 | 4.01 |
| | .469 | .421 | -.251 | .082 | 4.01 | 6.07 | 4.01 | 6.07 |
| Nov | .671 | .073 | -.131 | -.026 | 16.72 | 5.10 | 16.72 | 5.10 |
| | .417 | .400 | -.188 | .081 | 5.10 | 6.66 | 5.10 | 6.66 |
| Dec | .646 | .049 | -.051 | -.102 | 19.22 | 7.57 | 19.22 | 5.48 |
| | .361 | .397 | -.169 | .024 | 7.57 | 8.19 | 5.48 | 8.19 |

Table 21, continued.

b. Wet days

| | $\underset{\sim}{\Phi}_1$ | | $\underset{\sim}{\Phi}_2$ | | $\underset{\sim}{V}$ | | $\underset{\sim}{V}^*$ | |
|---|---|---|---|---|---|---|---|---|
| Jan | .295 | .520 | .146 | -.198 | 25.60 | 15.39 | 25.60 | 12.83 |
| | .016 | .771 | .014 | -.094 | 15.39 | 18.58 | 12.83 | 12.90 |
| Feb | .505 | .383 | .040 | -.211 | 23.47 | 11.24 | 23.47 | 11.24 |
| | .132 | .678 | .003 | -.056 | 11.24 | 14.84 | 11.24 | 14.84 |
| Mar | .563 | .368 | .034 | -.249 | 23.36 | 8.31 | 17.53 | 5.71 |
| | .172 | .699 | -.075 | -.104 | 8.31 | 11.74 | 5.71 | 7.38 |
| Apr | .616 | .210 | -.093 | -.054 | 16.41 | 6.38 | 16.41 | 5.40 |
| | .303 | .503 | -.121 | -.083 | 6.38 | 8.94 | 5.40 | 6.41 |
| May | .745 | -.029 | -.095 | -.049 | 12.10 | 3.72 | 12.10 | 3.72 |
| | .350 | .469 | -.171 | -.013 | 3.72 | 5.14 | 3.72 | 5.14 |
| Jun | .844 | .000 | -.233 | .084 | 7.73 | 2.69 | 11.71 | 4.11 |
| | .394 | .378 | -.185 | .052 | 2.69 | 3.44 | 4.11 | 3.44 |
| Jul | .889 | -.186 | -.214 | .224 | 6.39 | 2.44 | 17.13 | 7.97 |
| | .290 | .502 | -.184 | .040 | 2.44 | 2.33 | 7.97 | 5.02 |
| Aug | .924 | -.121 | -.276 | .159 | 6.56 | 2.16 | 11.11 | 4.73 |
| | .321 | .505 | -.239 | .119 | 2.16 | 2.33 | 4.73 | 3.57 |
| Sep | .702 | .273 | -.140 | -.111 | 11.70 | 4.56 | 11.70 | 4.56 |
| | .238 | .712 | -.207 | -.084 | 4.56 | 6.05 | 4.56 | 6.05 |
| Oct | .532 | .453 | -.073 | -.293 | 15.10 | 5.59 | 15.10 | 5.59 |
| | .212 | .646 | -.196 | -.152 | 5.59 | 9.04 | 5.59 | 9.04 |
| Nov | .570 | .420 | -.165 | -.233 | 18.24 | 6.79 | 18.24 | 2.64 |
| | .228 | .565 | -.165 | -.058 | 6.79 | 11.25 | 2.64 | 11.25 |
| Dec | .565 | .365 | -.051 | -.118 | 20.54 | 10.43 | 20.54 | 8.65 |
| | .250 | .602 | -.104 | .004 | 10.43 | 13.85 | 8.65 | 9.53 |

Table 22. As Table 21, for Box 2.

a. Dry days

| | $\underset{\sim}{\Phi}_1$ | | $\underset{\sim}{\Phi}_2$ | | $\underset{\sim}{V}$ | | $\underset{\sim}{V}*$ | |
|---|---|---|---|---|---|---|---|---|
| Jan | .941 | -.116 | -.139 | -.007 | 22.47 | 15.70 | 22.47 | 12.29 |
| | .657 | .282 | -.180 | .029 | 15.70 | 19.21 | 12.29 | 11.76 |
| Feb | .874 | .031 | -.122 | -.096 | 20.50 | 12.48 | 20.50 | 10.84 |
| | .669 | .398 | -.294 | .031 | 12.48 | 16.41 | 10.84 | 12.37 |
| Mar | .901 | .013 | -.064 | -.160 | 19.60 | 8.97 | 19.60 | 6.18 |
| | .555 | .416 | -.205 | -.069 | 8.97 | 10.60 | 6.18 | 5.02 |
| Apr | .911 | -.202 | -.080 | -.109 | 14.43 | 5.38 | 14.43 | 4.48 |
| | .572 | .205 | -.126 | -.152 | 5.38 | 6.96 | 4.48 | 4.83 |
| May | .901 | .114 | -.287 | -.091 | 8.42 | 4.17 | 8.42 | 4.85 |
| | .715 | .363 | -.350 | -.018 | 4.17 | 6.51 | 4.85 | 8.80 |
| Jun | 1.000 | -.130 | -.144 | -.115 | 4.79 | 2.97 | 3.47 | 1.76 |
| | .857 | .270 | -.233 | -.093 | 2.97 | 4.81 | 1.76 | 4.81 |
| Jul | 1.020 | -.085 | -.151 | -.141 | 3.70 | 2.40 | 3.70 | 2.29 |
| | .942 | .268 | -.371 | -.006 | 2.40 | 3.59 | 2.29 | 2.56 |
| Aug | 1.064 | .074 | -.324 | -.073 | 3.71 | 2.17 | 2.36 | 1.56 |
| | .734 | .616 | -.480 | .037 | 2.17 | 3.75 | 1.56 | 3.03 |
| Sep | .834 | -.043 | -.135 | -.023 | 8.21 | 4.26 | 10.54 | 6.80 |
| | .647 | .389 | -.290 | .047 | 4.26 | 7.36 | 6.80 | 7.36 |
| Oct | .817 | -.023 | -.179 | -.039 | 13.17 | 5.18 | 13.17 | 6.50 |
| | .683 | .224 | -.282 | .097 | 5.18 | 8.40 | 6.50 | 8.40 |
| Nov | .765 | .011 | -.098 | -.046 | 18.65 | 8.13 | 14.75 | 7.23 |
| | .536 | .243 | -.144 | .037 | 8.13 | 9.99 | 7.23 | 9.99 |
| Dec | .756 | .048 | -.095 | -.093 | 19.24 | 12.08 | 12.00 | 7.37 |
| | .611 | .275 | -.185 | .005 | 12.08 | 14.60 | 7.37 | 8.71 |

Table 22, continued.

b. Wet days

| | $\Phi_1$ | | $\Phi_2$ | | $V$ | | $V^*$ | |
|---|---|---|---|---|---|---|---|---|
| Jan | .525 | .272 | -.185 | .033 | 19.84 | 16.50 | 19.84 | 18.18 |
| | .255 | .568 | -.158 | .025 | 16.50 | 24.09 | 18.18 | 24.09 |
| Feb | .620 | .160 | -.102 | -.006 | 14.92 | 11.75 | 14.92 | 13.67 |
| | .408 | .478 | -.256 | .116 | 11.75 | 20.68 | 13.67 | 20.68 |
| Mar | .829 | .061 | -.119 | -.026 | 14.63 | 7.40 | 9.52 | 2.38 |
| | .507 | .426 | -.292 | .108 | 7.40 | 12.06 | 2.38 | 5.16 |
| Apr | .824 | .144 | -.185 | -.106 | 14.58 | 5.67 | 14.58 | 5.67 |
| | .476 | .369 | -.245 | .052 | 5.67 | 8.82 | 5.67 | 8.82 |
| May | .857 | .027 | -.177 | -.040 | 9.62 | 3.41 | 15.79 | 4.36 |
| | .479 | .458 | -.240 | .001 | 3.41 | 6.32 | 4.36 | 6.32 |
| Jun | .868 | .072 | -.266 | -.020 | 6.01 | 2.49 | 8.84 | 3.02 |
| | .588 | .380 | -.377 | .101 | 2.49 | 4.88 | 3.02 | 4.88 |
| Jul | .901 | .002 | -.233 | .050 | 4.24 | 1.95 | 4.24 | 1.95 |
| | .529 | .460 | -.352 | .079 | 1.95 | 3.57 | 1.95 | 3.57 |
| Aug | .875 | .052 | -.246 | .002 | 4.96 | 2.11 | 4.96 | 3.90 |
| | .505 | .467 | -.277 | -.030 | 2.11 | 4.32 | 3.90 | 6.73 |
| Sep | .779 | .139 | -.246 | -.087 | 9.40 | 4.12 | 14.06 | 8.92 |
| | .382 | .526 | -.252 | -.079 | 4.12 | 8.34 | 8.92 | 11.69 |
| Oct | .850 | .182 | -.269 | -.061 | 11.37 | 4.69 | 11.37 | 2.62 |
| | .520 | .480 | -.340 | -.048 | 4.69 | 10.05 | 2.62 | 10.05 |
| Nov | .647 | .278 | -.046 | -.180 | 13.86 | 8.18 | 9.52 | 4.74 |
| | .294 | .569 | -.147 | -.055 | 8.18 | 12.94 | 4.74 | 6.31 |
| Dec | .696 | .290 | -.217 | -.039 | 15.18 | 12.22 | 9.07 | 7.88 |
| | .371 | .608 | -.239 | .031 | 12.22 | 19.38 | 7.88 | 13.49 |

Table 23. As Table 21, for Box 3.

a. Dry days

| | $\underset{\sim}{\Phi}_1$ | | $\underset{\sim}{\Phi}_2$ | | $\underset{\sim}{V}$ | | $\underset{\sim}{V}^*$ | |
|---|---|---|---|---|---|---|---|---|
| Jan | .931 | -.045 | -.178 | .089 | 26.74 | 17.89 | 26.74 | 13.30 |
| | .760 | .196 | -.257 | .153 | 17.89 | 19.07 | 13.30 | 10.54 |
| Feb | .701 | .153 | .026 | -.138 | 24.13 | 15.89 | 24.13 | 15.89 |
| | .644 | .395 | -.116 | -.055 | 15.89 | 17.15 | 15.89 | 17.15 |
| Mar | .917 | -.075 | -.114 | -.004 | 18.61 | 10.44 | 18.61 | 6.56 |
| | .661 | .364 | -.379 | .131 | 10.44 | 13.46 | 6.56 | 5.32 |
| Apr | 1.023 | -.337 | -.150 | .089 | 17.17 | 5.78 | 17.17 | 4.07 |
| | .581 | .208 | -.261 | .097 | 5.78 | 6.64 | 4.07 | 3.29 |
| May | .771 | -.036 | -.142 | .020 | 13.04 | 6.14 | 13.04 | 6.14 |
| | .592 | .347 | -.258 | .055 | 6.14 | 6.49 | 6.14 | 6.49 |
| Jun | 1.007 | -.089 | -.186 | -.079 | 7.02 | 3.10 | 7.02 | 3.10 |
| | .664 | .363 | -.388 | .086 | 3.10 | 4.33 | 3.10 | 4.33 |
| Jul | 1.052 | -.275 | -.272 | .043 | 6.64 | 3.59 | 6.64 | 3.59 |
| | .705 | .336 | -.393 | .090 | 3.59 | 4.76 | 3.59 | 4.76 |
| Aug | 1.009 | -.185 | -.353 | .177 | 7.05 | 3.50 | 7.05 | 4.09 |
| | .695 | .342 | -.445 | .141 | 3.50 | 4.78 | 4.09 | 4.78 |
| Sep | .682 | -.052 | -.048 | -.123 | 14.84 | 6.18 | 23.27 | 11.82 |
| | .480 | .299 | -.182 | .048 | 6.18 | 7.41 | 11.82 | 10.47 |
| Oct | .689 | -.132 | -.049 | -.030 | 18.52 | 6.59 | 18.52 | 6.59 |
| | .468 | .145 | -.158 | .101 | 6.59 | 8.13 | 6.59 | 8.13 |
| Nov | .697 | -.064 | -.045 | .039 | 21.67 | 9.62 | 13.78 | 6.46 |
| | .460 | .332 | -.215 | .108 | 9.62 | 10.28 | 6.46 | 7.30 |
| Dec | .743 | .098 | .043 | -.168 | 26.64 | 18.68 | 14.22 | 10.05 |
| | .548 | .389 | -.171 | .014 | 18.68 | 19.42 | 10.05 | 10.53 |

Table 23, contnued.

b. Wet days

| | $\underset{\sim}{\Phi}_1$ | | $\underset{\sim}{\Phi}_2$ | | $\underset{\sim}{V}$ | | $\underset{\sim}{V}^*$ | |
|---|---|---|---|---|---|---|---|---|
| Jan | .694 | .084 | -.198 | .097 | 26.14 | 17.94 | 26.14 | 17.94 |
| | .499 | .315 | -.250 | .151 | 17.94 | 21.86 | 17.94 | 21.86 |
| Feb | .672 | .122 | -.185 | .047 | 21.39 | 16.63 | 21.39 | 12.25 |
| | .363 | .448 | -.295 | .190 | 16.63 | 23.49 | 12.25 | 12.75 |
| Mar | .729 | .085 | -.098 | .025 | 15.00 | 9.99 | 15.00 | 7.78 |
| | .402 | .492 | -.201 | .121 | 9.99 | 13.91 | 7.78 | 6.69 |
| Apr | .791 | .016 | -.142 | -.023 | 16.75 | 5.98 | 16.75 | 5.16 |
| | .349 | .440 | -.206 | .089 | 5.98 | 6.96 | 5.16 | 5.19 |
| May | .796 | -.023 | -.071 | -.089 | 14.00 | 4.61 | 14.00 | 4.61 |
| | .353 | .421 | -.178 | .014 | 4.61 | 6.12 | 4.61 | 6.12 |
| Jun | .850 | .061 | -.221 | -.002 | 8.37 | 2.69 | 11.69 | 3.58 |
| | .470 | .401 | -.298 | .127 | 2.69 | 4.42 | 3.58 | 5.59 |
| Jul | .888 | -.192 | -.216 | .146 | 6.94 | 2.41 | 9.91 | 4.36 |
| | .497 | .312 | -.314 | .165 | 2.41 | 3.72 | 4.36 | 5.52 |
| Aug | .911 | -.122 | -.194 | .091 | 8.47 | 3.14 | 8.47 | 3.14 |
| | .520 | .266 | -.319 | .179 | 3.14 | 4.86 | 3.14 | 4.86 |
| Sep | .650 | .191 | -.156 | -.015 | 15.99 | 6.78 | 15.99 | 6.78 |
| | .280 | .395 | -.160 | .051 | 6.78 | 7.97 | 6.78 | 7.97 |
| Oct | .623 | .145 | -.182 | .059 | 16.51 | 6.39 | 16.51 | 6.39 |
| | .293 | .391 | -.178 | .086 | 6.39 | 7.95 | 6.39 | 7.95 |
| Nov | .620 | .199 | -.124 | -.029 | 17.90 | 10.87 | 10.16 | 8.19 |
| | .324 | .521 | -.187 | .154 | 10.87 | 13.56 | 8.19 | 13.56 |
| Dec | .626 | .150 | -.013 | -.080 | 20.45 | 14.86 | 14.73 | 11.58 |
| | .312 | .495 | -.075 | .006 | 14.86 | 19.50 | 11.58 | 14.09 |

where the subscripts emphasize that the values vary from day to day on the basis of (3.6). Similarly, white-noise variances indicated in Tables 18 and 19 are adjusted multiplicatively, according to

$$\sigma^{2*} = [\ \sigma^2(\text{obs})\ \sigma^2(2X)\ ] \ /\ \sigma^2(1X) \quad . \tag{3.19}$$

Finally, significant differences in the white-noise correlations indicated in Table 20 are adjusted additively on the scale of the Fisher z-transformation:

$$z\,[r^*] = z\,[r(\text{obs})] + z\,[r(2X)] - z\,[r(1X)] \quad , \tag{3.20}$$

where

$$z\,[r] = \frac{1}{2} \ln [\ (1 + r)\ /\ (1 - r)\ ] \quad . \tag{3.21}$$

This procedure leads to

$$r^* = (\ R^* - 1\ )\ /\ (\ R^* + 1\ ) \quad , \tag{3.22}$$

where

$$R^* = \frac{[\ 1 + r(\text{obs})\ ]\ [\ 1 + r(2X)\ ]\ [\ 1 - r(1X)\ ]}{[\ 1 - r(\text{obs})\ ]\ [\ 1 - r(2X)\ ]\ [\ 1 + r(1X)\ ]} \quad . \tag{3.23}$$

Adjusted covariances (the off-diagonal elements in $\underset{\sim}{V}^*$) are then produced by multiplying $r^*$ in (3.22) by the factor ($\sigma^*\max\ \sigma^*\min$). Elements of $\underset{\sim}{V}$ and $\underset{\sim}{V}^*$ are presented for Boxes 1, 2, and 3 in Tables 21, 22, and 23, respectively.

### 3.5.2. Combined use of grid-scale stochastic weather models and the climate inverse procedure

Combination of stochastic generation of grid-scale daily weather elements with the climate inverse procedure described in Section 2.4.b is direct for the case of the $1X-CO_2$ (i.e., observed) world. Amplitudes of the leading rotated eigenvectors are calculated on the basis of the deviations of maximum and minimum temperatures from their respective means (i.e., $\underset{\sim}{T} - \underset{\sim}{\bar{T}}$) box-scale precipitation ($P_L$) and its square-root, using (2.10). Amplitudes of the smaller-scale modes are chosen randomly, and data for individual stations (scaled to standard normal form) are produced using (2.6). These scaled deviations are then redimensionalized using means and standard deviations derived from the observational data for each station.

Table 24 compares the average January and July monthly maximum temperatures produced by the above procedure for the 27 stations in Box 2 with the corresponding observations. Also included are the respective standard deviations of the monthly means from the overall means. The sample sizes are 36 years for the observations and 31 years for the synthetic data. The values are very well reproduced by the synthetic weather generation procedure, although the standard deviations for January synthetic data appear to be too low. The interpretation is the same for the corresponding minimum temperature data in Table 25.

The synthetic precipitation data, presented in Table 26, follow the observations less closely, as could have been anticipated on the basis of results presented in Section 2.4.c. Nevertheless, several

Table 24. January and July average maximum temperatures (C), with standard deviations, for Box 2 stations -- observed and synthetic data.

| | January | | | | July | | | |
|---|---|---|---|---|---|---|---|---|
| | Observed | | Synthetic | | Observed | | Synthetic | |
| Sta. | avg. | σ | avg. | σ | avg. | σ | avg. | σ |
| 1 | -4.7 | 3.0 | -4.8 | 2.5 | 29.3 | 5.3 | 29.2 | 5.5 |
| 2 | -3.0 | 3.0 | -3.0 | 2.5 | 29.5 | 5.3 | 29.3 | 5.5 |
| 3 | -2.0 | 3.0 | -1.9 | 2.3 | 30.3 | 5.4 | 30.1 | 5.6 |
| 4 | -3.1 | 3.0 | -2.9 | 2.3 | 30.4 | 5.4 | 30.1 | 5.6 |
| 5 | -.6 | 3.0 | -.6 | 2.5 | 30.8 | 5.4 | 30.5 | 5.7 |
| 6 | -4.6 | 3.1 | -4.7 | 2.6 | 29.1 | 5.2 | 29.0 | 5.4 |
| 7 | -.4 | 3.0 | -.4 | 2.3 | 31.2 | 5.6 | 31.0 | 5.8 |
| 8 | -.5 | 2.9 | -.5 | 2.3 | 31.4 | 5.7 | 31.2 | 5.8 |
| 9 | -2.0 | 2.9 | -1.9 | 2.3 | 30.4 | 5.4 | 30.2 | 5.6 |
| 10 | -1.0 | 3.0 | -1.1 | 2.5 | 30.9 | 5.5 | 30.6 | 5.7 |
| 11 | -3.7 | 3.0 | -3.7 | 2.6 | 29.3 | 5.2 | 29.2 | 5.5 |
| 12 | -3.3 | 3.2 | -3.1 | 2.4 | 31.0 | 5.5 | 30.7 | 5.7 |
| 13 | -1.6 | 2.9 | -1.6 | 2.3 | 30.9 | 5.5 | 30.7 | 5.7 |
| 14 | -5.0 | 3.1 | -5.1 | 2.6 | 28.8 | 5.2 | 28.8 | 5.4 |
| 15 | -1.9 | 3.0 | -1.8 | 2.3 | 31.0 | 5.5 | 30.9 | 5.7 |
| 16 | -5.1 | 3.0 | -5.2 | 2.6 | 28.1 | 5.0 | 28.1 | 5.3 |
| 17 | -1.1 | 2.9 | -1.2 | 2.5 | 30.7 | 5.5 | 30.5 | 5.7 |
| 18 | -3.4 | 3.0 | -3.3 | 2.5 | 30.0 | 5.3 | 29.8 | 5.6 |
| 19 | -5.1 | 3.3 | -4.8 | 2.5 | 29.0 | 5.2 | 29.0 | 5.4 |
| 20 | -6.1 | 3.4 | -6.0 | 2.7 | 28.5 | 5.1 | 28.4 | 5.3 |
| 21 | 1.1 | 3.1 | 1.0 | 2.4 | 31.4 | 5.7 | 31.1 | 5.8 |
| 22 | .3 | 3.0 | .3 | 2.1 | 31.8 | 5.8 | 31.5 | 5.9 |
| 23 | -.9 | 3.1 | -1.0 | 2.2 | 31.6 | 5.6 | 31.3 | 5.8 |
| 24 | -2.4 | 3.2 | -2.3 | 2.4 | 30.0 | 5.9 | 30.0 | 5.6 |
| 25 | -.4 | 2.8 | -.3 | 2.1 | 31.9 | 5.8 | 31.6 | 5.9 |
| 26 | -2.0 | 3.2 | -2.0 | 2.3 | 30.9 | 5.5 | 30.8 | 5.7 |
| 27 | -5.1 | 3.4 | -4.9 | 2.4 | 30.0 | 5.4 | 30.0 | 5.6 |

Table 25. As Table 24, for average minimum temperatures (C).

| | January | | | | July | | | |
|---|---|---|---|---|---|---|---|---|
| | Observed | | Synthetic | | Observed | | Synthetic | |
| Sta. | avg. | σ | avg. | σ | avg. | σ | avg. | σ |
| 1 | -15.1 | 4.1 | -15.1 | 3.8 | 16.4 | 3.1 | 16.3 | 3.1 |
| 2 | -13.3 | 3.7 | -13.1 | 3.6 | 17.2 | 3.2 | 17.2 | 3.3 |
| 3 | -13.5 | 3.6 | -13.6 | 3.6 | 16.9 | 3.3 | 16.8 | 3.2 |
| 4 | -14.0 | 3.6 | -13.8 | 3.6 | 16.4 | 3.2 | 16.3 | 3.2 |
| 5 | -12.0 | 3.7 | -12.0 | 3.5 | 17.2 | 3.3 | 17.2 | 3.3 |
| 6 | -14.8 | 4.2 | -14.9 | 3.9 | 16.5 | 3.1 | 16.5 | 3.2 |
| 7 | -11.7 | 3.4 | -11.6 | 3.2 | 18.0 | 3.4 | 18.0 | 3.4 |
| 8 | -11.8 | 3.4 | -11.8 | 3.3 | 18.2 | 3.4 | 18.2 | 3.5 |
| 9 | -13.1 | 3.6 | -13.1 | 3.5 | 17.5 | 3.3 | 17.3 | 3.3 |
| 10 | -12.0 | 3.8 | -11.9 | 3.5 | 17.6 | 3.4 | 17.5 | 3.3 |
| 11 | -14.4 | 4.0 | -14.3 | 3.8 | 16.4 | 3.1 | 16.4 | 3.1 |
| 12 | -14.9 | 4.0 | -14.9 | 3.7 | 17.0 | 3.3 | 16.8 | 3.2 |
| 13 | -12.8 | 3.5 | -12.7 | 3.4 | 17.9 | 3.4 | 17.9 | 3.4 |
| 14 | -15.5 | 4.1 | -15.5 | 3.9 | 16.2 | 3.1 | 16.3 | 3.1 |
| 15 | -13.5 | 3.6 | -13.6 | 3.5 | 17.7 | 3.3 | 17.5 | 3.3 |
| 16 | -15.3 | 4.2 | -15.4 | 3.9 | 16.5 | 3.2 | 16.5 | 3.2 |
| 17 | -11.6 | 3.6 | -11.3 | 3.4 | 18.0 | 3.3 | 18.0 | 3.4 |
| 18 | -14.1 | 3.8 | -13.9 | 3.6 | 17.0 | 3.1 | 17.0 | 3.2 |
| 19 | -16.4 | 4.2 | -16.3 | 3.9 | 16.0 | 3.1 | 15.8 | 3.1 |
| 20 | -16.2 | 4.6 | -16.1 | 4.0 | 16.7 | 3.1 | 16.7 | 3.2 |
| 21 | -9.8 | 3.6 | -9.7 | 3.1 | 18.7 | 3.4 | 18.7 | 3.5 |
| 22 | -11.1 | 3.1 | -11.2 | 3.0 | 18.7 | 3.4 | 18.6 | 3.5 |
| 23 | -13.9 | 3.5 | -14.0 | 3.3 | 17.2 | 3.2 | 17.0 | 3.3 |
| 24 | -12.5 | 3.7 | -12.2 | 3.3 | 18.9 | 3.8 | 18.8 | 3.5 |
| 25 | -11.3 | 3.2 | -11.3 | 2.9 | 18.6 | 3.4 | 18.6 | 3.5 |
| 26 | -14.6 | 3.8 | -14.8 | 3.6 | 16.8 | 3.1 | 16.5 | 3.2 |
| 27 | -16.7 | 4.4 | -16.6 | 3.9 | 16.7 | 3.3 | 16.4 | 3.2 |

Table 26. As table 24 for total monthly precipitation (mm).

| | January | | | | July | | | |
|---|---|---|---|---|---|---|---|---|
| | Observed | | Synthetic | | Observed | | Synthetic | |
| Sta. | avg. | σ | avg. | σ | avg. | σ | avg. | σ |
| 1 | 19.2 | 16.4 | 9.0 | 6.0 | 94.8 | 47.8 | 111.0 | 74.0 |
| 2 | 20.5 | 14.6 | 13.0 | 11.0 | 89.2 | 47.1 | 70.0 | 58.0 |
| 3 | 20.8 | 16.5 | 16.0 | 13.0 | 89.4 | 51.1 | 61.0 | 44.0 |
| 4 | 21.9 | 14.5 | 17.0 | 15.0 | 91.0 | 66.8 | 72.0 | 54.0 |
| 5 | 27.9 | 19.7 | 17.0 | 14.0 | 103.2 | 63.8 | 113.0 | 80.0 |
| 6 | 23.5 | 17.3 | 10.0 | 7.0 | 103.8 | 45.0 | 137.0 | 86.0 |
| 7 | 24.7 | 20.6 | 14.0 | 13.0 | 110.1 | 84.7 | 101.0 | 88.0 |
| 8 | 21.9 | 17.8 | 16.0 | 12.0 | 98.7 | 68.8 | 80.0 | 75.0 |
| 9 | 21.7 | 15.4 | 20.0 | 14.0 | 95.8 | 69.0 | 72.0 | 71.0 |
| 10 | 28.3 | 22.2 | 27.0 | 23.0 | 93.0 | 58.4 | 99.0 | 132.0 |
| 11 | 23.6 | 18.3 | 8.0 | 7.0 | 108.8 | 57.7 | 98.0 | 70.0 |
| 12 | 15.1 | 14.6 | 13.0 | 12.0 | 84.6 | 49.5 | 78.0 | 67.0 |
| 13 | 23.4 | 17.3 | 19.0 | 14.0 | 88.4 | 54.4 | 78.0 | 63.0 |
| 14 | 20.6 | 17.0 | 14.0 | 13.0 | 107.7 | 51.7 | 114.0 | 72.0 |
| 15 | 20.0 | 18.7 | 15.0 | 12.0 | 86.8 | 51.8 | 78.0 | 56.0 |
| 16 | 24.9 | 19.2 | 9.0 | 7.0 | 110.6 | 51.7 | 143.0 | 92.0 |
| 17 | 32.3 | 21.8 | 19.0 | 15.0 | 98.1 | 55.3 | 113.0 | 88.0 |
| 18 | 20.2 | 15.1 | 16.0 | 18.0 | 103.1 | 57.3 | 89.0 | 78.0 |
| 19 | 15.6 | 11.6 | 10.0 | 7.0 | 94.9 | 59.4 | 86.0 | 55.0 |
| 20 | 21.1 | 17.4 | 19.0 | 18.0 | 105.3 | 57.3 | 113.0 | 73.0 |
| 21 | 31.6 | 27.7 | 21.0 | 14.0 | 102.7 | 66.5 | 94.0 | 89.0 |
| 22 | 19.2 | 19.0 | 16.0 | 12.0 | 86.8 | 47.0 | 69.0 | 46.0 |
| 23 | 14.9 | 15.1 | 12.0 | 11.0 | 87.6 | 49.7 | 79.0 | 75.0 |
| 24 | 16.1 | 12.8 | 20.0 | 16.0 | 73.4 | 62.4 | 93.0 | 79.0 |
| 25 | 16.1 | 14.6 | 13.0 | 15.0 | 77.1 | 43.2 | 62.0 | 45.0 |
| 26 | 17.2 | 15.3 | 14.0 | 11.0 | 87.9 | 54.3 | 77.0 | 61.0 |
| 27 | 14.0 | 10.9 | 10.0 | 8.0 | 74.7 | 40.7 | 71.0 | 71.0 |

salient features of the observed data are reasonably well approximated by the synthetic data. First, the mean levels are approximately reproduced, as are the order-of-magnitude changes in average total precipitation between January and July. The standard deviations are of the same order of magnitude as the means in both data sets, indicating that strong positive skewness exists in the synthetic as well as the observational data. July standard deviations are typically too high in the synthetic data, which reflects the occasional production of very large daily precipitation amounts by the climate inverse scheme as discussed in Sections 2.4.b and 2.4.c. Finally, the east-west gradient of average monthly precipitation is evident in both data sets. Synthetic data for other months and gridboxes are similarly comparable to the respective observations.

For the case of grid-scale data generated using inferred 2X-$CO_2$ parameters (denoted with asterisks in Section 3.5.a) generation of local data elements (in standard normal form) using (2.1) and (2.6) is the same as described above for the 1X-$CO_2$ grid-scale time series. However, station-scale means and standard deviations for temperatures and precipitation in a 2X-$CO_2$ world are unknown, and some assumption must be made regarding them. Precipitation means and all standard deviations on the station scale are assumed here to be equal for the 1X-$CO_2$ and 2X-$CO_2$ climates. Absolute precipitation amounts, and the magnitudes of temperature variations are explicitly modeled in the procedure for generating gridscale weather data described in Section 3.3, and this information is transmitted to the climate inverse procedure. Accordingly, the above assumptions are consistent with an assumption implicit in this section; namely, that relationships among stations within a gridbox will be similar in the $1X$-$CO_2$ and $2X$-$CO_2$ worlds.

However, information regarding mean temperature has been removed from the procedure in (2.10), since the temperature predictors in that equation are deviations from mean levels. This procedure is desirable from the standpoint of not distorting the correlation structure between temperature and precipitation (particularly for the cool season, where the relative strength of the broad-scale precipitation mode depends substantially on temperature), which is based on observational data. Some adjustment is obviously required if the large temperature increases predicted by the GCM are to be reflected in the station-scale data. It is assumed here that $2X$-$CO_2$ temperature means at individual stations increase by amounts equal to increases at the gridscale, and that these means vary on a daily basis. That is,

$$\bar{\tilde{T}}^{*}_{j,t} = \bar{\tilde{T}}_{j,t}(\mathrm{obs}) + \bar{\tilde{T}}_{t}(2X) - \bar{\tilde{T}}_{t}(1X) \quad , \qquad (3.24)$$

where $\bar{\tilde{T}}^{*}(t)_{j,t}$ is the inferred $2X$-$CO_2$ station mean for station $j$ on julian date t, the first term on the right-hand side is the corresponding value from the observations in (2.4a), and the last two terms are the gridscale values from (3.6).

### 3.5.3. Specification of local solar radiation data

It would be desirable, in view of the anticipated use of the present procedure in conjunction with crop models, to incorporate solar radiation in the climate inverse formulation developed in Section 2. Unfortunately, each of the three gridboxes considered contains only a single location for which daily solar radiation data are available (National Climatic Center, 1978). These SOLMET stations are Dodge City, Kansas (Box 1, station 5), North Omaha, Nebraska (Box 2, station 24), and Bismarck, North Dakota (Box 3, station 1). The periods of record for radiation data at these stations are June 1957 through December 1976 for North Omaha, and July 1952 through December 1976 for Dodge City and Bismarck. Rather than include radiation in the climate inverse procedure directly, it is necessary to predict radiation values consistent with the generated surface weather data on the basis of observations at the available stations, and to assume that similar relationships hold at other stations within the same box.

Separate linear regression equations are developed relating daily global radiation (langleys) to maximum and minimum temperatures and total daily precipitation for each of these stations, and separately for each calandar month. Since it is intended that these equations represent the relationships among the variables throughout each gridbox, as well as under a 2X-$CO_2$ climate, temperature data are converted to standard normal form before fitting. Values in the SOLMET data sets greater than the maximum possible incoming solar radiation at the top of the atmosphere were discarded prior to the analysis.

The resulting regression parameters are tabulated in Table 27, which also includes the mean squared errors for each regression equation, and the coefficients of determination. In using these equations in a Monte Carlo setting, a Gaussian noise term (with variance equal to the mean squared error of that regression equation) is added, as is done in the implementation of (2.10) for simulation.

Table 27. Regression coefficients for prediction of daily global radiation (langleys) from maximum temperature, minimum temperature, and precipitation; and mean squared errors and coefficients of determination. Temperature coefficients are for predictors transformed to standard normal form.

a. Box 1 (Dodge City, Kansas)

| | Coefficients | | | | | |
|---|---|---|---|---|---|---|
| Month | Const (ly) | Max (ly) | Min (ly) | Ppt (ly/mm) | MSE | $R^2$ |
| Jan | 236.3 | 56.6 | -44.7 | -10.4 | 4515. | .9275 |
| Feb | 313.6 | 84.8 | -69.7 | -10.1 | 8596. | .9216 |
| Mar | 411.7 | 129.9 | -99.5 | -6.3 | 13290. | .9290 |
| Apr | 515.5 | 140.7 | -108.9 | -8.3 | 17230. | .9400 |
| May | 570.8 | 171.4 | -105.0 | -5.4 | 17300. | .9520 |
| Jun | 646.1 | 116.0 | -62.2 | -4.6 | 13080. | .9697 |
| Jul | 642.3 | 115.1 | -64.0 | -3.1 | 10660. | .9742 |
| Aug | 564.7 | 114.0 | -54.7 | -3.5 | 10280. | .9696 |
| Sep | 459.2 | 130.6 | -71.1 | -3.9 | 9937. | .9555 |
| Oct | 357.4 | 98.1 | -61.5 | -4.7 | 7287. | .9476 |
| Nov | 253.5 | 67.6 | -54.4 | -9.4 | 4655. | .9345 |
| Dec | 214.9 | 52.9 | -44.0 | -10.7 | 3767. | .9246 |

b. Box 2 (Omaha, Nebraska)

| | Coefficients | | | | | |
|---|---|---|---|---|---|---|
| Month | Const (ly) | Max (ly) | Min (ly) | Ppt (ly/mm) | MSE | $R^2$ |
| Jan | 197.1 | 32.9 | -46.0 | -10.7 | 4005. | .9053 |
| Feb | 275.5 | 72.1 | -91.9 | -10.1 | 7696. | .9070 |
| Mar | 361.5 | 100.1 | -115.4 | -11.0 | 12310. | .9143 |
| Apr | 445.7 | 161.6 | -129.1 | -9.8 | 14960. | .9314 |
| May | 532.4 | 168.9 | -130.2 | -5.0 | 15540. | .9487 |
| Jun | 599.7 | 132.1 | -93.8 | -4.8 | 13800. | .9623 |
| Jul | 587.2 | 121.6 | -98.1 | -4.4 | 13800. | .9612 |
| Aug | 514.9 | 115.4 | -81.2 | -3.5 | 12650. | .9543 |
| Sep | 399.2 | 131.4 | -94.1 | -3.2 | 13160. | .9224 |
| Oct | 290.6 | 98.5 | -83.8 | -4.1 | 7574. | .9236 |
| Nov | 187.9 | 69.6 | -75.5 | -6.0 | 4251. | .8987 |
| Dec | 162.6 | 51.0 | -63.3 | -6.3 | 3804. | .8706 |

Table 27, continued.

c. Box 3 (Bismarck, North Dakota)

| Month | Const (ly) | Max (ly) | Min (ly) | Ppt (ly/mm) | MSE | $R^2$ |
|---|---|---|---|---|---|---|
| | Coefficients | | | | | |
| Jan | 152.6 | 4.4 | -18.5 | -12.3 | 2180. | .9101 |
| Feb | 238.5 | 23.9 | -48.7 | -13.7 | 4721. | .9217 |
| Mar | 342.1 | 62.4 | -90.3 | -10.4 | 10580. | .9181 |
| Apr | 422.1 | 115.3 | -102.9 | -9.8 | 14910. | .9238 |
| May | 539.7 | 142.8 | -106.4 | -8.8 | 16820. | .9457 |
| Jun | 586.8 | 126.8 | -73.8 | -6.0 | 18430. | .9482 |
| Jul | 598.5 | 75.4 | -51.9 | -7.2 | 13110. | .9653 |
| Aug | 519.7 | 78.7 | -49.7 | -5.8 | 13250. | .9534 |
| Sep | 378.8 | 87.4 | -43.9 | -8.1 | 10580. | .9344 |
| Oct | 254.0 | 59.7 | -44.3 | -6.8 | 5750. | .9231 |
| Nov | 152.2 | 35.0 | -39.8 | -7.7 | 3166. | .8800 |
| Dec | 120.2 | 15.3 | -27.0 | -7.4 | 2183. | .8666 |

Possible spatial correlation of the noise term is ignored.

The pattern of the radiation regression parameters in time appears to be physically sensible for each of the three gridboxes. The constant terms and coefficients for maximum temperature exhibit annual cycles with maxima in June and minima in December, which reflects the astronomical forcing. The coefficients for maximum temperature are all positive, and the coefficients for minimum temperature and precipitation are all negative. These results reflect the positive correlation between maximum temperature and solar heating, the positive correlation between minimum temperature and cloud cover, the positive correlation of precipitation and cloud cover, and the negative correlation between cloud cover and solar radiation at the ground. Percent variance described by the regressions are typically 90% to 95%.

## 3.6 Summary and Conclusions

This section has developed a multivariate stochastic model for three daily surface weather model elements on the gridscale, and discussed the characterization of daily weather in terms of the parameters of this model. This stochastic model is then used to extrapolate to a climate scenario consistent with the relative changes in its parameters as derived from 1X-$CO_2$ and 2X-$CO_2$ realizations of the OSU GCM. The coupling of these grid-scale stochastic models with the stochastic climate inverse procedure described in Section 2.4.b was then described, and results were presented comparing summary statistics for the observations with a realization of the corresponding stochastic data.

This procedure appears to be well-suited as a link between large-scale GCMs, with which possible future climate changes are commonly explored, and crop simulation models, which are designed to represent much smaller spatial scales. The applicability of specific results derived from the particular GCM realizations treated here, however, is not clear. Apart from deficiencies inherent in the GCM, the data available here are not (at least for the 2X-$CO_2$ realization) a sample from its equilibrium climate. It is not clear that the transient response of the climate system to $CO_2$-induced warming will be qualitatively similar to the eventual equilibrium state (e.g., Schneider, 1984; Thompson and Schneider, 1982), although recent results indicate that the differences may not be large (Barnett, 1986). A case study of the applicability of the present procedure to assessment of agricultural consequences of $CO_2$-induced climatic changes is presented in Section 4, but the quality of the resulting agronomic "forecasts" derived from the particular GCM realizations treated here will be influenced by these considerations.

# Section 4

## Some Possible Consequences of $CO_2$-Induced Climate Change on North American Agriculture

### 4.1 Introduction

It is a widely held view that increasing atmospheric carbon dioxide concentrations are producing or will produce changes in the climate of the Earth. In particular, numerous modeling efforts project very substantial surface air temperature increases (Schlesinger, 1986). In addition to a general warming of the atmosphere, the possibility of increased summer dryness in the continental midlatitudes has been suggested on the basis of both historical analogs (Jager and Kellogg, 1983; Schneider, 1984; Wigley *et al.*, 1980) and GCM studies (Manabe and Wetherald, 1986; Manabe *et al.*, 1981).

Agricultural productivity is one area where the consequences of climate variations are felt particularly strongly (e.g., Bryson and Murray, 1977; Lamb, 1982; Sakamoto *et al.*, 1980; Thompson, 1975; Waggoner, 1983), so that agriculture may be particularly vulnerable to climatic changes induced by increasing carbon dioxide (Waggoner, 1983). It has been suggested that a warmer and dryer climate in central North America, for example, could result in crop yield decreases (Waggoner, 1983), and shifts of major cropping areas (e.g., Butzer, 1980; Newman, 1980; Rosenzweig, 1985). Large dislocations in global food supply could occur as a consequence, since this area is the principal world grain surplus region (Oram, 1985).

However, agriculture has been historically and continues to be adaptable (Clark, 1985; Kimball, 1985; Rosenberg, 1982; Waggoner, 1983), and it is anticipated that the accomodation of the climate system to carbon dioxide increases will be slow, as a consequence of the long response time of the deep ocean (Schlesinger, 1986). It is particularly important, therefore, that projections of agricultural potential in the future not assume that practices that are currently optimal will necessarily continue to be so. Indeed, a more reasonable assumption is that agriculture will be nearly fully adapted to prevailing climatic conditions at any stage of the warming (Clark, 1985).

One attractive means of studying the relationships between climatic variations and agricultural production is through the use of crop-climate models. There are two major types of these models: empirical-statistical; and process-oriented or physiological simulation models (Baier, 1977; Sakamoto, 1981; World Climate Applications Programme, 1984). The former seek to describe, through the parameters of multiple regression analyses, the historical relationships between averaged weather or climate data and crop yields. Typical examples are found in the work of Thompson (1969a,b). Although they are relatively simple to develop and use, the regression-based models suffer from a number of limitations. They are necessarily site-specific and highly aggregated in space and time. Moreover, the use of intercorrelated predictor variables may produce misleading results, particularly for conditions near the extremes or outside the range of the historical record (Katz, 1977c; World Climate Applications Programme, 1984). Empirical- statistical models are therefore not appropriate tools for the study of the impacts of a changed climate on agriculture (World Climate Programme, 1984).

Process-oriented crop models deterministically model crop growth on small spatial scales based on the physiology and phenology of the plant, the physics of evaporation, and the values of local meteorological variables. They are, in principle, fully generalizable to any location, and reliable for extreme as well as more "normal" conditions. The time resolution of this type of model, typically on the order of one day, is sufficient to respond to short-term weather events and their interactions with stages of plant development. This capacity may be critical to adequate representation of crop response (Mearns _et_ _al_., 1984; Neild _et_ _al_., 1979; Parry and Carter, 1985).

This section illustrates of the use of the climate scenarios constructed in Section 3, for agricultural impact analysis using physiological crop models for corn (maize) and wheat. In this analysis, possible relative changes in the yields of these crops in a 2X-$CO_2$ world are modeled. The gridboxes analyzed in earlier sections, which represent three important North American grain cropping regions, are treated separately. Section 4.2 describes the crop models employed, and Section 4.3 enumerates constants and initial conditions used in the crop simulations. Section 4.4 presents the results, and Section 4.5 contains a summary and conclusions.

## 4.2 Description of the Crop Simulation Models

### 4.2.1. Grain corn (maize)

The response of grain corn (maize) to the changed climate is studied using the physiological crop model CORNF (Stapper and Arkin, 1980). This model simulates growth and development of a hypothetical representative corn plant, based on daily values of maximum temperature, minimum temperature, precipitation, and solar radiation. Additional initial information, such as latitude, plant population density, seeding depth, soil characteristics, and initial soil moisture content, are also required. One major advantage to the use of CORNF in conjunction with the climate inverse procedure presented in Section 2 derives from the fact that it was developed using the method of Priestley and Taylor (1972) for estimation of potential evaporation. This is an energy balance approach which, in effect, assumes a Bowen ratio that varies as a function of temperature. The soil water balance submodel therefore does not use windspeed or humidity data, which are unavailable on the required scale.

The stages of development of the corn plant have been well characterized (Hanway, 1963), and this framework is the basis for the organization of CORNF. Progression from stage to stage within CORNF is controlled by the accumulation of growing degree days. This "thermal time scale" (Monteith, 1981) is a commonly and successfully used means of precicting corn development (e.g., World Meteorological Organization, 1977). Within a given phenological stage, the rates of physiological processes (e.g. photosynthesis and kernel growth) are controlled using rate functions derived from empirical results. These functions transform values of the meteorological data, soil water stress, and the previous history of the plant (as reflected in dry matter accumulation) to daily increments of the physiological processes. Influences of insects, diseases, weeds, suboptimal nutrient levels, or hail damage are not included in CORNF. More information concerning the details of the operation of CORNF is given in Stapper and Arkin (1980).

A very broad range of corn cultivars (i.e., varieties) exists, the characteristics of which are closely matched in practice to local growing conditions (e.g., Martin _et_ _al_., 1976). The most salient aspect of the differences among corn varieties from the standpoint of modeling phenology and yield is the rate of maturity. An "early" variety for a particular location requires fewer heat units to mature, but has a lower potential yield than a "late" variety. One essential attribute of a widely applicable corn model is the capacity to account for these differences in rates of maturity. This is accomplished in CORNF with discrete "maturity classes," which range from 1 (earliest) to 9 (latest).

An important aspect of crop simulation in the present context is adequate representation of the timing of plant development, since it is typically the case that crop plants are especially vulnerable to environmental extremes during particular phenological stages (e.g., Salter and Goode, 1967; Shaw, 1983). It has been shown that CORNF performs well in this regard (Stapper and Arkin, 1980; Wright and Keener, 1982). However, absolute levels of yield match observations less well, and cannot be literally relied upon (Stapper and Arkin, 1980; Wright and Keener, 1982).

4.2.2. Wheat

The possible effects of a changed climate on wheat agriculture is studied with the model TAMW (Maas and Arkin, 1980a). It is similar to CORNF in that it simulates crop response on the basis of the physiology of a single "average" plant. Also, potential evaporation is estimated using the Priestley-Taylor formulation, so that the same readily available meteorological variables are used to drive TAMW and CORNF.

The principal difference in the basic form of the two models is in the treatment of phenological development. Progression to succeeding phenological stages for the wheat plant (cf. Large, 1954) is accomplished by daily summation of reciprocal values of "duration" functions, rather than accumulation of heat units. This approach is taken in order to better model the processes of vernalization and tillering. The duration functions are particular to each stage of development, and depend on daily temperatures, soil water stress, and snow depth. Solar radiation is used in TAMW only in the estimation of potential evaporation.

As for the case of CORNF, rate functions control the daily levels of physiological activities within each stage of development. The rate functions respond to the same environmental variables as the duration functions, and the forms of both functions are derived from empirical results. Again, no impairments of plant growth or development due to pests, weeds, nutrient levels, or hail damage are included in TAMW. Also, TAMW does not account for whole-plant death due to excessively cold temperatures (winterkill), which can be important for winter wheat.

Characteristics of different wheat varieties are treated in TAMW through the suites of particular numerical values of the rate and duration functions. The values of these functions corresponding to specific cultivars, and further details on model operation in general are available in Maas and Arkin (1980a).

As is the case for CORNF, simulation of phenological development in TAMW compares well with observations, while absolute magnitudes of yield predictions reproduce the observations less well (Maas and Arkin, 1980b).

### 4.2.3. Modifications to the crop models

Several modifications to the soil water balance submodels of CORNF and TAMW were made prior to beginning crop simulations. Both crop models use the soil water model of Ritchie (1972), with potential evaporation estimated using the formulation of Priestley and Taylor (1972).

While the simplicity of the Priestley-Taylor formulation is attractive, it is prone to underestimation of potential evaporation, particularly at higher temperatures (Jury and Tanner, 1975). Its performance has been improved by Kanemasu _et al_. (1976) by increasing estimated evaporation by 10% for days on which maximum temperature exceeds 33 C. This correction is adopted in the present work as well.

The Ritchie (1972) model contains two soil-specific parameters, U and c. The parameter U specifies the amount of water which must be evaporated from a soil surface before the evaporation rate is limited by (in addition to available radiant energy) soil hydraulic properties. This parameter is an input variable for both crop models in the forms received from their authors. The parameter c controls the rate of evaporation after the initial energy-limited stage. The original soil water balance submodel in CORNF assumes a constant value for c, and the FORTRAN code for CORNF was modified to accept different values for different soils.

The final modification pertains to the treatment of loss of rainfall through the process of runoff from soil surfaces. Some formulation representing runoff is a desirable feature of any soil water model. It is particularly important for the present work, since the climate inverse procedure described in Section 2 occasionally produces unrealistically large daily precipitation amounts. The original FORTRAN code for TAMW contains no provision for loss of water from the soil/crop system by this mechanism. While CORNF contains code to calculate runoff, it is done in a way which does not depend on soil properties, following only a portion of the traditional procedure (Soil Conservation Service, 1972). Moreover, the calculation does not influence the model soil water balance as a consequence, apparently, of a programming error. The representation of runoff employed here for both crop models is equivalent to that developed in Appendix B. This formulation calculates the amount of precipitation absorbed by the soil on the basis of both daily precipitation amount and the soil parameter $A_{max}$, which specifies the maximum instantaneous rate at which the soil can absorb water.

Carbon dioxide is a limiting nutrient for plant growth at current concentrations (Strain, 1985). Aside from climatic effects, increasing carbon dioxide concentrations will affect crops directly, through changes in plant physiology (Acock and Allen, 1985; Cure, 1985; Waggoner, 1983). The consequences for crop yield may be quite large, and it would be desirable to include a treatment of these effects in the present modeling exercise.

It is unfortunately not straightforward to incorporate this influence into the crop models, due to interactions with other plant processes and with other environmental conditions, and it has not been attempted here. Direct effects of carbon dioxide on plant physiological processes are included in neither CORNF nor TAMW, and their alteration to adequately incorporate the many influences and interactions would be a large project in itself (Reynolds and Acock, 1985), and clearly beyond the scope of the present work.

The wheat model, TAMW, is relatively insensitive to snow depth (Arkin et al., 1983; Larsen 1983), and for simplicity this variable is assumed to be zero in all simulations.

## 4.3 Initial Conditions for Crop Simulations

Soil properties are assigned to stations on the basis of the "resource regions" of Austin (1972). These resource regions are generalized groupings of land on the basis of agricultural potential and use, using primarily soil and climate information. A single soil type is selected here as representative of each resource region (Austin, 1972), and the relevant soil properties are assigned to all stations within that resource region on the basis of soil descriptions taken from County Soil Surveys. Table 28 shows the profiles of soil texture representing Box 1 stations, Table 29 shows the soil profiles representing Box 2 stations, and Table 30 shows the soil profiles representing Box 3 stations. Soils are regarded as being comprised of homogeneous 10-cm thick layers, and having maximum depths of 150 cm.

Plant-available water capacity for each 10-cm soil layer is assigned on the basis of its textural designation following Buckman and Brady (1969), as indicated in Table 31. Also presented as a function of soil textural designation in Table 31 are effective values of the water absorption parameter, $A_{max}$, for the runoff formulation of Appendix B. These values of $A_{max}$ are taken from the lower limits of the ranges given as "typical" maximum infiltration rates for wet soils by Hillel (1971), in order to account somewhat for greater runoff due to slopes and "puddling" (Buckman and Brady, 1969). Values of $A_{max}$ characterizing each soil are calculated by depth-weighting the data presented in Table 31 according to the proportion of each textural class in the profile as presented in Tables 28, 29, and 30. Values of the soil evaporation parameters U and c are calculated according to the method of Jaafar _et al_. (1978), except in the case of Soil X (Table 30), for which this procedure is inappropriate. In this case the values are taken from Ritchie _et al_. (1972). Soil surface layers throughout the three study areas are generally dark (typical Munsell designation for dry soils is 10YR 4/2, dark greyish brown), and the surface albedo for all soils is accordingly assumed to be 0.08 (Geiger, 1965).

Soil moisture at time of seeding exhibits large interannual variations, and has a strong influence on crop yield in the regions considered here (e.g., Mathews and Army, 1960). One approach to

Table 28. Assumed soil textural profiles for Box 1 soils. The symbol "+" denotes finer than normal for the given textural designation. Key to abbreviations for textural designations is given in Table 4.4.

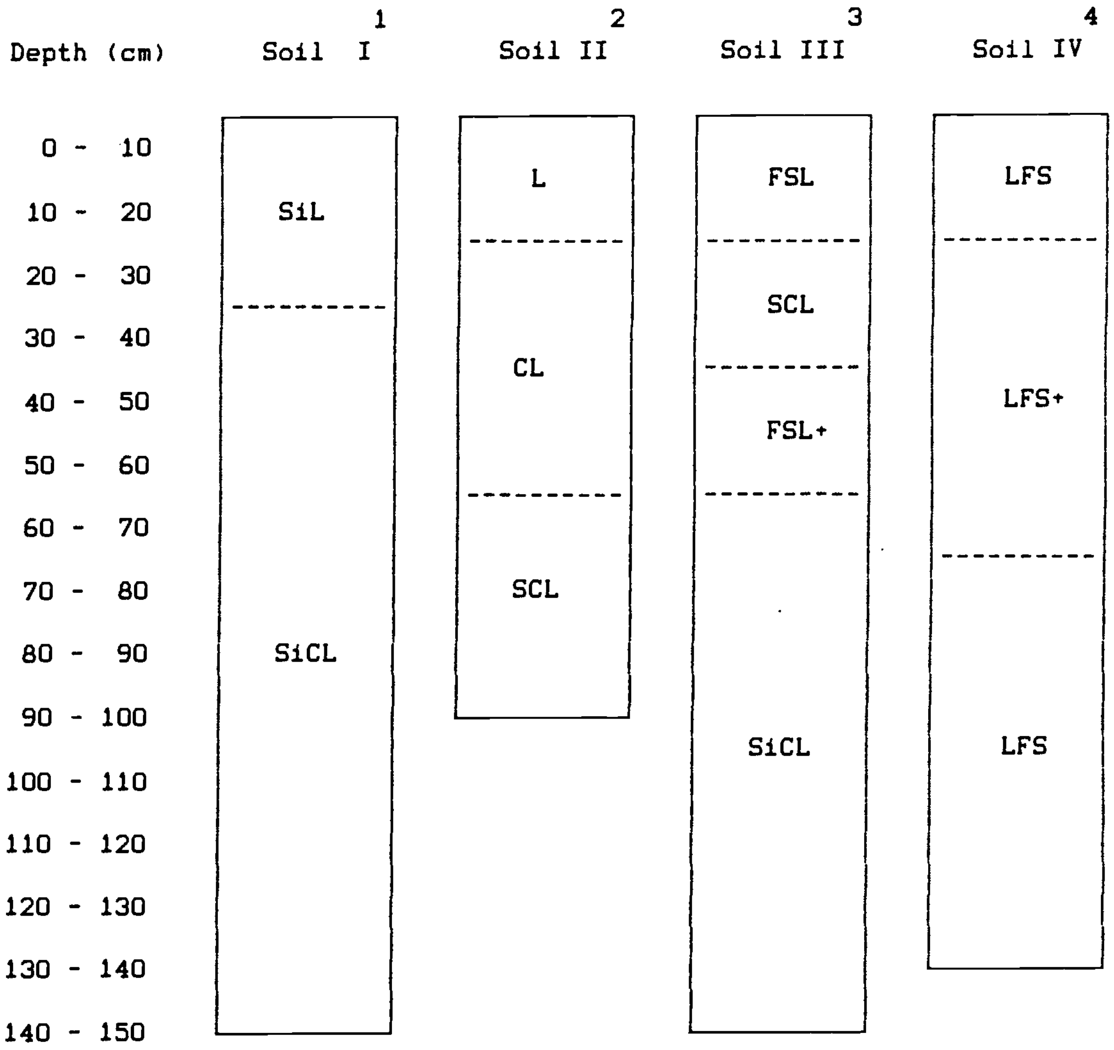


1 Hastings SiL (Soil Conservation Service, 1967). Assumed for stations 1-6, 8, 9, 13, 14, 16-21, 23, 24.
2 Lancaster L (Soil Conservation Service, 1980). Assumed for stations 12, 15.
3 Dalhart FSL (Soil Conservation Service, 1965). Assumed for stations 11, 22.
4 Pratt LFS (Soil Conservation Service, 1965). Assumed for stations 7, 10.

Table 29. As Table 28, for Box 2 soils.

| Depth (cm) | Soil V[1] | Soil VI[2] |
|---|---|---|
| 0 - 10 | | |
| 10 - 20 | | |
| 20 - 30 | | |
| 30 - 40 | | |
| 40 - 50 | | |
| 50 - 60 | | |
| 60 - 70 | | |
| 70 - 80 | L | SiCL |
| 80 - 90 | | |
| 90 - 100 | | |
| 100 - 110 | | |
| 110 - 120 | | |
| 120 - 130 | | |
| 130 - 140 | | |
| 140 - 150 | | |

1 Clarion L (Soil Conservation Service, 1981). Assumed for stations 1, 2, 6, 11, 14, 16, 18-20.

2 Sharpsburg SiCL (Soil Conservation Service, 1978). Assumed for stations 3-5, 7-10, 12, 13, 15, 17, 21-27.

Table 30. As Table 28, for Box 3 soils. The symbol "-" indicates coarser than normal for the given textural designation.

| Depth (cm) | Soil VII [1] | Soil VIII [2] | Soil IX [3] | Soil X [4] |
|---|---|---|---|---|
| 0 - 10 | L | SiL | L | SiC |
| 10 - 20 | | | | |
| 20 - 30 | CL- | | | C |
| 30 - 40 | | SiCL | | |
| 40 - 50 | CL | | | |
| 50 - 60 | | | | |
| 60 - 70 | CL- | | | |
| 70 - 80 | | L | | |
| 80 - 90 | | | | |
| 90 - 100 | | | | |
| 100 - 110 | | | | |
| 110 - 120 | | | | |
| 120 - 130 | | | | |
| 130 - 140 | | | | |
| 140 - 150 | | | | |

1 Williams L (Soil Conservation Service, 1974). Assumed for stations 1,16,19,20.

2 Morton SiL (Soil Conservation Service, 1974). Assumed for stations 8,10,11,15,23,26.

3 Svea L (Soil Conservation Service, 1975). Assumed for stations 2-7,9,12-14,17,18,22.

4 Promise SiC (Soil Conservation Service, 1985). Assumed for stations 21,24, 25.

Table 31. Assumed available soil water capacities (AWC) and maximum infiltration rates (Amax) for soil textural classes.

| Soil Textural Class | | AWC (mm/mm) * | $A_{max}$ (mm/hr) ** |
|---|---|---|---|
| Loamy fine sand | (LFS) | .09 | 12.0 |
| Fine sandy loam | (FSL) | .11 | 8.0 |
| Loam | (L) | .15 | 4.0 |
| Silt Loam | (SiL) | .16 | 3.5 |
| Sandy clay loam | (SCL) | .17 | 3.5 |
| Clay loam | (CL) | .18 | 2.5 |
| Silty clay loam | (SiCL) | .18 | 1.5 |
| Silty clay | (SiC) | .14 | 1.0 |
| Clay | (C) | .14 | 1.0 |

* From Buckman and Brady (1969)
** From Hillel (1971)

obtaining initial values for this variable would be to run the soil water balance submodels of the respective crop models continuously (i.e., between simulated harvest and the following planting date as well as during crop development). This was not done in order to reduce the computational burden. Instead, initial soil moisture is modeled as a random variable which is independent of past and subsequent growing season precipitation.

The Gaussian distribution is assumed for initial soil moisture for spring-sown crops (spring wheat and corn), and the Chi-square distribution is assumed for fall-sown crops (winter wheat). This distinction is natural in view of the precipitation climatologies for the respective fallow (i.e., between-cropping) periods. For the case of spring-sown crops, initial soil moisture may be regarded to a first approximation as the sum of precipitation from perhaps 6 or 7 cool-season months, for which the distributions of total precipitation exhibit only moderate positive skewness. The central limit theorem would lead one to consider the Gaussian distribution as a first approximation, and available data support this choice approximately (Baier, 1971; Mathews and Army, 1960; Shaw, 1965; Wadleigh et al., 1965). For the case of winter wheat, the corresponding random sum is comprised of only 2 or 3 warm-season months, for which the distributions of total precipitation are very highly skewed. In addition, increased evaporation during the warm season tends to emphasize the skewness since proportionally more of the smaller precipitation amounts is lost to the soil through this process. The Chi-square distribution is a simple means of incorporating the resulting skewness of the distrtibutions of inital soil moisture, and in a manner which is also consistent with observations (Mathews and Army, 1960; Zook and Weakley, 1944).

Observed planting-time soil moisture is very similar for the regions encompassed by Boxes 1 and 3 (Mathews and Army, 1960), and identical parameters are used for them. For the spring-planting Gaussian distribution, mean 6 cm and standard deviation 3.5 cm are assumed, and the mean of the Chi-square distribution for initial moisture in fall is taken to be 4 cm. For Box 2, mean 17 cm and standard deviation 8 cm are assumed for the spring (Gaussian) distribution, and mean 6 cm is assumed for the fall (Chi-square) distribution. The same parameters are assumed for the single- and double-$CO_2$ simulations. Initial soil moisture is set to zero for spring crops in years for which the stochastic realization produces a negative level. Identical amounts are assumed for all stations within the same box for a given year, and the initial moisture is assumed to be distributed uniformly through each soil profile.

Other parameters pertaining to cultural practices required as input by the crop models were prescribed on the basis of current practice (Martin et al., 1976). For corn these are 75-cm row spacing, 50000 plants per hectare, and 4-cm seeding depth. For wheat (both winter and spring) these are 20-cm row spacing, 1.5 cm spacing within rows, and seeding depth of 4 cm. These are assumed constant for all stations, and for both the single- and double-$CO_2$ simulations.

The adaptation and equilibration of the modeled agricultural systems to the changed climate is treated by allowing changes in seeding date and cultivar. This is achieved by calculating annual yields over 30-year "training periods," separately for each station and $CO_2$ level, for combinations of seeding date and cultivar over selected ranges of these parameters. That combination which produces maximum average yield for each station is selected for subsequent use in the crop simulations.

Of course maximization of average yield is not the only criterion which could have been employed, but investigation of other possible choices was not undertaken. These alternatives could include maximizing median yield; or use of a more complicated criterion, perhaps involving emphasized weighting of very low yields, designed to incorporate the effects of risk aversion on the part of the farmer. Note also that real-world crop seeding on different fields in a given area does not begin in unison, but rather proceeds over a period of weeks and is variable from year to year.

The same realizations of initial soil moisture, synthetic grid-scale weather, and the stochastic climate inverse procedure are used in the estimation of optimal cultivars and seeding dates at all stations within each gridbox. Identical sequences of initial soil moisture are used for the 1X- and 2X-$CO_2$ explorations, so that any differences in optimal cultural practices may be attributed to differences in the 30-year realizations of the respective synthetic climates. Trial seeding dates are spaced at 10-day intervals. For corn, consecutive maturity classes bracketing the optimum are explored. Developmental paramenters for two varieties of winter wheat ("TAM-101" and "Pawnee") are used. Parameters for different spring wheat cultivars are not available, so that planting date only is varied for this crop. The "cultivar" employed for spring wheat was constructed using the parameters for the winter wheat variety "Scout

66," modified to require only a very short vernalization period (S.J. Maas, private communication).

Table 32 presents the results of one such exploration, that for corn at Algonia, Iowa (Box 2, Station 1), using simulated 1X-$CO_2$ weather data. Maximum average yield occurs for seeding on 30 April, which corresponds to the beginning of the seeding period in actual practice (Martin et al., 1976); and maturity class 6, which represents long-season varieties for Iowa (Stapper and Arkin, 1980). Tables 33, 34, and 35 present planting dates and, for corn, maturity classes, selected as optimal for each set of meteorological data, for stations in Boxes 1, 2, and 3, respectively.

Best average model winter wheat yields are higher in all cases for the variety TAM-101, a cultivar adapted to the southern Great Plains. This is consistent with a general tendency to select earlier planting dates and later maturing cultivars (for the 1X-$CO_2$ simulations) than is usual in current practice. However, the geographical distribution of seeding dates and corn cultivars based on single-$CO_2$ synthetic weather data bears a qualitative resemblance to observed practices both within and between grid boxes. For example, the corn planting date tends to be increasingly later in the northern portions of the 3-box domain, although its distribution is complicated by the effects of cultivar. Corn maturity class 9 (the longest-season variety included in CORNF) is chosen as best only for the lower elevations of the southernmost gridbox (Box 1). Maturity classes 2, 3, and 4 are only selected in the northern and east-central portions of Box 3, while in the southeast portion of this northernmost gridbox maturity classes 5 and 6 are chosen. For Box 2, the selected maturity

Table 32. Simulated average corn yields (kg/ha) for Algonia, IA (Box 2, Station 1) as a function of seeding date and maturity class (cultivar). Averages are over 30 years of synthetic weather data representing the 1X-CO2 climate.

| Maturity Class | Planting Date (Julian) 80 | 90 | 100 | 110 | 120 | 130 | 140 |
|---|---|---|---|---|---|---|---|
| 4 | 4303 | 4286 | 4327 | 4433 | 4400 | 4517 | 4750 |
| 5 | 5281 | 5338 | 5366 | 5447 | 5658 | 5523 | 5521 |
| 6 | 5584 | 5638 | 5710 | 5827 | 6030 | 5761 | 5322 |
| 7 | 4900 | 4815 | 4843 | 4869 | 4859 | 3949 | 2786 |
| 8 | 2536 | 2448 | 2551 | 2574 | 2664 | 1924 | 1217 |
| 9 | 428 | 436 | 493 | 571 | 645 | 21 | 0 |

Table 33. Julian dates of seeding, and corn maturity classes for Box 1 stations.

| Sta. No. | 1X-CO2 Seeding Dates Spring Wheat | Winter Wheat | Corn | Corn Maturity Class | 2X-CO2 Seeding dates Spring Wheat | Winter Wheat | Corn | Corn Maturity Class |
|---|---|---|---|---|---|---|---|---|
| 1 | 30 | 260 | 80 | 7 | 10 | 300 | 130 | 8 |
| 2 | 50 | 230 | 90 | 8 | 10 | 240 | 100 | 9 |
| 3 | 40 | 240 | 90 | 8 | 40 | 240 | 120 | 9 |
| 4 | 40 | 250 | 90 | 9 | 10 | 240 | 170 | 8 |
| 5 | 50 | 260 | 130 | 8 | 20 | 250 | 120 | 9 |
| 6 | 30 | 260 | 80 | 7 | 20 | 290 | 90 | 9 |
| 7 | 30 | 260 | 90 | 9 | 10 | 230 | 100 | 9 |
| 8 | 60 | 240 | 120 | 8 | 10 | 280 | 170 | 8 |
| 9 | 30 | 250 | 80 | 8 | 10 | 260 | 100 | 9 |
| 10 | 40 | 240 | 120 | 9 | 10 | 240 | 170 | 9 |
| 11 | 20 | 250 | 80 | 9 | 10 | 260 | 170 | 8 |
| 12 | 40 | 240 | 100 | 9 | 10 | 260 | 130 | 9 |
| 13 | 30 | 240 | 80 | 9 | 10 | 250 | 120 | 9 |
| 14 | 30 | 240 | 80 | 9 | 10 | 240 | 170 | 8 |
| 15 | 40 | 240 | 90 | 9 | 10 | 250 | 140 | 9 |
| 16 | 40 | 230 | 100 | 8 | 10 | 240 | 100 | 9 |
| 17 | 60 | 250 | 120 | 8 | 10 | 250 | 100 | 9 |
| 18 | 30 | 240 | 110 | 8 | 10 | 260 | 120 | 9 |
| 19 | 50 | 280 | 80 | 9 | 10 | 240 | 170 | 8 |
| 20 | 40 | 280 | 90 | 7 | 10 | 270 | 130 | 9 |
| 21 | 30 | 250 | 120 | 9 | 10 | 240 | 170 | 8 |
| 22 | 20 | 270 | 90 | 8 | 10 | 310 | 110 | 9 |
| 23 | 30 | 250 | 90 | 9 | 10 | 240 | 170 | 9 |
| 24 | 20 | 250 | 120 | 9 | 10 | 240 | 170 | 9 |

Table 34. Julian dates of seeding, and corn maturity classes for Box 2 stations.

| Sta. No. | 1X-CO2 Seeding Dates Spring Wheat | Winter Wheat | Corn | Corn Maturity Class | 2X-CO2 Seeding dates Spring Wheat | Winter Wheat | Corn | Corn Maturity Class |
|---|---|---|---|---|---|---|---|---|
| 1 | 30 | 220 | 120 | 6 | 10 | 240 | 140 | 8 |
| 2 | 20 | 220 | 100 | 6 | 10 | 240 | 120 | 9 |
| 3 | 20 | 220 | 110 | 7 | 10 | 240 | 120 | 9 |
| 4 | 20 | 220 | 110 | 7 | 10 | 240 | 100 | 9 |
| 5 | 20 | 230 | 110 | 7 | 10 | 240 | 140 | 8 |
| 6 | 30 | 220 | 90 | 6 | 10 | 240 | 130 | 8 |
| 7 | 30 | 230 | 110 | 7 | 10 | 240 | 120 | 9 |
| 8 | 20 | 230 | 100 | 8 | 10 | 240 | 150 | 8 |
| 9 | 20 | 230 | 100 | 7 | 20 | 240 | 130 | 9 |
| 10 | 20 | 230 | 110 | 7 | 10 | 240 | 120 | 9 |
| 11 | 30 | 230 | 100 | 6 | 20 | 240 | 130 | 8 |
| 12 | 20 | 230 | 120 | 7 | 10 | 240 | 120 | 9 |
| 13 | 20 | 230 | 120 | 7 | 10 | 240 | 150 | 9 |
| 14 | 30 | 220 | 110 | 5 | 10 | 240 | 110 | 8 |
| 15 | 20 | 230 | 120 | 7 | 10 | 240 | 110 | 9 |
| 16 | 30 | 220 | 90 | 5 | 10 | 240 | 110 | 8 |
| 17 | 20 | 230 | 130 | 7 | 10 | 240 | 130 | 9 |
| 18 | 20 | 220 | 90 | 7 | 10 | 240 | 120 | 9 |
| 19 | 30 | 220 | 100 | 5 | 20 | 230 | 120 | 8 |
| 20 | 30 | 220 | 110 | 5 | 10 | 240 | 120 | 8 |
| 21 | 20 | 230 | 120 | 8 | 10 | 240 | 130 | 9 |
| 22 | 20 | 230 | 120 | 8 | 10 | 240 | 130 | 9 |
| 23 | 20 | 230 | 110 | 7 | 10 | 240 | 110 | 9 |
| 24 | 20 | 230 | 120 | 7 | 10 | 240 | 130 | 9 |
| 25 | 30 | 240 | 100 | 8 | 20 | 240 | 160 | 8 |
| 26 | 20 | 230 | 100 | 7 | 10 | 240 | 90 | 9 |
| 27 | 40 | 220 | 130 | 6 | 10 | 230 | 120 | 8 |

Table 35. Julian dates of seeding, and corn maturity classes for Box 3 stations.

| | 1X-CO2 | | | | 2X-CO2 | | | |
|---|---|---|---|---|---|---|---|---|
| | Seeding Dates | | | | Seeding dates | | | |
| Sta. No. | Spring Wheat | Winter Wheat | Corn | Corn Maturity Class | Spring Wheat | Winter Wheat | Corn | Corn Maturity Class |
| 1 | 70 | 230 | 130 | 2 | 20 | 230 | 120 | 7 |
| 2 | 20 | 210 | 120 | 4 | 10 | 220 | 120 | 6 |
| 3 | 40 | 210 | 130 | 3 | 20 | 230 | 120 | 7 |
| 4 | 20 | 220 | 100 | 4 | 10 | 230 | 120 | 7 |
| 5 | 40 | 230 | 120 | 4 | 20 | 240 | 120 | 7 |
| 6 | 30 | 220 | 120 | 4 | 20 | 230 | 120 | 7 |
| 7 | 50 | 220 | 120 | 3 | 50 | 230 | 130 | 6 |
| 8 | 70 | 250 | 130 | 4 | 40 | 250 | 130 | 7 |
| 9 | 40 | 220 | 120 | 3 | 10 | 230 | 120 | 6 |
| 10 | 50 | 230 | 120 | 4 | 20 | 240 | 120 | 7 |
| 11 | 60 | 240 | 120 | 3 | 20 | 230 | 130 | 7 |
| 12 | 30 | 220 | 90 | 4 | 20 | 230 | 100 | 8 |
| 13 | 30 | 220 | 90 | 4 | 10 | 230 | 100 | 8 |
| 14 | 20 | 230 | 90 | 5 | 10 | 230 | 90 | 7 |
| 15 | 30 | 250 | 100 | 4 | 10 | 240 | 90 | 8 |
| 16 | 40 | 220 | 120 | 4 | 10 | 240 | 120 | 7 |
| 17 | 50 | 220 | 100 | 5 | 10 | 230 | 90 | 8 |
| 18 | 20 | 220 | 90 | 6 | 10 | 240 | 80 | 8 |
| 19 | 30 | 220 | 90 | 6 | 10 | 240 | 90 | 8 |
| 20 | 30 | 220 | 100 | 5 | 10 | 230 | 90 | 8 |
| 21 | 30 | 260 | 150 | 4 | 20 | 240 | 90 | 8 |
| 22 | 20 | 220 | 90 | 6 | 10 | 240 | 80 | 8 |
| 23 | 30 | 250 | 100 | 3 | 10 | 240 | 140 | 6 |
| 24 | 20 | 260 | 120 | 6 | 40 | 260 | 90 | 9 |
| 25 | 30 | 220 | 100 | 6 | 20 | 230 | 100 | 9 |
| 26 | 50 | 220 | 150 | 4 | 20 | 230 | 90 | 8 |

classes range from 8 in the south to 5 in the north. Planting dates for winter wheat are increasingly later toward the southern part of the 3-box domain and exhibit reasonable continuity between the three gridboxes. Model planting dates for spring wheat are increasingly later in the northern parts of the domain, except for Box 1, where spring wheat culture is not well adapted to current conditions.

Similar considerations apply for planting dates and cultivars estimated from double-$CO_2$ synthetic weather data, although the specific optimal practices are substantially different for many stations. There is a tendency for corn planting dates to be later (in comparison to optimal values for 1X-$CO_2$ conditions) in Boxes 1 and 2, and about the same time or earlier for Box 3. Later maturing corn varieties are selected in nearly all cases, so that the earliest, selected again in the northern part of Box 3, are maturity classes 6 and 7. Only maturity classes 8 and 9 are selected in Boxes 1 and 2. It is interesting to note that for these southernmost boxes, maturity class 8 is often selected as best in conjunction with June (i.e., late) seeding dates. Spring wheat seeding dates tend to be shifted earlier in the spring, and winter wheat seeding dates tend to be shifted later in the summer and fall, although the previous latitudinal gradients are maintained in both cases.

An alternative to the foregoing, relatively expensive, procedure would be to simply match planting dates and cultivars to current agronomic practices. While this might result in more realistic simulations representing current climatic conditions, it will not in general represent practices which are well-adaped to the changed climate. As indicated above, "best" practices with respect to the synthetic $2X-CO_2$ climate are often substantially different, and disabling adaptive mechanisms in the modeling procedure will almost automatically introduce a negative bias to estimates of agricultural potential under the changed climate.

## 4.4. Results of Crop Simulation

Estimation of the agricultural impact (with respect to grain corn and wheat) of the climate change scenario constructed in Section 3.5 is investigated through Monte Carlo simulations of winter wheat, spring wheat, and corn. The two crop models described in Section 4.2 and the initial conditions described in Section 4.3 are employed. Separate simulations are undertaken for all stations using 250 years each of 1X- and $2X-CO_2$ synthetic weather data.

### 4.4.1. West and central Kansas: winter wheat region

Table 36 presents means, standard deviations, and medians of the yield distributions of winter wheat and grain corn for Box 1 stations. Spring wheat culture is not adapted to this relatively warm area, and yields of this crop are below or equivalent to winter wheat yields for all stations and for both climatic conditions. Spring wheat will therefore not be discussed further for this region. Statistical significance of differences between 1X- and $2X-CO_2$ yields of winter wheat and grain corn for each station, as judged by the Wilcoxon-Mann-Whitney rank-sum test (e.g., Steel and Torrie, 1980), are indicated in Table 36 by asterisks.

As might have been expected, model wheat yield levels for the

Table 36. Means, standard deviations, and medians of model winter wheat and grain corn yield distributions for Box 1. Significant differences between single- and double-CO2 distributions are indicated by "**" for the 1% level and "*" for the 5% level.

a. Winter Wheat

| | Single CO2 | | | | Double CO2 | | |
|---|---|---|---|---|---|---|---|
| Station | Mean | (Std.Dev.) | Median | | Mean | (Std.Dev.) | Median |
| 1 | 445 | ( 428) | 328 | * | 378 | ( 437) | 265 |
| 2 | 2345 | (1642) | 2182 | * | 2668 | (1548) | 2593 |
| 3 | 1372 | (1405) | 847 | | 1521 | (1388) | 1051 |
| 4 | 342 | ( 428) | 224 | | 580 | ( 902) | 224 |
| 5 | 344 | ( 461) | 235 | ** | 246 | ( 411) | 123 |
| 6 | 492 | ( 459) | 380 | ** | 390 | ( 389) | 297 |
| 7 | 979 | (1196) | 574 | ** | 1547 | (1414) | 1094 |
| 8 | 342 | ( 462) | 202 | ** | 413 | ( 520) | 233 |
| 9 | 469 | ( 565) | 297 | | 548 | ( 753) | 306 |
| 10 | 1513 | (1311) | 1116 | ** | 2059 | (1510) | 1932 |
| 11 | 264 | ( 387) | 159 | | 239 | ( 352) | 122 |
| 12 | 2483 | (1735) | 2297 | * | 2829 | (1651) | 2818 |
| 13 | 1625 | (1689) | 877 | ** | 2206 | (2039) | 1389 |
| 14 | 331 | ( 516) | 145 | * | 543 | ( 908) | 196 |
| 15 | 3500 | (2037) | 3767 | ** | 4140 | (2040) | 4735 |
| 16 | 1106 | (1269) | 666 | ** | 1716 | (1771) | 1133 |
| 17 | 434 | ( 553) | 272 | | 558 | ( 882) | 255 |
| 18 | 1388 | (1427) | 872 | ** | 1881 | (1745) | 1321 |
| 19 | 394 | ( 475) | 243 | ** | 302 | ( 599) | 131 |
| 20 | 440 | ( 467) | 287 | * | 370 | ( 497) | 242 |
| 21 | 325 | ( 551) | 161 | | 612 | ( 998) | 172 |
| 22 | 375 | ( 434) | 243 | ** | 275 | ( 371) | 155 |
| 23 | 938 | (1272) | 432 | ** | 1583 | (1661) | 1048 |
| 24 | 570 | ( 888) | 286 | | 1087 | (1540) | 340 |

Table 36, continued.

b. Grain Corn

| | Single CO2 | | | | Double CO2 | | |
|---|---|---|---|---|---|---|---|
| Station | Mean | (Std.Dev.) | Median | | Mean | (Std.Dev.) | Median |
| 1 | 428 | ( 809) | 2 | ** | 449 | ( 887) | 6 |
| 2 | 3828 | (2530) | 3618 | ** | 2734 | (2166) | 2810 |
| 3 | 1604 | (1658) | 1148 | * | 1289 | (1477) | 867 |
| 4 | 701 | (1070) | 45 | * | 463 | ( 917) | 1 |
| 5 | 834 | (1298) | 86 | ** | 696 | (1064) | 121 |
| 6 | 563 | ( 886) | 189 | | 492 | ( 854) | 33 |
| 7 | 1428 | (1853) | 646 | ** | 723 | (1208) | 152 |
| 8 | 419 | ( 812) | 0 | ** | 296 | ( 658) | 0 |
| 9 | 729 | (1022) | 275 | | 581 | ( 882) | 124 |
| 10 | 1359 | (1860) | 468 | | 995 | (1460) | 308 |
| 11 | 804 | (1252) | 105 | ** | 587 | ( 946) | 82 |
| 12 | 2369 | (2066) | 1989 | ** | 1564 | (1800) | 816 |
| 13 | 1498 | (1618) | 918 | ** | 692 | ( 993) | 272 |
| 14 | 592 | ( 874) | 141 | ** | 425 | ( 819) | 1 |
| 15 | 2675 | (2325) | 2055 | ** | 1550 | (1938) | 681 |
| 16 | 1065 | (1224) | 567 | * | 778 | (1125) | 288 |
| 17 | 420 | ( 801) | 0 | ** | 369 | ( 700) | 28 |
| 18 | 1475 | (1582) | 975 | | 1159 | (1428) | 559 |
| 19 | 349 | ( 760) | 0 | ** | 259 | ( 638) | 0 |
| 20 | 242 | ( 494) | 2 | ** | 282 | ( 590) | 0 |
| 21 | 643 | ( 960) | 72 | * | 409 | ( 785) | 10 |
| 22 | 794 | (1243) | 90 | ** | 549 | ( 937) | 77 |
| 23 | 1239 | (1432) | 641 | ** | 764 | (1184) | 18 |
| 24 | 1085 | (1529) | 335 | ** | 561 | ( 939) | 3 |

$1X\text{-}CO_2$ simulations do not correspond quantitatively to observations, but the general increase in yields toward the wetter (eastern) portion of the gridbox is qualitatively similar to that in the real world. Model yields are 50% to 100% higher than observed in the northeast corner, and perhaps half those observed in the western half of the gridbox (cf. Michaels, 1983). This latter discrepancy is probably related in part to the fact that alternate-year cropping (as a moisture conservation strategy) is practiced in this region, and is not incorporated into the present crop modeling procedure. Comparable figures for observed corn yields in this region are not readily available, since relatively little nonirrigated corn is grown even in the wetter portions of this gridbox (U.S. Bureau of the Census, 1982b). However, modeled corn yields are very low indeed (median model yields for several stations are zero) except in the wetter eastern portion of the gridbox, as is undoubtedly the case in the real world.

Relative changes in Box 1 yields are presented in Figure 33. Panels a and b show proportional changes in winter wheat and corn yields, respectively. Wheat yields are seen to increase, in some cases rather substantially, in the eastern portion of the box; and to decrease to a lesser degree in the drier western portion. These differences between the $1X\text{-}CO_2$ and $2X\text{-}CO_2$ distributions are statistically significant for most of these stations. In contrast, corn yields decline significantly almost everywhere within this gridbox.

Widespread decreases in potential corn yields in this region under the $2X\text{-}CO_2$ climate scenerio of Section 3 are to be expected, in

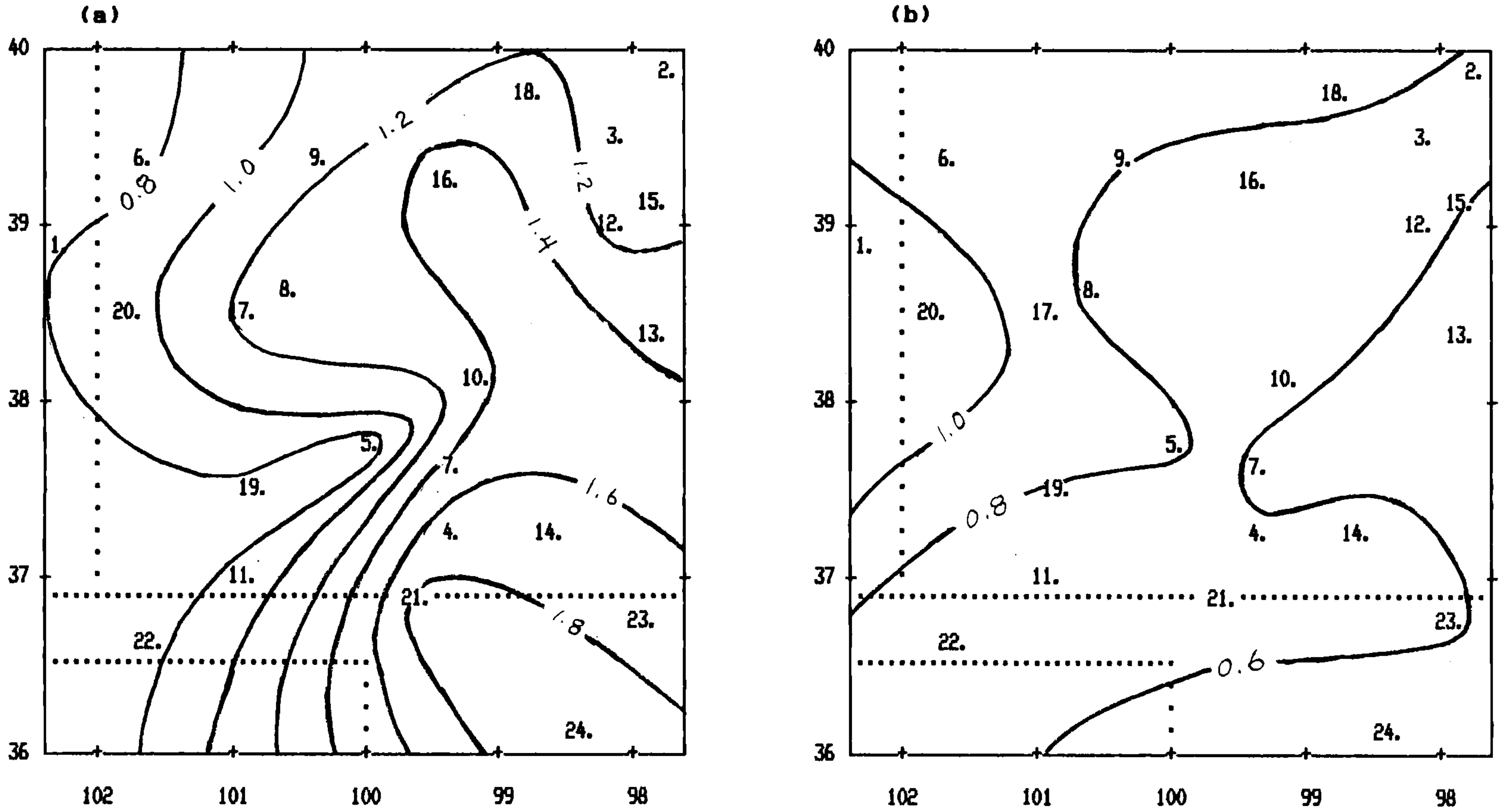


Figure 33. Relative change ( [2X-$CO_2$]/[1X-$CO_2$] ) in average simulated crop yields for Box 1: (a) winter wheat, (b) grain corn.

view of the very large temperature increases (Figure 21) and reduced precipititation probabilities (Table 16) during summer. Both these factors act to reduce available soil moisture during the tasseling and silking stages, when that moisture is most needed by the plant (Shaw, 1983). For most locations these developmental stages occur in the modeled crops during mid- to late July, which is the hottest part of the summer (cf. Figure 21). Model corn at those stations for which seeding is delayed until June (Table 33) does not reach these phenological stages until mid-August, after the highest potential for damaging heat in the 2X-$CO_2$ scenario has passed. (However, moisture is still insufficient for good yields.) Interestingly, this is a strategy sometimes employed for real-world irrigated corn production in western Kansas (Martin _et_ _al_., 1976).

The present results indicate that the potential for winter wheat production may increase in a 2X-$CO_2$ world. This is perhaps surprising, but may be viewed as an example of the potential adaptability of agriculture to changing environments. The crop calendar of winter wheat is such that no crop is present during July, so that the very harsh conditions in the 2X-$CO_2$ scenerio for this month do not affect yield potential. Winter temperatures are higher as well, but still cool enough that evapotranspiration is not drastically increased. The primary effect of increased winter temperatures on the modeled wheat crop is to accelerate vegetative development relative to the 1X-$CO_2$ simulations. In combination with delayed planting dates, this results in occurrence of the critical anthesis and grain filling periods for stations in the eastern part of the gridbox (where model yields increase) during April. Average temperatures during these critical stages are then somewhat cooler for the $2X-CO_2$ simulations, as the corresponding period occurs in May for the $1X-CO_2$ wheat crops. Also, there is a small increase in average March precipitation, which results from an increase in average precipitation intensity (cf. Table 16) in combination with the associated influence on the probabilities of successive wet days. Together the lower temperatures and higher precipitation effect a reduction in average daily water stress during the critical grain filling period. As a result, the duration of this stage is extended substantially and the yields are correspondingly increased.

For the stations in the western part of Box 1, both $2X-CO_2$ planting dates and onset of flowering and grain filling are later than for the eastern stations. Average daily water stress during the critical phenological stages increases over that for $1X-CO_2$ crops, and this is the apparent cause of the modeled yield decreases for these stations. Moisture is severely limiting in this area, and even modest increases in evapotranspiration would be expected to decrease yield potentials. The later planting dates may have been chosen so that the flowering period extends into the climatologically wetter period of late spring. This could have resulted in a few good harvests during the 30-year training sequence, which would have exerted a large influence on the mean yields over that period. Note in this regard that the near-equality of the means and standard deviations in Table 36, and the smaller magnitudes of the medians indicate that these distributions are strongly positively skewed.

4.4.2. West and central Iowa: western corn belt region

Table 37 presents means, standard deviations, and medians for the yield distributions of grain corn and winter wheat at Box 2 stations. Also indicated, as in the corresponding table for Box 1, are significance levels for the differences as judged by the Wilcoxon-Mann-Whitney test. Both winter wheat and spring wheat are grown in this area, although neither are of major importance (Martin et al., 1976). Since a warmer climate would likely favor winter wheat over spring wheat, discussion of the former will be emphasized in the present section.

Modeled 1X-$CO_2$ average corn yields compare moderately well with the corresponding observations, exhibiting a general increase toward the northeast, although the absolute magnitudes are perhaps 20% lower (cf. U.S. Bureau of the Census, 1982a). Modeled winter wheat yields are higher than observations, roughly by a factor of 2, but exhibit the same tendency for yields to decrease toward the northwest and southwest (U.S. Bureau of the Census, 1982a). Modeled spring wheat yields (not tabulated) exhibit much less spatial variation, and are comparable in magnitude to the observed values.

The relative changes in yields for modeled grain corn and winter wheat are shown in Figure 34. Panel (a) indicates increases in corn yields under the 2X-$CO_2$ climate in the northeast corner, several of which (stations 6, 14, 16, 19, and 20) are highly significant. An area of comparable size in the west-central portion of this box (stations 8, 9, 12, 13, 15, 23, 24, and 26) exhibits significant yield decreases. Half the stations exhibit no significant changes in corn

Table 37. Means, standard deviations, and medians of model grain corn and winter wheat yield distributions for Box 2. Significant differences between single- and double-CO2 distributions are indicated by "**" for the 1% level and "*" for the 5% level.

a. Grain Corn

| | Single CO2 | | | | Double CO2 | | |
|---|---|---|---|---|---|---|---|
| Station | Mean | (Std.Dev.) | Median | | Mean | (Std.Dev.) | Median |
| 1 | 5404 | (2866) | 5459 | | 5731 | (2997) | 5666 |
| 2 | 5538 | (2104) | 5493 | | 5615 | (2750) | 5485 |
| 3 | 4461 | (2187) | 4569 | | 4248 | (1774) | 4260 |
| 4 | 4961 | (2394) | 4899 | | 4602 | (2077) | 4553 |
| 5 | 4663 | (2296) | 4751 | | 4554 | (2178) | 4655 |
| 6 | 6423 | (2812) | 6792 | ** | 7551 | (2967) | 7967 |
| 7 | 4890 | (2307) | 5065 | | 4785 | (2158) | 4575 |
| 8 | 5558 | (2237) | 5593 | ** | 4908 | (2235) | 4995 |
| 9 | 5635 | (2309) | 5809 | ** | 5085 | (2046) | 5144 |
| 10 | 4482 | (2203) | 4555 | | 4183 | (2050) | 4192 |
| 11 | 6230 | (2708) | 6377 | | 6657 | (2906) | 6753 |
| 12 | 4091 | (2131) | 4211 | * | 3582 | (2094) | 3667 |
| 13 | 5328 | (2266) | 5303 | ** | 3884 | (2226) | 3837 |
| 14 | 6492 | (2335) | 6716 | ** | 7515 | (2802) | 7704 |
| 15 | 4873 | (2411) | 5156 | ** | 4333 | (1932) | 4395 |
| 16 | 6167 | (2634) | 6438 | ** | 7873 | (2886) | 8306 |
| 17 | 4938 | (2546) | 5117 | * | 4511 | (2262) | 4378 |
| 18 | 5699 | (2717) | 5841 | | 5475 | (3358) | 5188 |
| 19 | 4975 | (2254) | 4751 | ** | 6090 | (2802) | 6025 |
| 20 | 6029 | (2600) | 6419 | ** | 7233 | (3008) | 7691 |
| 21 | 4520 | (2356) | 4486 | | 4196 | (2252) | 3995 |
| 22 | 4395 | (2215) | 4451 | | 4141 | (2174) | 4197 |
| 23 | 4535 | (2369) | 4518 | * | 4112 | (2030) | 3903 |
| 24 | 5768 | (2358) | 5540 | ** | 5153 | (2108) | 4948 |
| 25 | 4394 | (2162) | 4484 | | 4082 | (2402) | 4110 |
| 26 | 4231 | (2065) | 4329 | * | 3920 | (1850) | 3911 |
| 27 | 3677 | (2185) | 3659 | | 4033 | (2069) | 4030 |

Table 37, continued.

b. Winter Wheat

| Station | Single CO2 Mean | Single CO2 (Std.Dev.) | Single CO2 Median | | Double CO2 Mean | Double CO2 (Std.Dev.) | Double CO2 Median |
|---|---|---|---|---|---|---|---|
| 1 | 3203 | (1782) | 3368 | ** | 1909 | (1384) | 1573 |
| 2 | 4739 | (1737) | 5232 | ** | 3250 | (1594) | 3537 |
| 3 | 4493 | (1687) | 4783 | ** | 2987 | (1521) | 3101 |
| 4 | 4379 | (1602) | 4699 | ** | 2848 | (1475) | 3029 |
| 5 | 3551 | (1749) | 3619 | ** | 2552 | (1550) | 2353 |
| 6 | 3219 | (1805) | 3195 | ** | 1886 | (1405) | 1694 |
| 7 | 3694 | (1755) | 3799 | ** | 2515 | (1491) | 2505 |
| 8 | 4935 | (1370) | 5171 | ** | 3409 | (1512) | 3644 |
| 9 | 5252 | (1175) | 5363 | ** | 3708 | (1401) | 3885 |
| 10 | 4185 | (1599) | 4426 | ** | 2895 | (1558) | 2888 |
| 11 | 2890 | (1829) | 2724 | ** | 1658 | (1345) | 1259 |
| 12 | 3183 | (1667) | 3151 | ** | 2022 | (1403) | 1740 |
| 13 | 4991 | (1288) | 5185 | ** | 3404 | (1480) | 3637 |
| 14 | 4556 | (1503) | 4893 | ** | 2851 | (1436) | 2973 |
| 15 | 4225 | (1516) | 4459 | ** | 2734 | (1453) | 2764 |
| 16 | 2938 | (1803) | 2754 | ** | 1671 | (1335) | 1461 |
| 17 | 3860 | (1777) | 4243 | ** | 2708 | (1495) | 2633 |
| 18 | 4317 | (1766) | 4720 | ** | 2667 | (1552) | 2681 |
| 19 | 4089 | (1633) | 4499 | ** | 2701 | (1486) | 2857 |
| 20 | 4345 | (1474) | 4773 | ** | 2621 | (1398) | 2647 |
| 21 | 3139 | (1863) | 3001 | ** | 2210 | (1381) | 2045 |
| 22 | 4329 | (1696) | 4638 | ** | 2846 | (1579) | 2923 |
| 23 | 3377 | (1715) | 3546 | ** | 1984 | (1521) | 1556 |
| 24 | 5230 | (1198) | 5380 | ** | 3805 | (1334) | 4045 |
| 25 | 3173 | (1746) | 3182 | ** | 1999 | (1464) | 1727 |
| 26 | 3688 | (1655) | 3863 | ** | 2326 | (1485) | 2128 |
| 27 | 2802 | (1556) | 2688 | ** | 1670 | (1274) | 1415 |

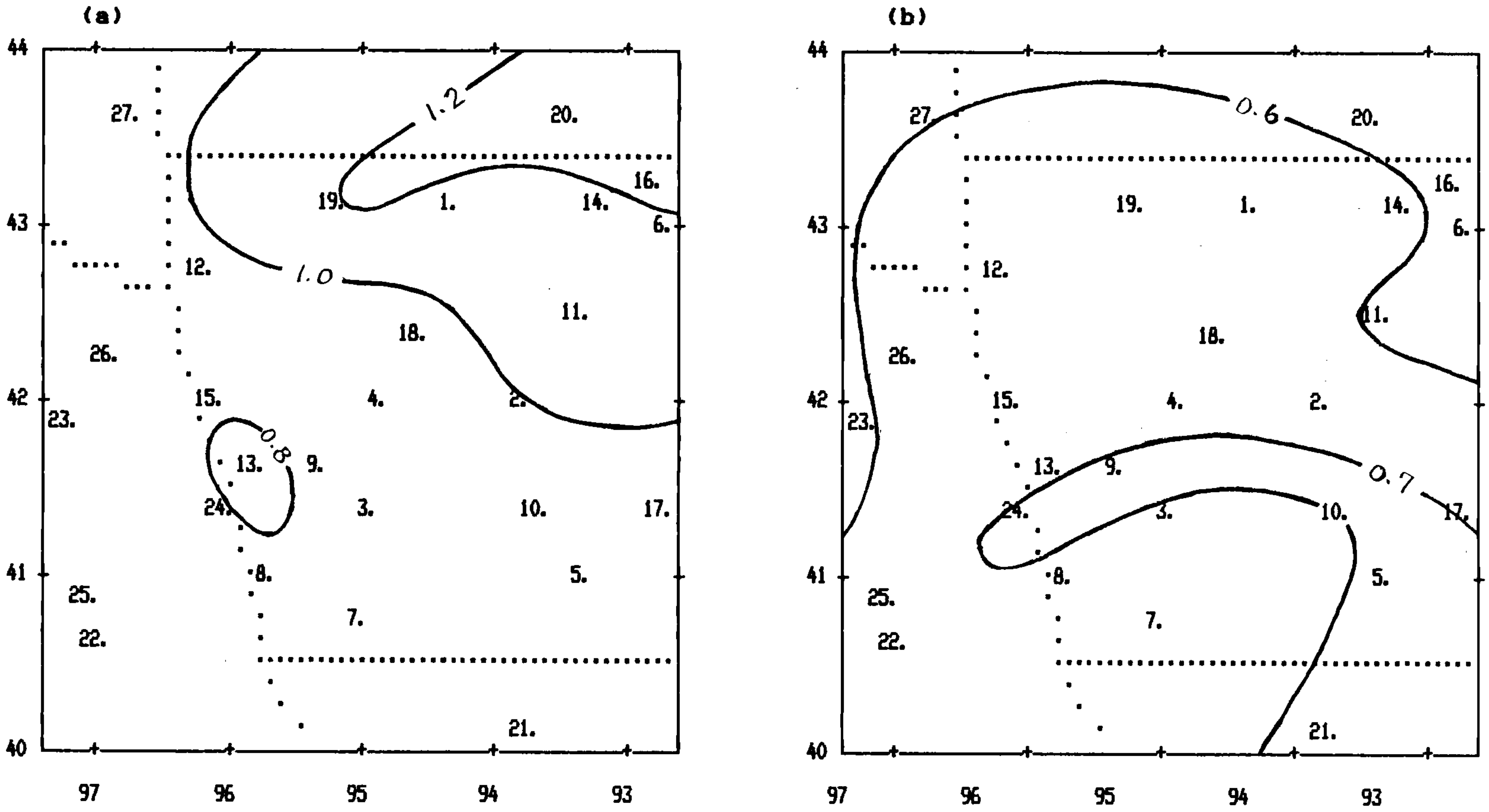


Figure 34. Relative change ( $[2X\text{-}CO_2]/[1X\text{-}CO_2]$ ) in average simulated crop yields for Box 2: (a) grain corn, (b) winter wheat.

yield potential.

In contrast, Figure 29b indicates sharp yield reductions for winter wheat throughout this gridbox, with the largest decreases occurring in the central and southeast portions. Spring wheat yields (not shown) exhibit decreases which are similar in magnitude and distribution. These decreases in potential wheat yields are rather clearly attributable to the higher temperatures (Figure 22) in conjunction with sharply lower spring rainfall frequencies (Table 16). Average model daily water stress during the anthesis and grain filling periods for winter wheat increase 30% to 100% throughout most of the gridbox, with catastrophic effects on yields.

For the case of corn yields, the possibly surprising relative increases at stations in the northeast portion of the box may be viewed as another example of the potential adaptability of agricultural production systems. Table 17 indicates a very substantial increase in July precipitation intensity while Table 16 shows no significant decrease in precipitation probability following dry days for this month. The result is a large (average of 66%) increase in July precipitation for all stations throughout the gridbox. The optimal combinations of seeding date and cultivar selected in Section 4.3.c result in the average dates of silking occurring in mid-July, thus minimizing water stress during this and the subsequent critical phenological stages. However, average water stress during the flowering period is still generally higher for the $2X-CO_2$ corn crops as compared to the $1X-CO_2$ realizations, and the differences are greater at those stations for which significant yield decreases are predicted. This is apparently a consequence of the higher temperatures in the 2X-$CO_2$ climate offsetting the beneficial effects of increased precipitation. Average 2X-$CO_2$ July maximum temperatures increase toward the southwest, being 34 C to 35 C in the region predicted to experience increased corn yields, and 36 C to 37 C for the area in which model yields decline significantly.

The compensating factor allowing overall yield to remain at nearly the same level, even though water stress is increased, follows as a consequence of the adaptability of cultural practices. More heat units are available, and over a longer growing season, in the warmer changed climate. It thus provides the opportunity for use of longer season varieties, which have a higher yield potential. If no increase in July precipitation were predicted, it is probable that the procedure of Section 4.3.c would select June planting of shorter-season varieties so that the flowering period could occur after the midsummer heat and drought. Modeled yields would clearly be lower than for the present 2X-$CO_2$ climate scenario, but not as low as would be the case if the opportunity to extend the growing season later into the fall were denied.

Taken together these results indicate that the regional corn production capacity may remain more-or-less constant. The tendency for corn yields to increase in the northeast portion of this gridbox support the possibility that the "corn belt" may shift in that direction, as has been suggested by Newman (1980). However, this may be compensated by declines in winter wheat yields in the southwest section of the gridbox, with the possible result that corn may still be the more profitable crop albeit at reduced yield levels.

4.4.3. North and South Dakota: spring wheat region

Finally, the summary yield statistics for Box 3 spring wheat and grain corn are presented in Table 38. Winter wheat results are not considered in this section, since modeled yields are quite high (ranging to several tons per hectare). This error derives from the absence of a mechanism for "winterkill" in TAMW. Very cold winters prohibit fall planting of wheat in this region for current climatic conditions, and the modest increases in winter (particularly maximum) temperatures in the 2X-$CO_2$ scenario (cf. Figure 23) for this gridbox suggest little change in the adaptability of winter wheat. Modeled magnitudes of yields for both spring wheat and corn are approximately two-thirds of those observed, although the general increase in average yields toward the wetter eastern portion of the box is preserved (cf. North Dakota Crop and Livestock and Reporting Service, 1984; U.S. Bureau of the Census, 1982c).

Figure 35a indicates substantial declines in modeled average spring wheat yields. Significant yield reductions occur over all but the southwestern portion of the gridbox, where both modeled and observed yields are low, and little wheat is grown in practice (e.g., Martin et al., 1976). Spring wheat is well adapted to the current climate in the remainder of this region, and while the 2X-$CO_2$ scenario does not specify reductions in probabilities of spring precipitation (as in the case of Box 2), increased temperatures and associated increases in evapotranspiration appear to be sufficient to impair yields.

For the case of grain corn, Figure 35b shows widespread yield

Table 38. Means, standard deviations, and medians of model spring wheat and grain corn yield distributions for Box 3. Significant differences between single- and double-CO2 distributions are indicated by "**" for the 1% level and "*" for the 5% level.

a. Spring wheat

| | Single CO2 | | | | Double CO2 | | |
|---|---|---|---|---|---|---|---|
| Station | Mean | (Std.Dev.) | Median | | Mean | (Std.Dev.) | Median |
| 1 | 505 | ( 495) | 375 | | 426 | ( 384) | 318 |
| 2 | 1518 | (1031) | 1321 | ** | 946 | ( 723) | 748 |
| 3 | 1185 | ( 927) | 923 | ** | 786 | ( 656) | 570 |
| 4 | 1268 | ( 941) | 1016 | ** | 862 | ( 708) | 692 |
| 5 | 1243 | ( 965) | 1033 | ** | 891 | ( 744) | 710 |
| 6 | 1369 | ( 995) | 1180 | ** | 885 | ( 717) | 701 |
| 7 | 951 | ( 787) | 667 | ** | 589 | ( 575) | 440 |
| 8 | 576 | ( 561) | 394 | * | 463 | ( 456) | 360 |
| 9 | 1379 | ( 958) | 1219 | ** | 934 | ( 770) | 705 |
| 10 | 545 | ( 533) | 388 | ** | 412 | ( 420) | 289 |
| 11 | 555 | ( 534) | 400 | * | 448 | ( 440) | 309 |
| 12 | 835 | ( 772) | 559 | ** | 630 | ( 619) | 445 |
| 13 | 819 | ( 706) | 609 | ** | 605 | ( 558) | 404 |
| 14 | 946 | ( 817) | 668 | ** | 738 | ( 726) | 489 |
| 15 | 328 | ( 310) | 220 | | 311 | ( 291) | 232 |
| 16 | 613 | ( 566) | 413 | | 514 | ( 469) | 392 |
| 17 | 688 | ( 650) | 502 | ** | 578 | ( 594) | 342 |
| 18 | 1234 | ( 996) | 951 | | 1069 | ( 902) | 789 |
| 19 | 622 | ( 636) | 395 | | 559 | ( 558) | 366 |
| 20 | 655 | ( 617) | 465 | ** | 519 | ( 508) | 364 |
| 21 | 265 | ( 260) | 176 | | 244 | ( 235) | 173 |
| 22 | 905 | ( 754) | 672 | * | 784 | ( 744) | 587 |
| 23 | 448 | ( 488) | 287 | * | 356 | ( 373) | 255 |
| 24 | 329 | ( 364) | 229 | | 342 | ( 334) | 247 |
| 25 | 331 | ( 342) | 209 | | 310 | ( 339) | 197 |
| 26 | 303 | ( 265) | 232 | * | 273 | ( 296) | 178 |

Table 38, continued.

b. Grain Corn

| | Single CO2 | | | | Double CO2 | | |
|---|---|---|---|---|---|---|---|
| Station | Mean | (Std.Dev.) | Median | | Mean | (Std.Dev.) | Median |
| 1 | 613 | ( 679) | 442 | | 810 | (1184) | 197 |
| 2 | 2065 | (2080) | 1404 | ** | 2630 | (2316) | 1984 |
| 3 | 1476 | (1510) | 1018 | | 1712 | (1825) | 1204 |
| 4 | 1777 | (1693) | 1190 | | 1893 | (1901) | 1363 |
| 5 | 1898 | (1753) | 1398 | | 2168 | (2125) | 1593 |
| 6 | 2316 | (2027) | 1832 | | 2506 | (2394) | 1913 |
| 7 | 1285 | (1302) | 917 | | 1491 | (1561) | 975 |
| 8 | 390 | ( 725) | 4 | ** | 645 | (1145) | 0 |
| 9 | 1682 | (1563) | 1250 | | 1980 | (1883) | 1416 |
| 10 | 508 | ( 808) | 95 | ** | 708 | (1033) | 105 |
| 11 | 685 | ( 861) | 389 | * | 822 | (1207) | 128 |
| 12 | 1310 | (1346) | 854 | | 1463 | (1656) | 915 |
| 13 | 1447 | (1416) | 994 | | 1654 | (1838) | 1116 |
| 14 | 1990 | (2015) | 1407 | * | 2312 | (2154) | 1781 |
| 15 | 334 | ( 486) | 151 | | 553 | ( 962) | 5 |
| 16 | 760 | ( 920) | 449 | * | 1105 | (1361) | 661 |
| 17 | 1040 | (1205) | 575 | | 1286 | (1581) | 665 |
| 18 | 2329 | (2193) | 1792 | * | 2871 | (2583) | 2376 |
| 19 | 1192 | (1413) | 682 | * | 1630 | (1904) | 870 |
| 20 | 1086 | (1215) | 625 | ** | 1567 | (1602) | 1292 |
| 21 | 251 | ( 376) | 51 | ** | 384 | ( 598) | 98 |
| 22 | 1328 | (1617) | 618 | ** | 1893 | (1867) | 1598 |
| 23 | 422 | ( 737) | 94 | ** | 641 | (1072) | 109 |
| 24 | 290 | ( 484) | 77 | | 379 | ( 682) | 3 |
| 25 | 415 | ( 501) | 229 | | 589 | ( 850) | 99 |
| 26 | 373 | ( 658) | 3 | ** | 732 | (1196) | 100 |

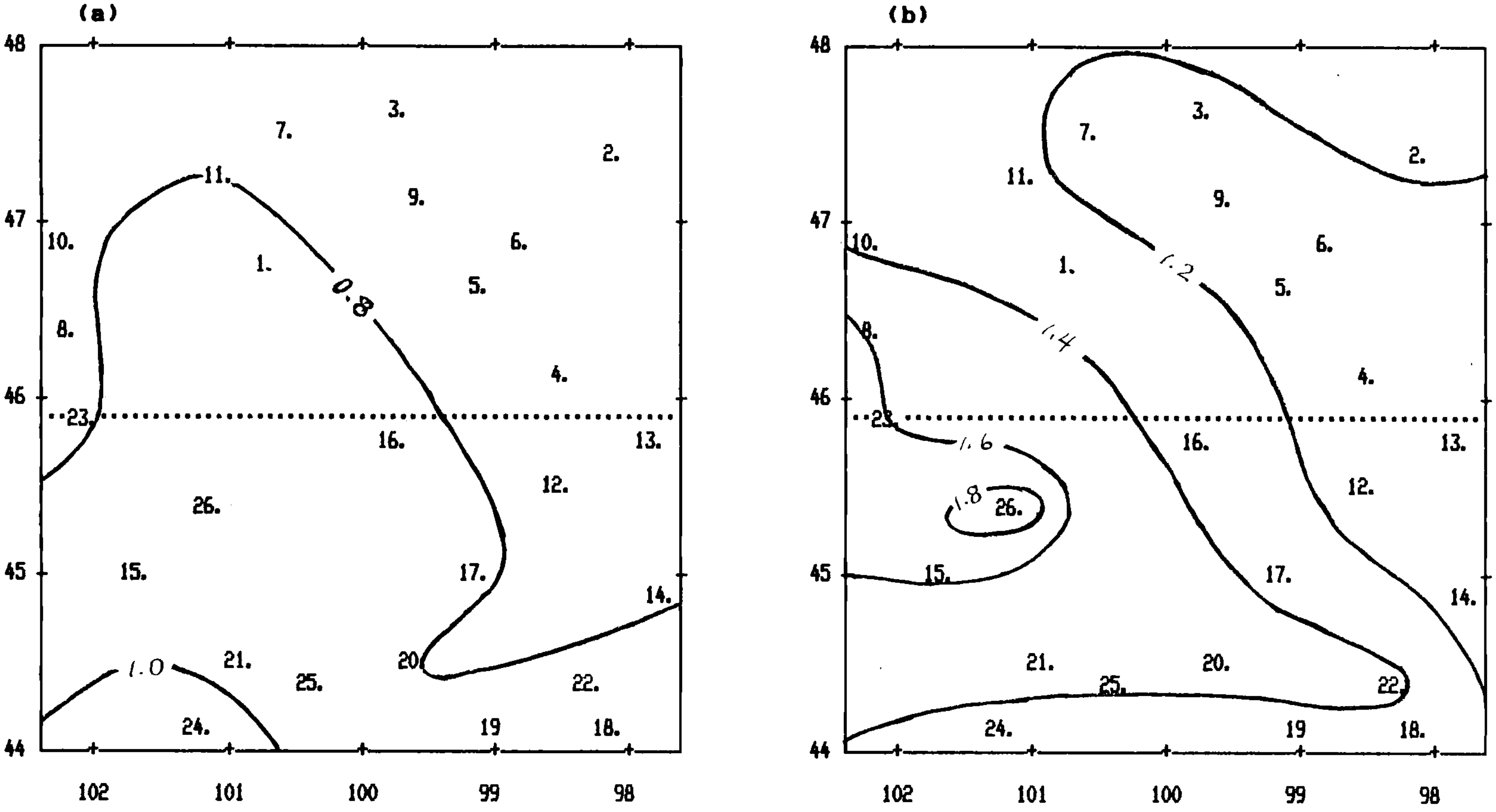


Figure 35. Relative change ( [2X-$CO_2$]/[1X-$CO_2$] ) in average simulated crop yields for Box 3: (a) spring wheat, (b) grain corn.

increases under the 2X-$CO_2$ climate scenario, many of which are highly statistically significant. While July precipitation intensity increases as in the case of Box 2 (Table 17), this is offset by a corresponding decrease in the probability of precipitation following dry days (Table 16). The result is that, at least in terms of average July precipitation, the moisture supply is approximately unchanged at most stations.

The observed yield increases appear to result from two temperature effects. First, the present climate of this region is cooler than the optimum for corn growth. Average 2X-$CO_2$ July temperatures (i.e., $[T_{max}+T_{min}]/2$ ) are between 25 C and 27 C through most of the gridbox, which is near the optimum for corn growth at the corresponding level of average July precipititaion (Shaw, 1983). Second, as is the case for Box 2 corn, warmer temperatures and the extended growing season allow use of longer-maturing varieties, with attendant increased yield potential.

Many of the stations exhibiting statistically significant yield increases are in the western half of the gridbox, where the large proportional increases would probably still be insufficient to produce economic corn crops. However, this is not the case for the east-central and southeastern portions of this gridbox (Newman, 1980; Wilks and Murphy, 1987), where the modeled increases would be agronomically as well as statistically significant. The combination of increasing corn yields and decreasing wheat yields in this gridbox indicate the potential for extension of the corn belt both northward and westward in this region.

## 4.5 Summary and Conclusions

This section has presented results describing possible consequences of $CO_2$-induced climate changes on several important aspects of North American grain agriculture. While some aspects of the changed climate in the scenario considered act to reduce crop yields, others present opportunities for adaptation which could result in compensation or even yield increases.

One important result is the illustration of means by which agriculture could effectively adapt to a changing climate. For example, warmer temperatures allow use of later-maturing varieties of grain corn as a consequence both of higher daily temperatures and an extended growing season. The resulting higher yield potential may be further enhanced by increased precipitation, even for a single month. This is particularly so if planting dates can be manipulated such that the occurrence of critical developmental stages of the crop can be made to occur at that time.

The particular climate scenario constructed in Section 3.5 produces some changes in the geographical distribution of the major cropping regions considered here. However, the picture is by no means complete since other important crops, most notably soybeans, have not been included in the present analysis.

For the case of grain corn, yields increase in the (presently temperature-limited) areas in the northern half of the three gridboxes considered, and yields decrease in the warmer southern areas. That portion of the continent well-adapted to grain corn production may accordingly increase; to the north as heat limitations are removed, and to the southwest to the extent that the yields of corn decline relatively less than those for wheat.

Evaluation of this latter point is complicated by the anticipated differences in the two types of plants to direct physiological effects of increased carbon dioxide, which are not treated in the present simulations. Plants such as wheat exhibit marked increases in net photosynthesis in response to increases in carbon dioxide concentrations, which may ultimately be 30% under favorable conditions in a doubled $CO_2$ atmosphere (Cure, 1985). Plants such as corn, which utilize a different biochemical pathway for carbon dioxide fixation, show little response in the rate of photosynthesis for $CO_2$ concentrations above the current levels of about 340 ppm, but do exhibit increased water use efficiency (Acock and Allen, 1985). However, the extent to which crop yields may be affected by these changes in plant physiology is not known (Acock and Allen, 1985; Bazzaz et al., 1985; Waggoner, 1983).

The potential changes in cropping regions are less clear for wheat than for corn. The modeled wheat crops fare worse in the 2X-$CO_2$ scenario nearly everywhere except in the very important production region of central Kansas. While this is an encouraging prospect, it is troubling that precisely the opposite result is encountered in the adjoining region of southeast Nebraska. The differences can be sensibly interpreted in terms of the separate projected climates for the respective gridboxes, but this spatial incoherence underscores the need to improve the present procedure to allow treatment of the statistical dependence between climates of nearby gridboxes.

Of course the specific results depend on many uncertainties in the antecedent components of the procedure. The two crop simulators employed do consider crop physiology and phenology on a daily basis, but are relatively simple examples of "process-oriented" models. Two particular shortcomings are in the treatment of winter wheat in very cold weather, and errors in quantitive yield predictions. It must be assumed that relative changes in crop yields are adequately portrayed. However, the two models are successful in relating developmental stages to weather events, which is critically important for examination of the capacity of agricultural producers to adapt. The climate inverse procedure does not completely reproduce the statistical character of station-scale meteorological data, but the most severe error from the standpoint of crop simulation, occasional very large precipitation amounts, is mitigated by the formulation for surface runoff presented in Appendix B. The appropriateness of the climate inverse procedure in a 2X-$CO_2$ world, and the means of extrapolating the statistical characteristics of the grid-scale time series, have both been assumed. Finally, the relative changes portrayed by the GCM have necessarily been accepted.

While the results presented here are moderately optimistic about the fate of North American grain agriculture in a doubled $CO_2$ world, the above considerations indicate that the present work may be best regarded as an exercise in the development of methods to examine this issue. Specific predictions should be taken seriously only to the extent that similar results are obtained using different GCM data sets and different or improved formulations linking the GCM data to the local conditions.

# Section 5

## Summary, Conclusions, and Future Work

The present work has formulated and demonstrated the use of specific procedures to implement the conceptual framework of Gates (1985) for estimation of local climate impacts using information derived from large-scale general circulation models. The development has consisted of three major parts. The first was refinement of the approach to the climate inverse problem of Kim et al. (1984) to allow its use with daily data. This extension consisted of a rotated principal component analysis of daily data for simultaneous treatment of maximum temperature, minimum temperature, and precipitation. It was found that this procedure produces pattern vectors that sensibly portray the different spatial scales of the variables and their cross-correlations, and that permit reasonable meteorological interpretation. Of particular utility in the context of stochastic simulation of the spatial distribution of weather elements is the representation of daily precipitation patterns that reflects, particularly in the warm season, its relatively isolated character.

The second major development presented here was a novel means of statistically constructing climate scenarios at the scale of resolution of GCMs, on the basis of the climates portrayed by two realizations of a GCM and a corresponding sample of observational data. This approach involved characterizing the climate states represented by each of these three data sources using the parameters of a multivariate parametric time-series model. The scenario for the changed climate was then constructed by adjusting parameters of this model that were derived from the observations on the basis of significant relative differences between the two GCM data sets. Although this method is conceptually no different than the usual approach to interpreting the results of climate change experiments with GCMs, it is carried out here with a much richer parameter set, and in such a way that stochastic realizations of daily data representing the present or inferred changed climate can be constructed in a straightforward manner.

Finally, these two procedures were coupled, and their applicability to investigations of climate impacts on agriculture was demonstrated with a case study. Stochastically synthesized local weather data were used in conjunction with two physiological crop simulation models to produce estimates of the climatic consequences of a doubling of $CO_2$ on grain yields, for selected regions of North America. The results of this investigation are moderately optimistic, and indicate that many potential disruptions may be mitigated by the adaptive capacity of agricultural producers, as has been emphasized by Clark (1985).

However, the specific predictions concerning relative crop yields and possible shifts in cropping regions generated here must be regarded with great caution. It could be tempting to use the present results in public policy or planning contexts (Figure 1, step 4), for example in conjunction with global economic models such as that described by Liverman (1986). Consideration of the many uncertainties present in the analysis indicates that such use of these initial results would be inappropriate.

First, the results depend rather strongly on the correctness of relative changes in surface climatic elements as portrayed by the particular GCM employed here. The global-averaged increase in surface temperature for this model at year 25 of the integrations (from which the assumed relative increases in temperature are calculated) is approximately 5°C (W.L. Gates, private communication). This increase is larger than results from comparable GCM studies reported in the literature (Schlesinger, 1986), although the potentially important contributions of radiatively active trace gases other than carbon dioxide to a global warming (e.g., Ramanathan et al., 1985) have not been considered. Also, the timing within the year of inferred climate changes (particularly for precipitation) with respect to the crop calendar influences the results very strongly.

The climate inverse procedure described in Section 2 appears to be a reasonably successful procedure for the estimation of local data using large-scale weather information, at least for current conditions. Particularly for the case of precipitation, however, it does not produce realizations of local climates possessing statistics that are identical to the observations. Also, the degree to which the statistical relationships embodied in the procedure will be representative of those in a warmer world is largely a matter of speculation.

Finally, there is uncertainty regarding the performance of the crop models employed. It is known that these models produce errors in absolute yield predictions, and it has been necessary to assume that relative changes in yields have been reasonably portrayed. In addition, the inability of these models to simulate the direct effects of $CO_2$ on plant physiology implies that the specific results pertaining to future crop yields contain considerable uncertainty.

It is probably best to regard the results presented here as a demonstration of the potential utility of the present method for climate impact assessments. Overall, the formulation appears to be an appropriate basis for such studies.

A number of refinements to the procedure are possible and should be pursued. These refinements may be regarded as being comprised of technical improvements to the climate inverse formulation, and extensions aimed at broadening the applicability of the approach:

1. Results presented in Section 2 indicate that the present station density is not adequate to fully capture the spatial variations of daily precipitation data, which in turn precludes adequate stochastic simulation of this variable between stations by interpolation. Precipitation has a very strong influence on agricultural response, and improvement of its representation would be highly desirable. An obvious potential remedy would be inclusion of more stations for which precipitation (but not necessarily temperature) observations are available. Many cooperative observing stations report only preciptitation, so that a larger pool of stations from which to choose is available. Increasing the density of stations appears to be unnecessary from the standpoint of representing spatial variations of temperature, and would primarily serve in this case to increase the computational burden.

2. The present formulation of the climate inverse procedure includes no weighting of the station data in the calculation of the correlation matrix, and the representation might be improved if some measure of relative station importance were incorporated at this stage. This issue is complicated by the fact that use of the correlation (rather than the covariance) matrix is dictated by simultaneous treatment of several variables. Possible starting points in the search for an optimal method of station weighting are the procedures suggested by Lorenz (Kutzbach, 1967) and Buell (1978).
3. The present procedure uses the GCM information at the very limit of its resolution, where its performance is expected to be least reliable. It would be desirable to devise a reasonable and consistent procedure for incorporation of information from surrounding gridboxes into the specification of climate scenarios. A successful treatment of this issue should minimize artificial discontinuities in the climates (and corresponding simulated crop yields) between nearby stations in adjacent gridboxes.

Finally, the applicability of the procedure presented here could be extended by explicit modeling of variations on time scales of months or seasons. Except when box-scale weather is specified from the observational record (which severely limits the applicability of the procedure for large-sample Monte Carlo simulations), the only source of intermonthly, interseasonal, or interannual variability in the present formulation is through a random-walk process (e.g., Feller, 1968; Katz, 1985). This limitation follows from treatment of the annual cycles of mean daily values, for example, as constant over the period of record (e.g., Trenberth, 1984).

There are several possible future lines of inquiry relative to this issue. One is explicit modeling of monthly and seasonal variations of mean values following, for example, Chu and Katz (1985). Another is stratification of the principal component amplitudes according to the value of some variable that may be produced by extended-range prediction efforts, such as monthly or seasonal mean temperature anomaly, or phase of the El Nino cycle. Refinement of climate-inverse procedures in this way could allow use of results from extended-range prediction groups in estimation of local impacts of weather fluctuations on monthly or seasonal time scales. For example, some current means of agricultural yield prediction, employing physiological crop models and daily values of climatological data (e.g., Duchon, 1986; Dugas _et al._, 1983b), could be improved through more sophisticated use of growing-season meteorological forecasts. As the performance of monthly and seasonal forecasting efforts improves, the procedure could then begin to provide information of economic and policy significance.

# Bibliography


Acock, B., and L.J. Allen, Jr., 1985: Crop responses to elevated carbon dioxide concentrations. In: B.R. Strain and J.D. Cure, eds., Direct Effects of Increasing Carbon Dioxide on Vegetation. U.S. Department of Energy, DOE/ER-0238, pp. 53-97.

Anderson, T.W., 1958: An Introduction to Multivariate Statistical Analysis. New York, Wiley, 374 pp.

Arkin, G.F, W.A. Dugas, and C.G. Ainsworth, 1983: Agricultural Drought Assessments Using a Crop Model. Final Report, Bureau of Reclamation 1-07-81-V0159, 154 pp.

Austin, M.E., 1972: Land Resource Regions and Major Land Resource Areas of the United States. Agriculture Handbook 296. Soil Conservation Service, U.S. Department of Agriculture, 82 pp.

Bach, W., H.-J. Jung, and H Knottenberg, 1984: Development of regional climate scenarios. In: H. Meinl and W. Bach, eds., Socioeconomic Impacts of Climatic Changes due to a Doubling of Atmospheric $CO_2$ Content. Report to Commission of the European Communities, Brussels, Contract No. CLI-063-D, pp 185-259.

Baier, W., 1971: An agroclimatic probability study of the economics of fallow-seeded and continuous spring wheat in southern Saskatchewan. Agricultural Meteorology, 9, 305-321.

Baier, W., 1977: Crop-weather models and their use in yield assessments. Tech. Note No. 151, WMO-No. 458. WMO, Geneva, 48 pp.

Barnett, T.P., 1986: Detection of changes in the global troposphere temperature field induced by greenhouse gases. Journal of Geophysical Research, 91(D6), 6659-6667.

Beaumont, G.P., 1980: Intermediate Mathematical Statistics. London, Chapman and Hall, 248 pp.

Bond, D.C., 1979: Generating daily weather values by computer simulation techniques for crop yield forecasting models. Washington, D.C., Econmics, Statistics, and Cooperative Service, US Department of Agriculture, 38 pp.

Box, G.E.P., and G.M. Jenkins, 1976: Time Series Analysis: Forecasting and Control. San Francisco, Holden-Day, 575 pp.

Box, G.E.P., and M.E. Muller, 1958: A note on the generation of random normal deviates. Annals of Mathematical Statistics, 29, 610-611.

Bratley, P., B.L. Fox, and L.E. Schrage, 1983: A Guide to Simulation. New York, Springer-Verlag, 383 pp.

Brower, B., 1984: Development of a U.S. historical climatology network. The State Climatologist, 8(3), 9-23.

Bryson, R.A., and T.J. Murray, 1977: Climates of Hunger. Madison, University of Wisconsin Press, 171 pp.

Buckman, H.O., and N.C. Brady, 1969: The Nature and Properties of Soils. New York, MacMillan, 653 pp.

Buell, C.E., 1978: The number of significant proper functions of two-dimensional fields. Journal of Applied Meteorology, 17, 717-722.

Butzer, K.W., 1980: Adaptation to global environmental change. Professional Geographer, 32, 269-278.

Changnon, S.A., Jr., 1981: Convective raincells. Journal of the Atmospheric Sciences, 38, 1793-1797.

Chin, E.H., and J.F. Miller, 1980: On the conditional distribution of daily precipitation amounts. Monthly Weather Review, 108, 1462-1464.

Chu, P.-S., and R.W. Katz, 1985: Modeling and forecasting the southern oscillation: a time-domain approach. Monthly Weather Review, 113, 1876-1888.

Clark, W.C., 1985: Scales of climatic impacts. Climatic Change, 7, 5-27.

Coe, R., and R.D. Stern, 1982: Fitting models to daily rainfall data. Journal of Applied Meteorology, 21, 1024-1031.

Cure, J.D., 1985: Carbon dioxide doubling responses: a crop survey. In: B.R. Strain and J.D. Cure, eds., Direct Effects of Increasing Carbon Dioxide on Vegetation. U.S. Department of Energy, DOE/ER-0238, pp. 99-116.

Deardorff, J.W., K. Ueyoshi, and Y.-J. Han, 1984: Numerical study of terrain-induced mesoscale motions and hydrostatic form drag in a heated, growing mixed layer. Journal of the Atmospheric Sciences, 41, 1420-1441.

Draper, N.R., and H. Smith, 1981: Applied Regression Analysis. New York, Wiley, 709 p.

Duchon, C.E., 1986: Corn yield prediction using climatology. Journal of Climate and Applied Meteorology, 25, 581-590.

Dugas, W.A., G.F. Arkin, and B.S. Jackson, 1983a: Factors affecting simulated crop yield spatial extrapolation. Transactions of the American Society of Agricultural Engineers, 26, 1440-1444.

Dugas, W.A., C.G. Ainsworth, and G.F. Arkin, 1983b: Operational drought evaluations using a crop model. Extended Abstracts, Sixth Conference on Agriculture and Forest Meteorology (Fort Collins, CO). Boston, American Meteorological Society, pp. 113-116.

Feller, W., 1968: An Introduction to Probability Theory and Its Applications, Volume I. New York, Wiley, 509 pp.

Gabriel, K.R., 1959: The distribution of the number of successes in a sequence of dependent trials. Biometrika, 46, 454-460.

Galliani, G. and F. Filippini, 1985: Climatic clusters in a small area. Journal of Climatology, 5, 487-501.

Garcia Guzman, A., and W.C. Torrez, 1985: Daily rainfall probabilities: Conditional upon prior occurrence and amount of rain. Journal of Climate and Applied Meteorology, 24, 1009-1014.

Gates, W.L., 1985: The use of general circulation models in the analysis of the ecosystem impacts of climatic change. Climatic Change, 7, 267-284.

Gates, W.L., and W. Bach, 1981: Analysis of a model-simulated climate change as a scenario for impacts studies. Report for the German Federal Environmental Agency, R & D No. 104-02-513, 163 pp.

Geiger, R., 1965: The Climate Near the Ground. Cambridge, Harvard University Press, 611 pp.

Ghan, S.J., J.W. Lingaas, M.E. Schlesinger, R.L. Mobley, and W.L. Gates, 1982: A documentation of the OSU two-level atmospheric general circulation model. Report No. 35, Climatic Research Institute, Oregon State University, 395 pp.

Griffith, C.G., J.A. Augustine, and W.L. Woodley, 1981: Sattelite rain estimation in the U.S. high plains. Journal of Applied Meteorology, 20, 53-66.

Han, Y.-J., K. Ueyoshi, and J.W. Deardorff, 1982: Numerical study of terrain-induced mesoscale motions in a mixed layer. Journal of the Atmospheric Sciences, 39, 2464-2476.

Hanway, J.J., 1963: Growth stages of corn (Zea mays L.). Agronomy Journal, 55, 487-492.

Harman, H.H., 1967: Modern Factor Analysis. Chicago, University of Chicago Press, 474 pp.

Harris, C.W., 1967: On factors and factor scores. Psychometrika, 32, 363-379.

Hendrick, R.L., and G.H. Comer, 1970: Space variation of precipitation and implications for raingage network design. Journal of Hydrology, 10, 151-163.

Hillel, D., 1971: Soil and Water. New York, Academic, 288 pp.

Hillmer, S.C., and G.C. Tiao, 1979: Likelihood function of stationary multiple autoregressive moving average models. Journal of the American Statistical Association, 74, 652-660.

Horel, J.D., 1981. A rotated principal component analysis of the interannual variability of the Northern Hemisphere 500 mb height field. Monthly Weather Review, 109, 2080-2092.

Houze, R.A., Jr., and P.V. Hobbs, 1982: Organization and structure of precipitating cloud systems. In: B. Saltzman, ed., Advances in Geophysics, volume 24. New York, Academic, pp. 225-315.

Ison, N.T., A.M. Feyerherm, and L.D. Bark, 1971: Wet period precipitation and the gamma distribution. Journal of Applied Meteorology, 10, 658-665.

Jaafar, M.N., E.T. Kanemasu, and W.L. Powers, 1978: Estimating soil factors for nine Kansas soils used in an evapotranspiration model. Transactions of the Kansas Academy of Science, 81, 57-63.

Jager, J., and W.W. Kellogg, 1983: Anomalies in temperature and rainfall during warm arctic seasons. Climatic Change, 5, 39-60.

Jenkins, G.M., and D.G. Watts, 1968: Spectral Analysis and its Applications. San Francisco, Holden-Day, 523 pp.

Johnson, R.A., and D.W. Wichern, 1982: Applied Multivariate Statistical Analysis. Englewood Cliffs, New Jersey, Prentice-Hall, 594 pp.

Jones, R.H., 1964: Prediction of multivariate time series. Journal of Applied Meteorology, 3, 285-289.

Jones, R.H., 1974: Identification and autoregressive spectrum estimation. IEEE Transactions on Automatic Control, AC-19, 894-897.

Jury, W.A., and C.B. Tanner, 1975: Advection modification of the Priestley and Taylor evapotranspiration formula. Agronomy Journal, 67, 840-842.

Kaiser, H.F., 1958: The varimax criterion for analytic rotation in factor analysis. Psychometrika, 23, 187-200.

Kaiser, H.F., 1962: Formulas for component scores. Psychometrika, 27, 83-87.

Kanemasu, E.T., L.R. Stone, and W.L. Powers, 1976: Evapotranspiration model tested for soybean and sorghum. Agronomy Journal, 68, 569-572.

Katz, R.W., 1977a: An application of chain-dependent processes to meteorology. Journal of Applied Probability, 14, 598-603.

Katz, R.W., 1977b: Precipitation as a chain-dependent process. Journal of Applied Meteorololgy, 16, 671-676.

Katz, R.W., 1977c: Assessing the impact of climatic change on food production. Climatic Change, 1, 85-96.

Katz, R.W., 1981: On some criteria for estimating the order of a Markov chain. Technometrics 23, 243-249.

Katz, R.W., 1982: Statistical evaluation of climate experiments with general circulation models: a parametric time-series modeling approach. Journal of the Atmospheric Sciences, 39, 1446-1455.

Katz, R.W., 1983: Statistical procedures for determining the statistical significance of changes in variability simulated by an atmospheric general circulation model. Report No. 48, Climatic Research Institute, Oregon State University, Corvallis, 23 pp.

Katz, R.W., 1985: Probabilistic models. In: A.H. Murphy and R.W. Katz, eds., Probability, Statistics, and Decision Making in the Atmospheric Sciences. Boulder, Westview, pp 261-288.

Kim, J.-W., J.-T. Chang, N.L. Baker, D.S. Wilks, and W.L. Gates, 1984: The statistical problem of climate inversion: determination of the relationship between local and large-scale climate. Monthly Weather Review, 112, 2069-2077.

Kimball, B.A., 1985: Adaptation of vegetation and management to a higher carbon dioxide world. In: B.R. Strain and J.D. Cure, eds., Direct Effects of Increasing Carbon Dioxide on Vegetation. U.S. Department of Energy, DOE/ER-0238, pp. 185-204.

Kutzbach, J.E., 1967: Empirical eigenvectors of sea-level pressure, surface temperature and precipitation complexes over North America. Journal of Applied Meteorology, 6, 791-802.

Lamb, H.H., 1982: Climate, History and the Modern World. London, Methuen, 387 pp.

Large, E.C., 1954: Growth stages in cereals: Illustration of the Feekes scale. Plant Pathology, 3, 128-129.

Larsen, G.A., 1983: Application of path coefficient analysis to a plant simulation model. Staff Report No. AGES830103, Statistical Reporting Service, U.S. Department of Agriculture, 38 pp.

Larsen, G.A., and R.B. Pense, 1982: Stochastic simulation of daily climatic data for agronomic models. Agronomy Journal, 74, 510-514.

Leith, C.E., 1973: The standard error of time-average estimates of climatic means. Journal of Applied Meteorology, 12, 1066-1069.

Lindgren, B.W., 1976: Statistical Theory. New York, MacMillan, 614 pp.

Liverman, D., 1986: The response of a global food model to possible climate changes: a sensitivity analysis. Journal of Climatology, 6, 355-373.

Livezey, R.E., and W.Y. Chen, 1983: Statistical field significance and its determination by Monte Carlo techniques. Monthly Weather Review, 111, 46-59.

Lough, J.M., T.M.L. Wigley, and J.P. Palutikof, 1983: Climate and climate impact scenarios for Europe and a warmer world. Journal of Climate and Applied Meteorology, 22, 1673-1684.

Maas, S.J., and G.F. Arkin, 1980a: TAMW: A wheat growth and development simulation model. Program and Model Documentation No. 80-3, Blackland Research Center, Texas Agricultural Experiment Station, Temple, Texas.

Maas, S.J., and G.F. Arkin, 1980b: Initial validation of a winter wheat simulation model. American Society of Agricultural Engineers Technical Paper No. 80-4010, 7 pp.

Madden, R.A., 1976: Estimates of the natural variability of time-averaged sea-level pressure. Monthly Weather Review, 104, 942-952.

Manabe, S., and K. Bryan, Jr., 1985: $CO_2$-induced change in a coupled ocean-atmosphere model and its paleoclimatic implications. Journal of Geophysical Research, 90(C6), 11689-11707.

Manabe, S., and R.T. Wetherald, 1986: Reduction in summer soil wetness induced by an increase in atmospheric carbon dioxide. Science, 232, 626-628.

Manabe, S., R.T. Wetherald, and R.J. Stouffer, 1981: Summer dryness due to an increase of atmospheric $CO_2$ concentration. Climatic Change, 3, 347-386.

Martin, J.H., W.H. Leonard, and D.L. Stamp, 1976: Principles of Field Crop Production. New York, MacMillan, 1116 pp.

Mathews, O.R., and T.J. Army, 1960: Moisture storage on fallowed wheatland in the Great Plains. Soil Science Society of America Proceedings, 24, 414-418.

McDonald, R.P., and E.J. Burr, 1967: A comparison of four methods of constructing factor scores. Psychometrika, 32, 381-401.

Mearns, L.O., R.W. Katz, and S.H. Schneider, 1984: Extreme high-temperature events: changes in their probabilitites with changes in mean temperature. Journal of Climate and Applied Meteorology, 23, 1601-1613.

Michaels, P.J., 1983: Price, weather, and "acreage abandonment" in western Great Plains wheat culture. Journal of Climate and Applied Meteorology, 22, 1296-1303.

Monteith, J.L., 1981: Climatic variation and the growth of crops. Quarterly Journal of the Royal Meteorological Society, 107, 749-774.

Morrison, D.F., 1976: Multivariate Statistical Methods. New York, McGraw-Hill, 415 pp.

Namias, J., 1980: Some concomitant regional anomalies associated with hemispherically averaged temperature variations. Journal of Geophysical Research, 85(C3), 1585-1590.

National Academy of Sciences, 1975: Understanding Climatic Change. Washington, National Academy of Sciences, 239 pp.

National Climate Center, 1978: SOLMET Hourly Solar Radiation-Surface Meteorological Observations. Washington, D.C., U.S. Department of Commerce, TD-9724.

Neild, R.E., H.N. Richman, and M.W. Seeley, 1979: Impacts of different types of temperature change on the growing season for maize. Agricultural Meteorology, 20, 367-374.

Newman, J.E., 1980: Climate change impacts on the growing season of the North American "Corn Belt." Biometeorology, 7, Part 2, 128-142 (Supplement to International Journal of Biometeorology, 24).

Neyman, J., and E.L. Scott, 1967: Some outstanding problems relating to rain modification. Proceedings of the Fifth Berkeley Symposium on Mathematical Statistics and Probability, 5, 293-326.

North Dakota Crop and Livestock Reporting Service, 1984: North Dakota Agricultural Statistics, No. 53. Fargo, North Dakota, 96 pp.

Oram, P.A., 1985: Sensitivity of agricultural production to climatic change. Climatic Change, 7, 129-152.

Palmen, E., and C.W. Newton, 1969: Atmospheric Circulation Systems. New York, Academic, 603 pp.

Parry, M.L., and T.R. Carter, 1985: The effect of climatic variations on agricultural risk. Climatic Change, 7, 95-110.

Pittock, A.B., and M.J. Salinger, 1982: Towards regional scenarios for a $CO_2$-warmed earth. Climatic Change, 4, 23-40.

Pollard, D., 1982: The performance of an upper-ocean model coupled to an atmospheric GCM: Preliminary results. Report No. 31, Climatic Research Institute, Oregon State University, Corvallis, 33 pp.

Priestley, C.H.B., and R.J. Taylor, 1972: On the assessment of surface heat flux and evaporation using large-scale parameters. Monthly Weather Review, 100, 81-92.

Ramanathan, V., R.J. Cicerone, H.B. Singh, and J.T. Kiehl, 1985: Trace gas trends and their potential role in climate change. Journal of Geophysical Research, 90(D3), 5547-5566.

Reed, D.N., 1986: Simulation of time series of temperature and precipitation over eastern England by an atmospheric general circulation model. Journal of Climatology, 6, 233-253.

Reynolds, J.F., and B. Acock, 1985: Modeling approaches for evaluating vegetation responses to carbon dioxide concentration. In: B.R. Strain and J.D. Cure, eds., Direct Effects of Increasing Carbon Dioxide on Vegetation. U.S. Department of Energy, DOE/ER-0238, pp. 33-51.

Richardson, C.W., 1981: Stochastic simulation of daily precipitation, temperature, and solar radiation. Water Resources Research, 17, 182-190.

Richman, M.B. 1981: Obliquely rotated principal components: An improved meteorological map typing technique? Journal of Applied Meteorology, 20, 1145-1159.

Richman, M.B. 1986: Rotation of principal components. Journal of Climatology, 6, 293-335.

Richman, M.B., and P.J. Lamb, 1985: Climatic pattern analysis of three- and seven-day summer rainfall in the central United States: Some methodological considerations and a regionalization. Journal of Climate and Applied Meteorlolgy, 24, 1326-1343.

Rind, D., 1986: The dynamics of warm and cold climates. Journal of the Atmospheric Sciences, 43, 3-24.

Ritchie, J.T., 1972: Model for predicting evaporation from a row crop with incomplete cover. Water Resources Research, 8, 1204-1213.

Ritchie, J.T., E. Burnett, and R.C. Henderson, 1972: Dryland evaporative flux in a subhumid climate. 3. Soil water influences. Agronomy Journal, 64, 168-173.

Rosenberg, N.J., 1982: The increasing $CO_2$ concentration in the atmosphere and its implication on agricultural productivity. II. Effects through $CO_2$-induced climatic change. Climatic Change, 4, 239-254.

Rosenzweig, C., 1985: Potential $CO_2$-induced climate effects on North American wheat-producing regions. Climatic Change, 7, 367-389.

Sakamoto, C.M., 1981: The technology of crop-weather modeling. In: W. Bach, J. Pankrath, and S.H. Schneider, eds., Food-Climate Interactions. Dordrecht, Reidel, pp. 383-398.

Sakamoto, C.M., S.K. Leduc, N. Strommen, and L.T. Steyaert, 1980: Climate and global grain yield variability. Climatic Change, 2, 349-361.

Salter, P.J., and J.E. Goode, 1967: Crop Responses to Water at Different Stages of Growth. Commonwealth Bureau of Horticulture and Plantation Crops, Research Review No. 2, 246 pp.

Santer, B., 1985: The use of general circulation models in climate impact analysis--a preliminary study of the impacts of a $CO_2$-induced climatic change on West European agriculture. Climatic Change, 7, 71-93.

Schlesinger, M.E., 1986: Equilibrium and transient climatic warming induced by increased atmospheric $CO_2$. Climate Dynamics, 1, 35-52.

Schneider, S.H., 1984: On the empirical verification of model-predicted $CO_2$-induced climatic effects. In: J.E. Hansen and T. Takahashi, eds., Climatic Processes and Climatic Sensitivity. Washington, D.C., American Geophysical Union, pp. 187-201.

Schwartz, G., 1978: Estimating the dimension of a model. Annals of Statistics, 6, 461-464.

Shaw, R.H., 1965: The prediction of soil moisture for the winter period in Iowa. Iowa State Journal of Science, 39, 337-344.

Shaw, R.H., 1983: Estimates of yield reductions in corn caused by water and temperature stress. In: C.D. Raper, Jr., and P.J. Kramer, eds., Crop Reactions to Water and Temperature Stresses in Humid, Temperate Climates. Boulder, Westview, pp. 49-65.

Soil Conservation Service, 1965: Soil Survey of Ford County, Kansas. Washington D.C., U.S. Department of Agriculture, 84 pp.

Soil Conservation Service, 1967: Soil Survey of Republic County, Kansas. Washington D.C., U.S. Department of Agriculture, 61 pp.

Soil Conservation Service, 1972: Hydrology. SCS National Engineering Handbook. Section 4. Washington. D.C., U.S. Department of Agriculture, Chapters 7-10.

Soil Conservation Service, 1974: Soil Survey of Burleigh County, North Dakota. Washington D.C., U.S. Department of Agriculture, 112 pp.

Soil Conservation Service, 1975: Soil Survey of Marshall County, South Dakota. Washington D.C., U.S. Department of Agriculture, 116 pp.

Soil Conservation Service, 1978: Soil Survey of Warren County, Iowa. Washington D.C., U.S. Department of Agriculture, 131 pp.

Soil Conservation Service, 1980: Soil Survey of Mitchell County, Kansas. Washington D.C., U.S. Department of Agriculture, 94 pp.

Soil Conservation Service, 1981: Soil Survey of Boone County, Iowa. Washington D.C., U.S. Department of Agriculture, 152 pp.

Soil Conservation Service, 1985: Soil Survey of Brule and Buffalo Counties, South Dakota. Washington D.C., U.S. Department of Agriculture, 191 pp.

Stapper, M., and G.F. Arkin, 1980: CORNF: A dynamic growth and development model for Maize (Zea mays L.). Program and Model Documentation No. 80-2, Blackland Research Center, Texas Agricultural Experiment Station, Temple, Texas, 91 pp.

Steel, R.G.D., and J.H. Torrie, 1980: Principles and Procedures of Statistics. New York, McGraw-Hill, 633 pp.

Stern, R.D., and R. Coe, 1984: A model fitting analysis of daily rainfall data. Journal of the Royal Statistical Society, A147, 1-34.

Strain, B.R., 1985: Background on the response of vegetation to atmospheric carbon dioxide enrichment. In: B.R. Strain and J.D. Cure, eds., Direct Effects of Increasing Carbon Dioxide on Vegetation. U.S. Department of Energy, DOE/ER-0238, pp. 1-10.

Terjung, W.H., D.M. Liverman, and J.T. Hayes, 1984: Climatic change and water requirements for grain corn in the North American Great Plains. Climatic Change, 6, 193-220.

Thompson, L.M., 1969a: Weather and technology in the production of corn in the U.S. corn belt. Agronomy Journal, 61, 453-456.

Thompson, L.M., 1969b: Weather and technology in the production of wheat in the United States. Journal of Soil and Water Conservation, 24, 219-224.

Thompson, L.M., 1975: Weather variability, climatic change, and grain production. Science, 188, 535-541.

Thompson, S.L., and S.H. Schneider, 1982: Carbon dioxide and climate: the importance of realistic geography in estimating the transient temperature response. Science, 217, 1031-1033.

Tiao, G.C., and G.E.P. Box, 1981: Modeling multiple time series with applications. Journal of the American Statistical Association, 76, 802-816.

Trenberth, K.E., 1984: Some effects of finite sample size and persistence on meteorological statistics. Part I: Autocorrelations. Monthly Weather Review, 112, 2359-2368.

United States Bureau of the Census, 1982a: Census of Agriculture, Part 15. Iowa State and County Data. Washington D.C., U.S. Department of Commerce, 435 pp.

United States Bureau of the Census, 1982b: Census of Agriculture, Part 16. Kansas State and County Data. Washington D.C., U.S. Department of Commerce, 460 pp.

United States Bureau of the Census, 1982c: Census of Agriculture, Part 41. South Dakota State and County Data. Washington D.C., U.S. Department of Commerce, 339 pp.

Wadleigh, C.H., W.A. Raney, and D.M. Herschfield, 1965: The moisture problem. In: W.H. Pierre, D. Kirkham, J.Pesek, and R. Shaw, eds., Plant Environment and Efficient Water Use. Madison, Wisconsin, American Society of Agronomy, pp. 1-19.

Waggoner, P.E., 1983: Agriculture and a climate changed by more carbon dioxide. In: Changing Climate, Carbon Dioxide Assessment Committee, National Academy Press, Washington, D.C., pp.383-418.

Walsh, J.E., and M.B. Richman, 1981: Seasonality in the associations between surface temperatures over the United States and the North Pacific Ocean. Monthly Weather Review, 109, 767-783.

Waymire, E., and V.K. Gupta, 1981: The mathematical structure of rainfall representations. 1. A review of stochastic rainfall models. Water Resources Research, 17, 1261-1272.

Whittle, P., 1963: On the fitting of multivariate autoregressions, and the approximate canonical factorization of a spectral density matrix. Biometrika, 50, 129-134.

Wigley, T.M.L., P.D. Jones, and P.M. Kelley, 1980: Scenarios for a warm, high $CO_2$ world. Nature, 283, 17-21.

Wilks, D.S., 1987: Sampling distribution of the time between effectively independent samples. Monthly Weather Review, in press.

Wilks, D.S., and A.H. Murphy, 1987: A decision-analytic study of the joint value of seasonal precipitation and temperature forecasts in a choice-of-crop problem. Atmosphere-Ocean, in press.

Williams, G.D.V., 1985. Estimated bioresource sensitivity to climatic change in Alberta, Canada. Climatic Change, 7, 5-69.

Williams, J., 1980: Anomalies in temperature and rainfall during warm Arctic seasons as a guide to the formulation of climate scenarios. Climatic Change, 2, 249-266.

Woolhiser, D.A., and G.G.S. Pegram, 1979: Maximum likelihood estimation of Fourier coefficients to describe seasonal variations of parameters in stochastic daily preciptation models. Journal of Applied Meteorology, 18, 34-42.

World Climate Applications Programme, 1984: Report of the WMO/UNEP/ICSU-SCOPE expert meeding on the reliability of crop-climate models for assessing the impacts of climatic change and variability. Geneva, WMO, 31 pp.

World Meteorological Organization, 1977: Agrometeorology of the Maize Crop. W.M.O. Publication No. 481, Geneva, 454 pp.

Wright, A.D., and M.E. Keener, 1982: A test of a maize growth and development model, CORNF. Agricultural Systems, 9, 181-197.

Zawadzki, I.I., 1973: Statistical properties of precipitation patterns. Journal of Applied Meteorology, 12, 459-472.

Zook, L.L., and H.E. Weakley, 1944: Summer fallow in Nebraska. Nebraska Agricultural Experiment Station Bulletin No. 362, 28 pp.

# APPENDICES

# APPENDIX A

## A Note on the Sampling Distribution of the "Time Between Effectively Independent Samples"

### A.1 Introduction

Meteorological and other geophysical time series exhibit positive serial correlation, or persistence. One popular and compact means of characterizing the degree of persistence in a data set is the "time between effectively independent samples," $T_0$ (e.g., Leith, 1973; Madden, 1976; Trenberth; 1984). This statistic has been employed in the meteorological literature to characterize and compare variations in monthly-averaged sea-level pressure (Madden, 1976), temperature (Madden and Shea, 1978), and daily geopotential height (Shukla and Gutzler, 1983; Trenberth, 1985).

The sampling distributions of estimates of $T_0$ have not been well documented, although this is an important consideration from the standpoints of both informal comparisons and formal statistical tests. Thiebaux and Zweirs (1984) investigated sample variances and measures of central tendency for several possible methods of calculating the "effective sample size," which is proportional to the reciprocal of $T_0$. Trenberth (1984) presents results indicating sample estimates of $T_0$ are negatively biased for sample sizes less than about 100.

The present note reports the results of an investigation into the sampling distribution of $T_0$ using Monte-Carlo techniques, with the aim of providing a basis for formal statistical tests involving this quantity. Section 2 describes the approach taken, results are reported in Section 3, and Section 4 contains some brief concluding remarks.

## A.2 Approach

Synthetic time series are generated using autoregressive processes of the form

$$X_t = \sum_{\ell=1}^{3} \phi_\ell X_{t-\ell} + \epsilon_t , \tag{A.1}$$

where $X_{t-\ell}$ is the value of the time series (which has zero mean) $\ell$ lags prior to time t, $\epsilon_t$ is a set of independent standard normal (i.e., Gaussian) variates, and the $\phi$s are the autoregressive coefficients. Table 39 lists autoregressive coefficients for the ten generating processes used in the study. These coefficients are representative of the sort of models that describe many meteorolological time series, and they are characterized by $T_0$ values (also listed in Table 39) which range from 1.7 to 18.2 time units.

Values of $T_0$ are calculated according to a weighted average of the autocorrelation function (e.g., Trenberth, 1984; Theibaux and Zwiers, 1984),

$$T_o = 1 + 2 \sum_{\ell=1}^{M} \left( 1 - \frac{\ell}{N} \right) r_\ell , \tag{A.2}$$

where $r_\ell$ is the autocorrelation at lag $\ell$, N is the sample size, and M

Table 39. Autoregressive coefficients for the ten generating processes considered, and corresponding theoretical values of $T_0$.

| Model | $\phi_1$ | $\phi_2$ | $\phi_3$ | $T_o$ |
|---|---|---|---|---|
| 1 | 1.00 | -0.50 | 0.00 | 1.67 |
| 2 | 0.40 | 0.00 | 0.00 | 2.33 |
| 3 | 0.60 | -0.20 | 0.10 | 2.86 |
| 4 | 0.90 | -0.50 | 0.20 | 3.25 |
| 5 | 1.00 | -0.40 | 0.10 | 4.46 |
| 6 | 1.20 | -0.40 | 0.00 | 5.57 |
| 7 | 1.00 | -0.20 | 0.00 | 7.33 |
| 8 | 0.90 | -0.20 | 0.10 | 8.79 |
| 9 | 0.85 | 0.00 | 0.00 | 12.25 |
| 10 | 0.90 | 0.00 | 0.00 | 18.24 |

is a truncation number. In the present work, M is taken to be 30, a value appropriate to daily data stratified by month.

Analytical values of $r_i$, and therefore for $T_0$, corresponding to a given autoregressive model are obtained using the Yule-Walker equations (e.g., Box and Jenkins, 1976). For autoregressive processes of maximum order 3 the recursions for calculation of autocorrelations are given by

$$r_1 = (\phi_1 + \phi_2 \phi_3) / (1 - \phi_2 - \phi_1 \phi_3 - \phi_3^2), \quad \text{(A.3a)}$$

$$r_2 = \phi_2 - r_1 (\phi_1 + \phi_3), \quad \text{(A.3b)}$$

$$r_3 = \phi_1 r_2 + \phi_2 r_1 + \phi_3, \quad \text{(A.3c)}$$

and

$$r_k = \sum_{\ell=1}^{3} \phi_\ell r_{k-\ell}, \quad k = 4,\ldots,M. \quad \text{(A.4)}$$

Estimates of the time between effectively independent samples, $\hat{T}_0$, are calculated according the procedure recommended by Jones (1975) and Trenberth (1984). First a sequence of (order zero to five) autoregressive processes are fit to the data, using the Yule-Walker equations (e.g., Box and Jenkins, 1976; Katz, 1982). The most appropriate order, p, is selected according the Bayesian information criterion statistic (Katz, 1982; Schwartz, 1978). Only the first p empirical autocorrelations are then used to estimate $\hat{T}_0$, with the remaining M-p coefficients being calculated from the Yule-Walker recursion on the basis of the initial p empirical autocorrelations. That is,

$$\hat{T}_o = 1 + 2 \sum_{\ell=1}^{M} \left( 1 - \frac{\ell}{N} \right) \hat{r}_\ell , \tag{A.5}$$

where

$$\hat{r}_k = \frac{1}{N-1} \sum_{t=1}^{N} ( X_t - \bar{X} ) ( X_{t-k} - \bar{X} ) , \quad k = 1,\ldots,p, \tag{A.6a}$$

and

$$\hat{r}_k = \sum_{\ell=1}^{p} \hat{\phi}_\ell \, \hat{r}_{\ell-k} , \quad k = p+1,\ldots,M. \tag{A.6b}$$

Here the $\hat{\phi}$'s are the fitted estimates of the autoregressive coefficients, and $\bar{X}$ is the usual sample mean over all N observations. Note that (A.5) is based on sample estimates of the autocorrelation function, while (A.2) employs the true autocorrelation values. The foregoing procedure is applied to obtain 1000 Monte-Carlo realizations for each of the 10 autoregressive generating processes, and each of eight values of N. These latter values are 2000, 1000, 600, 300, 200, 100, 70, and 50.

The proportion of effectively independent data decreases with increasing $T_o$, so that sample variances would be expected to increase with $T_o$. A flexible statistical model for quantifying this relationship is

$$V(\hat{T}_o) = A \, T_o^{\,B} \, e / N . \tag{A.7}$$

Here A and B are constants to be determined, the overbar denotes an average over the 1000 realizations, and e is a random residual error. The variance is assumed to be inversely proportional to N. Note that (A.7) implies that the errors are multiplicative (i.e., have magnitudes proportional to the fitted values), which indeed appears to be a feature of the data. The constants are determined by linear least-squares analysis after logarithms of both sides of (A.7) have been taken.

A.3 Results

Table 40 presents sample means and variances for $\hat{T}_0$ as a function of sample size for the 10 generating processes listed in Table 39. For the smaller sample sizes, some tendency toward negative bias of the sample means is evident, particularly for larger $\hat{T}_0$ values. This is in agreement with the result of Trenberth (1984). The bias steadily decreases with increasing N, however, and appears to be negligible for the larger sample sizes. The estimator (A.5) appears therefore to be asymptotically unbiased.

Figures 36 and 37 present histograms of $\hat{T}_0$ estimates, scaled to standard normal form (i.e., values minus sample means and divided by sample standard deviations), for autoregressive models 4 and 7, respectively. Panel (a) is for N = 100 and panel (b) is for N = 1000 in each case. Also shown in these figures for comparison is the standard Gaussian density. These figures illustrate that for the smaller values of N, the sampling distribution of $\hat{T}_0$ is distinctly non-normal, with moderately strong positive skewness. For the larger

Table 40. Theoretical $T_0$ values, and respective sample means and variances as a function of sample size, N, for the ten autoregressive models.

| Model | $T_o$ | $\bar{\hat{T}}_o$ | $\hat{V}(\hat{T}_o)$ | N |
|---|---|---|---|---|
| 1 | 1.667 | 1.666 | .011 | 2000 |
| | | 1.662 | .024 | 1000 |
| | | 1.671 | .039 | 600 |
| | | 1.657 | .074 | 300 |
| | | 1.646 | .112 | 200 |
| | | 1.597 | .242 | 100 |
| | | 1.670 | .596 | 70 |
| | | 1.672 | .995 | 50 |
| 2 | 2.333 | 2.334 | .014 | 2000 |
| | | 2.323 | .026 | 1000 |
| | | 2.336 | .045 | 600 |
| | | 2.312 | .082 | 300 |
| | | 2.299 | .135 | 200 |
| | | 2.269 | .274 | 100 |
| | | 2.241 | .403 | 70 |
| | | 2.227 | .593 | 50 |
| 3 | 2.858 | 2.854 | .075 | 2000 |
| | | 2.738 | .179 | 1000 |
| | | 2.624 | .268 | 600 |
| | | 2.712 | .456 | 300 |
| | | 2.760 | .572 | 200 |
| | | 2.781 | .711 | 100 |
| | | 2.772 | .998 | 70 |
| | | 2.745 | 1.510 | 50 |
| 4 | 3.250 | 3.251 | .075 | 2000 |
| | | 3.242 | .170 | 1000 |
| | | 3.198 | .264 | 600 |
| | | 3.124 | .687 | 300 |
| | | 2.899 | .999 | 200 |
| | | 2.776 | 1.612 | 100 |
| | | 2.812 | 2.915 | 70 |
| | | 2.821 | 4.328 | 50 |
| 5 | 4.457 | 4.421 | .179 | 2000 |
| | | 4.240 | .460 | 1000 |
| | | 4.046 | .625 | 600 |
| | | 3.946 | 1.054 | 300 |
| | | 3.823 | 1.341 | 200 |
| | | 3.978 | 3.356 | 100 |
| | | 4.025 | 4.948 | 70 |
| | | 4.219 | 7.262 | 50 |

Table 40, continued.

| Model | $T_o$ | $\hat{\bar{T}}_o$ | $\hat{V}(\hat{T}_o)$ | N |
|---|---|---|---|---|
| 6 | 5.571 | 5.558 | .174 | 2000 |
| | | 5.530 | .346 | 1000 |
| | | 5.507 | .619 | 600 |
| | | 5.396 | 1.115 | 300 |
| | | 5.325 | 1.799 | 200 |
| | | 5.219 | 5.657 | 100 |
| | | 5.595 | 12.840 | 70 |
| | | 5.824 | 20.550 | 50 |
| 7 | 7.333 | 7.279 | .328 | 2000 |
| | | 7.298 | .650 | 1000 |
| | | 7.153 | 1.267 | 600 |
| | | 7.396 | 3.729 | 300 |
| | | 7.777 | 6.323 | 200 |
| | | 7.967 | 11.060 | 100 |
| | | 7.858 | 14.210 | 70 |
| | | 7.414 | 18.370 | 50 |
| 8 | 8.788 | 8.677 | .889 | 2000 |
| | | 8.384 | 1.875 | 1000 |
| | | 8.278 | 3.042 | 600 |
| | | 8.198 | 4.165 | 300 |
| | | 8.000 | 5.194 | 200 |
| | | 7.768 | 8.286 | 100 |
| | | 7.288 | 10.790 | 70 |
| | | 7.136 | 14.300 | 50 |
| 9 | 12.250 | 12.130 | 1.025 | 2000 |
| | | 12.060 | 1.971 | 1000 |
| | | 11.850 | 3.186 | 600 |
| | | 11.680 | 5.747 | 300 |
| | | 11.370 | 8.897 | 200 |
| | | 10.510 | 13.730 | 100 |
| | | 9.807 | 18.730 | 70 |
| | | 9.289 | 24.100 | 50 |
| 10 | 18.240 | 18.030 | 2.706 | 2000 |
| | | 17.780 | 4.745 | 1000 |
| | | 17.620 | 8.059 | 600 |
| | | 16.720 | 14.710 | 300 |
| | | 15.840 | 19.200 | 200 |
| | | 14.470 | 30.860 | 100 |
| | | 13.040 | 38.440 | 70 |
| | | 11.980 | 44.110 | 50 |

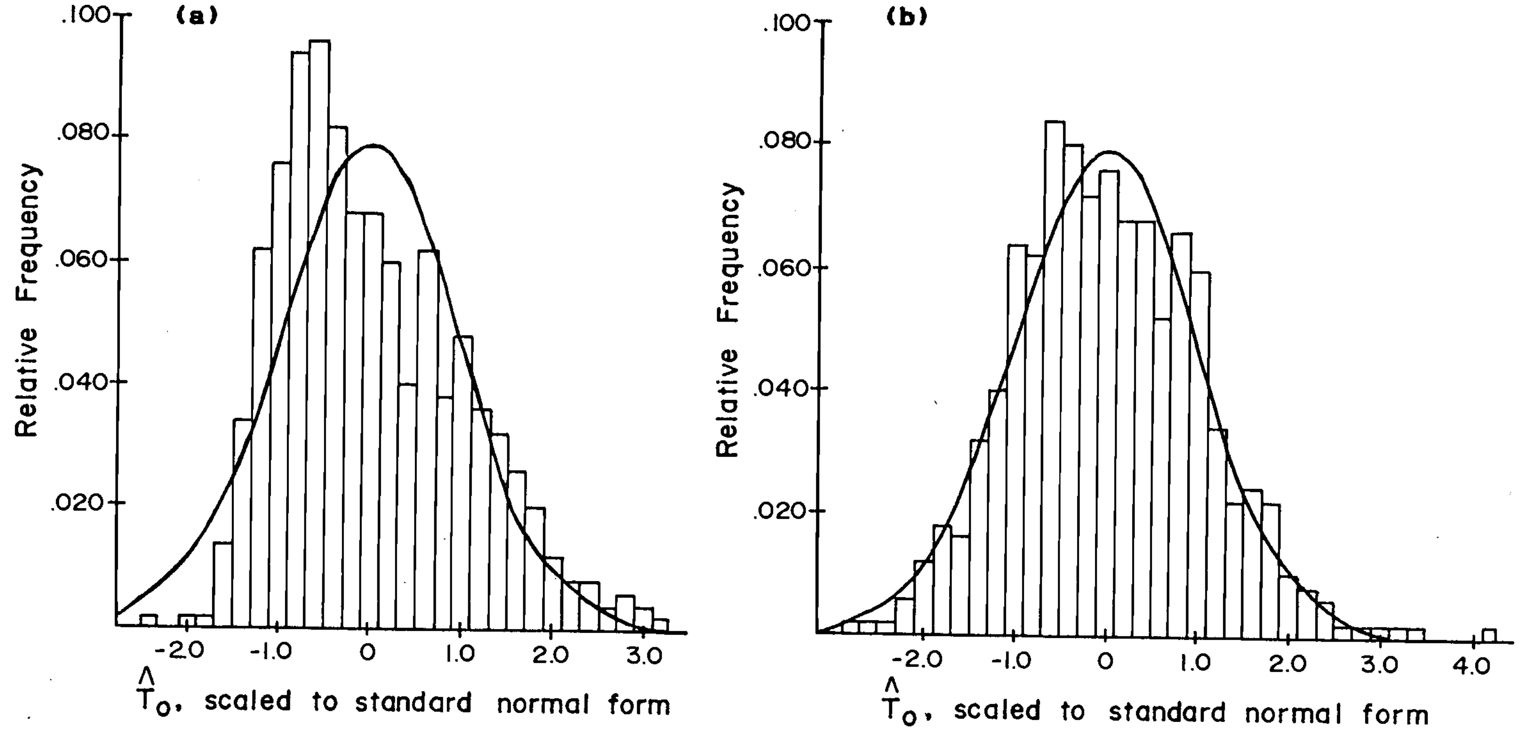


**Figure 36. Histograms of $T_0$ estimates, scaled to standard normal form, for autoregressive model 4.**

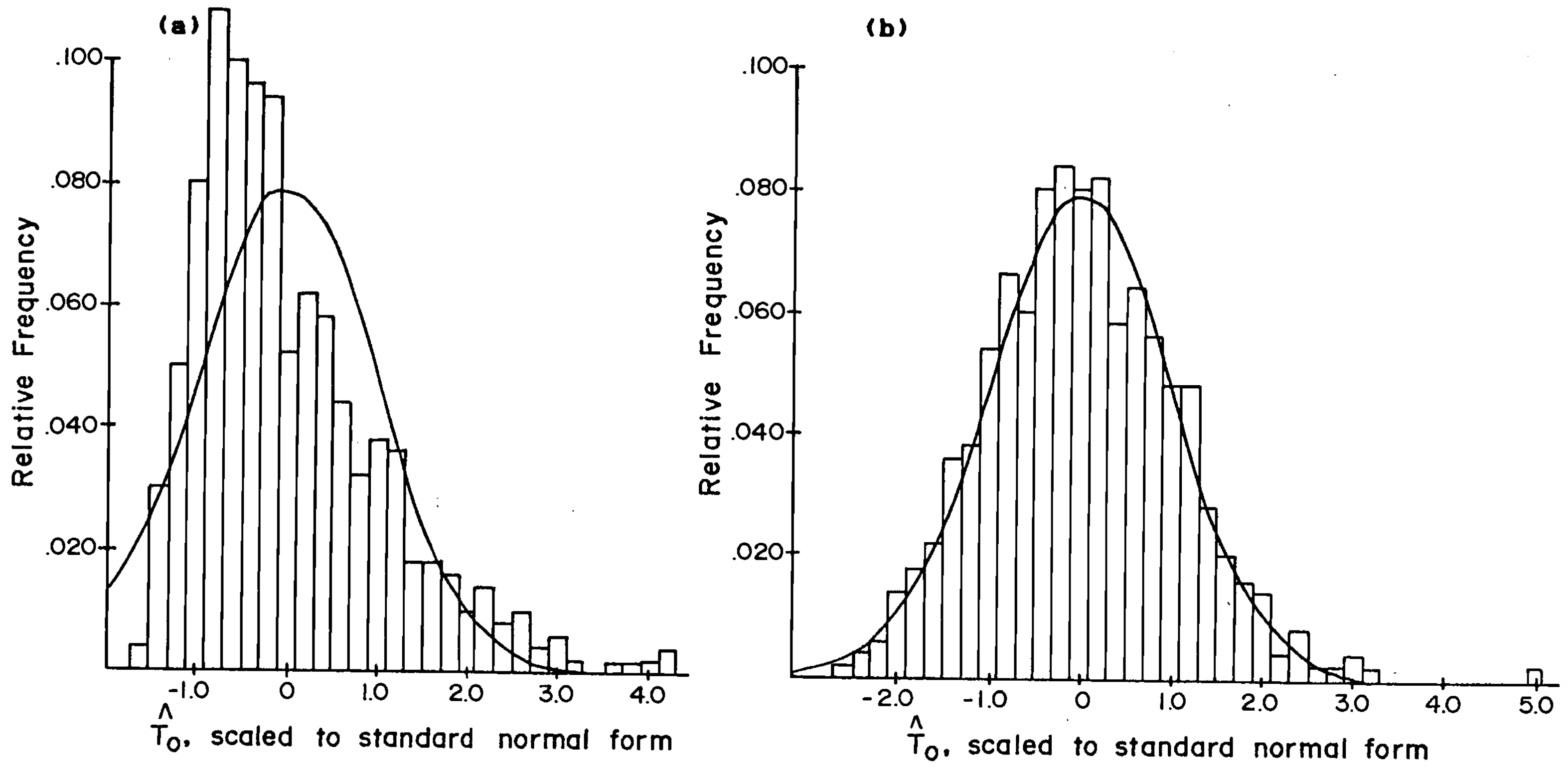


**Figure 37. Histograms of $T_0$ estimates, scaled to standard normal form, for autoregressive model 7.**

sample sizes, however, these distributions appear to be approximately Gaussian. This general impression is supported by the data in Table 41, which indicate proportions of the estimates lying beyond ±1.960 and ±2.576 standard deviations (the two-tailed 5%- and 1%-points for the normal distribution, respectively). Positive skewness of the sampling distributions for smaller N is evident here also, as well as the tendency to converge toward Gaussian distributions as sample sizes increase.

The best linear least-squares fit of the Monte-Carlo data to the transformed (A.7) is

$$\log [V(\hat{T}_o)] = \underset{(.246)}{2.47} + \underset{(.070)}{2.24} \log [\hat{T}_o] - \underset{(.039)}{1.03} \log [N] , \qquad (A.8)$$

where the numbers in parentheses below the parameter estimates indicate standard errors and log denotes natural logarithm. The coefficient of the last term in (A.8) is evidently not significantly different from unity, indicating that $V(\hat{T}_o)$ may indeed be regarded as inversely proportional to sample size, as assumed in (A.7). The resulting values for A and B in (A.7) are 11.8 and 2.2, respectively. Estimates of $V(\hat{T}_o)$ using this relationship are plotted in Figure 38 for selected values of N, together with the corresponding data points. The degree of fit is good ($R^2$ = 0.956 over all the transformed data), and deviations from the regression lines do indeed appear to increase with higher values of the predictand (note log scale on the ordinate).

Table 41. Proportion of standardized $\hat{T}_0$ values in the tail regions of the empirical distribution functions corresponding to one-tailed tests at the 0.5%- and 2.5%-levels.

| Model | N | Proportion of Standardized Data Values | | | |
|---|---|---|---|---|---|
| | | < -2.576 | < -1.960 | > +1.960 | > +2.576 |
| 1 | 2000 | .006 | .020 | .027 | .011 |
| | 1000 | .000 | .014 | .040 | .012 |
| | 600 | .001 | .012 | .038 | .014 |
| | 300 | .000 | .006 | .037 | .014 |
| | 200 | .000 | .006 | .036 | .011 |
| | 100 | .001 | .008 | .038 | .015 |
| | 70 | .000 | .000 | .034 | .023 |
| | 50 | .000 | .001 | .058 | .034 |
| 2 | 2000 | .005 | .020 | .030 | .007 |
| | 1000 | .001 | .019 | .026 | .009 |
| | 600 | .003 | .015 | .033 | .007 |
| | 300 | .004 | .015 | .033 | .008 |
| | 200 | .002 | .014 | .041 | .013 |
| | 100 | .000 | .005 | .040 | .014 |
| | 70 | .000 | .010 | .042 | .022 |
| | 50 | .000 | .013 | .036 | .015 |
| 3 | 2000 | .008 | .033 | .029 | .007 |
| | 1000 | .001 | .005 | .024 | .006 |
| | 600 | .000 | .001 | .034 | .013 |
| | 300 | .000 | .005 | .020 | .009 |
| | 200 | .000 | .006 | .021 | .005 |
| | 100 | .001 | .012 | .027 | .010 |
| | 70 | .000 | .006 | .033 | .012 |
| | 50 | .000 | .000 | .039 | .016 |
| 4 | 2000 | .002 | .020 | .027 | .006 |
| | 1000 | .001 | .020 | .029 | .008 |
| | 600 | .002 | .024 | .029 | .008 |
| | 300 | .000 | .005 | .039 | .014 |
| | 200 | .000 | .000 | .043 | .016 |
| | 100 | .000 | .000 | .052 | .018 |
| | 70 | .000 | .000 | .044 | .026 |
| | 50 | .000 | .000 | .032 | .015 |
| 5 | 2000 | .012 | .034 | .022 | .008 |
| | 1000 | .000 | .011 | .022 | .005 |
| | 600 | .000 | .003 | .038 | .011 |
| | 300 | .000 | .000 | .047 | .025 |
| | 200 | .000 | .001 | .047 | .028 |
| | 100 | .000 | .000 | .056 | .024 |
| | 70 | .000 | .000 | .059 | .023 |
| | 50 | .000 | .000 | .046 | .024 |

Table 41, continued.

| Model | N | Proportion of Standardized Data Values < -2.576 | < -1.960 | > +1.960 | > +2.576 |
|---|---|---|---|---|---|
| 6 | 2000 | .002 | .020 | .031 | .008 |
| | 1000 | .000 | .017 | .031 | .016 |
| | 600 | .003 | .009 | .033 | .010 |
| | 300 | .000 | .011 | .037 | .012 |
| | 200 | .000 | .006 | .036 | .016 |
| | 100 | .001 | .002 | .037 | .022 |
| | 70 | .001 | .001 | .053 | .029 |
| | 50 | .002 | .002 | .051 | .028 |
| 7 | 2000 | .000 | .018 | .029 | .008 |
| | 1000 | .002 | .013 | .028 | .008 |
| | 600 | .000 | .008 | .032 | .014 |
| | 300 | .000 | .003 | .053 | .023 |
| | 200 | .000 | .000 | .043 | .014 |
| | 100 | .000 | .001 | .039 | .014 |
| | 70 | .000 | .000 | .041 | .017 |
| | 50 | .000 | .000 | .037 | .019 |
| 8 | 2000 | .005 | .023 | .025 | .009 |
| | 1000 | .003 | .018 | .023 | .004 |
| | 600 | .000 | .005 | .032 | .009 |
| | 300 | .000 | .011 | .031 | .006 |
| | 200 | .000 | .011 | .027 | .014 |
| | 100 | .000 | .002 | .039 | .015 |
| | 70 | .000 | .000 | .036 | .015 |
| | 50 | .000 | .000 | .052 | .027 |
| 9 | 2000 | .000 | .015 | .033 | .011 |
| | 1000 | .004 | .017 | .028 | .007 |
| | 600 | .001 | .013 | .033 | .014 |
| | 300 | .000 | .010 | .037 | .008 |
| | 200 | .000 | .007 | .045 | .012 |
| | 100 | .000 | .002 | .048 | .014 |
| | 70 | .000 | .001 | .046 | .019 |
| | 50 | .000 | .000 | .059 | .024 |
| 10 | 2000 | .004 | .023 | .022 | .007 |
| | 1000 | .003 | .019 | .027 | .011 |
| | 600 | .001 | .016 | .031 | .008 |
| | 300 | .001 | .017 | .030 | .004 |
| | 200 | .000 | .006 | .033 | .011 |
| | 100 | .000 | .002 | .038 | .014 |
| | 70 | .000 | .000 | .044 | .022 |
| | 50 | .000 | .001 | .054 | .030 |

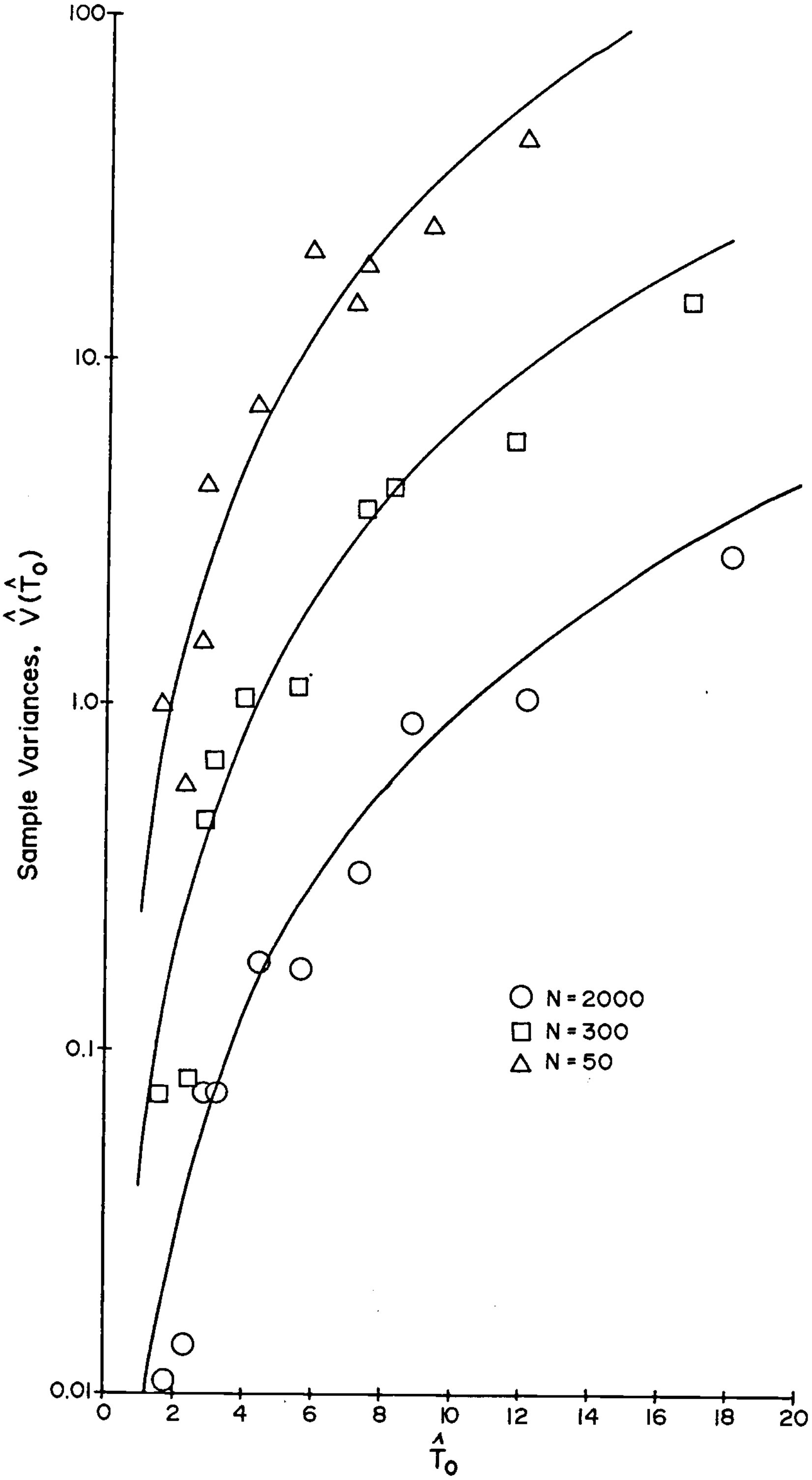


Figure 38. Estimates of $V(\hat{T}_0)$ as a function of $\hat{T}_0$.

## A.4 Concluding Remarks

The present results indicate that estimates of $T_0$ calculated according to (A.5) are asymptotically normally distributed. This result may be viewed as a consequence of the central limit theorem, since the statistic is a linear combination of sample autocorrelation estimates which are themselves asymptotically normally distributed (Hannan and Heyde, 1972). However, the sample size must be fairly large, perhaps on the order of 1000, for the sampling distribution of $\hat{T}_0$ to well approximate the Gaussian distribution.

Other important results include the fact that the sampling distribution of $\hat{T}_0$ appears to be asymptotically unbiased, and that its variance may be well represented as a simple nonlinear function of its mean. It is therefore possible to perform formal statistical procedures (for example, confidence statements concerning mean values, or approximate tests of equality of $T_0$ for two time series) by making use of the approximation to the normal distribution given time series of adequate length. This procedure would be appropriate, for example, when dealing with daily data from a 30-year record stratified by month or season.

For smaller sample sizes the Chebyshev inequality (e.g., Lindgren, 1976) can be used together with (8) for formal testing or to aid qualitative judgments. The present results indicate that, particularly for small samples and large estimates of $T_0$, caution in the interpretation of differences in this statistic is warranted.

# References


Box, G.E.P., and G.M. Jenkins, 1976: Time Series Analysis: Forecasting and Control. San Francisco, Holden-Day, 575 pp.

Hannan, E.J., and C.C. Heyde, 1972: On limit theorems for quadratic functions of discrete time series. Annals of Mathematical Statistics, 43, 2058-2066.

Jones, R.H., 1975: Estimating the variance of time averages. Journal of Applied Meteorology, 14, 159-163.

Katz, R.W., 1982: Statistical evaluation of climate experiments with general circulation models: A parametric time series modeling approach. Journal of the Atmospheric Sciences, 39, 1446-1455.

Leith, C.E., 1973: The standard error of time-average estimates of climatic means. Journal of Applied Meteorology, 12, 1066-1069.

Lindgren, B.W., 1976: Statistical Theory. New York, Macmillan, 614 pp.

Madden, R.A., 1976: Estimates of the natural variablilty of time-averaged sea-level pressure. Monthly Weather Review, 104, 942-952.

Madden, R.A., and D.J. Shea, 1978: Estimates of the natural variability of time-averaged temperatures over the United States. Monthly Weather Review, 106, 1695-1703.

Schwartz, G., 1978: Estimating the dimension of a model. Annals of Statistics, 6, 461-464.

Shukla, J., and D.S. Gutzler, 1983: Interannual variability and predictability of 500 mb geopotential heights over the Northern Hemisphere. Monthly Weather Review, 111, 1273-1279.

Thiebaux, H.J., and F.W. Zwiers, 1984: The interpretation and estimation of effective sample size. Journal of Climate and Applied Meteorology, 23, 800-811.

Trenberth, K.E., 1984: Some effects of finite sample size and persistence on meteorological statistics. Part I: Autocorrelations. Monthly Weather Review, 112, 2359-2368.

Trenberth, K.E., 1985: Persistence of daily geopotential heights over the Southern Hemisphere. Monthly Weather Review, 113, 38-53.

# APPENDIX B

## A Meteorologically-Based Formulation of Absorption and Runoff of Daily Rainfall

### B.1. Introduction

Runoff of rainwater from soil surfaces occurs when rainfall intensity exceeds the absorption capacity of the soil. Estimation of the proportion of rainfall which runs off, as a function of rainfall amount and soil properties, is desirable for many purposes. These include estimation of water available to crops, watershed yield, and soil loss due to erosion.

Most frequently precipitation data are available only as daily accumulations. However, drastic variations in precipitation intensity occur on much shorter time scales (e.g., Bodtmann and Ruthroff, 1976; Brown et al., 1985), and it is during periods of greatest precipitation intensity that most runoff occurs (e.g., Stallings, 1957).

The purpose of this note is to develop a method for estimation of absorption and runoff based on the statistical characteristics of point rainfall intensity, which can be applied using relatively coarse (i.e., daily) precipitation data.

## B.2. Development

It is assumed that the instantaneous rate of rainfall may be regarded as an exponentially distributed random variable. That is, that the probability density function for instantaneous rainfall rate, r, is given by

$$f(r) = \frac{1}{\mu} \exp\left[\frac{-r}{\mu}\right], \qquad r > 0, \tag{B.1}$$

where $\mu$ is a scaling constant. This formulation is consistent with observations of rainfall accumulated over short time periods (e.g., Bodtmann and Ruthroff, 1976; Brown et al., 1985; Drufuca, 1977; Huff, 1967; Jones and Simms, 1978) in that it implies that a large proportion of total rainfall occurs over relatively short durations, and therefore at high intensities. This is evidently a consequence of the concentration of the most intense convective activity in relatively small-scale regions, even within synoptic-scale storms (e.g., Austin and Houze, 1972; Hobbs and Locatelli, 1978; Houze et al., 1976).

The parameter $\mu$ in (B.1) is the mean of the distribution, and represents the average rainfall rate over the day. Its numerical value (in mm/hour) therefore depends on total daily rainfall (in mm), P, according to

$$\mu = P / 24 . \tag{B.2}$$

Let $A_{max}$ be the maximum (instantaneous) rate at which a soil can absorb rainfall, with units of mm/hour. So long as rainfall intensity is below this threshold, all precipitation will be absorbed and no runoff will occur. This will be the case during the proportion of the day given by

$$D_{full} = \int_0^{A_{max}} f(r)\, dr$$

$$= \int_0^{A_{max}} \frac{1}{\mu} \exp\left[\frac{-r}{\mu}\right] dr$$

$$= 1 - \exp\left[\frac{-A_{max}}{\mu}\right] . \qquad (B.3)$$

The probability-weighted (i.e., statistically expected) absorption rate during this time is given by the conditional expectation

$$A_{full} = \int_0^{A_{max}} r\, f(r \mid r < A_{max})\, dr$$

$$= \int_0^{A_{max}} \frac{r}{\mu\, D_{full}} \exp\left[\frac{-r}{\mu}\right] dr$$

$$= \left\{ \mu - ( A_{max} + \mu ) \exp\left[\frac{-A_{max}}{\mu}\right] \right\} / D_{full} , \qquad (B.4)$$

since the probability that r is less than $A_{max}$ is equal to $D_{full}$.

Similarly, that proportion of the day for which the precipitation rate exceeds the absorption capacity of the soil is given by

$$D_{part} = \int_{A_{max}}^{\infty} f(r)\, dr$$

$$= \int_{A_{max}}^{\infty} \frac{1}{\mu} \exp\left[\frac{-r}{\mu}\right] dr$$

$$= \exp\left[\frac{-A_{max}}{\mu}\right] , \qquad \text{(B.5)}$$

during which time the absorption rate takes on the limiting value

$$A_{part} = A_{max} . \qquad \text{(B.6)}$$

The weighted-average (hourly) rate of absorption throughout the day is then given by

$$A_{ave} = D_{full} A_{full} + D_{part} A_{part} , \qquad \text{(B.7)}$$

and the total amount of water absorbed over 24 hours is

$$W = 24\ A_{ave}$$

$$= 24\ (\ \mu - \mu \exp\left[\frac{-A_{max}}{\mu}\right]) . \qquad \text{(B.8)}$$

Runoff is of course given by P - W.

## B.3. Examples and Discussion

The relationship between daily rainfall, P, and water absorbed, W, given by (B.8) and (B.2) is illustrated in Figure 39. Curves for five values of $A_{max}$, representing typical values for very fine-textured to very coarse-textured soils (Hillel, 1971) are shown. As precipitation increases, absorption approaches a limit which depends on $A_{max}$. For P less than approximately 5 mm full absorption is specified, and no runoff occurs for even very slowly permeable ($A_{max}$=1) soils. For highly permeable ($A_{max}$=20) soils runoff is not specified unless P is greater than about 50 mm.

The specifications of the present method are similar to those derived from the more cumbersome traditional method of calculating rainfall absorption (Soil Conservation Service, 1972), which is based on empirical "rainfall/runoff" data from small watersheds and is oriented primarily toward prediction of streamflow. The present formulation has the advantages of being based on a single continuously variable parameter that directly influences absorption, $A_{max}$, and gives explicit consideration to the nature of variations in precipitation rate during a given day. Also, extension of the method for use with rainfall data accumulated over shorter periods (e.g., hourly) is immediate.

Incorporation of the present formulation into soil water balance models would be straightforward, and could be done at various levels of sophistication. The parameter $A_{max}$ can be considered constant for

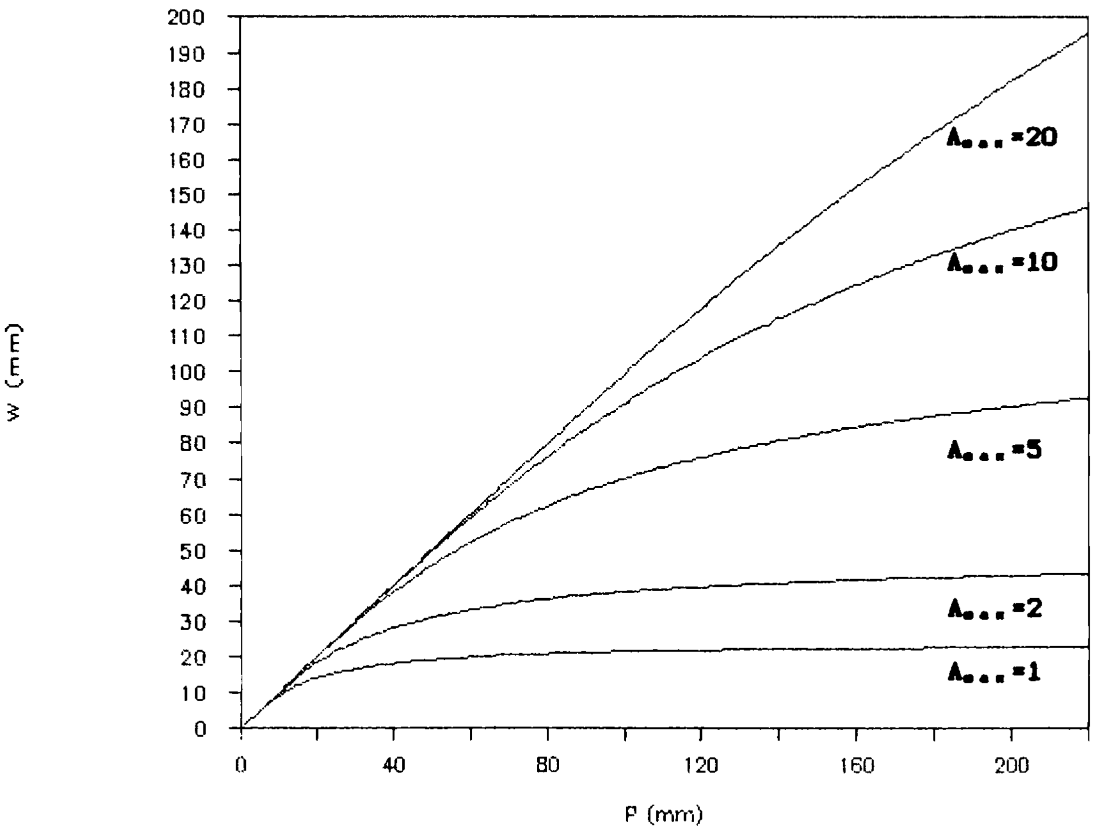


**Figure 39. Predicted daily water absorption, W, as a function of total daily precipitation, P, for five values of maximum absorption rate.**

a particular soil depending, for example, on soil texture and slope. Alternatively, it could be made to vary dynamically as a function of such variables as soil water content or leaf area index.

A more faithful representation of the instantaneous rainfall rate might result if (B.1) were replaced by a more complicated probability density function, such as the Chi-square or two-parameter gamma. These distributions would allow the possibility of low probabilities of small precipitation intensities, although at a higher computational expense. It is doubtful that the overall specification of rainfall absorption would be much improved, however, since the essential feature of precipitation intensity influencing runoff and absorption is the strong positive skewness of the distribution, which is well represented in (B.1).

# References


Austin, P.M., and R.A. Houze, Jr., 1972: Analysis of the structure of precipitation patterns in New England. Journal of Applied Meteorology, 11, 926-935.

Bodtmann, W.F., and C.L. Ruthroff, 1976: The measurement of 1 min rain rates from weighing raingage recordings. Journal of Applied Meteorology, 15, 1160-1166.

Brown, B.G., R.W. Katz, and A.H. Murphy, 1985: Exploratory analysis of precipitation events with implications for stochastic modeling. Journal of Climate and Applied Meteorology, 24, 57-67.

Drufuca, G., 1977: Radar-derived statistics on the structure of precipitation patterns. Journal of Applied Meteorology, 16, 1029-1035.

Hillel, D., 1971: Soil and Water. New York, Academic, 288 pp.

Hobbs, P.V., and J.D. Locatelli, 1978: Rainbands, precipitation cores, and generating cells in a cyclonic storm. Journal of the Atmospheric Sciences, 35, 230-241.

Houze, R.A., Jr., P.V. Hobbs, K.R. Biswas, and W.M. Davis, 1976: Mesoscale rainbands in extratropical cyclones. Monthly Weather Review, 104, 868-878.

Huff, F.A., 1967: Time distribution of rainfall in heavy storms. Water Resources Research, 3, 1007-1019.

Jones, D.M.A., and A.L. Sims, 1978: Climatology of instantaneous rainfall rates. Journal of Applied Meteorology, 17, 1135-1140.

Soil Conservation Service, 1972: Hydrology. SCS National Engineering Handbook. Section 4. Washington. D.C., U.S. Department of Agriculture, Chapters 7-10.

Stallings, J.H., 1957: Soil Conservation. Englewood Cliffs, N.J., Prentice-Hall, 575 pp.